Cell mechanics and cell-cell interactions of fibroblasts from Dupuytren's patient: Atomic Force Microscopy Investigation

Dissertation submitted towards the degree
Doctor of Natural Sciences

- Dr. rer. Nat. -

M.Tech Prem Kumar Viji Babu

Bremen, January 16, 2020

Referees: Prof. Dr. Manfred Radmacher

Prof. Dr. Ursula Mirastschijski

Universität Bremen

INSTITUT FÜR BIOPHYSIK

If you want to find the secrets of universe, think in terms of energy, frequency and vibration

-Nikola Tesla

Abstract

Cells as a biological entity of tissue, itself made of biomolecules such as mostly proteins, lipids and carbohydrates, creates its own meshwork of biopolymers named extracellular matrix (ECM) particularly fibroblasts. With the advanced light and force microscopies, inter-cellular, cell-ECM and intracellular signaling pathways are deeply explored either by tagging the biomolecule of interest with fluorophores or by applying certain forces (in the order of pN to nN). In the field of mechanobiology, interplay between cell function and physical forces are studied using biophysical tools that probe their diverse mechanisms.

Cells exert forces ('inside-out' signalling) and also respond to physical forces from their micro-environment ('outside-in' signalling) through participation of chain of varying protein signaling molecules. Actin molecules from cytoskeleton family form filaments in the cytoplasmic side of the cell and myosin walk on these filaments generates contractile tension. These traction forces get transmitted to the extracellular matrix of the cell or to the neighboring cells through protein complexes such as integrin and cadherins, respectively.

Fibroblasts, from the mesenchymal family, are the abundant cells found in the connective tissue. Basically, fibroblasts synthesize, degrade and maintain the extracellular matrix components of the tissue. Fibroblasts, by acquiring different phenotypes called protomyofibroblast/myofibroblast, play a huge participation in various connective tissue related diseases. Myofibroblast are large cells possessing large bundles of actin filaments of isomers named alpha smooth muscle actin (α-SMA). On the other hand, protomyofibroblast share the similar characteristic appearance but shows α-SMA negative large stress fibres. In Dupuytren's disease, these myofibroblasts persists and deform the surrounding matrix environment thus results in tissue stiffening and further leads to tissue contracture.

Existing various biophysical tools maps forces such as tractile force, cell-cell interaction force and cell-ECM interaction force. One among such tool is Atomic Force Microscopy, a multifunctional toolbox in cellular biology to observe various cell types mechanics. Observing cell viscoelastic properties by application of controlled force (nanonewton) to the adherent cell become more common in the biomedical community. This thesis demonstrates the measurement of viscoelastic properties of fibroblast of different phenotypes extracted from a Dupuytren's diseased patient and ECM derived from various tissues. The bio-mechanical interplay between cell and ECM has been studied with careful design of the AFM experiments. Fibroblasts extracted from the cords and nodular region of the palmar fascia exhibits myofibroblast phenotype and migrate slower than the fibroblast extracted from dermal and scar region. Normal and scar fibroblasts migrate faster in the wound healing assay. On the decellularized matrices, scar fibroblasts exhibit protomyofibroblast phenotype by expressing large stress fibres. Whereas, normal fibroblasts derived from the dermal region express the healthy phenotypic appearance. From AFM based Single-cell force spectroscopy (SCFS), cell-cell interaction force measurements evaluate the homophilic and heterophilic cadherin pairs mechanical bond strength expressed in homo-cellular (fibroblast of similar phenotype) and hetero-cellular (fibroblast-epithelial cell) arrangements. SCFS measurements also illustrate the significant role of actomyosin contractile apparatus in cadherin extracellular

domain binding dynamics. With this evidence, SCFS setup has become an excellent spectroscopic tool to study the intracellular signaling cascades that are linked to the extracellular domain consisting transmembrane proteins such as cadherins.

Therefore, an understanding of the unique fibroblasts mechanobiology is necessary to study the healthy and diseased tissue dynamics. The cell-cell and cell-ECM bio-chemical and bio-mechanical cues are strongly interdependent. Finally, the current thesis opens the basic understanding of the fibroblasts biophysical properties using AFM nano-mechanical tool and unravels the fibroblasts biomechanical function in sub-tissue level biology.

Table of Contents

Acknowledgements

The loving upbringing of my beloved parents and the support of my family especially my younger sister, Hema has always set the seed of mental stability and they will always stay with me in my heart and thought.

A doctoral thesis in any subject brings out the deepest knowledge and trueness of life science in a researchers life. The creativity, the dedication and the freedom of science exploration in any laboratory makes a doctoral life an unforgettable experience. I have experienced such a warm welcome to an abroad land by Prof. Manfred Radmacher and his creative approaches towards discussing the results has been very important to me throughout the projects. Manfred has always made sure that I had all the resources I need to conduct my project and helped me a lot in the data analysis which I admired a lot. Manfred gave me lot of freedom to learn and conduct experiments. He made sure that he always there for me to show progress in my work and mould me a good presenter. By giving this huge opportunity, I sincerely thankful and I hope I worked hard to his expectations.

With the fine collaboration, one can always share their enthusiasm and dedication in the respective field. To that, Prof. Dr. Ursula Mirastschijski, a medical doctor was introduced on a project and from that moment, she became a true inspiration for me in science. She always there for me throughout the projects right from sample preparation, results and discussion to manuscript preparation. Her inputs in my project really shaped me better professionally and personally. I am always excited to present my results with her because of her enthusiasm and motivation that amaze me every time and made me perform even better. For all this, I thank you once again.

Furthermore, I would like to thank from the bottom of my heart Prof. Monika Fritz and Prof. Dorothea Brüggemann for all the inputs given on my presentation skills. I thank Dorothea for letting me share all the facilities from her lab specifically fluorescence microscopy. I am also very grateful to Prof. Gazanfer Belge and his other lab members for providing me cells and other materials.

During the years in Bremen, my lab member Dr. Carmela Rianna, soon to be a mother has been like an elder sister, a dear friend and a great inspiration for me. She is one of the best postdoctoral members anyone can get in their research life. I am really going to miss such a lovely being. She taught me all the things in the lab and helped me a lot in upbringing my career. Also, I would like to thank my lab technician Holger Doschke for all his efforts in instrumentation setup and data analysis. I would like to thank other members of the biophysics institute: Naiana, Karsten, Dennis, Klaudia, Kathrin, Achu, Eva, Anja, Sandra, Shruthi, Saurabh and Janka for all the fun and joy.

I take this opportunity to thank my past PIs: Prof. Uma Maheshwari, Prof. Thorben Cordes, Prof. Deepak Saini and Prof. Gautam Soni for their support in my research career.

x

I   Introduction

Chapter 1

1.1 Atomic Force Microscopy and Cell mechanics

1.1.1 AFM Imaging

In the current biophysics field, the invention of AFM (Binnig et al., 1986) has become a milestone in the nano-biotechnology and increasingly been employed for obtaining both topography images and mechanical maps (stiffness, molecular recognition) of the various cellular and sub-cellular structures. AFM allows the characterization of these structures on live cell/tissue samples at high resolution. Originally invented as scanning tunneling microscope to perform measurements on non-conducting samples, AFM is a mechano-nanoscope to study biomolecules and cells at higher spatiotemporal resolution. With the basic principle, AFM is a force sensor, with a sharp tip attached to a tiny spring named cantilever, which interacts vertically with the sample and scans the specimen in a zigzag manner. The most common imaging methods from AFM for applications in cellular and molecular biology are illustrated in figure 1.1.
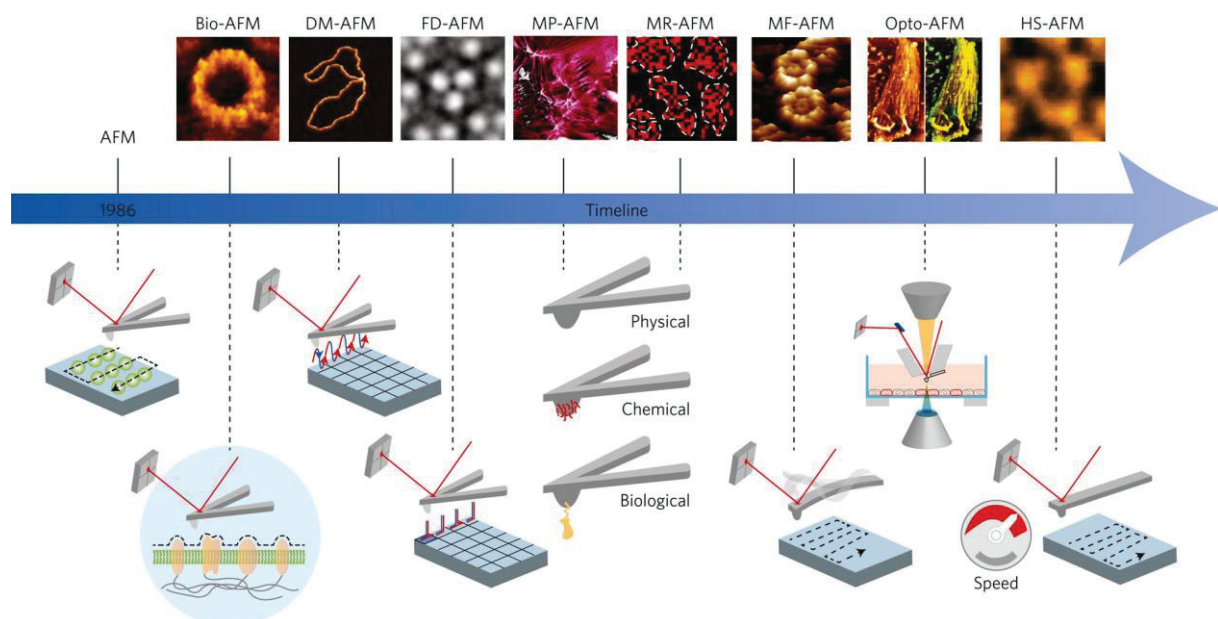
Figure 1.1 AFM imaging-common methods (Biological (Bio-), Dynamic mode (DM-), force-distance curve based (FD-), multiparamteric (MP-), molecular recognition (MR-), multifrequency (MF-), correlated optical imaging (Opto-) and high-speed (HS-) AFM) in cellular and molecular biology. Since the invention in 1986, AFM has been used as a imaging tool to study the structure of membrane proteins expressed in cell membranes, protein and DNA conformations, protein subunits dynamics, F-D curve based biological samples elastic properties, cell stiffness, biomolecular recognition by mapping the specific interactions of molecules attached to tip, correlated optical imaging of complex biological systems and cell processes. Reproduced from the (Dufrêne et al., 2017) with the license. To view the copy of the license, visit http://creativecommons.org/licenses/by/4.0/.

The key breakthrough that led to biological AFM is the advancement of laser detection system reflected from the cantilever surface and followed by enabling AFM imaging in native physiological environment. The simple AFM imaging modes are categorized mainly into contact (DC) and non-contact (AC) to measure the sample topography. In contact mode, the cantilever deflection is measured while the AFM tip is brought into physical contact with the sample. "In the constant height mode, while the tip raster scans the sample and the sample is kept at a constant height. The topographic information is inferred from the deflection of the cantilever as the tip scans over areas of different heights. This particular mode is generally used for flat and rigid samples, since, due to the deflection of the cantilever the loading force will change. For soft biological samples, especially for cells and softer tissues such as brain, this mode will damage such soft bio-samples as they will be exposed to large loading forces. In order to image soft samples, a feedback is introduced to adjust the z height such that the deflection, and therefore the loading force, is held constant. This mode is called constant force or constant deflection mode. In constant deflection mode, the output of the feedback corresponds to the height signal image which shows the overall sample topography. Since the feedback will react with a finite response time, the main time limiting factor will be the piezo transducers used in AFM, there are some residual changes in deflection, which are not perfectly compensated. In control theory this behaviour is called the error (of the feedback loop); therefore, in AFM the phrase error signal image is also often used. To reduce lateral forces exerted to the sample in contact mode, which can be substantial and destroy or detach samples, the tip is periodically retracted from the sample and the cantilever height is modulated at the cantilever's resonance frequency. This mode is called the tapping mode and is used largely in imaging biomolecules such as DNA, proteins, and lipids" (quoted content reprinted from Viji Babu and Radmacher, 2019). Tapping mode is further classified into amplitude- and frequency- modulation AFM dynamic modes from which various properties such as mechanical, electrical, magnetic and so on are measured. Like in contact deflection mode, tapping mode produces two images: a height and an amplitude error image.

A novel variant of the tapping mode, the peak force mode is one of the off-resonant modes, where the data during one oscillation cycle are captured and analysed online to control the maximum interaction force, which usually kept constant, seems to be favourable for cell imaging (Schillers et al., 2016). Among the other off-resonant modes (HybriD mode, QI mode, Jumping mode, Digital Pulse-Force, HarmoniX, AM-FM Viscoelastic Mapping, Pulse-Force- modes), PeakForce Tapping mode from Bruker manufacturer also provides the analysis of viscoelastic properties of the sample surface. Being a fast scanning mode by applying faster indentation to the sample such that it obtains quantitative mechanical properties, it also brings fast imaging. Instead of triangular wave implementation to Z modulation, PeakForce Tapping mode feeds the sinusoidal wave and this creates a sinusoidal background to the cantilever deflection and the measured interaction force. Through data analysis algorithm this background is subtracted to obtain the true interaction force, which shows an increase in signal to noise ratio that provides high resolution images of soft

A
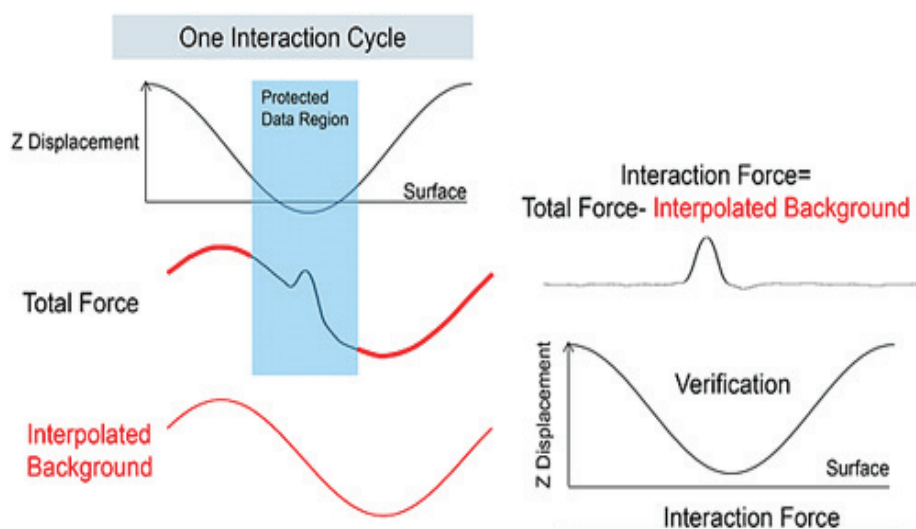
B
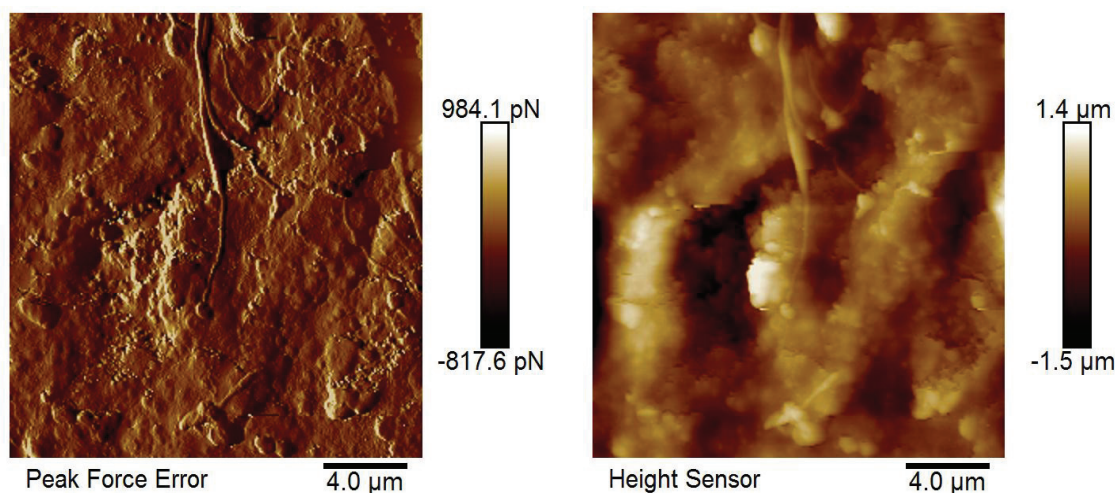
Figure 1.2 AFM PeakForce Imaging. (A) The schematics illustrates the sinusoidal Z modulation input to the total force with the peakforce region and outside force region, which is eliminated by the interpolated background subtraction from the total force. Reproduced from the (Schillers et al., 2016) with the license. To view the copy of the license, visit http://creativecommons.org/licenses/by/4.0/. (B) Height and peak force error images recorded with AFM peak force tapping mode in human decellularized matrix, which shows the surface topography of the matrix (Rianna et al., 2018).

biological samples even scanned at very low forces (Schillers et al., 2016). Figure 1.2 shows the schematics of peak force event extrapolation using certain algorithm and also shows the height and peak force error images of human decellularized dermal matrix obtained for carrying investigations on cell and ECM mechanics interplay (Rianna et al., 2018) (Chapter 4).

Overall, these AFM based resonance and off-resonance methods of fast imaging provide better resolution images and also determine various mechano-chemical properties of the biological sample.

1.1.2 Cell mechanobiology

Cells in tissues are constantly undergoing changes in their shape, composition and function induced by mechanical loads. Mechanical load sensitive cells includes fibroblasts, osteoblasts, smooth muscle cells and endothelial cells *in vivo* that possess the specific genotype responsible for the generation of mechanical force such as contractile stress that are applied to their extracellular matrix (ECM) environment and also to their neighbouring cells. These cellular genotypes mediate the focus of proteins involved in the cellular mechanotransduction pathways. Although the exact mechanisms by which cells generate mechanical forces are known through measuring intracellular contractile stresses, converting them into biochemical signals are still unknown and only some possible signalling pathways and associated proteins are under investigation. More focus on sensing and converting mechanical forces into biochemical responses is concerned in finding the exact signalling mechanisms. Exploring the right mechanotransductory pathways and finding out both cell and ECM proteins participation in such complex pathways are the key areas of mechanobiology research. The process of participation of mechanoproteins in biophysical force sensing, transmitting and responding through cell adhesion to the neighbouring cells and ECM environment is called cellular mechanotransduction (Fig. 1.3). The main players of the mechano-transduction pathways include: intracellular cytoskeleton, cell membrane adhesion receptors and extracellular ECM

macromolecules. In the current mechanobiology field, studying the mechanically stimulated living cells and tissues and then determining their mechanical properties in response are of huge interest. Setting up experiments at the single cell and tissue levels are quite challenging and it made possible by the recent experimental developments in the biophysical instrumentation. Mostly these biophysical instruments applies and in response measures the forces only, but the actual potential lies in measuring biochemical signals output in response to mechanical stimuli. This should give even more detailed overview in addressing the questions still persists in cellular mechanotransduction. The quantification of cellular contractile forces in cell traction force microscopy help to understand the underlying biological mechanisms at the cellular and molecular level (Wang et al., 2007). AFM nanoindentation experiments elicited the dependency of cellular stiffness on the cell underlying substrate stiffness (Solon et al., 2007). This create huge impact on the need of understanding the signalling molecules, basically mechanoreceptors and mechanoproteins roles in complex mechanotransdcution pathway.
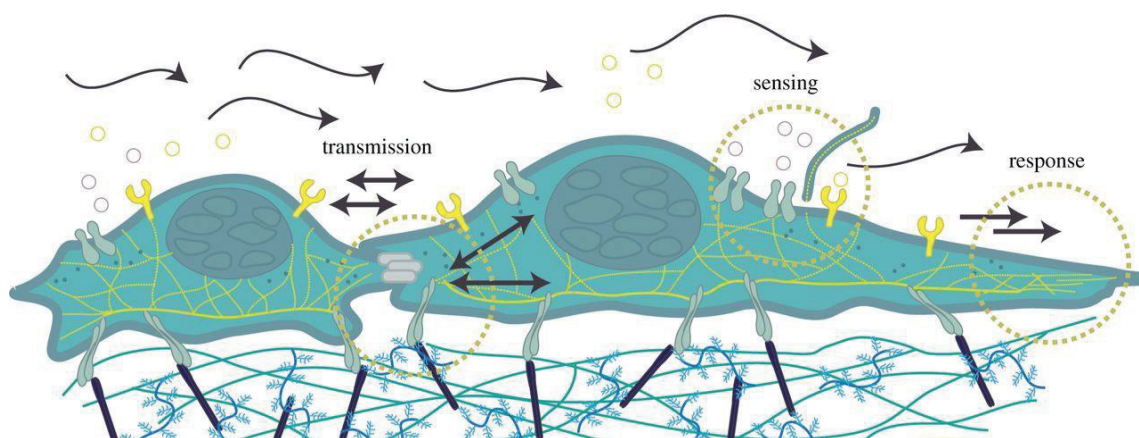
Figure 1.3 The process of cellular force sensing, transmitting and responding through specific membrane receptors and participation of such mechano-sensitive protein complexes (focal adhesion complexes) is called mechanotransduction (Haase and Pelling, 2015). Reproduced and modified with permission and for licence visit (https://s100.copyright.com/AppDispatchServlet#formTop)..

Normally, cells generate, sense, transmit and respond to forces from its ECM microenvironment using integrin-actin cytoskeleton enriched focal adhesion complexes. Transmembrane adhesion receptors-integrin and cadherin act as a mechanosensor that interconnects both intra- and extracellular protein networks (Geiger and Bershadsky, 2002). Focal complexes (FC) acts as a biochemical and biophysical hub that anchors integrin along with other adaptor proteins to the actin cytoskeleton and to the extracellular RGD peptide sequence containing ECM molecule. The maturation of focal complex (1 μm in size) to focal adhesion (FA) (3-5 μm in size) assembles other adaptor proteins and the ECM substrate

stretching leads to the mechanical activation of integrin signalling and FA assembly (Jungbauer et al., 2008; Tondon et al., 2012). The mechanosensing process starts at the integrin checkpoint which makes the initial cell-ECM contacts along with other associated protein molecules together termed as focal complexes (Fig. 1.4). These structures later transformed into mature focal adhesions consists of other signalling protein molecules with
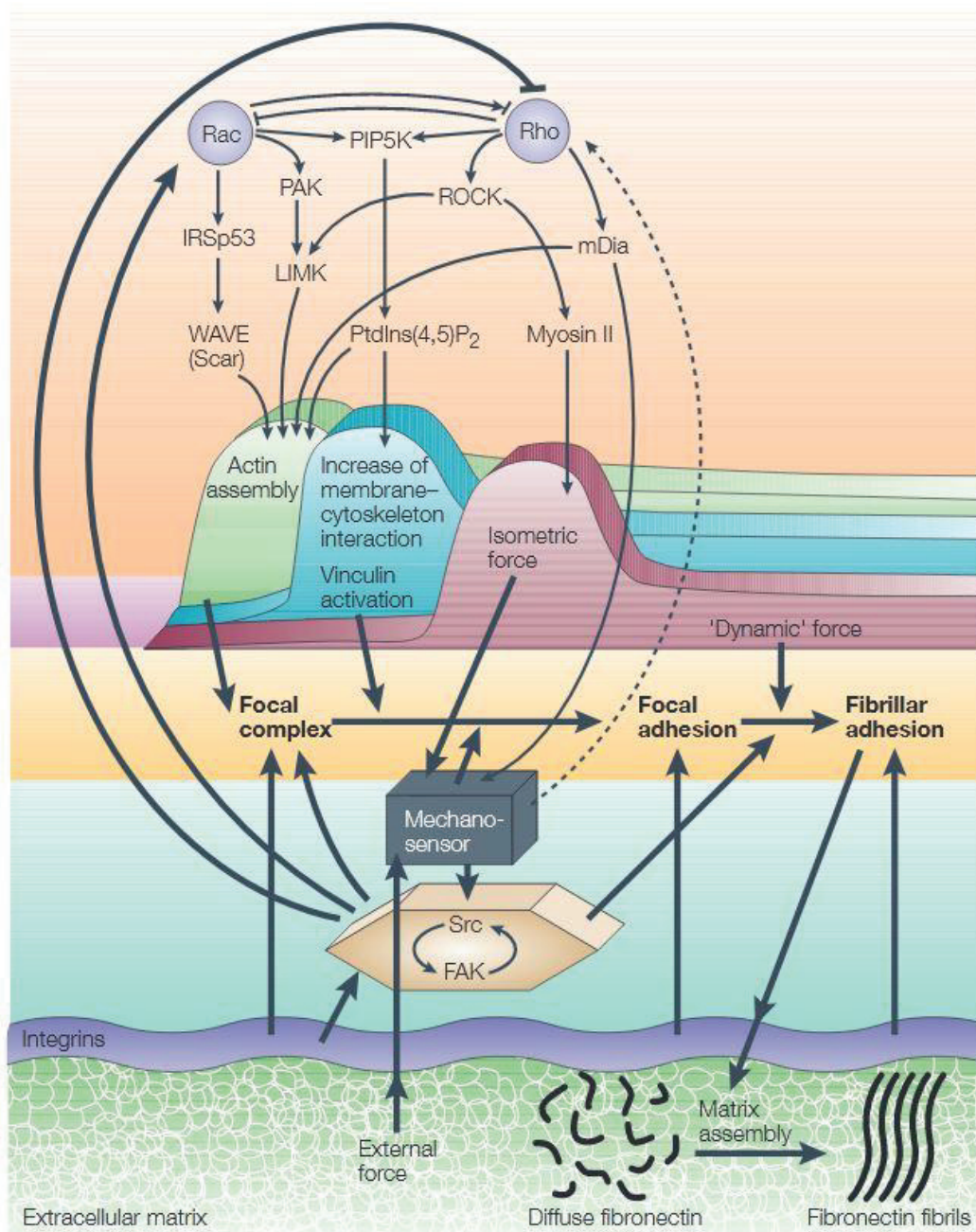
Figure 1.4 A cartoon representation of mechanotransduction signalling systems that are associated with various protein complexes formation and involvement in signal transduction pathways through generation and transduction of forces. Here, the contractile (isometric) force generated by actomyosin contraction is transmitted to the stiff ECM through focal complexes which assembles integrins and focal complex maturation to focal adhesion complexes thus to fibrillar adhesion complexes (Geiger et al., 2001). Reproduced with permission and for licence visit (https://s100.copyright.com/AppDispatchServlet#formTop).

larger size in appearance. These mature FAs further evolve to supermature FAs called fibrillar adhesions driven by 1) rigid ECM, 2) the activation of plaque proteins (such as vinculin) and 3) the increase in cellular tension force. Intracellular actin assembly, myosin crosslinking the actin filaments, increase of membrane-actin cytoskeleton interaction and associated isometric and dynamic force plays an important in the FC and FAs growth, activation and regulation. The isometric force is defined by the force developed in response to cell adhesion formed with stiff ECM. Meanwhile, the dynamic force helps to mobilize both focal adhesion complexes and the ECM. ECM in every tissue provide structural support and mechanical strength to the tissues and also generate attachment sites for cells together constitute tissue integrity and function. ECM components such as collagen, elastin and fibronectin provide biochemical signals to cells and promote cell-ECM adhesion. The stiff matrix triggers the growth of cell anchoring FAs. The fibrillar adhesion structures involved in the matrix assembly specifically in the formation of fibronectin fibrils from diffused fibronectin. The entire system is regulated by the cascade of signalling events which are categorized into local and global regulatory system. The local regulatory system consists of mechanosensor and FAK (focal adhesion kinase)-Src phosphorylation system that activates the Rac and Rho signalling system which plays a role in myosin II mediated isometric force generation. The global regulatory system consists of Rho and Rac and other associated proteins and enzymes which are activators and regulators of the actin assembly, vinculin activation and isometric force generation events.

1.1.3 Cell mechanics and viscoelastic properties

As a biophysical parameter, cell mechanics is correlated with many human diseases (C. Rianna and Radmacher, 2017) and the mechanical cues between cell and ECM determine the cell fate and phenotype escpecially in case of fibroblast and myofibroblast mechanics (Guilak et al., 2009; Huang et al., 2012). Mostly cells in tissue are experienced to various forces through interaction which surrounding cells and surrounding matrices through various protein complexes enriched signaling pathways. These mechanotransduction pathways consist of three main processes such as force sensing, transmitting and responding in the typical signaling ways of 'inside-out' and 'outside-in' signaling. The key protein components present in the mechanotransduction pathways are the (i) cytoskeleton, which are present as large filaments made of actin in the intracellular region and connects the neighboring cells through

(ii) cadherins, which are transmembrane, cell-cell adherens junction protein molecules, and connects the ECM microenvironment through (iii) integrins, which are transmembrane protein receptors that binds to RGD ligand peptide of the ECM protein complexes. These transmembrane proteins (integrins and cadherins) are connected to the actin filaments through multi-protein complexes called adaptor proteins. Focal adhesion complexes (integrin-adaptor proteins-actin filaments) direct the multiple mechanosensor protein molecules and direct many intracellular responses. Similarly, cadherins mediate the intracellular tractile force generation and direct the mechanosensor and mechanotransmitter protein molecules in the signaling transduction pathway. In force generation within the cell, tractile force generation through actomyosin assembly and myosin walk includes signaling pathways such as Rac and Rho dependent pathways.

The integration of the force output generated by these mechanotransduction pathways and actomyosin contractile apparatus mediated cell mechanics govern the cellular shape and function. Intermediate filaments also play an important role in cellular mechanics through providing stiffness to the cell. Mostly, actin filaments in the vicinity of the AFM mechanical force loading provide the stiffness of the cell (figure 1.5). Cell deformation from the AFM applied force measures the local elastic response of the underlying cell actin filaments. Usually, by fitting the F-D curve (explained in section 2.1) with suitable contact models, Young's moduli of actin filaments expressing certain cell types can be measured. Measuring cell stiffness has become more common in order to characterize and identify the diseased and healthy cells. The main advantage of measuring cell stiffness from AFM mechanical maps combined with fluorescence imaging of fluorescently tagged actin filaments is the evaluation of highly heterogeneous cell region with varying stiffness correlated to the presence of actin filaments. Cell stiffness depends not only on the cell type but also on the AFM tip geometry,

Height Sensor   2.0 µm / -2.2 µm   20.0 µm

Peak Force Error   1.7 nN / -1.2 nN   20.0 µm

8
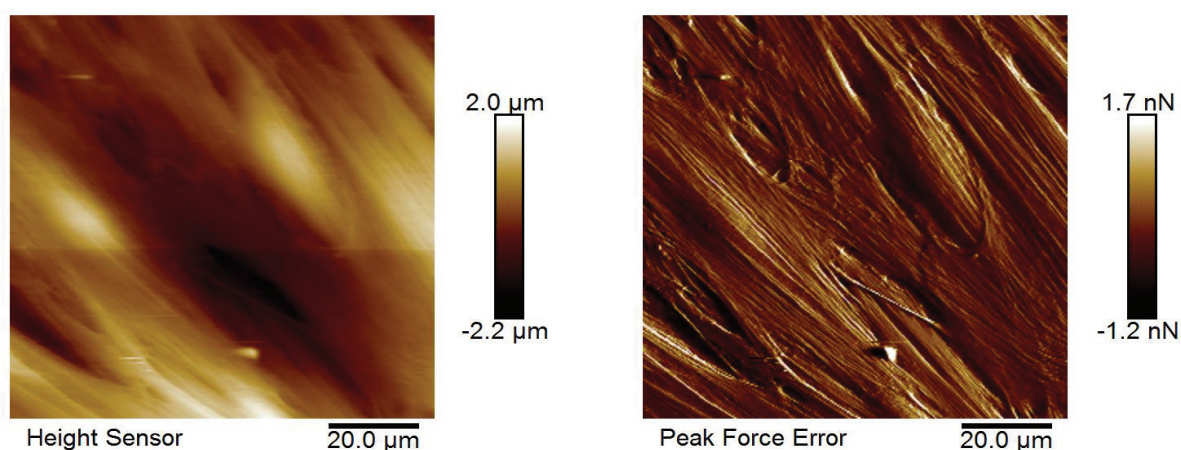
Figure 1.5 Actin filaments in the vicinity of cell stiffness. In the AFM mechanical loading regime to evaluate the cell stiffness, the visible actin filaments beneath the cell membrane contribute to the cell's elastic modulus value.

force ramp frequency and force magnitude. It is always necessary to measure and compare the elasticity of cells of various origins (diseased and healthy) with the similar tip geometry and force parameters. AFM mechanical studies are often carried on adherent cells, which are seeded on biochemically modified petriplates or other substrate gels such as polyacrylamide gel coated with collagen or direct collagen gels. Effect of substrate stiffness on cell stiffness can also be measured by AFM. The durotaxis effect are studied on gel stiffness gradient, where on a stiff region of the substrate cells exhibit stiff mechanics by expressing large stress fibres and exert larger traction force and on a soft substrate region, cells migrate faster and exert low traction force by expressing less stress fibres. Cell adhesion, cell tractile force generation and cell migration are the fundamental processes in biological phenomenon such as tissue morphogenesis and homeostasis. The actin cytoskeleton plays an important role in all these processes and an interconnected cellular mechanical evaluation demonstrates the cell functions at different phenotypic determinants.

AFM mechanical force mapping consist of many force curves and provides better resolution cell elasticity maps which shows larger picture of different parts (cell body, nucleus and cell periphery) of cells rheology. In order to determine the viscoelastic properties of cells, other than Hertzian model which only provides elastic modulus, a step response AFM technique with standard linear model fitting has been implemented (Yango et al., 2016). This method measures the true elastic modulus by means of storage modulus and also the dynamic viscosity of the cells by means of loss modulus. Using this method, viscoelastic properties of normal and cancer thyroid cells are studied and compared on different stiffness substrates (Carmela Rianna and Radmacher, 2017). In chapter 3, the viscoelastic properties of different fibroblast phenotypes are measured by obtaining stress relaxation data and by calculating the force ramp data by standard linear solid model (see Appendix). The stress relaxation data is obtained by applying a force to the cell and within a dwell time of 2 seconds the creep response of the cell is measured by applying a small step in Z-height in contact. And by employing the standard linear solid model as the fit model to the step force with step response data, the elastic constants, the friction damping coefficients and the relaxation time are extrapolated to calculate the viscoelastic properties of the cell. Alternatively, using power-law rheology quantitative viscoelastic properties of live cells are measured, where the force clamp is introduced after the AFM tip approach to the cell of shorter dwell time and the power-law parameters (elastic modulus, power-law exponent from which viscosity is measured) are

calculated by fitting the power law equation to the indentation creep data (Hecht et al., 2015). Here, the step response technique is used to calculate the viscoelastic properties of fibroblasts that are even more appropriate with the easy method implementation and force curve analysis.

1.2 Fibroblasts and Dupuytren's Disease

1.2.1 Fibroblast and Myofibroblast cells

Every tissue and organ of the body is constituted with biomechanical and biochemical cushion provided by the connective tissue. Mostly, connective tissues are enriched with the primary mesenchymal cells called fibroblasts that produce, degrade and maintain the extracellular matrix (ECM). Non-contractile fibroblasts are spindle like shaped and more motile cells that are the central mediators in physiological tissue mechanics. Being part of many organs, fibroblasts show a distinctive morphology like cardiac fibroblasts present a normal flattened stellate shape in the heart (Porter and Turner, 2009). *In vitro* studies of fibroblasts were carried out on 2D and 3D gels in order to study their proliferation, migration and matrix degradation properties (Bott et al., 2010). To study fibroblast-matrix interactions, a fibroblast-induced collagen gel contraction assay was established (Bell et al., 1979). They interact and modulate the ECM components such as collagen, laminin, fibronectin through αβ integrin receptors. Contracting fibroblasts in fibrillar collagen matrices provide mechanical cues for macrophages to interact with them and thus coordinating tissue repair (Pakshir et al., 2019). Co-culturing of fibroblast-epithelial cells paves the way for the retaining of fibroblast metabolic activity (Walimbe et al., 2017) and also to study the epithelia-mesenchyme interactions (Omelchenko et al., 2001). Fibroblasts play a very important role in tissue homeostasis by tissue remodeling and in wound healing by differentiating into large cells named myofibroblasts (Tomasek et al., 2002). Generally, during the healing of an open wound or following tissue injury, the stress shielding effect in surrounding collagen matrix pulls the non-contractile fibroblast to the site. The dermal wound is lately filled by fibrin clot that stimulates fibroblasts invasion into the provisional matrix. Then the fibroblast produce one of the biochemical characteristics of myofibroblast such as ED-A fibronectin (ectodomain-A FN) and these migrating fibroblasts exert traction forces on the collagen matrix. This further stimulates fibroblasts to develop large stress fibres and also to produce more collagen. In this event, fibroblast has acquired a new phenotype named proto-

myofibroblast. Mostly this particular phenotype has been observed in petriplates when normal fibroblasts are seeded and they create stronger cell-cell junctions. Tensional forces and other cytokines especially transforming growth factor-β1 (TGF- β1) together stimulate proto-myofibroblast to show increased levels of myofibroblast biochemical cues-ED-A FN collagen, TGF- β1, and alpha-smooth muscle actin (α-sma). Thus, myofibroblasts, the differentiated fibroblasts, synthesize more α-sma and generate larger contractile forces. This force generation aids in the closure of the open wound and further tissue remodeling by shortening of the collagen matrix. The persistence of these myofibroblasts in the wound region leads to more ECM remodeling and thus results in connective tissue disorder (section 1.2.2). The stiffness map for the fibroblast to myofibroblast differentiation as a function of substrate stiffness is shown in figure 1.6.
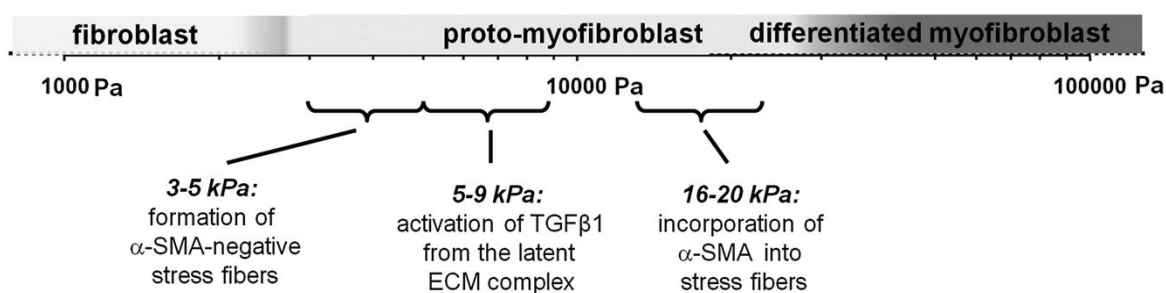
Figure 1.6 The stiffness map of the three fibroblast phenotypes. Young's modulus values determined using AFM explains the stiffness of fibroblasts at different phenotypes through formation of stress fibres and other biochemical promoters and activators (Hinz, 2010). Reproduced with permission and for licence visit (https://s100.copyright.com/AppDispatchServlet).

The overall mechanotransduction mechanism of myofibroblasts and the key biomolecular players involved in such force transduction mechanism are of huge interest to clinical researchers. Force generated within the myofibroblast by α-sma positive stress fibres are transmitted to their microenvironment through supermature focal adhesion (larger protein assemblies) containing integrins (αvβ3, α5β1, αvβ5) and other adaptor proteins such as paxillin, tensin, vinculin, talin 1 and FAK (focal adhesion kinase) (Hinz, 2010). TGF- β1 signalling plays an important role in fibroblast differentiation into myofibroblast and also in myofibroblast biochemical and biomechanical functions. TGF- β1 is released from protomyofibroblast/myofibroblast (autocrine production) and gets deposited in the ECM as latent inactivated form. Integrins from protomyofibroblasts bind to the latent TGF- β1 complex which is sitting in the remodelled stiffened matrix and integrin-intracellular actin mediated force exertion trigger the complex and release the activated TGF- β1. This further

binds and activates the intracellular pathways thus resulting in increased levels of α-sma, collagen and ED-A FN. Also, TGF- β1 helps in the recruitment of α-sma into the stress fibres of the myofibroblast. Active TGF- β1 induces other pathways such as Rho kinase and FAK that promotes myofibroblast mechanical contraction. TGF- β1 activated myofibroblasts also express OB-cadherin that reinforce stronger cell-cell adheren junction. They have mechanosensitive jucntions and gap junctions as other cell-cell junctions. Myofibroblasts coordinate such intercellular junctions mainly for force transmission and mechanosensitive ion channels activation.

1.2.2 Myofibroblast in connective tissue disorder

In tissue fibrosis, myofibroblast plays a huge role in connective tissue stiffening by continuous tissue remodelling and thus results in fibrotic environment. The pathogenic characteristic of pathogenic scarring and organ fibrosis is myofibroblast persistence. Most connective tissue disorders are skin, heart, lung, liver, kidney fibrosis where myofibroblast phenotypes are found in the histopathological specimens. Fibrosis can affect almost every tissue of the body and is a pathological characteristic of chronic inflammatory diseases (Baranyi et al., 2019). Bronchial asthma is one of such disease with key mechanisms of fibroblast to myofibroblast transition (FMT) followed by elevated ECM protein secretion and an increased number of myofibroblasts. The overview of this FMT and their source, function and pathology were schematically represented in figure 1.7. In most of the organ fibrosis, myofibroblasts produce excess ECM deposition and larger contractile force generation that results in tissue stiffening and thus totally modulating the tissue morphology. Interstitial lung disease (ILD) is a life threatening lung fibrosis happens due to the respiratory failure characterized by the progressive scarring of the lungs (Bongartz et al., 2010). Systemic sclerosis (SSc) and rheumatoid arthritis (RA) are the autoimmune rheumatic diseases caused by the organ fibrosis. Idiopathic pulmonary fibrosis (IPF) is the most common lung fibrotic disease and myofibroblasts in the fibrotic lung are derived through mesothelial-to-mesenchymal transition (MMT) which is nothing but epithelia-to-mesenchymal trasition (EMT) (Rock et al., 2011). Even in liver and kidney fibrosis, EMT plays a key role for myofibroblast histopathological appearance and activation (Grande et al., 2015; Li et al., 2013). In lung fibrosis, ECM stiffening can modulate fibroblast resistance to apoptosis and resulting in profibrotic and prosurvival genes upregulation (Sisson et al., 2015; Zhou et al.,

2013). TGF-β1 induces transdifferentiation of mesothelial cells, BM-derived fibrocytes, pericytes, mesenchymal stem cell (MSC)-like cells into fibrogenic myofibroblasts in many organ fibrosis. The abnormal depositions of ECM by myofibroblasts and fibroblast activation by fibrotic signalling molecules such as integrins are the main targets for developing new therapeutic drugs. CWHM 12 is a αv-integrin specific pharmacological blocking drug that reduces the liver and lung fibrosis (Fausther and Dranoff, 2014).
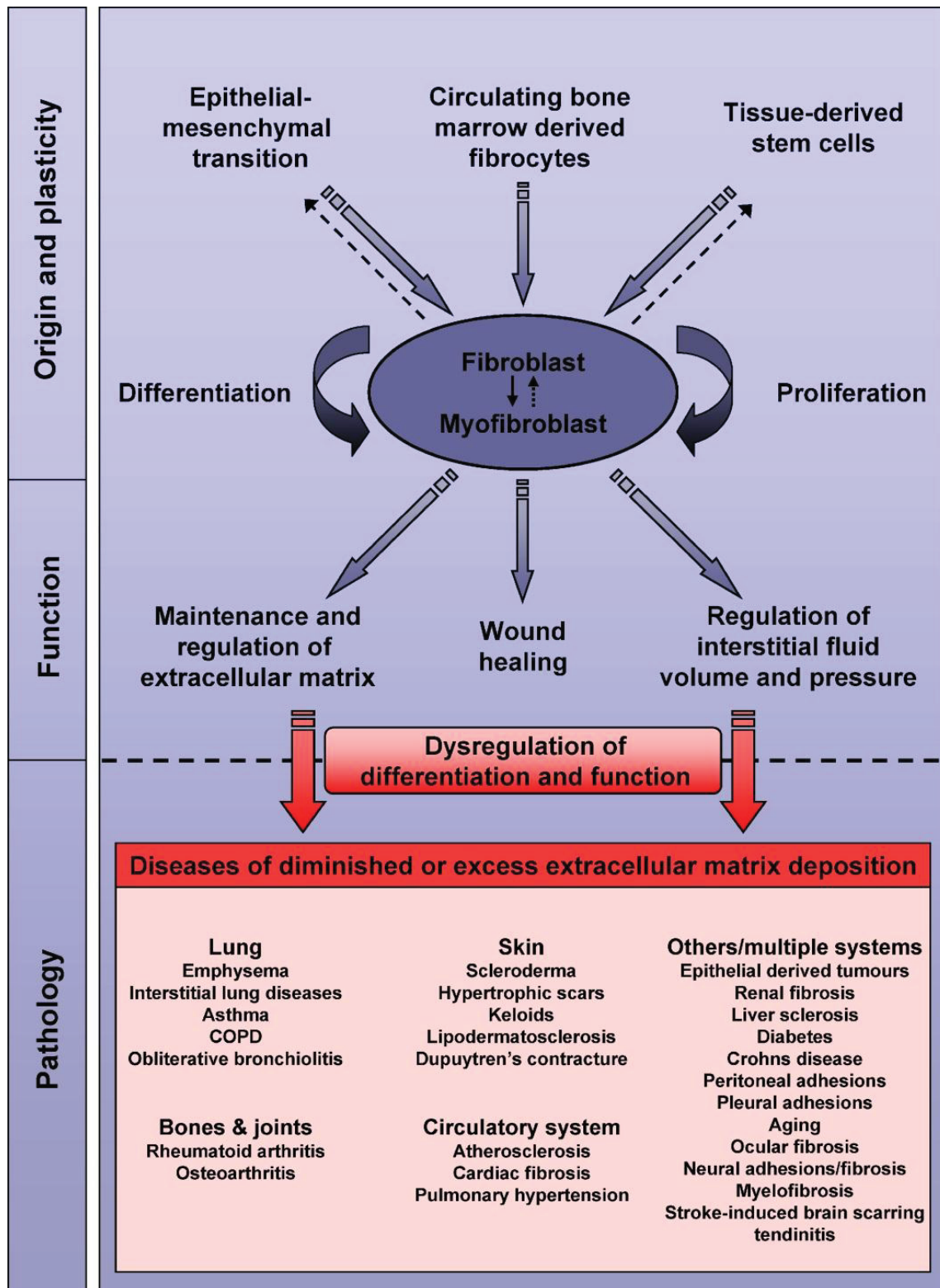
Figure 1.7 Normal and Pathological role of fibroblasts in various connective tissue disorders/organ fibrosis. This schematic diagram summarizes the origin and plasticity, functional role and pathology of fibroblasts to myofibroblasts differentiation (FMT). From the source of EMT, fibrocytes and tissue derived stem cells; these fibroblasts originate and play a functional role in a respective manner-ECM regulation, wound healing and regulation of interstitium. Dysregulated functionalities in FMT results in organ fibrosis that leads to severe diseases (McAnulty, 2007). Reproduced with permission and for licence visit (https://s100.copyright.com/AppDispatchServlet).

14

Myofibroblasts requires energy for the ECM synthesis and contraction, which it gained with high metabolic rates. ECM degradation and restoration of the biochemical and biomechanical properties of the ECM is the main characterization of the organ fibrosis resolution.

1.2.3 Dupuytren's disease

Dupuytren's Disease (DD) is a fibro-proliferative disorder of the palmar and digital fascia of the hand and fingers, which causes cords and nodules development later results in the contracture of the fingers. Contractile tension is the known contributing factor of Dupuytren's contracture. Dupuytren's diseased fibroblasts extracted from the cord and nodular region express α-sma and respond well to TGF-β1 stimulation, thus exhibiting a myofibroblast phenotype (Bisson et al., 2003). The mechanical environment in Dupuytren's disease's tissue is mainly altered by myofibroblasts that secrete, deposit and contract ECM. These further leads to changes in the production of matrix metalloproteinases (MMPs), produced by hyper-contractile myofibroblasts, that function in the ECM degradation and hence controlling matrix remodelling. Dupuytren's myofibroblast (DMF) achieve tensional homeostasis by applying higher contractile forces to their surroundings. The excessive ECM contractility by myofibroblasts are interpreted in two scenarios, either the myofibroblast impaired ability to sense its surrounding matrix stress or the biochemical or biomechanical signals received by myofibroblasts promotes the hyper-contractile action. Experimental evidence supports the latter and the hypothesis that the Dupuytren environment itself promotes the disease progression. In the similar fashion of myofibroblasts in other connective disorders, Dupuytren's myofibroblasts interacts with the ECM through integrin mediated attachment points, focal adhesions and intracellular α-sma recruited stress fibres. DMFs respond to biomechanical and biochemical signals from the ECM through these focal points and exert traction force through actomyosin contraction. Collagen I is the major collagen type found in cords and nodules (van Beuge et al., 2016). Dupuytren's disease mechanical environment determines the myofibroblast contractility and the associated MMP-mediated matrix remodeling (Verhoekx et al., 2013a). MMP inhibitor, ilomastat inhibited the development of contractile tension created by the DMFs extracted from the cords and nodules of the fascia (TOWNLEY et al., 2009). An *in vitro* study shows that DMFs in 3D collagen matrices exhibit three cell-cell junctions- adherens, mechanosensitive and gap junctions. Blocking of these

juncitons inhibited the contraction of the matrices and also downregulated the myofibroblast phenotype (Verhoekx et al., 2013b).

Mechanical properties of myofibroblasts activated by TGF-β1 are stiffer than normal fibroblasts that are not TGF-β1 treated. In chapter 3, the cell mechanics of three different fibroblast phenotypes extracted from the same Dupuytren's diseased patient are investigated using AFM nano-indentation experiments. The correlative α-sma stress fibres are observed by tagging them specific antibodies under fluorescence microscopy. Also, the substrate stiffness dependent cell stiffness is also seen for Dupuytren's myofibroblasts other than normal and scar fibroblasts.

1.3 ECM and decellularized matrices

A diverse mixture of macro-molecules such as proteins, glycoproteins and proteoglycans that are the secreted product of the cells, aggregate, assemble and form a structural scaffold called extracellular matrix (ECM). ECM serves a scaffold not only for cells but also for other cells associated growth factors representing as a source of bioactive cryptic peptides (Colorado et al., 2000; Houghton et al., 2006). The key biomolecular components of ECM are collagen, elastin, proteoglycans, glycoproteins and hyaluronic acid. Mostly collagen, proteoglycans and hyaluronic acid represents the structural components (Mouw et al., 2014). The non-cellular ECM components from different tissues provides the biochemical and biomechanical cues required for tissue development, morphogenesis, differentiation and homeostasis (Frantz et al., 2010).

Biosynthesis and assembly of the ECM molecules through enzyme and biochemical pathways enriched interactions brings the evolving cellular microenvironment. Normally, the biosynthesis and assembly of collagens (fig 1.8) involves various pathways from the intracellular and extracellular environment, respectively. At the initial step, the intracellular production of procollagen polypeptides are carried with the help of gene transcription and followed by post-translational modification. After the secretion of triple procollagen molecules to the microenvironment, the collagen crosslinking to form self-assembled collagen fibrils is carried out by lysyl oxidase. The number and proportions of the various crosslinks are highly dependent on the tissue specific types and also depends on other biochemical reactions such as glycosylation and hydroxylation of the amino acid residues of collagen. A

simple amino acid and biochemical reaction dependent initiated crosslinking step leads to differentiate the soft (lysine aldehyde crosslinkers) and stiff (hydroxylysine aldehyde crosslinkers) connective tissue. Non-fibrillar part of ECM include major proteoglycans and glycoproteins which are synthesized and secreted by the cells and are self-assembled or connected to the fibrillar ECM portion through expression of specific collagen binding domains. These domains containing proteins such as laminin and fibronectin also express cell specific protein, integrin binding domain as well. In such a way, these non-fibrillar ECM molecules promote ECM integrity and bring cell-ECM interactions. The architecture of ECM is a highly organized scaffold resulted from highly controlled self-assemblies and well interconnected chains of fibrillar and non-fibrillar ECM molecules. ECM is not only a collection of proteins, also holds unique role in tissue-specific functions including structural support and transmission of cellular forces.
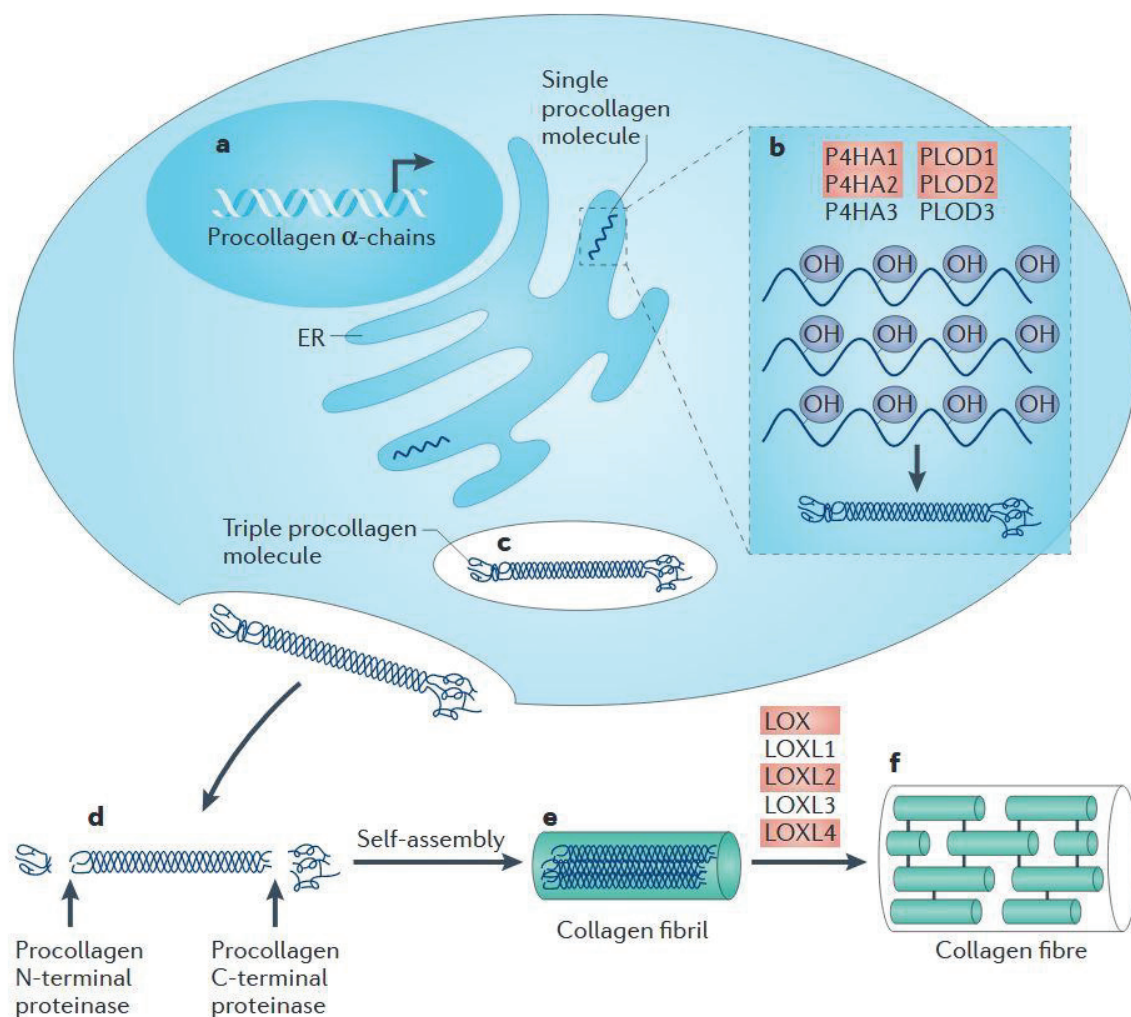
Figure 1.8 The cartoon representation depicts the biosynthesis of collagen and their assembly to form collagen bundles and also shows the cellular steps (biochemical pathway) that involves the ECM synthesis and assembly (Gilkes et al., 2014). Reproduced with permission and for licence visit (https://s100.copyright.com/AppDispatchServlet).

Generally, ECM scaffolds plays a crucial role in wound healing, tissue engineering and reconstruction. For these platforms, design and synthesis of biocompatible scaffolds provide the active components for cell-ECM and cell-cell interaction in any kind of tissue. Preparing such tissue specific scaffolds gives rise to the emerging trend of using decellularized matrices in the tissue engineering field. The functional role of such matrices intend to accompany the tissue repair processes by providing the utmost biomolecules and also performing as the natural scaffolds to the native cells.

"A novel and emerging strategy to fabricate matrices able to mimic the natural ECM is based on a process of decellularization of natural biological tissues. Removing cells from their tissue and slicing the remnant matrix with a cryostat, will provide a natural network that can be used for studying cell-ECM interactions in physiological conditions. In fact, once primary cells are removed, these matrices consist only of ECM components and resemble the natural surroundings of cells as *in vivo* contexts. Unlike 3D hydrogels, which mimic only few properties of ECM, decellularized tissue matrices provide a more variegated and natural ECM meshwork. Tissue decellularization can be performed through physical, chemical or enzymatic procedures. Physical procedures include mainly freezing/thawing processes, sonication and mechanical agitation. Trypsin and/or detergents (such as Triton X100 and sodium dodecyl sulfate - SDS) are mostly employed for enzymatic and chemical approaches, respectively.

Several types of tissues have been used for producing and characterizing several decellularization methods. For example, the mechanical properties of lung decellularized tissues have been studied recently with AFM (Jorba et al., 2017); in this work Jorba et al. used 0.1% Triton X100 and 1% SDS as an effective chemical decellularization process that maintained ECM structure, composition and mechanics. In order to obtain human decellularized dermal matrix, primary cells were removed using a freezing and thawing protocol and the surface topography of the matrix characterized using peak force tapping mode, implemented in a Bruker AFM Bioscope Resolve (Figure 4). Without any further treatment, these matrices can be directly used as cell culture scaffold, where cells can grow on top and within the matrix to form an artificial tissue. In some preliminary studies, biological response has been observed on decellularized tissues. For example, human fibroblasts were investigated on six different groups of decellularized matrices (prepared with enzymatic methods) in order to optimize a specific group of decellularized dermal matrix as an autologous skin graft (Łabuś et al., 2018). Decellularized matrices proved to play also a major

role as xenogenous dermal matrices for breast reconstruction and hernia repair (Mirastschijski et al., 2013). In this study, Mirastschijski et al. investigated the vertical proliferation, apoptosis and differentiation of fibroblast cells on human decellularized dermal matrix and matriderm (a commercially available matrix). In addition to decellularized matrices derived from human tissues, another interesting approach, recently reported, propose the use of decellularized plant leaves as a "green technology" in tissue engineering to fabricate scaffolds for biological applications. In this study, they prove that human mesenchymal stem cells and human pluripotent stem cell derived cardiomyocytes are able to adhere and maintain their functionality when seeded on these plant-based scaffolds (Gershlak et al., 2017).

Unlike synthetic or hybrid 2D and 3D systems, native ECM accurately present a wide number of signals and components that are fundamental for discerning intrigued mechanisms happening at the cell-matrix level. Recently, a comparative study on 2D monolayers, 3D spheroids and 3D native decellularized tissue models, showed that 3D decellularized models serve as a better platform to recapitulate the mechanical properties of human native dermal tissue and conduct biological experiments (Pillet et al., 2017).

Exploiting the possibility to preserve fundamental features of natural ECM, like composition, stiffness, ligand presentation and topography, decellularized matrices will potentially provide scientists and biomedical specialists with ideal platforms to gain deep insights in cellular functions. In particular, for elucidating processes of complex diseases, like cancer, employing these decellularized matrices could be an interesting approach that may help in understanding many critical processes, like mechanics, invasion and migration during metastasis formation. So far, only few applications have been reported in the field of cancer research. For example, engineered acellular tumor 3D scaffolds were developed to study the MCF-7 breast cancer cell proliferation and growth factor expression (Lü et al., 2014). In this study, they compared the repopulation of different cancer cells on acellular tumor matrix treated with Tris-Trypsin-Triton (both enzymatic and chemical procedures) and found an improved modeling of 3D tumor scaffold to perform cancer cell studies. Moreover, Hoshiba et al. showed an increase in chemo-resistance with tumor progression on decellularized matrices (Hoshiba and Tanaka, 2016). They also prepared the matrices from tumor tissues at different stages of malignancy and studied the 5-fluorouracil resistance among these matrices.

Therefore, in cancer and tissue fibrosis research, these decellularized 3D matrices could provide a realistic route that could bring much more information on cell behavior and functions, compared to studies on Petri-dishes or 2D monolayer. Exploiting their physiological properties, these matrices might potentially become an extraordinary model to

mimic natural microenvironment, emulating the *in vivo* context" (quoted content reprinted from Rianna et al., 2018).

1.4 AFM based Single cell force spectroscopy (SCFS)

Cells interact with their environment and neighbouring cells through their lipid, protein and saccharide constituted membrane. Within such biochemical and biomechanical membrane surface, many transmembrane proteins such as integrins and cadherins connect the extracellular side of the cell to the intracellular cytoplasmic side protein filaments. Every cell biological phenomena such as signalling, communication, adhesion and sensing occurs through such transmembrane proteins. In case of cell-cell adhesion, cadherins, of adherens junctions, from one cell interacts with their identical (homophilic) or not identical (heterophilic) partner in the neighbouring cells. These cadherins form dimers and multimers to enhance adhesion or the selectivity: homo-dimers or hetero-dimers. In the cellular adhesion mechanobiology, three important strategies have been followed by the cells to control its cell adhesion strength. (1) Availability of binding competent molecules in the membranes that are accessed by the binding partner molecules. (2) The strength of the bond formed by the partners in terms of measuring the unbinding force (pN) and the molecular bond potential. (3) The presence of the interacting adhesion molecules linked to the cell membrane and intracellular regions (anchoring). This relates to the interdependent strength of protein molecule clustering at the membrane and anchoring to the cytoskeleton by dimerization of many binding partners. Cell-cell adhesion studies were initially done with cell aggregation assay, where the ratio of single, double, triple and multi-aggregates are noted and quantified. With the technical advancement in AFM and other spectroscopies, a simple AFM based SCFS setup is used to measure the interaction forces between two cells arranged as a cell that can be attached to a AFM cantilever and cells that are grown on the substrate.

An AFM tipless cantilever-force sensor surface is functionalized with molecules such as concanavalin A, a lectin that binds to the sugar residues of the cell membrane. This functionalized cantilever is later used to pick up freshly detached trypsinized cells that initially adhere to the substrate, using controlled force, dwell time and pulling velocity. SCFS is a sensitive and quantitative method to measure the cell-cell adhesion molecule, cadherin mechanical bond unbinding/rupture forces. By varying the pulling rate of the cantilever, the binding strength of the bond can be studied.

In chapter 5, cell-cell interactions of fibroblast phenotypes extracted from the same Dupuytren's patient were studied using AFM based SCFS. Also, epithelial cells attached to a cantilever were used, making it possible to study interaction between epithelial cell and fibroblast, i.e. in a hetero-cellular arrangement. Immunofluorescence studies show the specific cadherin (N-, OB- and E-) expression at the cell-cell interaction sites of homo- and hetero-cellular cell cultures and also demonstrated cadherin homophilic and heterophilic interaction.

II Materials and Methods

Chapter 2

2 AFM- Young's modulus and rupture force measurement

2.1 Force-distance curve and Young's modulus measurement

A force-distance (F-D) curve is a force graph represented by the AFM cantilever deflection versus the distance between the AFM tip and the sample surface. To start with the practical notation, basically the AFM tip is approached in Z-/vertical direction towards the sample surface with the help of Z-piezoelectric transducer until the tip makes the initial contact with the sample, which is denoted as contact point (z_0) and further movement of the tip into the sample and following deformation is denoted as indentation (δ). Before making the initial contact, the AFM tip travel range without any deflection will be denoted as deflection offset (d_0). After the tip-sample interaction, the tip is withdrawn from the sample and shows unspecific interaction force in F-D curve, which is due to van der Waals forces (in water) and capillary forces (in air). One can visualize these parameters in the F-D graph (approach curve shown in figure 2.1).
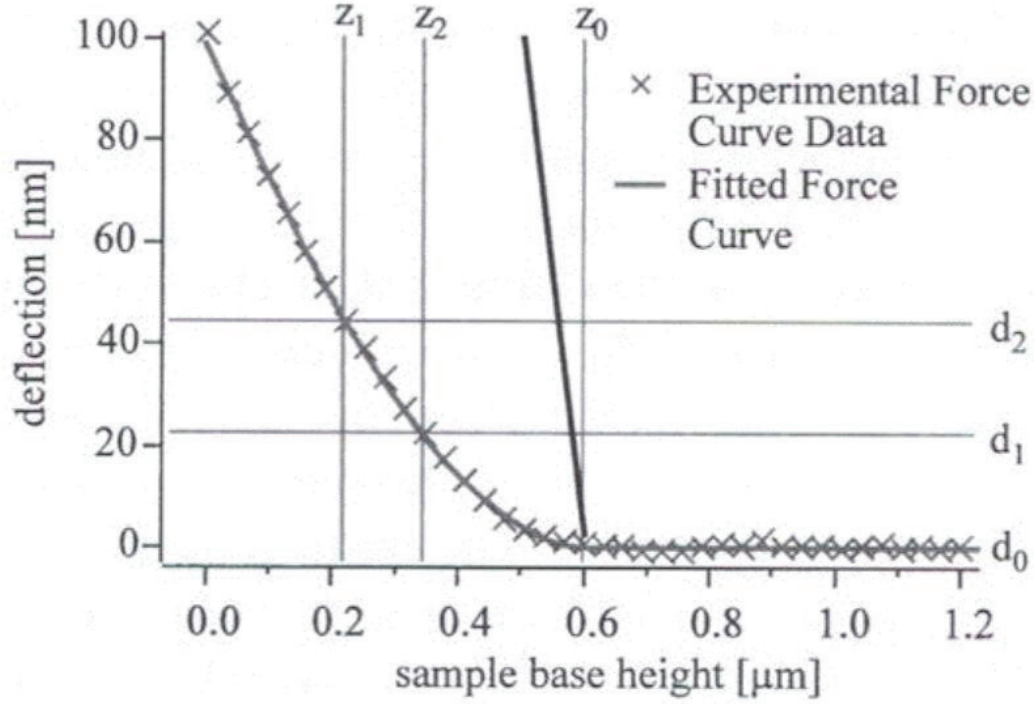
Figure 2.1 Example of the force curve with certain parameters. The deflection (nm) *versus* sample base height (μm) shows the approach curve with the deflection offset (d_0), contact point (z_0) and the indentation (δ) measured as compared to the stiff curve (*vertical thick line*). By fitting the approach curve (from retract curve possible if there is no viscous contribution of the sample) with Hertz model, Young's modulus value is calculated. Reproduced with the permission from the author (Radmacher, 2002).

Initially, the F-D curve will be shown as deflection-displacement curve because the deflection of the AFM cantilever and displacement of the Z-piezoelectric transducer both with respect to time are measured and later converted to the F-D curve and analyzed for sample elastic modulus measurement with the following equations and derivations.

For respective loading force (F) exerted by the cantilever onto the sample, Hooke's law can be applied for cantilever springs that are linear springs for small deflections which is as follows:

$$F = k_c. \, d \qquad (2.1)$$

Where k_c is the force constant of the cantilever and d is the cantilever deflection. Now the other influential parameters such as contact point (z_0) pointed in figure 2.3, deflection offset (d_0) which will be subtracted from deflection (d) and indentation (δ) which is the difference between the sample base height and cantilever deflection, are derived and substituted to the equation 1.1.

$$\delta = z - d \qquad (2.2)$$

The offsets are substituted and equation 2.2 is rewritten as,

$$\delta = (z - z_0) - (d - d_0) \qquad (2.3)$$

$$d = z - z_0 - \delta + d_0 \qquad (2.4)$$

Then finally equation 2.1 becomes,

$$F = k_c . (z - z_0 - \delta + d_0) \qquad (2.5)$$

For estimating the Young's modulus of the biological sample, an appropriate model such as Hertzian model is fitted to the F-D curve and is as follows,

$$F_{pyramidal} = \frac{1}{\sqrt{2}} * \frac{E}{1-v^2} * tan(\alpha) * \delta^2 \qquad (2.6)$$

$F_{pyramidal}$ is the force required to indent the given sample with the given three-sided pyramidal AFM tip. Here, E is the elastic or Young's modulus, v is the Poisson ratio and α is the half-opening angle of the pyramid.

To combine equations (2.5) and (2.6) in the case of pyramidal indenter to obtain,

$$k_c . (z - z_0 - \delta + d_0) = \frac{1}{\sqrt{2}} * \frac{E}{1-v^2} * tan(\alpha) * \delta^2 \qquad (2.7)$$

and rearranging the parameters to obtain E,

$$E = \frac{k_c.(z - z_0 - \delta + d_0)}{tan(\alpha) * \delta^2} * (1 - v^2) * \sqrt{2} \qquad (2.8)$$

Thus the Young's modulus of the sample is determined from AFM nano-indentation experiments. Here most of the parameters in equation (2.8) either are known or can be measured from the experiments. A standard procedure for doing AFM nano-indentation experiments is as follows,

1. Spring constant of the cantilever determination and calibration by recording thermals both in air and water.
2. Taking a F-D curve on a stiff sample and determining the deflection sensitivity of the instrument through setting the slope of the attract or retract curve.

Then proceed with AFM force mapping experiments. In all the AFM experiments, both E and z_0 are used as fit parameters for fitting F-D curve using equation (2.8) to calculate Young's modulus. The soft cantilevers of spring constant 10 pN/nm which possess low resonance

frequency are used for all AFM experiments to estimate cell and ECM elastic properties. The spring constant is determined by measuring the amplitude of the cantilever random motion driven by the Brownian motion of the surrounding medium. From the Boltzmann's equipartition theorem, each degree of freedom of any system possess an average energy of

$$<E> = 0.5 \; k_B. \; T \qquad\qquad (2.9)$$

where k_B is the Boltzmann's constant and T is the absolute temperature. Assuming the cantilever undergoes bending vibrations at its resonance frequency, the force constant from the fluctuations in AFM cantilever position can be estimated as follows,

$$<E> = 0.5 \; k_c. \; <d^2> \qquad\qquad (2.10)$$

where $<d^2>$ is the mean square displacement of the cantilever. The spring constant can be calculated from the below equation by combining equations (2.9) and (2.10),

$$k_c = k_B. \; T/<d^2> \qquad\qquad (2.11)$$

As the AFM detects all cantilever bending modes (higher harmonics) and has been seen in the thermal graphs, this leads to underestimation of spring constant. Thus to obtain more accurate spring constant value, the resonance frequency peak from the power spectral density of the deflection signal as a function of frequency was fitted using a model function and the spring constant is calculated. With the optical lever sensitivity (OLS) technique, deflection sensitivity in nm/V is measured after adjusting the position of the photodiode, in order to relate the reflected laser spot displacement to the cantilever deflection, from obtaining a F-D curve on a stiff surface (petriplate with medium or glass with a droplet) and putting the slope of the fitting equal to one. The deflection sensitivity is nothing but the conversion factor between the deflection in metres and the deflection in volts (Cappella, 2016). After these two critical calibrations-cantilever spring constant and deflection sensitivity, the mechanical properties such as Young's modulus of the biological samples are measured.

2.2 cadherin-cadherin bonds rupture force measurement-SCFS

Cell adhesion receptors like cadherins plays a crucial role in cell-cell adhesion processes and also plays an important role in cell signalling pathways by sensing and transducing signals from the neighbouring cellular environment. Various cell adhesion assays have been

employed to measure the cell-cell interaction force mediated by the cadherin-cadherin mechanical bond. Among many quantitative assays, AFM-SCFS is particularly useful to measure the cell-cell interaction at the single molecule resolution. This technique works on large range of applicable forces and provide high force resolution and good control of contact conditions. The following procedure describes the steps taken from cell capture to the SCFS data analysis for the cell-cell interaction study.

(1) AFM tipless cantilever functionalization. The tipless cantilever was cleaned in Helizyme and SDS for 2 hours. Then the cantilever was incubated for 1 hour and washed thrice with Milli-Q water. Then the cantilever was cleaned with plasma cleaner for 3 minutes. Plasma treated cantilevers were treated with concanavalin A (con A) and incubated for 1 hour at room temperature. This step allows the functionalization of the cantilever with con A. Con A is a lectin which specifically binds to mannose residues present in the cell membrane constituents. Then the con A functionalized cantilevers were stored up to 1 week at 4 ^{o}C with BSA-PBS solution.

(2) cell culture and immobilization to the AFM cantilever. The functionalized cantilever which is used to pick up cell, was recorded with thermals and F-D graph for the determination of spring constant and deflection sensitivity, respectively. At 1 hour before SCFS experiments, the cells in the tissue flask was washed with PBS and incubated with trypsin-EDTA for 2 min in the 37 ^{o}C incubator. At room temperature, the cells were span down by centrifugation at 1300 rpm for 3 min. The supernatant was removed carefully and the cells were resuspended in medium and gently pipetted up and down to end up with individual cell. Then these cells were introduced to the petridish containing cell monolayer grown for 2 days. This setup was kept at 37 ^{o}C incubator for 2 min before taking it to the SCFS setup.

(3) cadherin mechanical bond rupture force measurement

In a typical AFM-SCFS experiment, the living cell is captured at the tip of the con A functionalized cantilever and the recorded force-distance (F-D) curve represented by the AFM cantilever deflection versus the distance between the AFM tip and the sample surface is shown in Fig. 2.2. During this step, the cantilever position was corrected in such a way that the cell attach to the apex of the cantilever. For cell attachment, the suitable parameters were contact force of 3 nN, a contact time of 3 sec and the approach and retract velocity of 3 μm sec^{-1}. After the cell pickup, the cantilever was retracted from the cell monolayer a few μms away manually. Now the whole setup was left undisturbed for 10 min. During this recovery

time, the cell enables firm attachment to the cantilever surface. To confirm the firm attachment of cell to the cantilever, gently move the setup and observe the cell movement. If there is no such movement, proceed to the next step of measuring cell-cell adhesion force SCFS experiment.
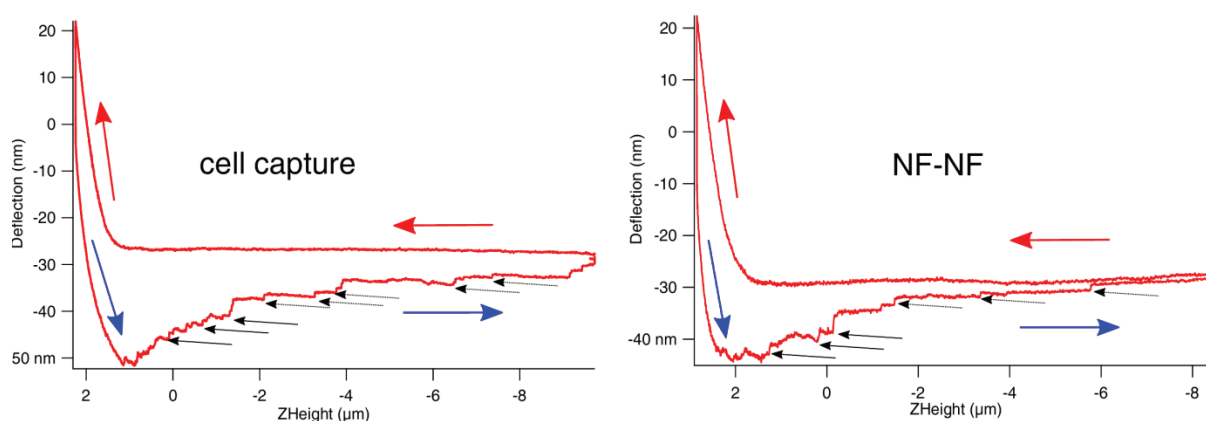

Figure 2.2 F-D curve of picking up a cell and of cell-cell interaction. Force curve recorded during cell pick up was shown and retract curve (blue arrow) contains jumps (continuous line black arrow) and tether (discontinuous line black arrow) events. 4- After a recovery time of 10 min, the interaction between cell attached to the cantilever and cell grown as monolayer was conducted. Cell-cell interaction force curve shows jump/rupture events that corresponded to the extracellular cadherin-cadherin bond breakage. Here, multiple rupture events were recorded.

The entire SCFS experimental procedure followed to measure cadherin mediated cell-cell interaction force is briefly explained in Chapter 5, section 5.6. Now the cell attached cantilever was approached towards a cell in the monolayer and with suitable parameters- 1 nN contact force, 2 sec contact time and 3 μm sec^{-1} approach and retract velocity, a F-D curves were recorded (Fig. 2.2). At different approach and retract velocities (3, 5, 7.5 and 10 μm sec^{-1}) cell-cell interaction force is measured to estimate the binding strength of cadherins at varying mechanical load.

(4) data analysis

The F-D curves usually show characteristic force patterns in the retract curve. Initially the force curves are corrected for baseline offset and tilt correction steps (Fig. 2.3). F-D retract curves contains two discrete force events- jumps/rupture (continuous line black arrow in Fig 2.2) and tethers (discontinuous line black arrow in Fig 2.2). These two force events are distinguished by the preceding force plateau corresponds to rupture events and followed by the tether events.
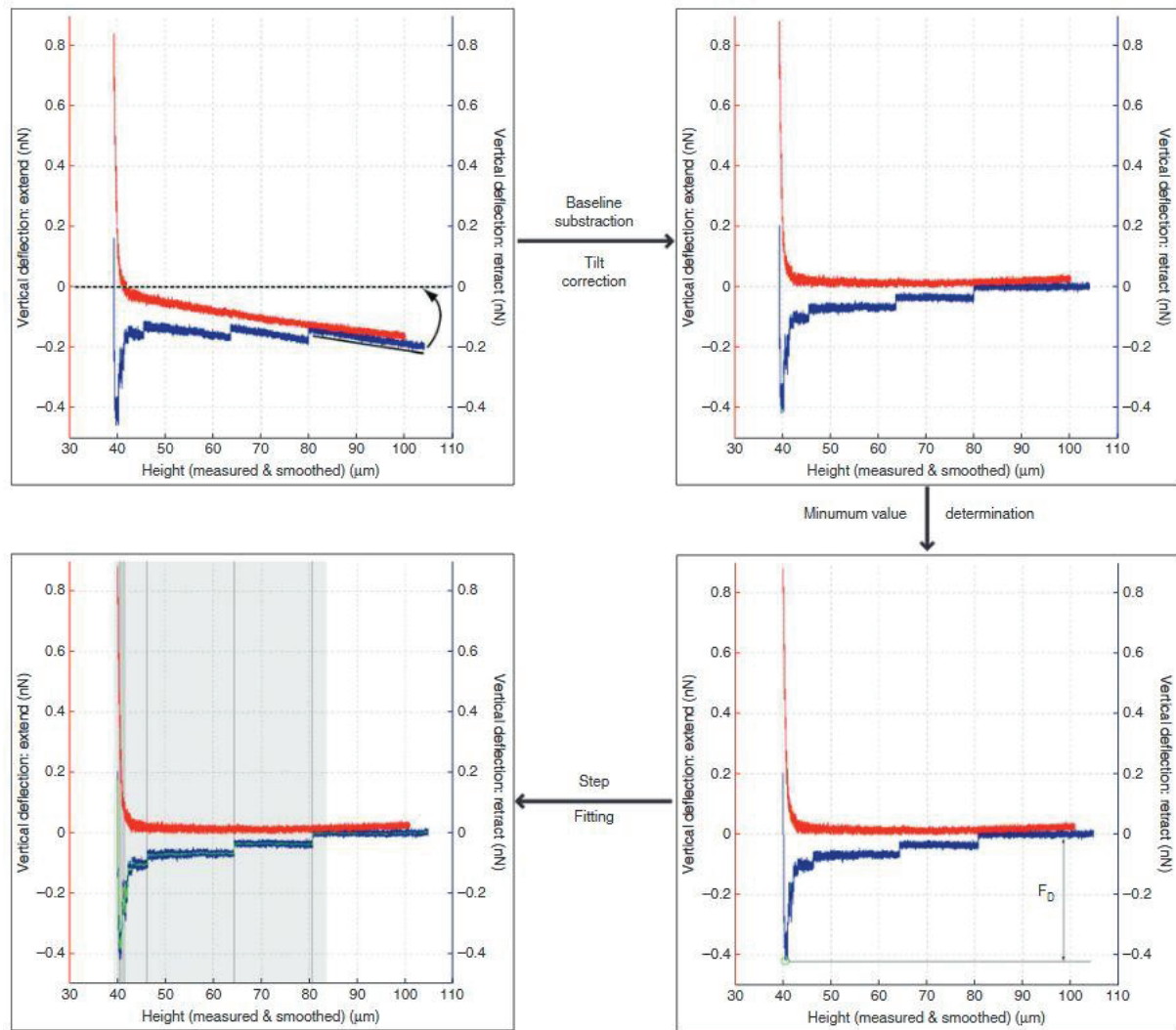
Figure 2.3 Data analysis procedure that involves important steps such as 1) Baseline subtraction and tilt correction, 2) Minimum value determination (rupture force measurement) and 3) detachment force calculation. The analysis has been performed in the grey shaded area for last two steps (Friedrichs et al., 2010). Reproduced with permission and for licence visit (https://s100.copyright.com/AppDispatchServlet#formTop).

In cell-cell adhesion SCFS experiments, the rupture event corresponds to the rupture of cadherin-cadherin mechanical bonds; whereas the tether events corresponds to the rupture of the membrane nanotubes which holds the unbound cadherin molecule that are supposed to be interconnected to the intracellular actin cytoskeleton. When the cadherin-cadherin bond breaks, the rupture events look staircase-like patterns. The rupture force is calculated by multiplying the cantilever spring constant and the decreasing deflection of the individual rupture events. Then the histogram is generated which gather all the rupture force and finds out the maximum rupture force of the cadherin mechanical bonds. To ensure the rupture events corresponds to cadherin bond unbinding, calcium depletion have been assigned as control experiments where the rupture events gets decreased.

III   Results and Discussions

Chapter 3

This is a verbatim copy of an article that has been published in a peer reviewed journal: Viji Babu, P.K., Rianna, C., Belge, G., Mirastschijski, U. and Radmacher, M., 2018. Mechanical and migratory properties of normal, scar, and Dupuytren's fibroblasts. *Journal of Molecular Recognition*, *31*(9), p.e2719.

Fibroblast and Myofibroblast viscoelastic properties

Prem Kumar Viji Babu[1,4], Carmela Rianna[1], Gazanfer Belge[2],   Ursula Mirastschijski[3], Manfred Radmacher[1,4]

[1]Institute of Biophysics, University of Bremen, Bremen, Germany

[2]Faculty of Biology and Chemistry, University of Bremen, Bremen, Germany

[3]Wound Repair Unit, Centre for Biomolecular Interactions Bremen, University of Bremen, Bremen, Germany

[4]Authors to whom any correspondence should be addressed.

3.1 Abstract

Mechanical properties of myofibroblasts play a key role in Dupuytren's disease. Here, we used atomic force microscopy (AFM) to measure the viscoelastic properties of three different types of human primary fibroblasts derived from a same patient: normal and scar dermal fibroblasts and palmar fascial fibroblasts from Dupuytren's nodules. Different stiffness hydrogels (soft ~1 kPa and stiff ~50 kPa) were used as cell culture matrix to mimic the mechanical properties of the natural tissues, and AFM step response force curves were employed to discriminate between elastic and viscous properties of cells. Since transforming

growth factor-β1 (TGF-β1) is known to induce expression of α-Smooth Muscle Actin (α-SMA) positive stress fibres in myofibroblasts, we investigated the behavior of these fibroblasts before and after applying TGF-β1. Finally we performed an *in vitro* cell motility test, the *wound healing or scratch assay,* to evaluate the migratory properties of these fibroblasts. We found that i) Dupuytren's fibroblasts are stiffer than normal and scar fibroblasts, the elastic modulus E ranging from 4.4, 2.1 to 1.8 kPa, for Dupuytren, normal and scar fibroblasts, respectively; ii) TGF-β1 enhances the level of α-SMA expression and thus cell stiffness in Dupuytren's fibroblasts (E ~ 6.2 kPa); iii) matrix stiffness influences cell mechanical properties most prominently in Dupuytren's fibroblasts iv) Dupuytren fibroblasts migrate slower than the other fibroblasts by a factor of 3. Taking together, our results showed that mechanical and migratory properties of fibroblasts might help to discriminate between different pathological conditions, helping to identify and recognize specific cell phenotypes.

3.2 Introduction

Dupuytren's disease is a fibromatosis of the connective tissue of the palm that can lead in certain cases to the immobility of one or more fingers due to formation of nodules and cords in the palmar fascia (Schleip et al., 2005; van Beuge et al., 2016). Connective tissue represents the architectural and supportive framework of many tissue and organs in animal body and it is mainly composed by fibroblasts. In the palmar fascia of patients with Dupuytren's disease, there is an increase of the type-III collagen to type-I collagen ratio in the ECM (Brickley-Parsons et al., 1981) and an increase of the myofibroblast population in the Dupuytren's nodule (Rudolph and Vande Berg, 1991).

Fibroblasts constitute the predominant cell type in connective tissues. They secrete and deposit extra-cellular matrix (ECM) components to establish a scaffold for neighbouring cells. In wound healing, fibroblast migration and their transdifferentiation into α-SMA expressing myofibroblasts results in the exertion of mechanical stress on the ECM and thus contributes to tissue remodeling (Jemec et al., 2000). The transition from fibroblasts into myofibroblasts depends on the activation of the latent transforming growth factor-β1 (TGF-β1) that is deposited in the ECM via binding to decorin and the TGF-β latency associated complex (Kloen et al., 1995; Wipff et al., 2007). TGF-β1 is a multifunctional protein that increases the expression of α-SMA (Desmoulière et al., 1993) in concert with the fibronectin ectodomain-A (ED-A FN) (Serini et al., 1998) and α-SMA enhances the contractile activity of myofibroblast. The increased contractility of myofibroblasts leads to stiffening of the ECM.

In addition, during the process of wound healing, migrating fibroblasts create mechanical stress on the ECM matrix by adopting a myofibroblast phenotype in order to generate stress fibre formation and secretion of additonal ECM molecule (collagen) (Tomasek et al., 2002). Numerous studies support the idea that myofibroblasts are a key cell responsible for the tissue contraction in Dupuytren's disease. In vitro models have been developed to study the underlying cellular basis of myofibroblast differentiation and contraction. Several studies suggest that the growth factor TGF-β1 combined with mechanical stress can promote the differentiation of fibroblasts into myofibroblasts (Desmoulière et al., 1993; Orlandi et al., 1994). However, there are no studies reporting the comparison of mechanical properties of fibroblasts extracted from different sites of the same patient affected by Dupuytren's disease.

Atomic Force Microscopy (AFM) can be used to study cell stiffness (Radmacher, 1997; Radmacher et al., 1996), cell-cell interaction (Beckmann et al., 2013; Friedrichs et al., 2007b; Lehenkari and Horton, 1999) and cell-ECM interactions (Friedrichs et al., 2013; Taubenberger et al., 2013). Measuring cell stiffness by micro-indentation using AFM yields information about many biological processes, like migration (Kole et al., 2004), cytoskeletal structure (Rotsch and Radmacher, 2000), myosin activity, as well as pathological conditions, in which the alteration in cell mechanical properties allows the discrimination between normal and diseased cells (Dulińska et al., 2006; Guedes et al., 2016; Carmela Rianna and Radmacher, 2017; Rianna and Radmacher, 2016; Stolz et al., 2009).
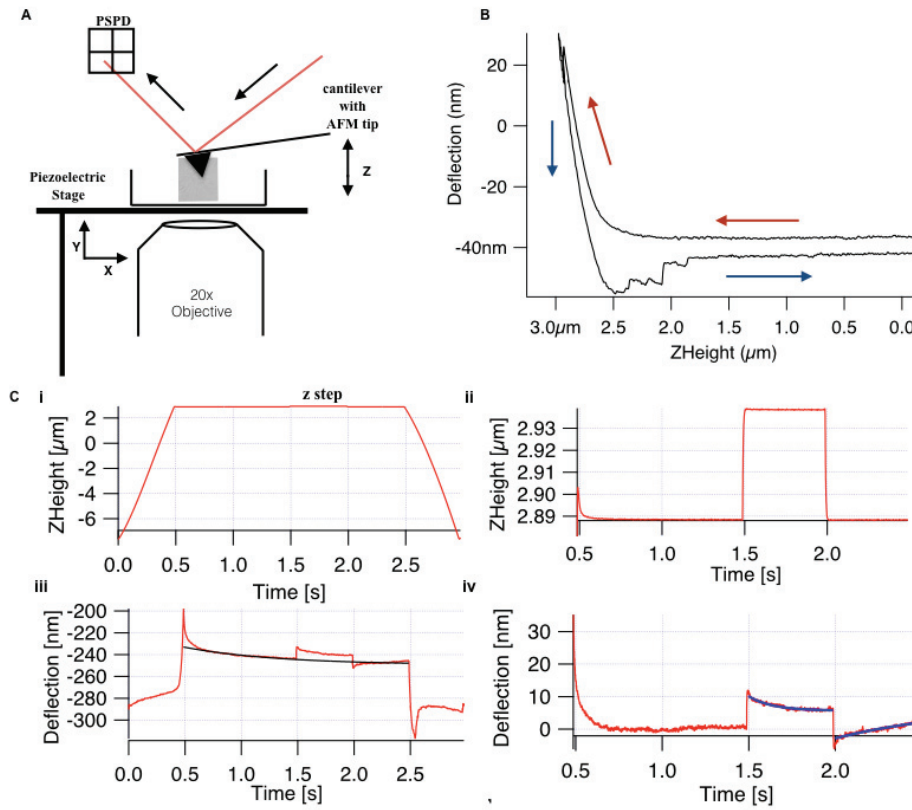
Figure 3.1 Basic components of AFM (A) and force curve (B) with viscoelastic creep response measurement (C), **(A)** The basic four components of AFM- i) a laser diode, ii) a cantilever of 0.01 N/m spring constant with 30 nm radius AFM pyramidal tip, iii) a position sensitive photo detector (PSPD) and iv) *xyz*- piezo stage. (B) Sample indentation by the AFM tip obtains the force curve which gives the approach (red arrow) and retract (blue arrow) curve on Deflection *vs* Z-Height graph and apparent Young's modulus was calculated by applying Hertz model to the approach curve. In creep response curve (C), the Z-Height profile (i) shows the approach and retract ramp towards the cell for 3 seconds and in-between there is a z step which is applied at t=1.5 which is enlarged in (ii). (iii) The deflection data shows global creep of the cell which includes the creep after loading and unloading step which is enlarged in (iv) and global creep was determined by the exponential fit (black curve) and was subtracted for qualitative analysis.

Here, by using AFM, we measured the viscoelastic properties of three types of fibroblasts: normal, scar and Dupuytren's fibroblasts, extracted from the same patient. Specifically, employing AFM step response force curves and analysing the data using the standard linear solid model, we could compare viscous and elastic properties of the cells. In this experimental scheme, after the step, the force (being proportional to the deflection) and the sample indentation (calculated as z height minus deflection) will relax to a new equilibrium situation. Thus, our experimental scheme is neither equivalent to a strain relaxation experiment, where stress is kept constant, nor a stress relaxation experiment, where strain is kept constant. Technically, we could apply a step in force, which would require an additional feedback to employ, which will reduce the time resolution of our setup (Yango et al., 2016). Moreover, we

studied the effect of TGF-β1 on the mechanical properties of the three fibroblasts, as well as on their cytoskeleton organization acquiring fluorescent images of cells where α-SMA has been stained. Since viscoelastic properties of cells strongly depend on substrate stiffness (Solon et al., 2007), we used polyacrylamide (PA) gel with different stiffness values as cell culture supports, namely soft (~1 kPa) and stiff (~50 kPa) gels to further investigate the response of cells to different mechanical signals. Finally, to gain insights in the migratory properties of these fibroblasts and to emulate the conditions of wound healing, we performed a migratory test, so called *wound healing or scratch assay*. We could find differences in mechanical properties of the different fibroblasts. Specifically, Dupuytren's fibroblasts were stiffer than the others and their mechanical properties and cytoskeleton organization were mainly influenced from TGF-β1, as well as from different stiffness of underlying materials. Concerning motility features, α-SMA expressing Dupuytren myofibroblasts were slower than the other fibroblasts investigated in this study.

3.3 Results

The microenvironment of every cell is composed of chemical and physical components which play a key role in influencing and determining cell fate and functions. Releasing specific components, cells modify the extracellular matrix (ECM) and, *vice versa*, ECM influences cell processes in a dynamic interplay. In order to mimic certain properties of natural cellular environments, like mechanical properties, we provided cells with specific mechanical cues by employing synthetic gels as cell culture supports. Specifically, we prepared polyacrylamide (PA) gels with two different stiffness values: a soft (E ~1 kPa) and a stiff gel (E ~50 kPa). We measured the different stiffness values of the respective gels by AFM, recording force maps of 6 x 6 force curves within a 1 μm area on the cell body. Force curves (figure 3.2A & B) show the separation between approach and retract curves, which indicates that the viscosity is larger in stiff gels compared to soft gels. The difference between stiff and soft gels can be seen also in the graph showing force versus indentation in Supplementary figure 3.7. Moreover, with the step response experiment, the median values of apparent Young's modulus and elastic modulus were obtained and listed in supplementary table 3.5. The apparent Young's modulus was calculated by using Hertz model on the approach curve of the force curve, which does not include the contribution of viscosity of the sample. Whereas, the elastic modulus was calculated from step response data by using the standard linear model which also yields the dynamic viscosity of the sample. The difference in the apparent Young's modulus and elastic modulus values is due to negligence of sample viscosity in the simple

analysis using the Hertz model, whereas the standard linear model includes the viscous effect of the sample and thus gives the true elastic modulus value of the sample.
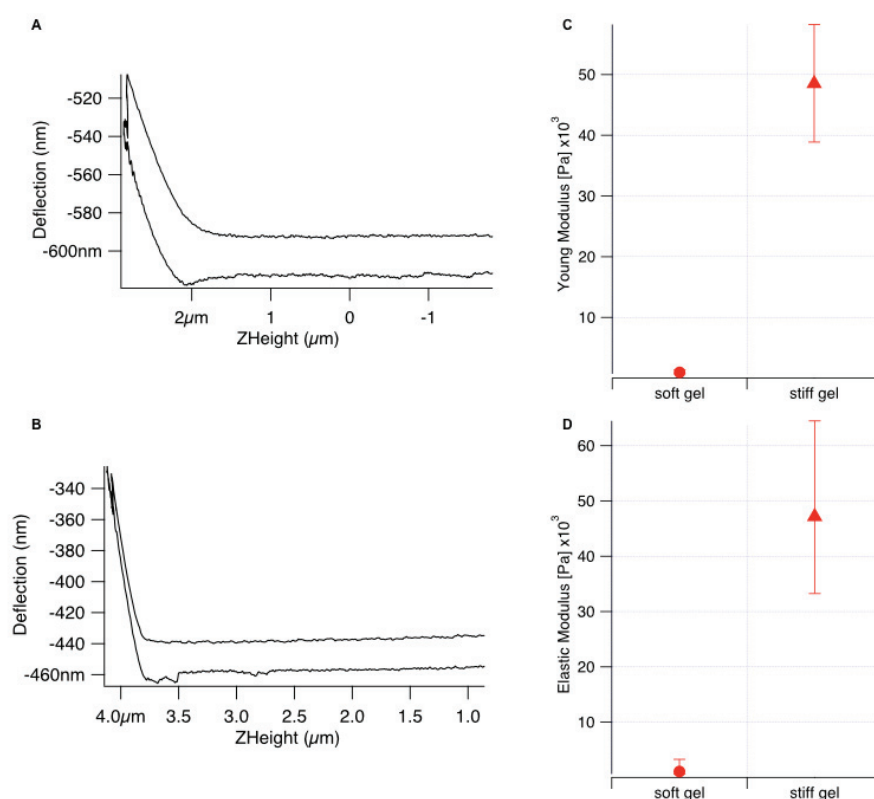
Figure 3.2 Force curve from soft (A) and stiff gel (B) and comparison of apparent Young's modulus (C) and elastic modulus (D), The force curves are obtained on soft and stiff gel shows the separation of approach and retract curve which is due to viscous contribution, is larger in soft gel than in stiff gel force curve. Due to which, there is a change in apparent Young's modulus and elastic modulus values. The error bars of first and third quartiles are shown in Supplementary Table 3.5.

The mechanical properties of cells can often be related to their physiological or pathological state. In fact, cell mechanics has been previously used to discriminate between many healthy and diseased cells, like in the case of cancer, blood and cardiovascular diseases (Dulińska et al., 2006; Guedes et al., 2016; Rianna and Radmacher, 2016; Stolz et al., 2009). In this study, we used AFM to study mechanical properties of normal, scar and Dupuytren's fibroblasts (from the same patient) in order to investigate whether Dupuytren's fibroblasts could show a different mechanical phenotype compared to the other cell types. Moreover, we investigated the effect of TGF-β1 (5 ng/mL) on stress fibre formation in fibroblasts, hence in their stiffness. With this aim, we took 30 μm scan size force maps of 128 x 2 step response force curves over the nuclear, cell body and periphery region of a cell and we could measure median values of elastic modulus of 2.1, 1.8 and 4.4 kPa for normal, scar and Dupuytren's

fibroblasts, respectively (figure 3.3A, filled circles).
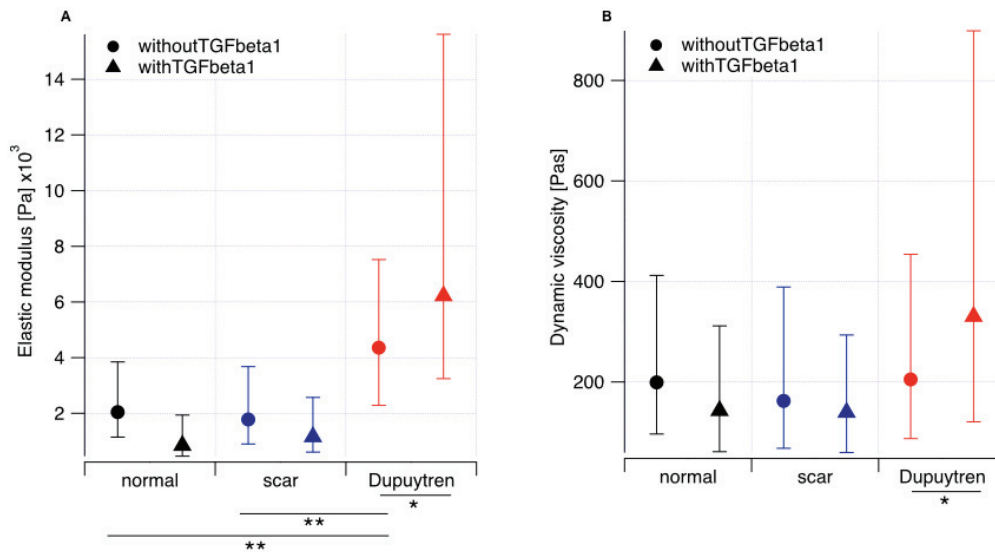
Figure 3.3 Elastic modulus (A) and dynamic viscosity (B) of fibroblasts with and without TGFβ1. The elastic modulus and dynamic viscosity graph for normal, scar and Dupuytren's fibroblasts seeded on petridish in the presence (*filled circle*) and absence (*filled triangle*) of TGFβ1 clearly show that the Dupuytren's fibroblasts are stiffer and more viscous than the other fibroblasts in the presence of TGFβ1. For each category, maximum 29 number of cells were studied. The error bars of first and third quartiles are shown in Table 3.1 & 3.2.

Our results showed that Dupuytren's fibroblasts were much stiffer than the other two cell types, in both conditions, with and without TGF-β1 (figure 3.3A, filled circles and triangles, respectively and Supplementary figure 3.8A & B). Results are shown in figure 3.3 and the respective values of the elastic modulus and the dynamic viscosity are listed in Table 3.1 and Table 3.2. Moreover, we found that Dupuytren's fibroblasts increased their elastic modulus and becomes stiffer (Supplementary figure 3.8C) in presence of TGF-β1 (from 4.4 to 6.2 kPa), whereas we did not find significant changes in the elastic moduli of scar and normal fibroblasts, before and after addition of TGF-β1. In order to check whether cytoskeleton organization could have an influence on the mechanical properties of fibroblasts, we then acquired fluorescent images of the three cell types, staining α-SMA stress fibres.

Table 3.1: The median (bold values) elastic modulus values of normal, scar and Dupuytren's fibroblasts treated with and without TGF-β1

Elastic modulus (kPa)	without TGF- β1			with TGF- β1		
	25th	median	75th	25th	median	75th
Normal	0.8	**2**	1.8	0.3	**0.8**	1.0
Scar	0.8	**1.8**	1.9	0.3	**1.1**	1.4
Dupuytren	2.1	**4.4**	3.2	2.9	**6.2**	9.3

We found large differences in structure and organization of the cytoskeleton network in Dupuytren's fibroblasts compared to the other cells. In fact, Dupuytren's fibroblasts were characterized by a wide number of thick and well organized stress fibres (Supplementary figure 3.9 left row) and bundles of stress fibres were even thicker in presence of TGF-β1 (Supplementary figure 3.9 right row). In normal and scar fibroblast instead, cytoskeleton

Table 3.2: The median (bold values) dynamic viscosity values of normal, scar and Dupuytren's fibroblasts treated with and without TGF-β1

Dynamic viscosity (Pas)	without TGF- β1			with TGF- β1		
	25th	median	75th	25th	median	75th
Normal	102.8	**199**	212.9	81.7	**142.8**	168.6
Scar	94.3	**162.3**	226.7	79.8	**139.2**	154
Dupuytren	117.8	**204.8**	248.8	209.8	**330.3**	568.3

network did not undergo dramatic changes in presence of TGF-β1. Therefore, we found that variations in cytoskeleton structure, and specifically in α-SMA fibres number and conformation, could be related to an increase in elastic moduli in Dupuytren's fibroblasts. Additionally, we investigated the viscous properties of fibroblasts by performing step response force curves and we found that Dupuytren's fibroblasts are also affected from TGF-β1 as they become more viscous (from 204 to 330 Pas) after application of TGF-β1 (figure 3.3B). Therefore, from this first set of experiments we could find that viscoelastic properties of Dupuytren's fibroblasts increase in presence of TGF-β1, while instead the other two types of fibroblasts are less affected. Moreover, we could associate the increase of Dupuytren's fibroblast stiffness to the presence of α-SMA stress fibres.
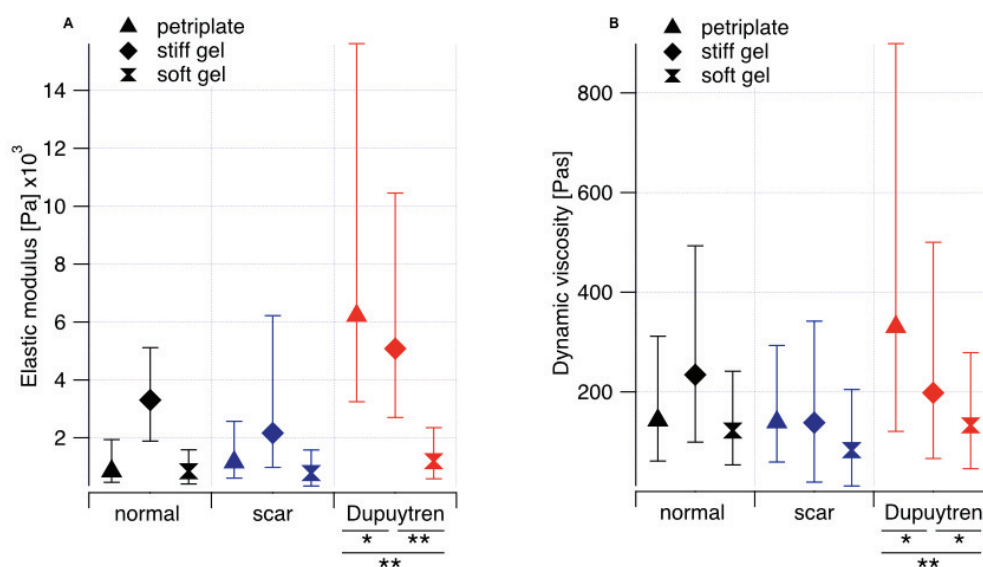
Figure 3.4 Elastic modulus (A) and dynamic viscosity (B) of fibroblasts on different stiffness substrates. The elastic modulus data for normal, scar and Dupuytren's fibroblasts on a Petri dish (*filled triangle*), soft gel (*filled rhombus*) and stiff gel (*filled double triangle*) clearly show that the matrix stiffness influences cell stiffness is most pronounced in Dupuytren's fibroblast, whereas in the others it is rather negligible. The dynamic viscosity data for all fibroblasts show the differing viscous properties of normal, scar and Dupuytren's fibroblasts on substrates. For each category, maximum 29 number of cells were studied. The error bars of first and third quartiles are shown in Table 3.3 & 3.4.

The relative stiffness of the matrix, that surrounds the cell, can have a strong influence on the biochemical (expression of biomolecules) and mechanical (stiffness) properties of the cell. To check whether mechanical properties of ECM could have an influence on the mechanical properties of the fibroblasts used in this study, we prepared different stiffness PA gels as cell substrates and we used AFM to study the elastic and viscous response of normal, scar and Dupuytren's fibroblasts seeded on them. Specifically, experiments were performed on cells

seeded on PA gels with two different stiffness values (1 and 50 kPa) and on conventional Petri dishes as a control. Therefore, we took force maps with 128 x 2 force curves over the nuclear, cell body and periphery regions of 30 μm scan size (for cells on petri dish and stiff gels) and 10 μm scan size (for cells on soft gels, since cells tended to be smaller and less spread on this substrate) and measured the elastic modulus and dynamic viscosity for the fibroblasts in the presence of TGF-β1. Results are shown in figure 3.4 and the respective values of the elastic modulus and the dynamic viscosity are listed in Table 3.3 and Table 3.4. We found a direct correlation between cell stiffness and substrate stiffness in Dupuytren's fibroblasts, i.e. elastic moduli of fibroblasts decrease with decreasing stiffness of the underlying substrate. For the other two fibroblasts we did not find this correlation.

Table 3.3: The median (bold values) elastic modulus values of normal, scar and Dupuytren's fibroblasts on Petri dish, soft gel and stiff gel in the presence of TGF-β1

Elastic modulus (kPa)	Petridish			soft gel			stiff gel		
	25th	median	75th	25th	median	75th	25th	median	75th
Normal	0.3	**0.8**	1.0	0.4	**0.8**	0.7	1.4	**3.3**	1.8
Scar	0.5	**1.1**	1.4	0.4	**0.7**	0.8	1.2	**2.2**	4.1
Dupuytren	2.9	**6.2**	9.3	0.6	**1.2**	1.1	2.4	**5.1**	5.4

Moreover, in order to evaluate the stiffness, force versus indentation data were plotted for three fibroblasts (Supplementary figure 3.10A, B) on soft and stiff gel and specifically for Dupuytren's fibroblast (Supplementary figure 3.10C). We therefore confirmed that Dupuytren's fibroblasts were stiffer than other two fibroblasts and that they could adapt their stiffness to those of the underling gels. Fluorescent images presenting the expression of α-SMA stress fibres for different cell types on soft and stiff gels are reported in Supplementary figure 3.11, showing that all three fibroblast cells are more spread on stiff gel than on soft gel and they present α-SMA stress fibres on less compliant materials.

Table 3.4: The median (bold values) dynamic viscosity values of normal, scar and Dupuytren's fibroblasts on Petridish, soft gel and stiff gel in the presence of TGF-β1

Dynamic viscosity (Pas)	Petridish			soft gel			stiff gel		
	25th	median	75th	25th	median	75th	25th	median	75th
Normal	81.7	**142.8**	168.6	68.9	**122.5**	118.8	135.1	**234.4**	258.8
Scar	79.8	**139.2**	154	71.9	**83.2**	121.7	119.4	**138.1**	203.6
Dupuytren	209.8	**330.3**	568.3	86.8	1**32.9**	145.9	131.6	**198.2**	302

Cell migration plays an important role in wound healing. One of the most used assays to study cell migratory activity is the so-called *wound healing or scratch assay.* With this assay, a gap is mechanically created on a confluent layer of cells and the migration of cell within the scratch is observed. We used this assay to gain information on cell velocity and motility. In our experimental setting, the migration of normal, scar and Dupuytren's fibroblasts within the scratch area was monitored using light microscopy over an observation period of 24 h with images being taken every 2 minutes. In supplementary figure 3.12, images are shown for 0 and 24h from left to right, respectively taken from movies, which are provided in supplementary materials (movie 1, 2 & 3).
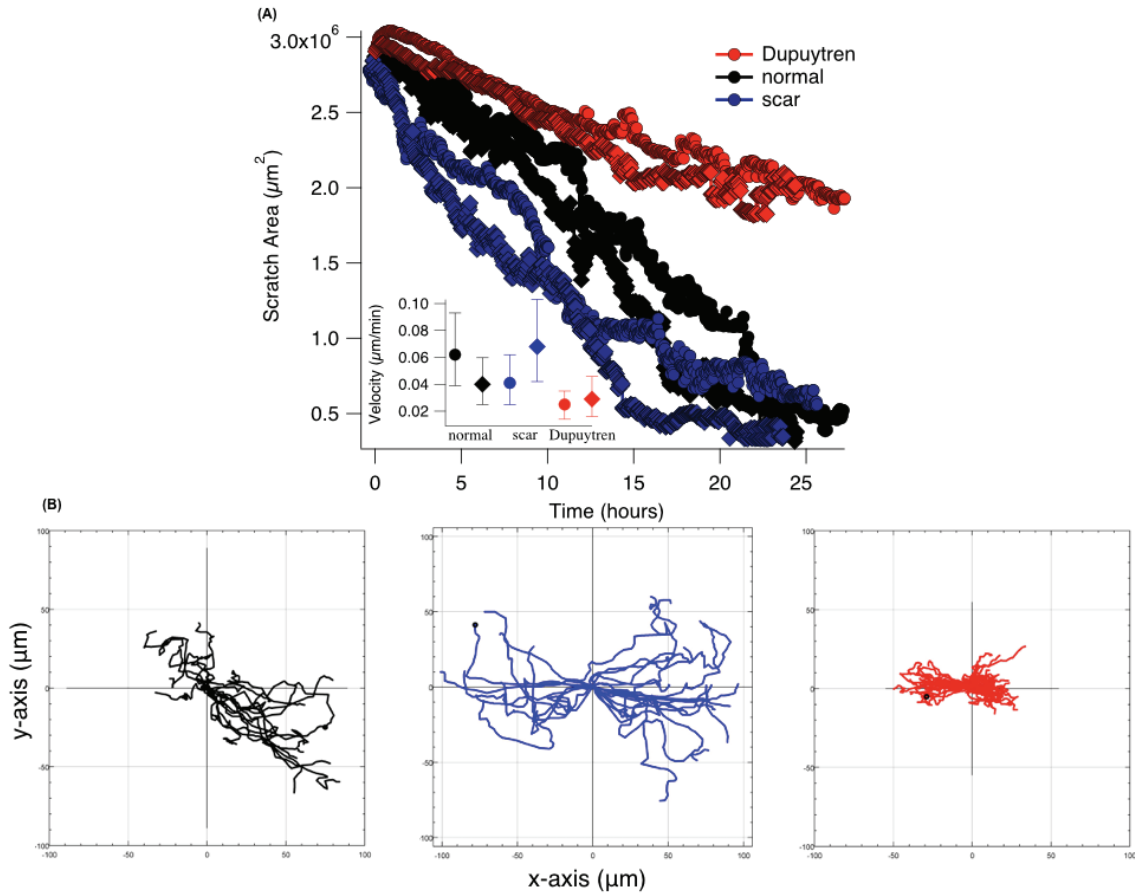
Figure 3.5 (A) Scratch area as a function of time in the wound healing assay. For each cell type we followed two samples over 24 to 28 hours. Closing of the gap was slowest for Dupuytren's cell (red trace), and faster for normal (black) and scar fibroblasts (blue). Closing of the gap correlates nicely with migration speed as calculating from tracks following individual cells in these experiments. The inset shows the median value of velocity values calculated by following individual cells from the supplementary videos. Dupuytren's fibroblast migrates at the speed of 0.026 μm/min, whereas normal and scar fibroblasts show migration speeds between 0.04 and 0.06μm/s. (B) Trajectories of normal (black), scar (blue) and Dupuytren's (red) fibroblasts were plotted by tracking individual cells from supplemental movies1, 2, and 3 respectively. Dupuytren's fibroblast migrates collectively and thus closure of the gap is much slower over the 24 hour time window.

The scratch area (~300 μm^2) was calculated by using ImageJ software for each frame from the 24 hour movie as described in the experimental section. The scratch area (figure 3.5A) was plotted against the time (each experiment was repeated twice) and found that α-SMA stress fibres expressing Dupuytren's fibroblasts could move at slower speed (figure 3.5A, inset) within the scratch area compared to normal and scar fibroblasts. Moreover, from the single cell trajectories (figure 3.5B), we could see that Dupuytren's fibroblasts cover a vertical distance (x axis) of ~50 μm within 24hrs. While instead, within the same range of time, scar and normal fibroblasts were able to cover longer distances (of ~100 μm). Thus, Dupuytren's

fibroblast showed clear differences in their migratory properties compared to the other two fibroblasts.

3.4 Discussion

Determining viscoelasticity by the standard linear solid model. The cytoskeletal filaments and the cytosol determine the elastic and viscous properties of cells. Most importantly, polymerisation of monomer G-actin to filamentous F-actin affects the elastic properties of a cell. The concept of viscosity of a cell seems to be very complicated, e.g. measured values depend on the length scale of the experiment, due to the complexity of the liquid, being a highly concentrated solution of molecules (proteins, RNA, oligosaccharides and the corresponding monomers, and ions and small organic molecules) and a mixture of larger structures like polymeric networks and organelles (Kalwarczyk et al., 2011). Elastic properties can be measured using magnetic twisting cytometry (Coughlin and Fredberg, 2013), particle tracking (Gal and Weihs, 2012) and high-force magnetic tweezers (Kollmannsberger and Fabry, 2007) applying a force or torque on the cell. Viscous properties of cells can be measured by micropipette aspiration; however, this is restricted to non-adherent cells and will yield only one global value for the entire cell. AFM (Binnig et al., 1986) gives us amble opportunities to determine the elastic properties of any area of interest in the cell by picking the appropriate tip geometry to choose a local measurement (e.g. by using pyramidal tips) or a more extended global measurement by using spherical tips. In most cases data are analysed by using the Hertz model (Sneddon, 1965; "Ueber die Berührung fester elastischer Körper." 1882), which neglects the effect of viscous properties. Thus, we should rather term the derived quantities apparent Young's modulus. Here, by applying a small step of 50 nm during the contact with the cell and analysing our step response data in the framework of standard linear solid model (figure 3.3), we were able to determine the true elastic modulus and dynamic viscosity (Yango et al., 2016) (see Appendix). In this model, the sample is modelled by a Zener element with spring k_1 running parallel to Maxwell element consists of spring k_2 and a viscous damping coefficient f plus the cantilever spring of constant k_c in series. Z-height motion resulted in the deflection of the cantilever d which can be fitted with the exponential function and indentation δ of the sample with the mathematic equation of $z = d + \delta$. We chose this very simple model (Yango et al., 2016) although there are many other models available for cell viscoelasticity like tensegrity model (Ingber, 1997), SGR model (Sollich, 1998) and poro-elastic model (Moeendarbary et al., 2013), since it is most appropriate to our experimental design, basically measuring only one relaxation time, i.e. one

mode of relaxation.

PA hydrogels with regulated stiffness to mimic ECM. Mechanical properties of the ECM play a major role in cell development and morphogenesis (Enemchukwu et al., 2016). The ECM microenvironment exerts physical stimuli which result into mechano-chemical and genetic alterations of cells. The mechanically compliant ECM provides cell adhesion and spreading by creation of cell focal adhesion points on ECM. ECM microenvironment tackles the force created by cells and this helps to study the mechano-response of cells on ECM substrate. The ECM consists of collagen, proteoglycans, fibrin, glycoproteins and glycosaminoglycans (GAG) and other proteins. In some experimental settings, cells are studied on collagen hydrogels or collagen-GAG artificial matrixes, but tuning the stiffness of these gels to values close to those in tissues and presenting the cells adequately for AFM (i.e. well adherent on the surface of the gel) turned out to be difficult. Thus, we choose to use here non-physiological, but bio-inert PA gels. The stiffness of thin PA hydrogels can be easily modulated by tuning the concentration of monomer and crosslinker, namely acrylamide and bis-acrylamide (Denisin and Pruitt, 2016). Here, we chose two values for the stiffness, i.e. soft gels around 1kPa that resemble the stiffness of most tissues (50 Pa- 12 kPa) (Cox and Erler, 2011) and a stiffer value of 50 kPa that is considered as very stiff with regard to cellular properties even though this value is much softer than conventional cell culture substrates, such as Petri dishes.

Dupuytren's fibroblasts are stiffer than normal or scar fibroblasts. By using AFM step response curves, we observed that pathological Dupuytren's fibroblasts are stiffer than other two types of fibroblasts, presumably due to the presence of α-SMA expression in intracellular stress bundles. This shows that the Dupuytren's fibroblasts are present in myofibroblast phenotype. In our experimental setting, the addition of 5 ng/ml TGF-β1 increased the expression of α-SMA and thus the elastic modulus predominantly in Dupuytren's fibroblasts, which further confirms their myofibroblast phenotype. Whereas there is no significant response from normal and scar fibroblast to TGF-β1. Obviously, palmar fascial fibroblasts from Dupuytren's nodules and cords seem to react more rapidly to the TGF-β1 stimulus by expressing morphological and biochemical characteristics of smooth muscle cells (Tomasek and Rayan, 1995). The prominent biochemical α-SMA expression of vascular smooth muscle is also seen in fibroblasts from Dupuytren's environment other than β- and γ- cytoplasmic actins. These specialised fibroblasts that express α-SMA, exert high contractile force on ECM

and synthesis and remodel ECM are called myofibroblast. α-SMA is a cell specific actin iso-form and its intracellular gene expression are activated by extracellular latent-TGF-β1 which gets activated either by myofibroblast derived ECM stretching (Wipff et al., 2007) or autocrine production (Dabiri et al., 2006).

The cell mechanics of myofibroblasts is not thoroughly investigated yet. Our results from step response measurements support the assumption that the expression of α-SMA in Dupuytren's fibroblasts is associated with increased stiffness and viscosity compared to normal and scar fibroblasts. After addition of TGF-β1 the stiffness of Dupuytren's fibroblasts increased further. Although previous studies (Desmoulière et al., 1993) reported on the role of TGF-β1 on α-SMA expression and myofibroblast differentiation, there are no reports on the comparison of mechanical measurement of fibroblasts of different origins, mostly from normal and diseased tissue. Here, we measured cellular viscoelasticity, which reveals the different levels of intracellular force generation from each fibroblast type and their phenotype varied with regard to α-SMA expression. Even when seeded on an "infinite" stiff substrate, as a Petri Dish occurs to cells, normal fibroblasts and scar fibroblasts do not show a myofibroblast phenotype. This seems to be related to their different cytoskeleton organization, as we found a lack of stress fibre formation though they show low level α-SMA expression (supplementary figure 3.9).

Substrate stiffness influences the stiffness of Dupuytren's fibroblasts. Mechanical stress regulates myofibroblast differentiation and function. Fibroblasts are influenced by cell-ECM interactions, where they will for instance undergo stress-dependent maturation and form focal adhesion. The mechanical stress of the ECM is transmitted through the integrin-focal adhesion protein complex, which activates downstream signaling cascades in the cell resulting in the recruitment of α-SMA into stress fibres. Matrix stiffness plays a pivotal role in the fibroblast to myofibroblast transition (Li et al., 2007; Smithmyer et al., 2014). In our study, we clearly observed the adaptive nature of Dupuytren's fibroblasts stiffness to matrix stiffness which was less prominent with the other two types of fibroblasts in the current experimental setting. Dupuytren's fibroblasts were well adherent and well spread on Petri dishes as compared to normal fibroblasts and scar fibroblasts cells. As a consequence, they showed a larger cell area. In soft gels all three types of fibroblasts are reduced in area and exhibit a more roundish shape. Generally, soft substrates led to the formation of less stress fibres, resulting in low values of elastic moduli for all three fibroblasts. Previous studies (Goffin et

al., 2006) showed that the focal adhesion area and α-SMA localisation depends on matrix compliance. This explains that through focal adhesion (FA) points, Dupuytren's fibroblasts makes stronger cell-ECM contacts on Petri dish and stiff gel (immunofluorescence data not performed) where α-SMA is recruited into stress fibres and becomes stiffer on both substrate. Even though normal and scar fibroblasts stiffness was influenced by PA substrate stiffness, they were soft even on a virtually incompressible stiff substrate (Petri dish) as they did not form more stress fibres even in the presence of TGF-β1. In the previous studies (Solon et al., 2007), it was reported that NIH-3T3 fibroblasts show adaptive increasing cell size and stiffness with increasing gel stiffness coated with fibronectin. This could be due to the presence of fibronectin which brings stronger adhesion, hence cell stiffness and also due to fibroblast cell line from mice which attained different morphology and function than the cells used here. We used fibroblasts from human origin cultured on soft and stiff gels that enable good adhesion to the PA hydrogel. Recently it was reported (Achterberg et al., 2014a) that human dermal fibroblast cultured in 3D collagen matrix, needed three weeks to form stress fibres and with TGF-β1 presence this still required one week. But in our study, prior to viscoelastic measurement within 48 h of growth for all three cells in the presence and absence of TGF-β1, Dupuytren's fibroblasts are stiffer than the other two types of fibroblasts due to the myofibroblast phenotype. In order to prove the statement on myofibroblast differentiation, all three fibroblasts were grown for a week with TGF-β1 treatment. Differentiated myofibroblasts showed an increase in elastic moduli in all three cell types (Supplementary figure 3.13 and Supplementary Table 3.6).

Dupuytren fibroblast migration. Here, we studied the wound healing assay for fibroblasts of three different origins and observed the difference in their migration pattern to close a mechanically created "wound gap". From figure 3.5 and the supplementary video1, 2 and 3, it can be clearly seen that the Dupuytren's fibroblasts migrate slowly compared to the other ones, which might be due to their phenotypic presence of expressing α-SMA stress fibers. Previously, it was discussed that filamentous α-SMA stress fibers expression immobilized the cells by forming prominent focal adhesion and thus reduced their motility (Rønnov-Jessen and Petersen, 1996). Dupuytren's fibroblasts, which exhibit the myofibroblast phenotype, tend to move collectively to close the gap. The distance travelling within 24 hours is smaller than 50 μm. These myofibroblasts are the mechanically active cells that communicate through intercellular adherent junctions (Follonier et al., 2008) and are also participating in the fibrosis *in vivo* (Bochaton-Piallat et al., 2016). Thus, exhibiting stronger cell-cell contact, Dupuytren's

fibroblast from the fibrosis microenvironment migrate slowly in the scratch area. Scar fibroblasts are basically extracted from the wounded region. Apparently they can sense the free space, enabling them to migrate and close the scratch faster than Dupuytren's cells. Recently, (Ascione et al., 2016) a cell motility assay on skin fibroblasts from wild type and transgenic mice overexpressing PEA-15 protein showed that the wildtype cells sensed and closed the scratch faster than transgenic mice. Here, normal fibroblasts migrate individually in the same way as scar fibroblasts. In comparing the individual cell trajectories, scar fibroblast motility is more directed than the motility of normal fibroblasts, whereas Dupuytren's fibroblasts move in a 'zig-zag' manner within the cell layer and thus were not able to achieve closing the gap within the observation period of 24 hours.

3.5 Conclusion

We measured the viscoelastic properties of three types of fibroblast cells extracted from different tissues of the same patient: normal, scar and Dupuytren's fibroblasts. We investigated the effect of TGF-β1 and microenvironment stiffness on fibroblast mechanical properties and cytoskeleton organization. We used different stiffness polyacrylamide gels as cell culture substrates to reproduce an environment similar to the natural ECM (from the mechanical point of view) to study cell response to different mechanical signals. We could find differences in the way normal and diseased cells perceive and react to these external factors. Specifically, we found that Dupuytren's fibroblasts were stiffer and more viscous than normal and scar derived fibroblasts. Also, a pronounced relation between cell and matrix stiffness was found only for Dupuytren's fibroblasts, i.e. the stiffness of these fibroblasts increased increasing the stiffness of the underling gels. Finally, from a *wound healing assay*, we found differences in the way different fibroblasts migrate, in terms of migration pattern and migration velocity: Dupuytren's fibroblasts migrated slowly, thus covering only shorter distances. Our findings show that the use of biophysical tools to investigate mechanical and migratory properties can help to discriminate between different cell phenotypes, highlighting differences between the way normal and diseased cells interact with their ECM and adapt their features.

3.6 Methods and Experimental Design

General Materials. Acrylamide and bisacrylamide solutions were purchased from Bio-Rad. N,N,N',N'-Tetramethylenediamine(TEMED), N-[3-(Trimethoxysilyl)propyl]ethylenediamine silane and dichlorodimethylsilane solutions were purchased from Sigma. Anti-alpha-actin

(smooth muscle) rabbit monoclonal antibody, Sodium hydroxide, Dulbecco Modified Eagle's Medium (DMEM) and ammonium persulphate (APS) were purchased from Merck, TGF-β1 from Peprotech and Alexa Fluor 488 secondary antibody from Life Technologies. Glutaraldehyde, ethanol and other solvents were purchased from Panreac AppliChem.

Gel substrate Preparation. Polyacrylamide (PA) gels were prepared following a well-established protocol (Tse and Engler, 2010) based on the polymerisation of the gel solution between two glass slides, silanized with amino- or chloro- silanes, respectively. For the amino-silanization process, round cover slips were first washed with absolute ethanol and ultra-pure water (MilliQ systems, Molsheim, FR), then covered with 0.1 M NaOH for 3 min and finally activated with N-[3-(Trimethoxysilyl)propyl]ethylenediamine silane for 3 min and treated with 0.5 % glutaraldehyde for 30 min. For the chloro-silanized glass preparation, a dichloromethylsilane solution was poured on the cover slides for 5 min; glasses were later extensively washed with ultrapure water and dried with paper tissues. PA gel solution was prepared by mixing 40 % acrylamide with 2 % bisacrylamide in ultra-pure water. Polymerisation was initiated by APS and TEMED. The gel solution was then poured on the amino-silanized glass and covered with the chloro-silanized one to avoid the presence of oxygen that would inhibit the polymerization. After 30 min, the upper slide was removed while the gels were attached on the amino-silanized supports. By varying the amount of bisacrylamide we obtained gels with different stiffness values. Here, we made soft and stiff gels with elastic moduli of ~1 kPa and ~50 kPa respectively (values were measured by using AFM) to study the mechanics of fibroblasts from three different origins. Before cell seeding on PA gel, the substrates were sterilised in ethanol, extensively washed in PBS, and incubated with DMEM medium along with 20 % fetal bovine serum for a few hours to promote serum protein adsorption on the gels.

Cell isolation and cell culture. Primary fibroblasts were isolated from three surgically removed skin tissues of a 55-year old female patient's left hand palmar fascia regions. The skin tissues were minced and enzymatically disaggregated using a 0.5% collagenase solution (250 U/ml Serva, Heidelberg, Germany) at 37∘C in 5% CO_2 for 6 h. After centrifugation, the pellet was resuspended in culture medium (TC 199 with Earle's salts supplemented with 20 % fetal bovine serum, 200 IU/ml penicillin, 200 μg/ml streptomycin) and incubated at 37 °C in 5% CO_2 air. The culture medium was changed after attachment of the cells. Primary fibroblasts of the three different skin tissues were passaged using trypsine / EDTA solution

(0.05% / 0.02% w/v in PBS w//o Ca^{2+}, Biochrom, Berlin, Germany) a split ratio of 1:2 one time a week to preserve monolayer formation. The patient had given informed consent. The study was approved by the local Ethics Committee (Ärztekammer Bremen, #336/2012). The guidelines of the declaration of Helsinki are followed.

All fibroblasts were cultured in DMEM medium and incubated at 37 °C in a humidified atmosphere of 95 % air and 5 % CO_2. Medium was supplemented with 10 % fetal bovine serum (FBS) and 2 % penicillin-streptomycin. Prior to cell seeding, PA gel substrates were sterilised in ethanol, extensively washed in PBS, and incubated with DMEM medium along with 20 % fetal bovine serum for a few hours to promote serum protein adsorption on the gels, hence, cell adhesion ((Carmela Rianna and Radmacher, 2017), see the supplementary figure 3.11). Cells were seeded 48 h prior to AFM measurements; either plated on gels placed in Petri dishes, or directly on Petri dishes. Passages between three and seven were used for the experiments.

AFM experiments. A MFP3D AFM (Asylum Research, Santa Barbara, CA, USA) was used to measure mechanical properties of three fibroblast types. AFM consists of four important components: 1) cantilevers with a pyramidal tip (in our case), 2) laser diode, 3) position sensitive photodetector and 4) xyz piezoelectric scanner (figure 3.1A). An optical microscope was combined with the AFM to be able to control tip and sample positioning. Soft cantilevers (MLCT Bio, Bruker, nominal spring constant 0.01 N/m) were used to investigate cell properties. The Petri dishes with cell samples were fixed to an aluminum holder with vacuum grease and mounted on the AFM stage with two magnets. The AFM head including the sample was enclosed in a homebuilt polymethacrylate (PMMA) box in order to inject and maintain 5 % CO_2.

We used two cantilevers (same batch, same nominal spring constant) to minimize systematic errors due to calibration. The deflection sensitivity was adjusted offline based on the thermal tune and a spring constant of 10 mN/m as described in reference (Schillers et al., 2017)

AFM force maps. Step response force curves were recorded on all three fibroblasts to study their viscoelastic properties. All force measurements were performed with two cantilevers. First, the spring constant of the cantilever was calibrated by using the thermal tune method (Sader et al., 1995) and then force curves were recorded over different regions of cells (nuclear region, cell centre and periphery). For step response force curves, we used typically a scan rate of 1 Hz, corresponding to a maximum loading rate of 1 nN/s and a maximum force

of 1nN. Indentation depths were always greater than 500 nm in order to average the stiffness over a large contact area, which gives values that do not depend on local variations of the cytoskeleton structures. At least 25 cells were measured for each substrate; 256 force curves were acquired over a cell of scan size 30 µm called force maps. To apply the step, z motion was stopped for a dwell time of 2 s after the trigger threshold was achieved (cantilever deflection of 100 nm). After 1 s, the z height was changed by 50 nm towards the cell and after an extra 0.5 s this step was reversed (Yango et al., 2016).

AFM data analysis. The data analysis package IGOR (wave metrics, Lake Oswego, OR, USA) was used to evaluate mechanical data of the cells. Details have been described elsewhere (Carmela Rianna and Radmacher, 2017). Recording force curves (figure 3.1B), by approaching (red arrows) and retracting (blue arrows) the cantilever towards and from the sample, we obtained information on its mechanical properties. Force curves are usually analysed within the framework of the Hertz model (Rico et al., 2005; Sneddon, 1965; "Ueber die Berührung fester elastischer Körper.," 1882). However, this model only considers the elastic response of the sample, neglecting the viscous response from certain samples (like cells), which is visible from a large hysteresis between approach (red arrows) and retract curves (blue arrows) (figure 3.1B).

In step response curves, a well-defined z-step is applied while the tip is in contact with the sample (figure 3.1C). After applying a loading force of 1 nN, the z-height was kept constant for 2 seconds to allow the cells to reach an equilibrium and then a small step of 50 nm in z-height was applied at 1.5 s (figure 3.1C). This small step is reversed after 0.5 s, the relaxation of the cell is observed, and after another 0.5s the tip is fully brought out of contact from the cell after a short time of period. Even though we waited for 1 s before applying the step to minimise creep caused by the approach ramp of the force curve, it was essential to subtract an exponential fit to remove residual creep. The individual exponential fits were applied to the data after the loading and unloading step. Each fit resulted in two spring constants and one value for the friction-damping coefficient. Step response data were collected and fitted with the standard linear solid model (Supplementary figure 3.6), which is a combination of two springs and a dashpot (also called a Zener model) (Fung, 1985). The spring constant k_1 correspond to the stiffness of the sample after relaxation. The sum of k_1 and k_2 correspond to the initial stiffness of the sample after the step is applied, whereas the friction-damping f is responsible for the strain and stress relaxation. The spring constants and the friction damping coefficient can be converted to true elastic moduli and dynamic viscosity, respectively,

assuming a Hertzian response of the sample taking in account the final loading force during the step. The equations and fit parameters used for creep response data and elastic modulus and dynamic viscosity calculation were presented in the Supplementary information.

Immunofluorescence staining. Forty-eight hours after seeding of cells on gels and Petri dishes, cells were fixed with 3.7 % formaldehyde for 15 min and permeabilized with 0.1 % Triton X100 for 3 min. Samples were washed with PBS after each step and then incubated with a rhodamine phalloidin solution (5:200 dilution in PBS) for F-actin staining for 30 min at 20 °C. For α-SMA staining, cells were incubated with primary antibody Anti-alpha-actin (smooth muscle) rabbit monoclonal antibody (1:100 dilution in 0.1 % BSA/PBS) and followed by incubation with secondary antibody Alexa Fluor 488 (1:200 dilution in 0.1 % BSA/PBS) for 30 min each at 20 °C and samples were washed after every step with 0.1 % BSA/PBS. Finally, cells were stored in PBS at 4 °C prior to image acquisition. An Axiovert 135 TV epifluorescence microscope (Carl Zeiss MicroImaging GmbH, Germany) with 40x objective lens was used to observe cells and collect fluorescent images.

Wound Healing Assay. All three fibroblast cell types were seeded at a density of 2 x 10^5 on Petri dishes and incubated at 37 °C in a 5 % CO_2/air atmosphere until 100 % confluence. Cell monolayers were scratched manually with a 10 μL pipette tip and then washed with PBS twice to remove cellular debris followed by replenishing with the fresh medium. To observe the migratory activity of the cells, we used a light microscopy (Axiovert 135, Carl Zeiss MicroImaging GmbH, Germany) with 20x objective lens. Images were recorded every 2 minutes for a total time of 24 hours. In the end the scratch area before and after closure was calculated using Fiji software (Schindelin et al., 2012). Specifically, we applied image thresholding and segmentation to separate our object of interest from the background (in this case the scratch area from the cell layer). Then, by using the macro *MRI Wound Healing Tool* (Carmela Rianna and Radmacher, 2017) we measured the area of the gap for each image and plot these data versus time. We used Manual Tracking Tool of Fiji software to monitor the velocity and trajectory of single cells at the scratch edge of the wound healing assay. More than 26 cells were tracked in each video and totally two videos were studied for each cell types.

Statistical Analysis. Statistical differences for the median values of elastic moduli and dynamic viscosity of fibroblasts between different conditions of the AFM measurements were

determined by Wilcoxon test, calculated in IGOR software. * and ** indicate statistically significant differences for p-values <0.05 and p<0.005, respectively.

3.7 Acknowledgements

3.8 Author contributions

PK was performing AFM experiments, gel preparation, wound healing assay, data analysis and manuscript preparation. GB was establishing cell lines from primary cells. CR was preparing gels and was involved in data analysis. UM designed the experimental scheme. MR designed the experimental scheme and was involved in data acquisition, data analysis and preparation of the manuscript.

3.9 Additional information

Competing financial interests: The authors declare no competing financial interests.

3.10 Supporting Information
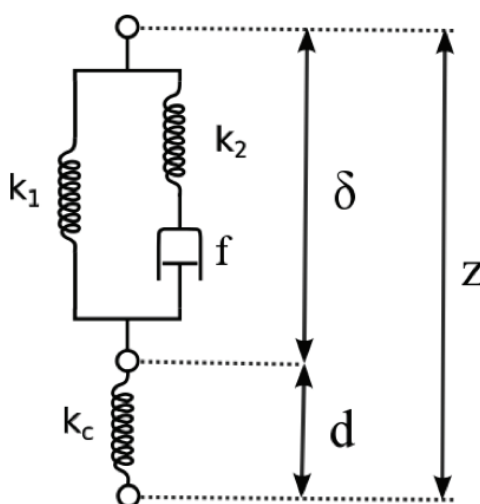
Supplementary figure 3.6 Standard linear solid model, Viscoelastic behavior of cells is calculated using this model which consists of two springs (k_1 and k_2) and a viscous damping dashpot (f), whereas the cantilever is characterized by its spring constant k_c only. Sample height is represented by z, cantilever deflection by d and indentation of the sample by δ.
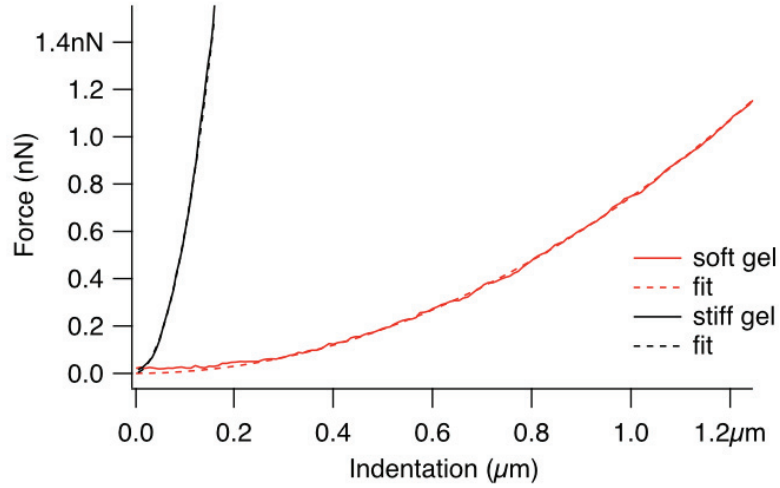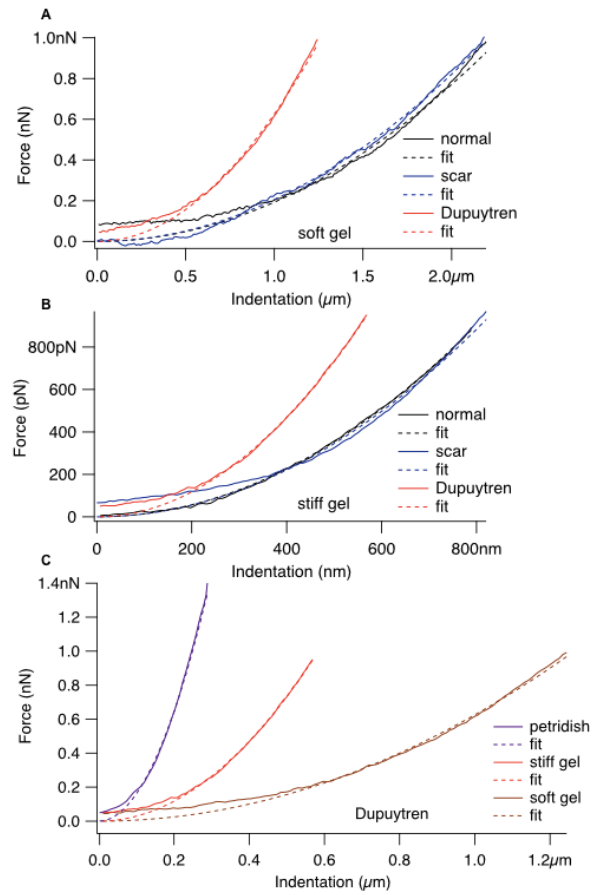
Supplementary figure 3.7 Force *vs* indentation graph with Hertz fit (discontinuous line) evaluates the stiffness of the soft gel (red) and stiff gel (black)
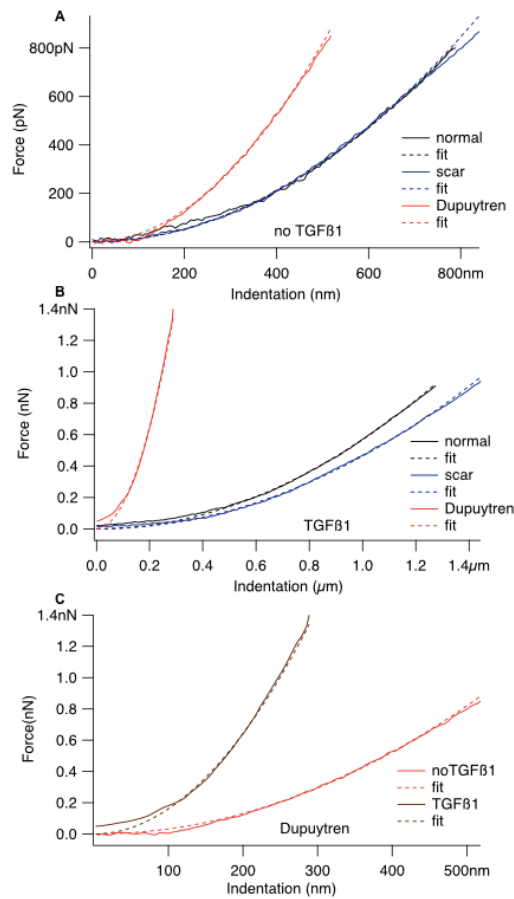
Supplementary figure 3.8 Force *vs* indentation graph with Hertz fit (discontinuous line) evaluates the stiffness of fibroblasts (A) In the absence and (B) presence of TGFβ1 where Dupuytren's fibroblast is more stiff than other two fibroblasts in two cases. (C) Particularly, Dupuytren's fibroblast looks stiffer in presence of TGFβ1.

51
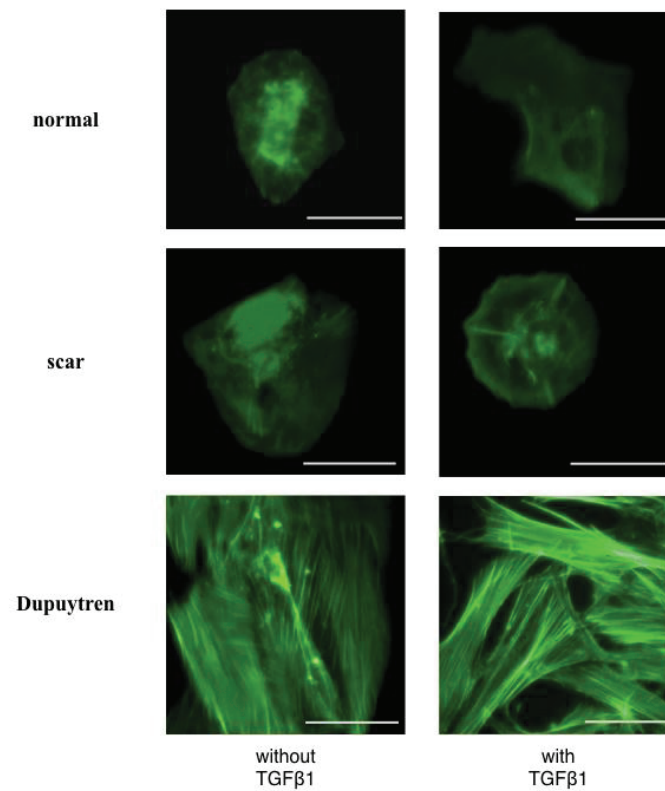
Supplementary figure 3.9 The α-SMA staining of normal, scar and Dupuytren's fibroblasts on petridish shows the high level of α-SMA expression of Dupuytren's fibroblasts before (-) and after (+) addition of TGFβ1. Scale bar 50 μm
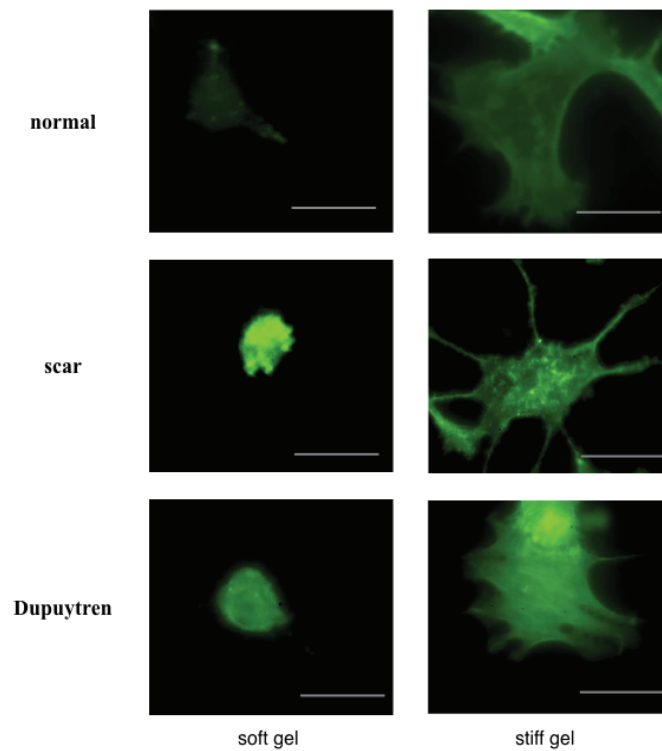
Supplementary figure 3.10 Force *vs* indentation data with Hertz fit (discontinuous line) evaluates the stiffness of fibroblasts (A) In soft gel and (B) in stiff gel where Dupuytren's fibroblast is stiffer than the other two fibroblast types. (C) Dupuytren's fibroblast cell stiffness on a Petri dish, soft gel and stiff gel is strongly influenced by substrate stiffness.
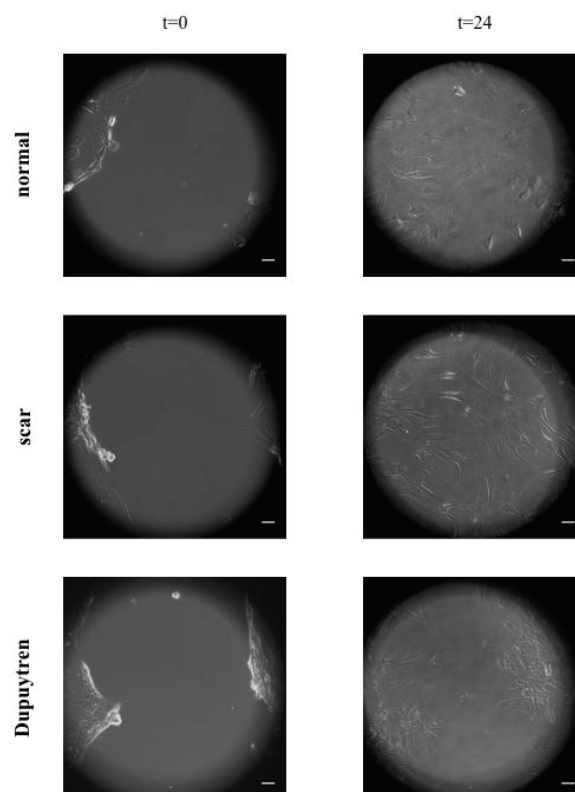
Supplementary figure 3.11 α-SMA staining of normal, scar and Dupuytren's fibroblasts on a Petri dish shows the level of α-SMA expression on cells on soft and stiff gel in the presence of TGFβ1. Scale bar 50 μm.

Supplementary figure 3.12 Migration of fibroblasts in wound healing experiment. Normal, scar and Dupuytren's fibroblasts cell migration studied at t=0 hr and 24 hr time-scales shows the individual cell migration

seen mostly in normal and scar fibroblasts than in Dupuytren's fibroblast due to strong cell-cell contact. Scale bar 50 μm.
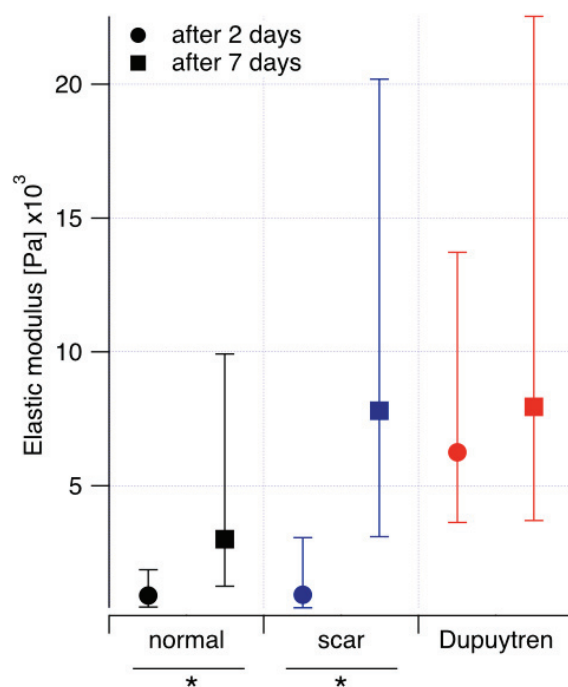
Supplementary figure 3.13 The elastic modulus of three fibroblasts cell types after two and seven days of TGFβ1 treatment. Although expression of a-SMA and subsequent formation of stress fibres is most prominent in Dupyuteren's fibroblasts, all three cell types show an increase in stiffness. represents the activation of fibroblasts after one week. For each category, maximum 11 number of cells were studied. The error bars of first and third quartiles are shown in Supplementary Table 3.2.

Supplementary Table 3.5: The median (bold values) apparent Young's modulus, elastic modulus and dynamic viscosity values of soft gel and stiff gel

	soft gel			stiff gel		
	25th	median	75th	25th	median	75th
apparent Young's modulus (kPa)	0.2	**0.9**	0.4	9.6	**48.5**	9.7
Elastic modulus (kPa)	0.4	**1.1**	2.1	13.9	**47.1**	17.2
Dynamic viscosity (Pas)	63.1	**29.6**	75.5	1126.9	**976**	3888.5

Supplementary Table 3.6: The median (bold values) elastic modulus of normal, scar and Dupuytren's fibroblast treated with TGF-β1 after 2 days and after 7 days

Elastic modulus (kPa)	after 2 days			with TGF- β1		
	25th	median	75th	25th	median	75th
Normal	0.4	**0.8**	0.9	1.7	**2.9**	6.9
Scar	0.4	**0.9**	2.1	4.7	**7.8**	12.3
Dupuytren	2.6	**6.2**	7.4	4.2	**7.9**	14.5

Chapter 4

Nano-mechanical mapping of interdependent cell and ECM mechanics

Prem Kumar Viji Babu[1,3], Carmela Rianna[1], Ursula Mirastschijski[2], Manfred Radmacher[1,3]

[1]Institute of Biophysics, University of Bremen, Bremen, Germany

[2]Wound Repair Unit, Centre for Biomolecular Interactions Bremen, University of

Bremen, Bremen, Germany

[3]Authors to whom any correspondence should be addressed.

4.1 Abstract

Extracellular matrix (ECM), as a dynamic component of the tissue, influences cell behavior and plays an important role in cell mechanics and tissue homeostasis. Reciprocally, this three-dimensional scaffold is dynamically, structurally and mechanically modified by cells. In the field of biophysics, the independent role of cell and ECM mechanics has been largely investigated; however, there is a lack of experimental data reporting the interdependent interplay between cell and ECM mechanics, measured simultaneously. Here, using Atomic Force Microscopy (AFM) we have characterized five different decellularized matrices diverse in their topography, ECM composition and stiffness and cultured them with normal and pathological fibroblasts (scar and Dupuytren's). We investigated the change in topography and elasticity of these matrices due to cell seeding, by using AFM peak force imaging and mechanical mapping, respectively. We found normal fibroblasts soften these matrices more

than pathological fibroblasts, suggesting that pathological fibroblasts are profoundly influencing tissue stiffening in fibrosis. We detected different ECM composition of decellularized matrices used here influences fibroblast stiffness, thus highlighting that cell mechanics not only depends on ECM stiffness but also on their composition. We used confocal microscopy to assess fibroblasts invasion and found pathological fibroblasts were invading the matrices deeper than normal fibroblasts.

4.2 Introduction

The extracellular matrix (ECM) is a structural scaffold made of non-cellular, fibrous and non-fibrous proteins that are able to influence cellular functions, tissue homeostasis and organ development (Bonnans et al., 2014). Highly dynamic three-dimensional (3D) scaffolds provide environmental signals that directly regulate stem cell fate (Watt and Huck, 2013). The ECM microenvironment mediates cell adhesion by providing the anchoring sequence tripeptide Arg-Gly-Asp (RGD) to cell transmembrane anchoring proteins such as integrins, which are an integral part of focal adhesions (FA) (Boudreau and Jones, 1999; Ohashi et al., 1999; Raines, 2000). This molecular assembly connects cells and ECM via force pinpoints and contributes to cellular signaling such as mechano-sensation and mechanotransduction (García and García, 2014; Hoffman et al., 2011; Ingber, 2006). The mechanical signals provided by the ECM have an impact on cell mechanics and in response, cells have also huge impact on the ECM by modifying its composition, its architecture, and hence its mechanics and thus creating a reciprocal interplay between mechanics of cells and ECM. The bidirectional bio-chemical and bio-mechanical relationship between cells and ECM that is defined as dynamic reciprocity (Schultz et al., 2011) is a principal component of 3D tissues.

In order to evaluate cell and ECM mechanics in physiological conditions we have used the AFM, since it allows to record high resolution images and force-distance curves, often in forms of force maps, on biological samples in their physiological condition. The components that play a major role in determining cell and ECM elasticity are the actin cytoskeleton, collagen and elastin network structures (Martens and Radmacher, 2008; Muiznieks and Keeley, 2013; Rotsch and Radmacher, 2000).

Under either normal or pathological conditions, tissues are subjected to various mechanical forces such as tension, compression and shear force that alter cell and ECM mechanics (Wells, 2013). Several studies explored the influence of ECM topography and stiffness on cell mechanics (C. Rianna and Radmacher, 2017; Solon et al., 2007) and of cells on ECM topographic cues (Friedrichs et al., 2007a; Kusick et al., 2005) using AFM force

spectroscopy. Previously, employing AFM nanoindentation, it has been reported that the leading edge of individual and collective cell migration deform the fibrillar collagen substrate and the substrate undergoes reversible non-linear strain stiffening (van Helvert and Friedl, 2016; Wen and Janmey, 2013). The cellular proteolytic activity brings permanent changes to ECM composition, structure and mechanics (Helvert et al., 2018; Jorba et al., 2017). Cellular traction forces induce permanent deformation of ECM collagen bundles suggesting a mechanical remodeling of the ECM by cells (Kim et al., 2017). However, there is a lack of knowledge in following the permanent changes of ECM structure and mechanics by cells.

So far, cell elasticity was determined on individual ECM protein gels, mostly collagen (Achterberg et al., 2014b) and fibronectin (Solon et al., 2007). The tremendous complexity of the 3D microenvironment makes the deep understanding of the mechanical reciprocity between cells and ECM very complicated which in turn results in difficulties to follow the changes in cell and ECM mechanics at the same time. To overcome this issue, there is a strong need to employ more complex and heterogeneous matrices able to provide the full range of signals, where cells are exposed to, in near physiological conditions.

The emerging trend using decellularized samples provides cells with an enormously rich and tunable chemical and mechanical microenvironment. With the already reported decellularization protocols (Rianna et al., 2018), a natural ECM scaffold can be prepared through chemical, physical or enzymatic procedures. Interestingly, decellularized tissues offer a more physiologically relevant microenvironment to cells than 3D cultures using single or only a very limited variety of ECM components (Alcaraz et al., 2018). Different decellularization protocols preserve the chemical and mechanical integrity of the native ECM scaffold in order to study ECM micromechanics. In order to study their mechanical properties, AFM indentation experiments were set up to probe the decellularized lung ECM micromechanics and to study the anatomical specific regional heterogeneities (Jorba et al., 2017).

Here, we characterised five matrices that will be further termed "decellularized": human DED (de-epidermized dermis), human Amnion (allogenic, acellular), Epiflex (allogenic, acellular) and porcine XenoDerm (xenogenic, acellular), and MatriDerm (alloplastic, artificial). Each one differs in composition, topography and stiffness. Some of these decellularized matrices are seeded with cells and often used in wound repair and organ regeneration (Haslik et al., 2007; Kim et al., 2013; Rana et al., 2017). We have chosen these matrices in order to study the role of fibroblasts in ECM maintenance by mechanical and topographical evaluation. DED was prepared by us in a physical decellularization procedure (Rianna et al., 2018), whereas

the others are commercially purchased. In general, ECM secretion, deposition and degradation are highly regulated by fibroblasts (Fan et al., 2012; Kalluri and Zeisberg, 2006). For this study, three types of primary fibroblasts of different origin (normal fibroblasts from normal healthy skin and scar fibroblasts from cutaneous scar tissue and Dupuytren's fibroblasts from the palmar fascia of the same patient with Dupuytren's disease) were seeded onto these matrices to monitor the interdependent cell and ECM mechanics. As the fibroblasts-scar and Dupuytren's are extracted respectively from the pathological environment- scar region and cord and nodule of palmar fascial region, we termed them as pathological fibroblasts. The aim of this work was to visualize and observe changes in ECM structure and mechanics caused by cells. To achieve this aim, we recorded AFM peak force tapping mode images and mechanical force maps on the five decellularized matrices for different categories: bare matrix, matrix populated by cells, and the same matrices after cell removal for each fibroblast (normal, scar and Dupuytren's). This setup allows to probe quantitatively the ECM topography and mechanics in all different categories and allows to study the effect of fibroblasts on ECM features. We found that fibroblasts had a strong effect on decellularized matrices topography and stiffness and were able to modify the matrix, causing a change in mechanical properties before and after cell culture, even after the cells were removed. Also, we hypothesized that decellularized matrices provide the natural and biomimetic microenvironment to study both cell and ECM mechanics. Furthermore, we show that the Young's modulus of fibroblasts differs when fibroblasts are seeded on different matrices, possibly due to the peculiar matrix composition, thus implicating the dependence of cell mechanics to ECM composition. Finally, we were able to obtain z stack images using confocal fluorescence microscopy, demonstrating the degree of cell invasion into decellularized matrices by three different fibroblast types.

4.3 Results

General setup and characterisation of decellularized matrices

The overviews of the different steps of the experiment are schematically shown in Figure. 4.1A. First, AFM measurements were performed on bare matrices, and then cells were seeded on the matrices and cultured for two weeks. This was followed by repeated AFM measurements of these matrices populated with cells. Finally, cells were removed and bare, but possibly restructured or modified matrices were investigated again by AFM. By obtaining PeakForce Tapping AFM images (Figure. 4.1B) and mechanical maps (Figure. 4.1C) at each step, we were able to observe changes in ECM topographical and mechanical properties and

also cell stiffness within the same matrix, investigating the reciprocal effect of cell and ECM mechanics on each other. Finally, by performing confocal microscopy z stack imaging for cells on matrices (Figure. 4.1D), we were able to study fibroblast invasion into the matrix, visualizing the stress fibre network and relating this information to the cell stiffness measurements.
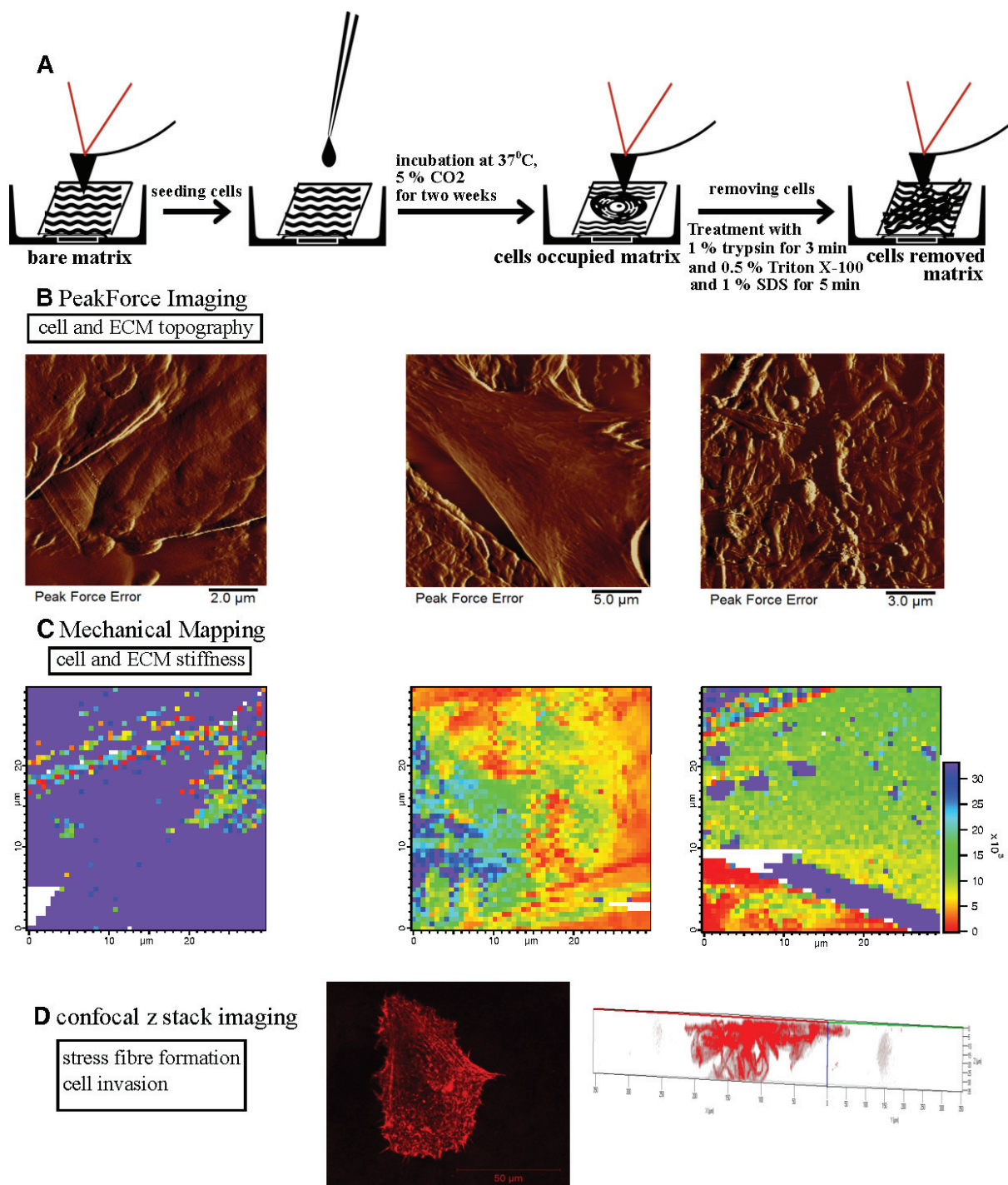
Figure 4.1. Schematic representation of the overall experimental setup for cell and ECM topography and mechanics investigation on decellularized matrix. (A) Decellularized matrices were seeded with fibroblasts (normal, scar or Dupuytren's) and incubated at 37°C for two weeks. Thereafter, cells were removed by chemical treatment (1% trypsin, 0.5% Triton X-100 and 1% SDS) to follow the changes in matrix topography and

mechanics. (B) AFM Peak force imaging shows the topography of native Epiflex matrix, matrix with cells and matrix after removal of cells. (C) AFM mechanical mapping illustrates the stiffness of bare Epiflex matrix, matrix with cells and matrix after removal of cells (the maps have the same scale and show values of Young Modulus, Pa). (D) z stack imaging from confocal microscopy displays the stress fibre formation in fibroblasts and also creates 3D maps that evaluate the degree of cell invasion into the decellularized matrices.

Since in our experimental setup the matrices were incubated for 14 days with cells prior to AFM measurements, we decided to test the bare matrix stiffness and topography at day 1 and day 14, i.e. the first day and after 14 days of culture in PBS in the incubator (as a control for other samples, which were incubated with cells for up to 14 days). Figure. 4.2A shows the height and peak force error images of decellularized bare matrices (without cells) imaged in PBS on day 1 and day 14 (left and right panel, respectively). Height and peak force error images from AFM Peak Force Tapping Imaging show the respective overall topography and fine details such as fibre thickness of the decellularized matrices. The topographical and mechanical characterisation of the five decellularized matrices at different times gives the possibility to track the influence of liquid environment on ECM topography and stiffness. Height and peak force error images of Amnion matrices show the presence of cross-linked thick and thin fibres with some other ECM remnants. Thickness of thick and thin fibres varied between 0.5-0.7 µm and 0.15-0.2 µm, respectively The microscopic appearance of DED and Epiflex matrices shows no proper fibre alignment but irregular blobs and corrugated surfaces with few fibres. Traces of thin fibres of 0.25-0.3 µm thickness were observed in DED matrix. A well oriented fibre alignment was observed in MatriDerm and XenoDerm. MatriDerm images show thin fibres of 0.125-0.275 µm thickness running parallel to each other and sometimes tailored structures. XenoDerm images show large thick fibres of fibre thickness 0.9-1.4 µm and thin fibres of 0.235-0.375 µm thickness, which are bundled closely together. Although few fibres (0.45-0.5 µm thickness) running along the matrices were observed in DED after 14 days in PBS, there was no particular fibre alignment or pattern. Despite the small topographic differences due to measurements taken on different positions in the Epiflex and MatiDerm matrices, there was no change in pattern or disruption or misalignment of fibres observed between day 1 and day 14. Mostly, no larger variability in Amnion and XenoDerm topography were found between day 1 and day 14. Additionally, no effect of aging of matrices observed microscopically and also macroscopically no change in texture of matrices witnessed.

We also recorded high resolution force maps (each map = 50 x 50 = 2500 force curves) in at least 10-12 different positions on the decellularized matrices on day 1 and day 14. These force

maps recorded on the decellularized matrices showed ECM fibers (indicated by *blue arrows* in Supplementary Figure. 4.11A). From the force measurements the mechanical properties are obtained by fitting each force curve with the Hertz model to obtain and plot the respective median Young's modulus values (Figure. 4.2B). In some cases, we could observe a decrease in Young's modulus after 14 days, especially in Epiflex (from 199.5 kPa to 95.8 kPa – a two-fold decrease), MatriDerm (Young modulus significantly changed from 27.1 kPa to 2.3 kPa – a ten-fold decrease) and XenoDerm (from 114.2 kPa to 85.3 kPa). An explanation for this discrepancy could be the influence of the liquid environment over the incubation time of two weeks. In contrast, for DED there was no significant change in Young's modulus apparent (144.4 kPa on day 1 and 181.4 kPa on day 14). In contrast to macroscopic appearance as a
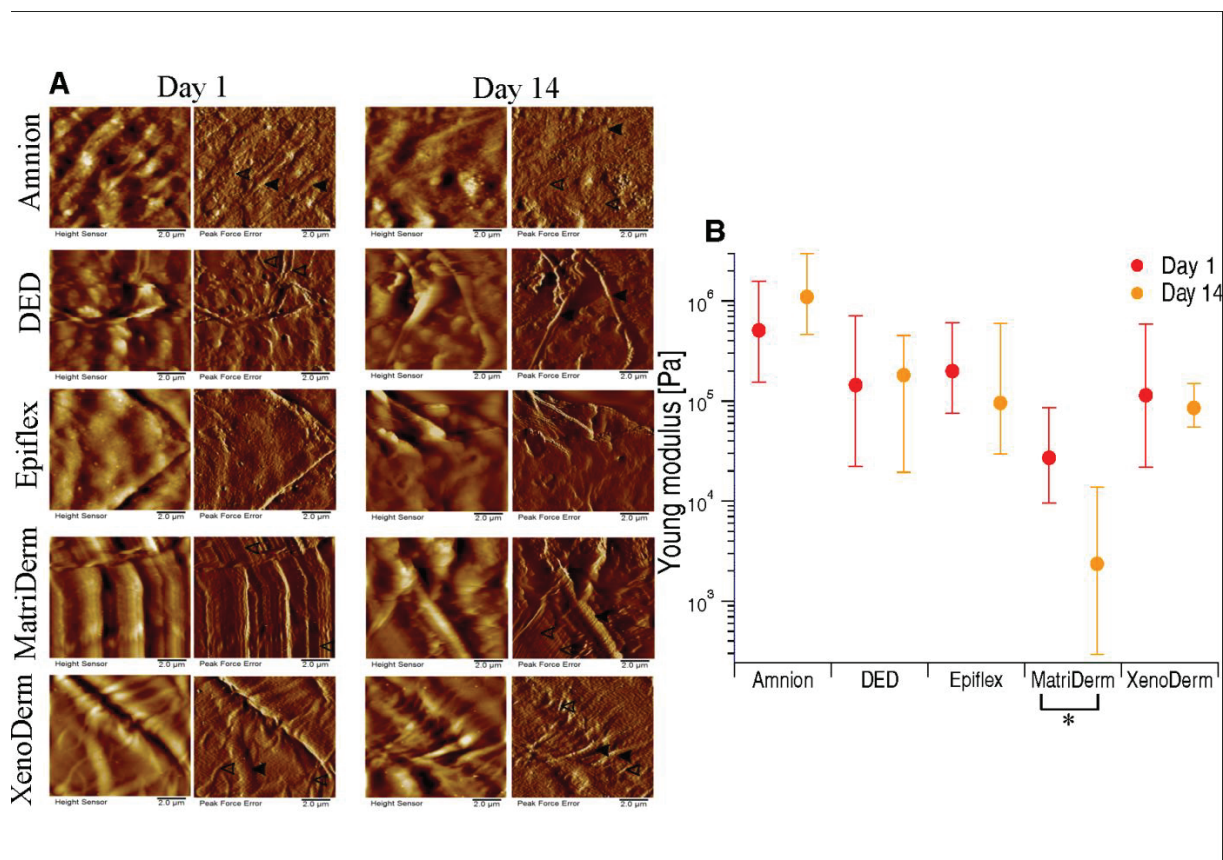

Figure 4.2. Influence of liquid environment on decellularized matrix topography and mechanics. (A) Height and Peak force error images from PeakForce Tapping imaging show no larger effect of liquid between day 1 and day 14 on Amnion and XenoDerm matrix topography. In MatriDerm, some collapsed fibres were observed along with well aligned fibres on day 14. Random fibres were running along DED and plain surfaces were seen in Epiflex. (B) The median of Young's modulus values were obtained from force maps that enable the assessment of the stiffness of decellularized matrices between day 1 and day 14. There is a change in Young's modulus value observed in Epiflex, MatriDerm and XenoDerm matrices but not in DED or Amnion on day 14 which is due to the impact of liquid environment. *Filled* and *open arrow heads* indicates the thick and thin fibres, respectively. Statistical results are reported in Methods and Experimental Design section.

shiny membrane, Amnion was characterized to be a "super stiff" ECM substrate. We could not quantify the Young's modulus due to the soft cantilever used. The quoted values (0.5 MPa on day 1 and 1.09 MPa on day 14) shown in Figure. 4.2B reflects the comparatively softest areas (calculated from fewer force curves- Supplementary Figure. 4.11B) within the sample and should not be over interpreted. Together, our results show that the liquid environment has no significant effect on the structures of the decellularized matrices except for DED and Epiflex and has a large effect on the mechanics of MatriDerm over a period of 14 days. As a consequence, any notable effect seen after the incubation with cells was due to the presence of the cells and not exclusively an effect of the liquid environment.

Changes in decellularized matrices topography and mechanics by fibroblast

The structure and mechanics of tissues are constantly altered biochemically as well as by cellular traction forces, which results in permanent topographical and mechanical changes of the extracellular matrix microenvironment. Earlier reports observed a reversible nonlinear strain stiffening (van Helvert and Friedl, 2016) and irreversible plasticity (Kim et al., 2017) of collagen ECM networks due to cell traction forces. In order to measure the resulting ECM topographical and mechanical changes induced by cellular activity, three different fibroblast types derived from different sites of the same patient (normal, scar and Dupuytren's fibroblast) were grown on the five different decellularized matrices used here. As presented above, we monitored the effect of liquid environment on the topography and stiffness of decellularized matrices. In a similar way, matrices were topographically imaged and mechanically mapped (at least 10 different positions) before cell culture, with cells seeded on them and finally after removing cells.

As stated above, the topography of all five decellularized matrices before adding cells was recorded using PeakForce Tapping AFM mode and the corresponding height and peak force error images are shown in Figure. 4.3A (Amnion), in Figure. 4.4A (DED), in Figure. 4.5A (Epiflex), in Figure. 4.6A (MatriDerm) and in Figure. 4.7A (XenoDerm). From the topographic images of Amnion, DED and XenoDerm, we did not find any larger structural differences within the three independent experiments of individual matrices (before adding cells) proving that matrices were quite homogenous within the same category. In contrast, three independent experiments on individual Epiflex and MatriDerm matrices showed some variability in their topography. In Epiflex (Figure. 4.5), two distinct regions were observed: corrugated surface and very thin fibres (0.078 µm thickness) running under the corrugated surface. In some specimen, only the
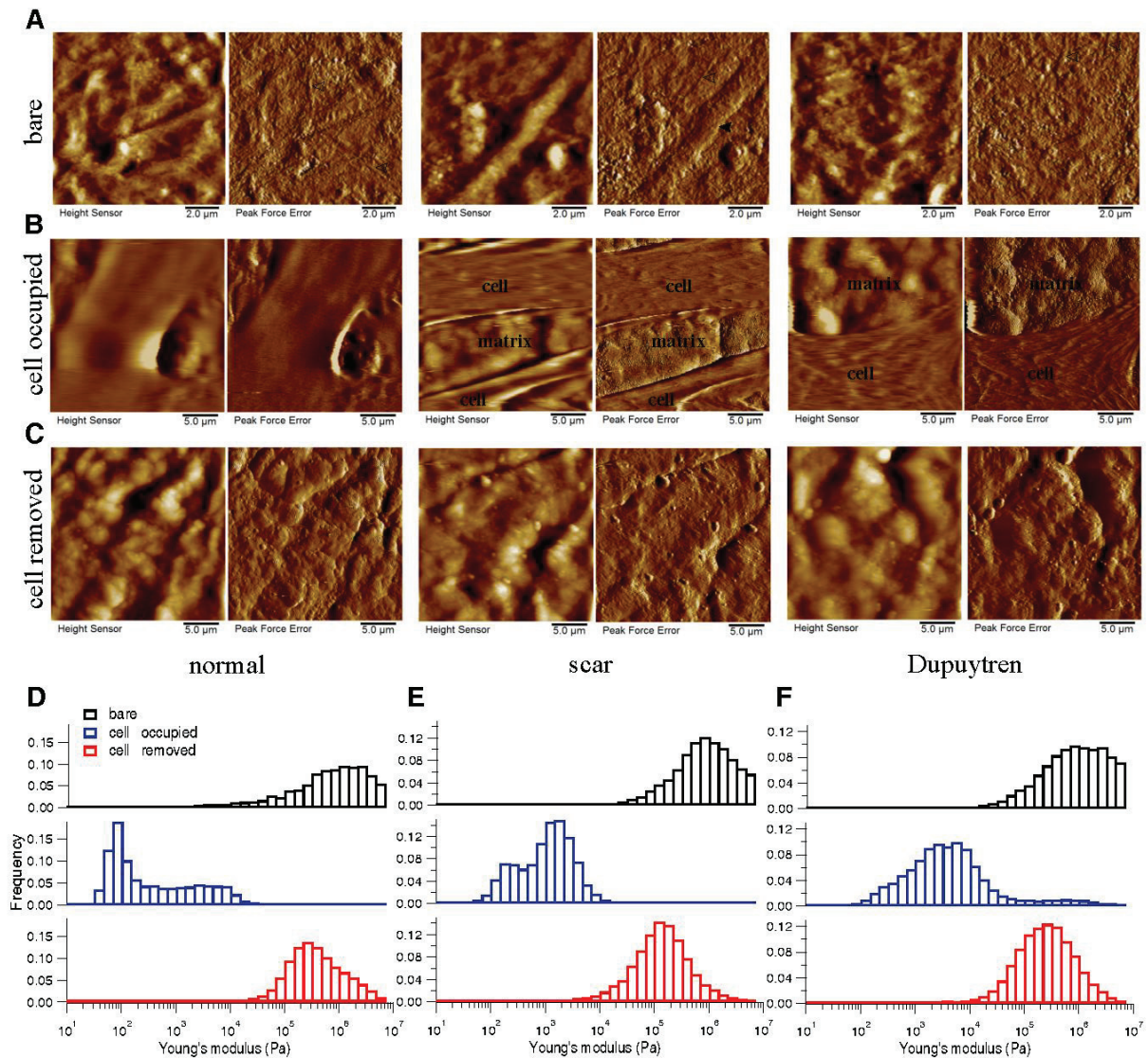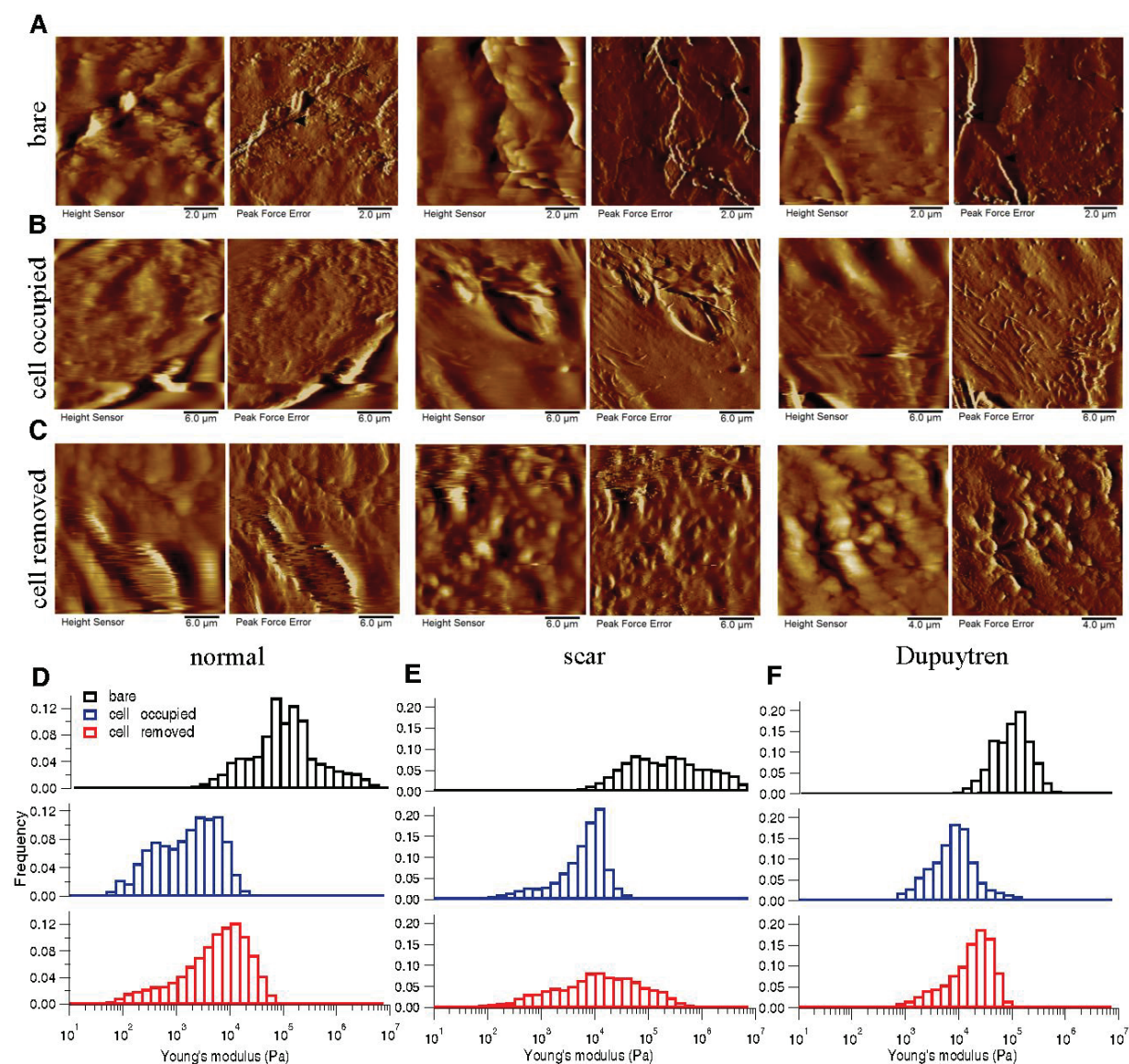
Figure 4.3. Changes in decellularized matrix topography and mechanics assessed in Amnion. (A) Height and PeakForce error images of the bare matrix show the presence of very thin and thick irregular fibres in bare matrix. (B) After seeding and culture of normal, scar and Dupuytren's fibroblasts for two weeks, height and PeakForce error images show the presence of fibroblasts on Amnion matrix. (C) After removing the cells, height and PeakForce error images show the disappearance of fibres. Histograms of Young's modulus values of bare (*black bar*), cell-occupied (*blue bar*), and cell- removed Amnion matrix (*red bar*), for normal (D), scar (E) and Dupuytren's fibroblasts (F). The shifts in the histograms show the change in Amnion matrix mechanics effected by all three fibroblast types. The respective medians of Young's modulus values are shown in Supplementary Figure. 4.12A. *Filled* and *open arrow heads* indicates the thick and thin fibres, respectively.

corrugated surface was observed. In MatriDerm, thick fibres were seen with different geometries like tailored and totally compacted shapes. Histograms from AFM mechanical maps for bare matrix before adding fibroblasts were plotted for each matrix, i.e. Amnion (Figure. 4.3D, E & F), DED (Figure. 4.4D, E & F), Epiflex (Figure. 4.5D, E & F), MatriDerm (Figure. 4.6D, E & F) and XenoDerm (Figure. 4.7D, E & F) (black bar plots). Their respective medians of Young's modulus values were plotted in Supplementary Figure. 4.12A, B, C, D & E (black filled circles) and listed in Table 4.1. A large difference in the modulus values was

observed for all three independent experiments with regard to each decellularized matrix: Amnion (mostly infinite pascal for all three independent experiments- 760.6 kPa, 751.3 kPa and 851.7 kPa), DED (65.7 kPa, 171.6 kPa and 73 kPa), Epiflex (250.6 kPa, 139 kPa and 101.6 kPa), MatriDerm (51.4 kPa, 29.8 kPa and 28.1 kPa) and XenoDerm (119.2 kPa, 82.9 kPa and 70.8 kPa) which show the heterogeneity within each decellularized matrix mechanical properties but are not significant.

Figure 4.4. Changes in decellularized matrix topography and mechanics assessed in DED. (A) Height and PeakForce error images of bare matrix show the presence of irregular structures of ECM components in the bare matrix. (B) After cell culture for two weeks, height and PeakForce error images show the matrix with normal, scar or Dupuytren's fibroblasts. (C) After removing the cells, height and PeakForce error images show the matrix topography. Histograms of Young's modulus values of bare (*black bar*), cell-occupied (*blue bar*), and cell-removed DED matrix (*red bar*), for normal (D), scar (E) and Dupuytren's fibroblasts (F). The shifts in the histograms show the change in DED matrix mechanics by all three fibroblast types. The respective medians of Young's modulus values are shown in Supplementary Figure. 4.12B. *Filled* and *open arrow heads* indicates the thick and thin fibres, respectively.

Three fibroblast cell types were grown on these five decellularized bare matrices for two weeks in order to evaluate the topography and stiffness of our cell populated matrices. Amnion (Figure. 4.3B), DED (Figure. 4.4B), Epiflex (Figure. 4.5B), MatriDerm (Figure. 4.6B) and XenoDerm (Figure. 4.7B) shows the overall topography of cells on decellularized matrices in which all three fibroblasts remains viable and exhibit regular cell shape and spread and cytoskeletal organisation. In some of the PeakForce AFM micrographs, we were able to show both cell and ECM topography and revealed the change in ECM topography (Figure. 4.3B & 4.5B). Histograms from AFM mechanical maps for cells occupied matrix of all three fibroblasts were plotted for each matrix - Amnion (Figure. 4.3D, E & F), DED (Figure. 4.4D, E & F), Epiflex (Figure. 4.5D, E & F), MatriDerm (Figure. 4.6D, E & F) and XenoDerm (Figure. 4.7D, E & F) (blue bar plots). These histograms showed a shift in the cell occupied matrix bar (blue) comparative to bare matrix bar (black). To measure quantitatively the mechanical heterogeneity of cell and ECM stiffness, the median of Young's modulus values was plotted in Supplementary Figure. 4.12A, B, C, D & E- blue filled circles and listed in Table 4.2. Comparatively, the median Young's modulus of normal fibroblast populated matrices (0.2 kPa on Amnion, 1.5 kPa on DED, 0.3 kPa on Epiflex, 1.9 kPa on MatriDerm and 0.4 kPa on XenoDerm) are smaller than those of scar (0.9 kPa on Amnion, 5.9 kPa on DED, 1.4 kPa on Epiflex, 11.5 kPa on MatriDerm and 1.8 kPa on XenoDerm) and Dupuytren's fibroblasts (2.9 kPa on Amnion, 6.7 kPa on DED, 3.3 kPa on Epiflex, 13.2 kPa on MatriDerm and 2 kPa on XenoDerm) populated matrices. Here, Young's
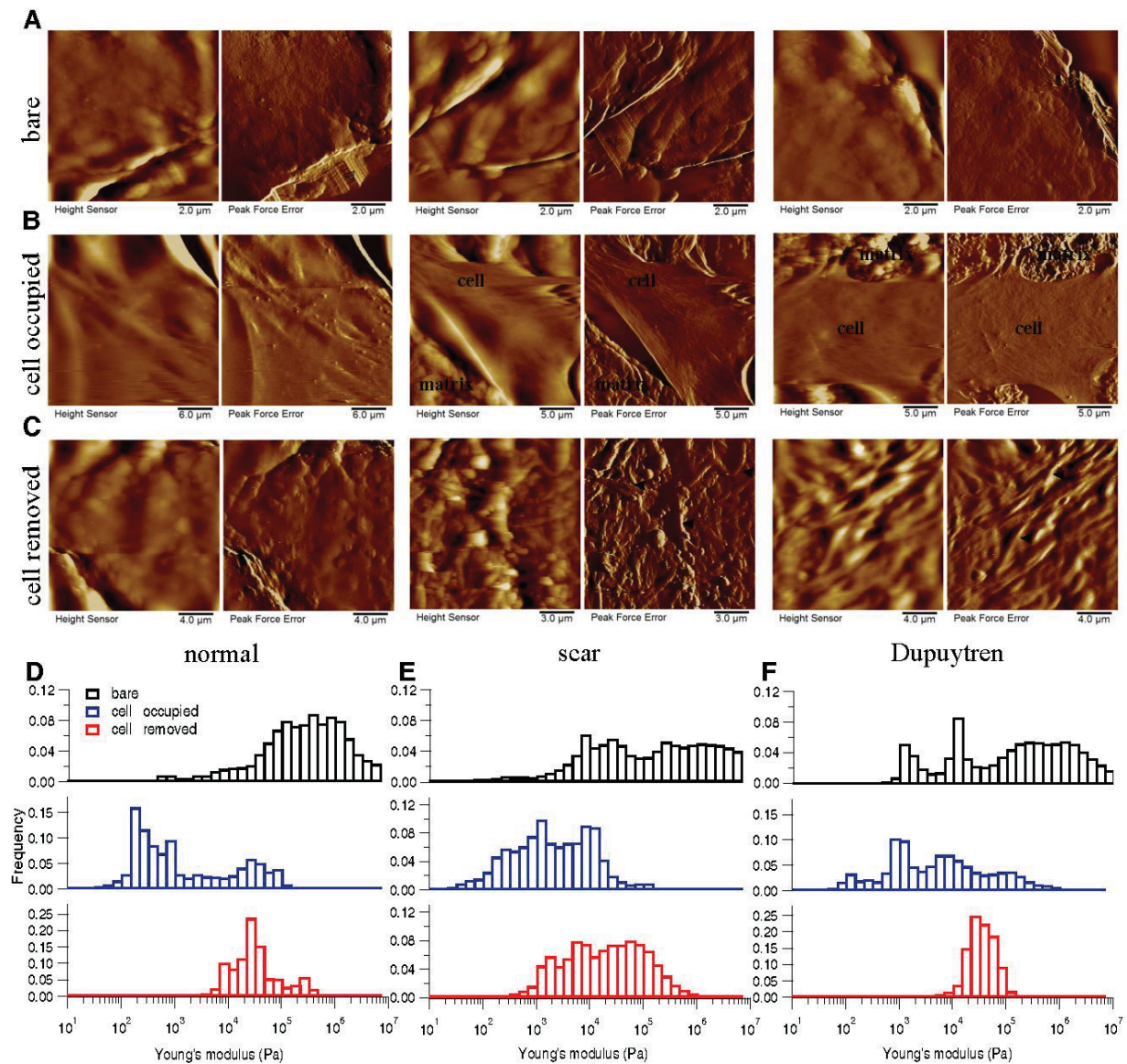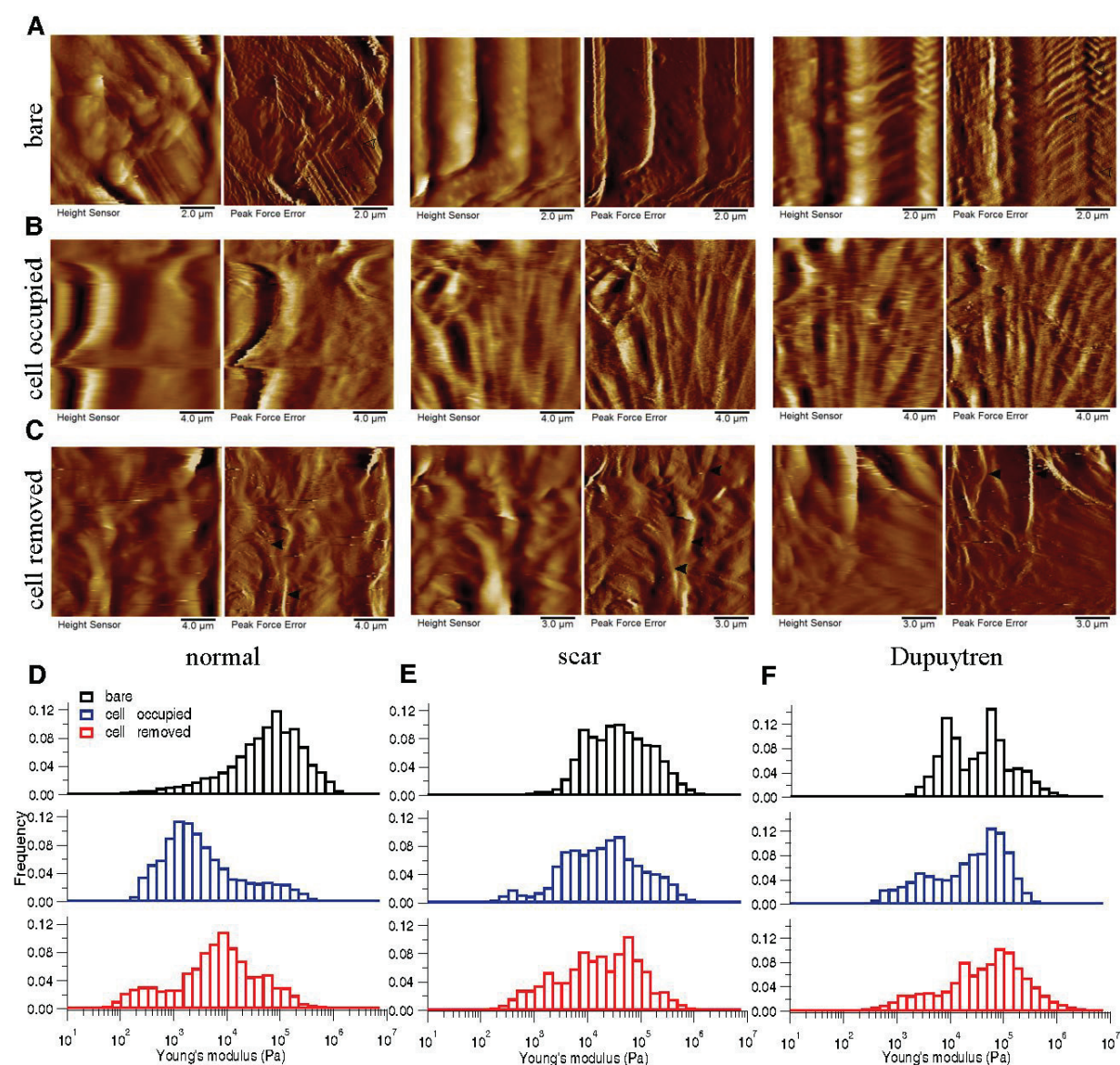
Figure 4.5. Changes in decellularized matix topography and mechanics assessed in Epiflex. (A) Height and PeakForce error images of bare matrix show the presence of bigger blobs with some very thin fibres in the bare matrix. (B) After culture the three fibroblast types for two weeks, height and PeakForce error images show the topography of matrix with respective cells. (C) After removing the cells, height and PeakForce error images shows the change in matrix topography. Histograms of Young's modulus values of bare (*black bar*), cell-occupied (*blue bar*), and cell-removed Epiflex matrix (*red bar*), for normal (D), scar (E) and Dupuytren's fibroblasts (F). The shifts in the histograms show the change in Epiflex matrix mechanics by all three fibroblast types. The respective medians of the Young's modulus values are shown in Supplementary Figure. 4.12C. *Open arrow heads* indicates the thin fibres.

modulus median values reflect both cell and ECM stiffness properties as some force maps were recorded on cell and ECM regions. Fluorescence images (Figure. 4.8) show the stress fibre network of normal, scar and Dupuytren's fibroblasts on Amnion, DED, Epiflex, MatriDerm and XenoDerm. On all matrices, we observed that normal skin fibroblasts exhibited no stress fibres than scar or Dupuytren fibroblasts, which correlates to their respective lower and higher Young's modulus values.

To determine if the fibroblast culture could alter the topography and mechanics of the decellularized matrices themselves, we repeated the measurements after removing the cells by chemical treatment (see Methods and Experimental Design). Height and Peakforce error images (Figure. 4.3, 4.4, 4.5, 4.6 & 4.7C) show enormous differences between the decellularized matrices, before cell seeding and after cell removal. From AFM imaging, we were not able to see any cellular debris or remnants on the matrices. With regard to Amnion (Figure. 4.3C), we found no ECM fibres after cell removal and the matrix structure was more corrugated from all three fibroblast removed matrices. For DED matrix after fibroblasts removal (Figure. 4.4C), it was difficult to find any difference in ECM topography, we could only appreciate a decrease in the number of fibres and the presence of bigger blobs after cell removal. Despite of the corrugated surface in Epiflex (Figure. 4.5C), we could see thicker and uneven fibres (0.7-0.9 µm thickness) exclusively
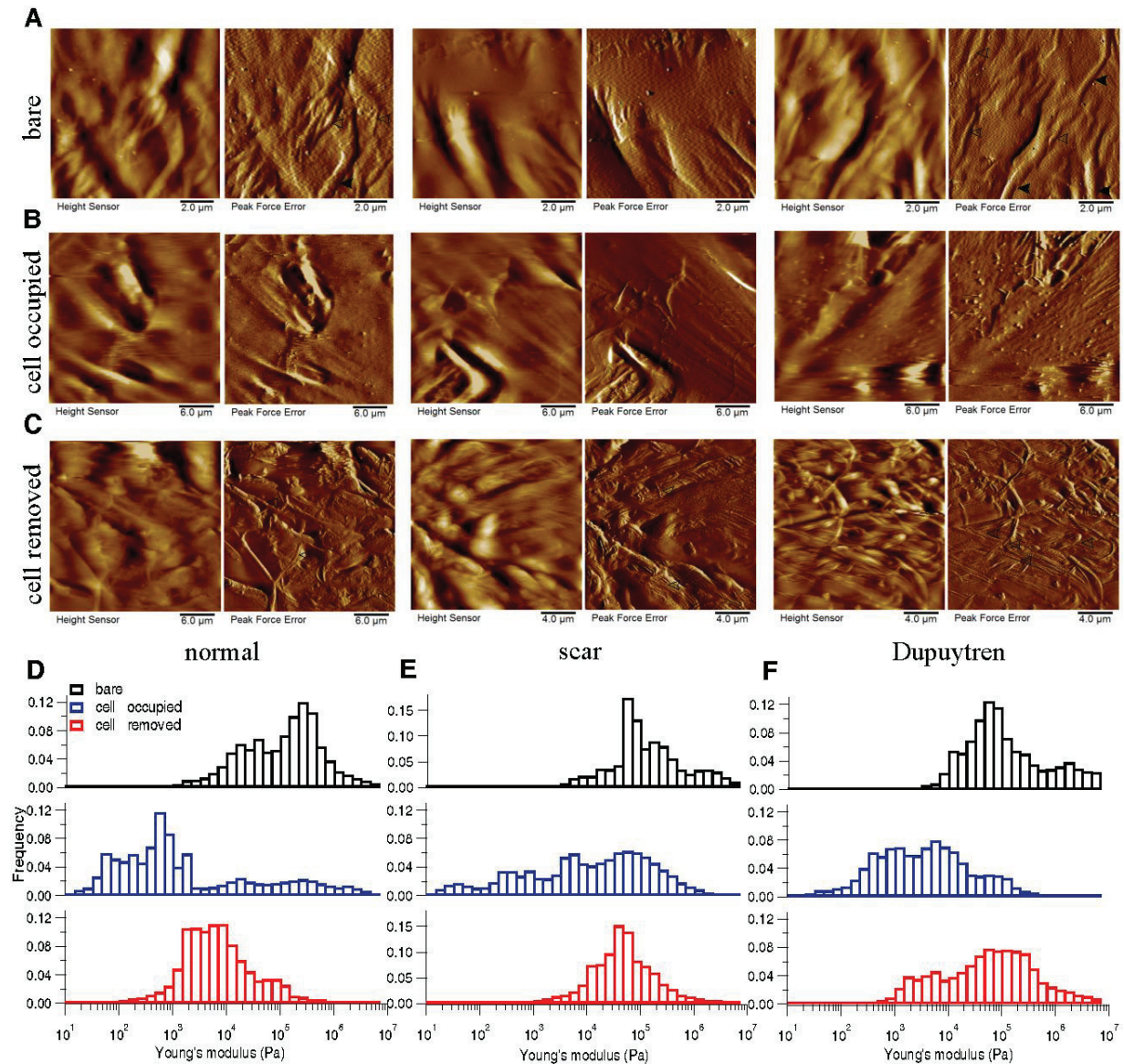
Figure 4.6. Changes in decellularized matix topography and mechanics assessed in MatriDerm. (A) Height and PeakForce error images of bare matrix show the presence of tailored and more dense fibres running along the bare matrix. (B) After fibroblast culture for two weeks, height and PeakForce error images show the matrix with cells. (C) After removing the cells, height and PeakForce error images show the change in matrix topography. Histograms of Young's modulus values of bare (*black bar*), cell-occupied (*blue bar*), and cell-removed MatriDerm matrix (*red bar*), for normal (D), scar (E) and Dupuytren's fibroblasts (F). The shifts in the histograms show the change in MatriDerm matrix mechanics by all three fibroblast types. The respective medians of the Young's modulus values are shown in Supplementary Figure. 4.12D. *Filled* and *open arrow heads* indicates the thick and thin fibres, respectively.

on samples that were previously populated with scar or Dupuytren's fibroblasts, whereas there were only smaller blobs when matrices had been seeded with normal fibroblast. In case of MatriDerm, thin fibres initially found in the bare matrix (Figure. 4.6A) disappeared after cell removal (Figure. 4.6C), giving place to more irregularly aggregated and thick fibres (1.3-1.4 µm thickness) in all three fibroblast removed matrices. In XenoDerm (Figure. 4.7C), the thick and bundled fibres were disrupted to form irregular and disarranged thin fibres (0.2-0.4 µm thickness) after fibroblasts removal.

These topographical modifications after fibroblast culture were accompanied by a softening of the matrices. In fact, from the mechanical mapping data, we observed a shift in the histograms bar compared to bare (black) and cell occupied (blue) matrix in Amnion (Figure. 4.3D, E & F), DED (Figure. 4.4D, E & F), Epiflex (Figure. 4.5D, E & F), MatriDerm (Figure. 4.6D, E & F) and XenoDerm (Figure. 4.7D, E & F) (red bar plots) matrices after cell removal, for all three fibroblast types. The corresponding median of Young's modulus values for all fibroblast-removed matrices were plotted in Supplementary Figure. 4.12A, B, C, D & E (red filled circles) and listed in Table 4.3. The median Young's modulus values of bare, cell-populated and cell-removed of all five decellularized matrices that were seeded with normal or pathological (scar and Dupuytren's)

Figure 4.7. Changes in decellularized matix topography and mechanics assessed in XenoDerm. (A) Height and PeakForce error images of bare matrix show the presence of thick fibres running along the bare matrix. (B) After culturing normal, scar or Dupuytren's fibroblasts for two weeks, height and PeakForce error images show the matrix with cells. (C) After removing the cells, height and PeakForce error images show the change in matrix topography. Histograms of Young's modulus values of bare (*black bar*), cell-occupied (*blue bar*), and cell-removed XenoDerm matrix (*red bar*), for normal (D), scar (E) and Dupuytren's fibroblasts (F). The shifts in the histograms show the change in XenoDerm matrix mechanics by all three fibroblast types. The respective medians of the Young's modulus values are shown in Supplementary Figure. 4.12E. *Filled* and *open arrow heads* indicates the thick and thin fibres, respectively.

Table 4.1: The median (bold values) Young's moduli (kPa) values of bare matrices before seeding with normal, scar or Dupuytren's fibroblasts.

Matrix	Amnion			DED			Epiflex			MatriDerm			XenoDerm		
Fibroblast type	25th	**Median**	75th	25th	**Median**	75th	25th	**Median**	75th	25th	**Median**	75th	25th	**Median**	75th
normal	552.50	**760.67**	1383.11	37.74	**65.72**	83.95	182.60	**250.62**	557.33	36.21	**51.4**	78.84	94.79	**119.25**	165.97
scar	445.19	**751.33**	1131.38	124.71	**171.64**	461.16	125.86	**139.03**	934.30	19.67	**29.86**	58.54	35.25	**82.93**	185.75
Dupuytren	563.50	**851.72**	1582.59	35.54	**73.06**	46.18	94.13	**101.62**	487.37	20.41	**28.17**	34.80	39.73	**70.89**	321.44

Table 4.2: The median (bold values) Young's moduli (kPa) values of cell-occupied matrices when seeded with normal, scar or Dupuytren's fibroblasts.

Matrix	Amnion			DED			Epiflex			MatriDerm			XenoDerm		
Fibroblast type	25th	**Median**	75th	25th	**Median**	75th	25th	**Median**	75th	25th	**Median**	75th	25th	**Median**	75th
normal	0.09	**0.16**	1.43	1.08	**1.49**	2.10	0.16	**0.33**	0.73	1.10	**1.92**	5.55	0.31	**0.41**	0.67
scar	0.61	**0.94**	0.85	3.51	**5.94**	3.32	1.01	**1.45**	5.01	7.89	**11.48**	20.88	1.53	**1.79**	14.55
Dupuytren	1.94	**2.96**	5.31	3.44	**6.76**	4.30	2.47	**3.27**	11.73	10.66	**13.2**	22.62	1.51	**2.03**	5.49

Table 4.3: The median (bold values) Young's moduli (kPa) values of cell-removed matrices after seeding with normal, scar or Dupuytren's fibroblasts.

Matrix	Amnion			DED			Epiflex			MatriDerm			XenoDerm		
Fibroblast type	25th	**Median**	75th	25th	**Median**	75th	25th	**Median**	75th	25th	**Median**	75th	25th	**Median**	75th
normal	109.16	**228.73**	261.16	3.52	**5.18**	6.49	10.18	**23**	16.82	4.14	**5.82**	11.62	2.96	**4.89**	8.09
scar	578.42	**108.15**	115.15	7.43	**9.83**	27.14	12.34	**16.49**	41.83	10.51	**14.15**	33.42	20.71	**37.1**	50.40
Dupuytren	110.82	**193.75**	240.72	9.25	**16.41**	11.05	8.82	**27.22**	14.53	25.82	**35.4**	61.27	34.40	**42.57**	113.11

fibroblasts, respectively, are presented in Table 4.1, 4.2 or 4.3, accordingly. The comparative change in Young's modulus values of bare and cell-removed matrices reveals the extent of matrix mechanics and remodelling induced by fibroblasts. Bare Amnion is a very stiff matrix and shows high Young's modulus values (MPa) – even the calculated Young's modulus values (Table 1) from fewer force curves which are recorded in comparatively softest areas within the stiff matrix. Mostly, all force curves evaluated from cell-removed Amnion matrices show a gradual decrease in Young's modulus. The shift in the peak of the histograms (Figure. 4.3,4.4,4.5,4.6&4.7 D, E and F) clearly shows the unique changes in ECM elasticity before adding cells (black bar), with cells (blue bar), and after removing the cells (red bar). In particular, normal fibroblasts soften the matrices by a factor of 10 compared to scar and Dupuytren's fibroblasts in all matrices contrasting scar and Dupuytren's fibroblasts that have a minor effect on matrix softening. This important finding is highlighted by biophysical measurements with MatriDerm. Here, we observed the median Young's modulus values from bare matrices before adding cells (29.86 kPa and 28.17 kPa) and cell-removed matrices (14.15 kPa and 35.4 kPa) only when pathological (scar and Dupuytren's) fibroblasts were seeded on MatriDerm matrices (Figure. 4.6). Taking into account the influence of liquid on MatriDerm mechanics (Figure. 4.2B), these pathological fibroblasts greatly maintained the matrix
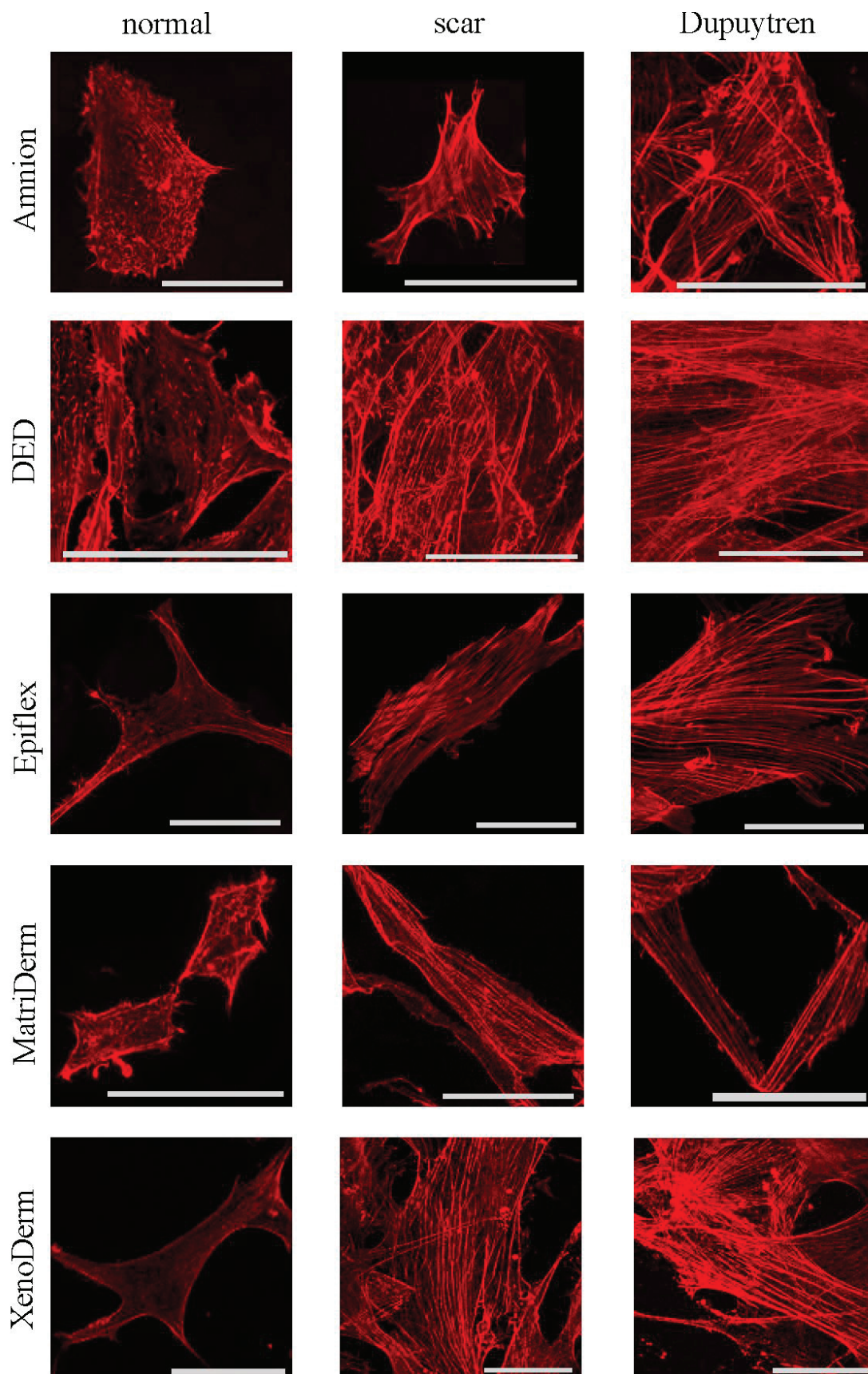
Figure 4.8. Confocal images of normal, scar and Dupuytren fibroblasts seeded on different matrices. Fibroblast stress fibre formation in decellularized matrices is assessed by rhodamine phalloidin actin fluorescent staining. Fluorescence images show the presence of thick stress fibres in pathological fibroblasts (scar and Dupuytren's) that results in higher values of cell mechanics compared to normal fibroblasts that express less or

74

no stress fibres on all decellularized matrices and therefore impress as softer. Scale bar are 50 μm.

stiffness. Finally, these results clearly demonstrate that fibroblasts reciprocally influence their ECM microenvironment topography and mechanics in general and that the pathological scar and Dupuytren's fibroblasts may play an important role in fibrosis by tissue stiffening in particular.

ECM composition dependent cell stiffness

Many studies have reported that ECM stiffness largely influences many cell characteristics such as spreading, adhesion and mechanics (C. Rianna and Radmacher, 2017; Solon et al., 2007; Vertelov et al., 2016; Yeh et al., 2017). However, the relevance of ECM composition on cell mechanics has been scarcely explored. Here, we studied the mechanical properties of normal, scar and Dupuytren's fibroblast on five different decellularized matrices. In order to evaluate the mere cell stiffness, the mechanical maps obtained from matrices after plating cells were carefully analyzed and treated to eliminate the stiffness contribution of the matrix. As shown in Supplementary Figure. 4.13, the slope of force curves of the matrices greater than 0.375 were filtered out from the mechanical maps thus resulting in the force curves that only identify cell stiffness (see Methods and Experimental Design section). This value was identified by carefully measuring the slope on matrix and cells from each force map which is able to distinguish cell and matrix regions in better resolution force maps and finding a threshold value between the two. The median Young's modulus (Figure. 4.9) of normal, scar and Dupuytren's fibroblasts and their respective values in Table 4.4 show that they were softer on three matrices, i.e. Amnion, Epiflex and XenoDerm. In contrast, all three fibroblast cell types were stiffer when seeded on DED and MatriDerm. This mechanical difference could be possibly due to different ECM composition of these decellularized matrices, since their stiffness is quite comparable, except for Amnion (Figure. 4.2B). In fact, all decellularized matrices used here consist of different compositions of collagen, elastin and other varying ECM structural and functional components (Haslik et al., 2007; Kim et al., 2013; Mirastschijski et al., 2013; Roessner et al., 2012; von Versen-Hoeynck et al., 2008). In each decellularized matrix that was seeded
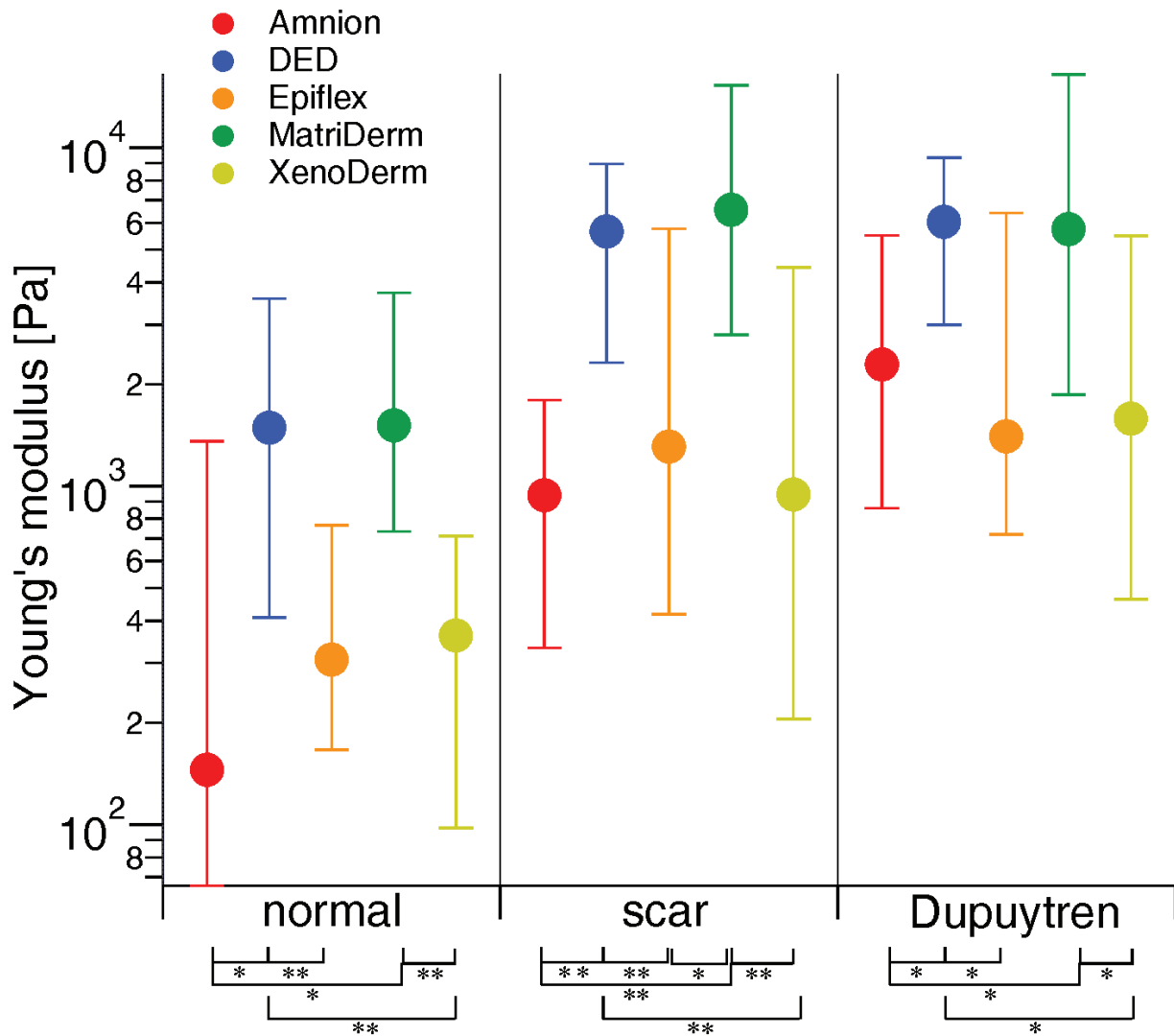
Figure 4.9. Cell stiffness is influenced by ECM composition, measured with AFM. After filtering the values of native matrices Young's modulus values from cell-occupied matrices, the median of Young's modulus values of normal, scar and Dupuytren's fibroblasts shows that the composition of the different decellularized matrices, e.g. Amnion, DED, Epiflex, MatriDerm or XenoDerm, determines the fibroblast mechanics. The respective medians of the Young's moduli values were presented in Table 3.4. Statistical results are reported in Methods and Experimental Design section.

with cells, even after exclusion of the matrix stiffness, the pathological (scar and Dupuytren's) fibroblasts were stiffer than normal fibroblasts. Fluorescence images (Figure. 4.8) clearly show that the cell's stress fibre network has a strong role in determination of cell stiffness. Interestingly, cell stiffness depends as well on the decellularized matrix composition along with its stiffness. Note that the error bars from Figure. 4.9 are large, which is due to the fact that force maps were recorded on different cellular regions (nucleus, cell body and periphery), presenting therefore a larger range of Young's modulus values.

Table 4.4: The median (bold values) Young's moduli (kPa) values of normal, scar and Dupuytren's fibroblasts from cell-populated matrix category filtering the matrix modulus values.

Matrix	Amnion			DED			Epiflex			MatriDerm			XenoDerm		
Fibroblast type	25th	**Median**	75th	25th	**Median**	75th	25th	**Median**	75th	25th	**Median**	75th	25th	**Median**	75th
normal	0.07	**0.14**	1.21	1.07	**1.49**	2.09	0.14	**0.31**	0.46	0.77	**1.51**	2.21	0.26	**0.36**	0.35
scar	0.60	**0.94**	0.85	3.33	**5.65**	3.29	0.89	**1.31**	4.45	3.76	**6.55**	8.71	0.74	**0.94**	3.47
Dupuytren	1.43	**2.28**	3.22	3.03	**6.03**	3.30	0.68	**1.4**	5.01	3.88	**5.75**	10.71	1.12	**1.58**	3.90

Fibroblast invasion into the decellularized matrices

Cellular invasion into a matrix is found both in physiological and pathological conditions. While fibroblasts invade the wound bed and initiate repair processes by synthesizing new matrix components, excessive matrix production is found in various fibrotic diseases like idiopathic pulmonary fibrosis and Dupuytren's contracture. In malignancies, e.g. scirrhous gastric carcinoma (SGC), stromal fibroblasts mediate the ECM microenvironment mechanical remodeling and the invasion of carcinoma cells (Yamaguchi et al., 2014). To quantitatively address the invasion of fibroblasts into the decellularized matrices, we acquired confocal z stack images on matrices for normal and pathological (scar and Dupuytren's) fibroblasts, which were fluorescently labeled for actin with rhodamine phalloidin. Typical 3D plots (Figure. 4.10A) generated from z stacks taken at different positions on individual matrices show a distinct pattern of invasion for each fibroblast type. This invasive pattern made it possible to distinguish between normal, scar and Dupuytren's fibroblast in decellularized matrices. Viewing the z-axis (µm) of 3D plots, the degree of invasion by fibroblast can be seen. In Amnion (Figure. 4.10A), DED (Supplementary Figure. 4.14), MatriDerm (Supplementary Figure. 4.16) and XenoDerm (Supplementary Figure. 4.17), pathological (scar and Dupuytren's) fibroblasts were more invasive than normal fibroblasts. This contrasted findings with Epiflex (Supplementary Figure. 4.15) where normal fibroblasts showed higher invasiveness than pathological fibroblasts. The fluorescence intensity versus invasion depth calculated from z stacks were plotted for the three fibroblast cell types

A
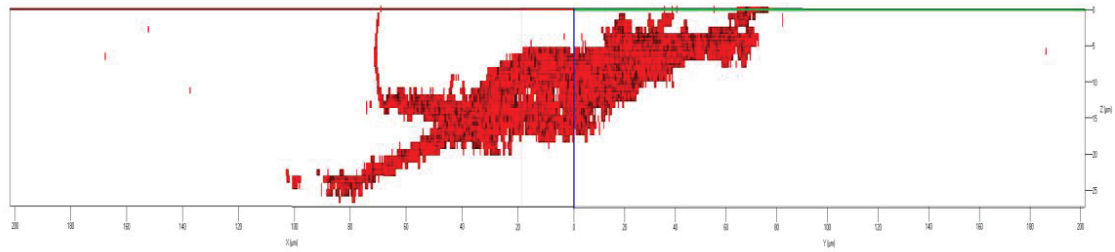
normal
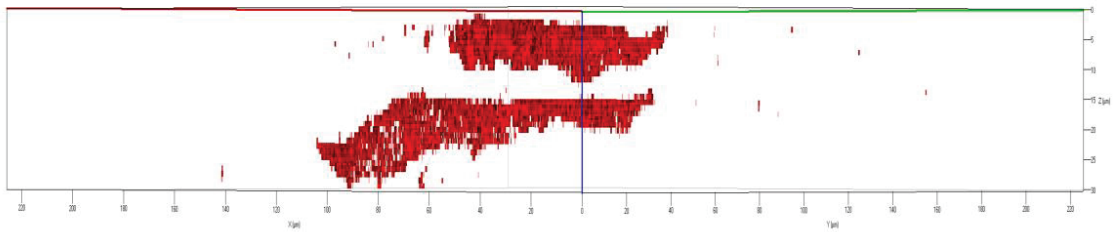
scar
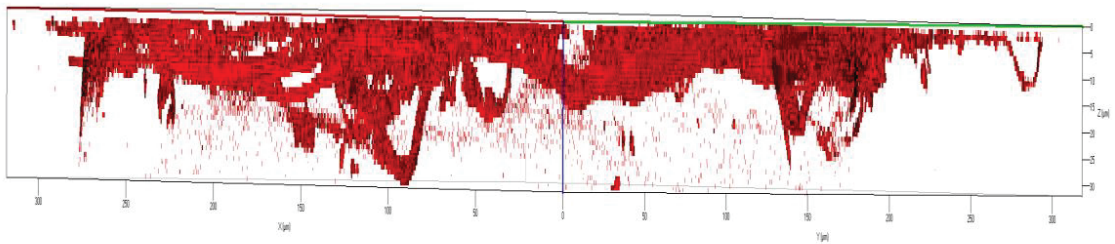
Dupuytren

B
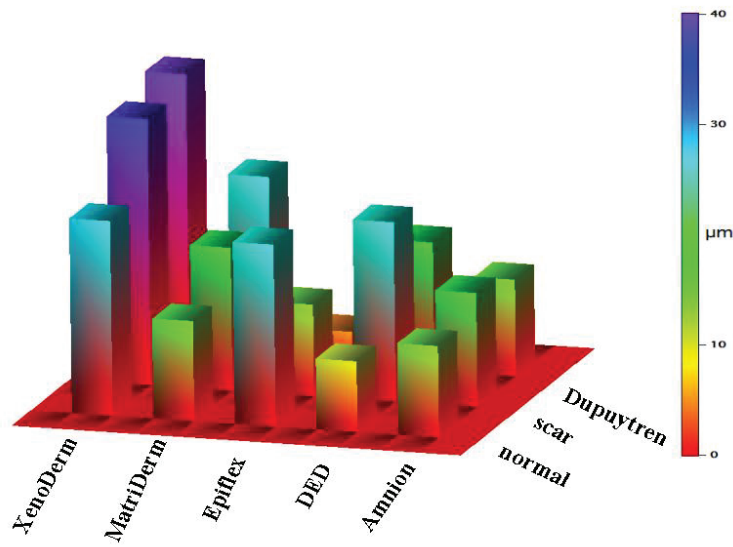
Figure 4.10. Fibroblast invasion into decellularized matrices, studied with the confocal microscope. (A) Representative 3D plots were created from the z stack images and show the invasion of normal, scar and Dupuytren's fibroblasts into the Amnion decellularized matrix. Pathological (scar and Dupuytren's) fibroblasts

are more invasive than normal fibroblasts into this matrix. The remaining plots of fibroblasts invading into the other matrices are shown in Supplementary Figure. 4.14-4.17 (B) The 3D color category plot extrapolated from Supplementary Figure. 4.18 represents the value range of normal, scar and Dupuytren's fibroblast invasion into all five decellularized matrices.

(Supplementary Figure. 4.18A-E). From this plot, a 3D color category plot (Figure. 4.10B) was generated by calculating the 50th percentile of the invasion depth for every fibroblast cell type on individual matrices. Within the matrices, normal fibroblasts invaded largely in Epiflex and XenoDerm with an invasion depth falling in the range of 20-25 µm and 25-30 µm, respectively. With regard to Amnion, DED and MatriDerm, they invaded with an invasion depth falling in the range of 10-15 µm. Pathological fibroblasts invaded DED and MatriDerm matrices with an invasion depth in the range between 20 µm and 25 µm while invasion of the XenoDerm matrix was very high with a depth in the range of 35 µm and of Amnion and Epiflex matrix with a smaller depth of 5-15 µm. Among all the decellularized matrices, all three fibroblast types showed highest invasiveness in collagen rich XenoDerm matrix. Even in XenoDerm matrix, scar and Dupuytren's fibroblasts were more invasive than normal fibroblasts. From the AFM PeakForce Tapping images, no micro scale pores were seen on any of the five decellularized matrices. This implies that the presence of fibroblasts inside the matrix or the tendency to infiltrate it depends on the invasive behaviour of the corresponding cell type. These results clearly demonstrate a higher invasive behaviour of pro-fibrotic scar and Dupuytren's fibroblasts in contrast to normal dermal fibroblasts.

4.4 Discussion

We have demonstrated that different types of fibroblasts isolated from the same patient are capable of remodelling the topography and elasticity of decellularized matrices in different ways. In particular, by obtaining AFM peak force images and mechanical force maps, we showed the interdependency of cell and ECM mechanics in these various decellularized matrices. Z stack images from confocal microscopy provided additional quantitative information on cell invasion into matrices, revealing the variable degree of cell invasion and actin stress fibre formation of fibroblasts in different matrices. Additionally, we showed that cell stiffness strongly varies depending on respective decellularized matrix which has different mechanical and biochemical properties (Figure. 4.9). In order to follow the cell and ECM mechanics simultaneously, the experimental setup was designed in such a way that the same decellularized matrices were used for obtaining AFM peak force images and mechanical force maps in each category, e. g bare, cell-occupied and cell-removed matrices. This was done to establish the effect of cell culture on matrix topography and mechanics with respect to

each fibroblast type (normal, scar and Dupuytren). As these matrices are basically created for wound healing and tissue regeneration applications, we have selected these five matrices in order to investigate ECM maintenance of fibroblasts by topographical and mechanical evaluation. These matrices have different topography, mechanical stiffness and biochemical compositions. Taking into account the presence of collagen in all matrices, there are other varying ECM components present in these matrices. Histochemical and immunofluorescence analysis from earlier studies shows that Amnion contains collagen I, III and IV, laminin, elastin and fibronectin (Wilshaw et al., 2006), DED contains collagen I, III, IV, V and VI, other glycosaminoglycans and glycoproteins (Rana et al., 2017), Epiflex contains collagen I, III and IV, laminin, fibronectin, vitronectin and hyaluronic acid (Roessner et al., 2012), MatriDerm contains collagen and elastin (Haslik et al., 2007) and XenoDerm contains collagen (Kim et al., 2013). Mostly, the topographic images of these matrices show the presence of fibres (thick and thin)- which could be both collagen and elastin. These fibres are harder to distinguish biochemically without any histochemical or fluorescence analysis. To favor the aim of this study, these mechanical, topographical and biochemical compositional varying matrices are suitable enough to observe the matrix remodeling by fibroblasts. While the hydration of elastin (Lillie and Gosline, 2002) and water sequestration by proteoglycans (Culav et al., 1999) modify ECM elasticity and swelling, we found that the liquid environment did not change the topography and elasticity of most of our decellularized matrices, at least within a range of 14 days (Figure. 4.2). A big change in Young's modulus value was solely found for MatriDerm matrix, even if the elasticity changes due to the liquid environment did not affect matrix topography. Previously, the exploration of cell mechanics and its influence on ECM mechanics was carried out on ECM protein coated polyacrylamide (PA) hydrogels (Shi et al., 2011; Solon et al., 2007) or directly on individual ECM components, mostly collagen (Friedrichs et al., 2007a; Kim et al., 2017; van Helvert and Friedl, 2016), which limits their mechanical evaluation in *in vivo* environments. Here, we prepared a decellularized human dermal matrix (DED) by the freezing and thawing method (Mirastschijski et al., 2013). This procedure preserves the ECM mechanical properties (Elder et al., 2010; Gilpin and Yang, 2017) and enables measuring direct cell and ECM micromechanics in their natural microenvironment, providing the cells with a complex and variegated amount of ECM signals. Along with other decellularized matrices, these natural scaffolds provide a more physiological support to conduct biological and biophysical experiments on the fundamental reciprocal interplay between cells and ECM.

Cells exert traction forces on their microenvironment which leads to ECM protein

realignment through reversible strain stiffening (van Helvert and Friedl, 2016) and as a consequence, ECM fibres enable long range stress transmission between cells (Ma et al., 2013). Intracellular actomyosin contractility enables wound closure (Abreu-Blanco et al., 2012; Sakar et al., 2016) and increases tissue stiffness (Samuel et al., 2011). Contractile stress fibres (Kreis and Birchmeier, 1980) act as a key element in fibroblast mechanics. Here, we performed mechanical force measurements and correlated our results with confocal microscopic images. Thereby, we could demonstrate that cutaneous scar and palmar fascial Dupuytren's fibroblasts expressed large stress fibres on all decellularized matrices which contributed to an increase in Young's modulus values of these cells in contrast to normal fibroblasts. Under the influence of mechanical tension and transforming growth factor-beta, fibroblasts differentiate into myofibroblasts during wound healing or tissue fibrosis (Hinz, 2009). In these environments, they exert larger traction stresses on substrates through expression of alpha smooth muscle actin (α-SMA) stress fibres. Our earlier results showed the existence of a myofibroblast like phenotype in Dupuytren's fibroblasts that expressed α-SMA positive stress fibres (Babu et al., 2018). In case of the dermal scar fibroblasts which previously (Babu et al., 2018) showed α-SMA positive but no large stress fibres, we observed the presence of large actin stress fibres in the present experiment. This phenomenon can be explained by the fact that the matrix biophysics governs the activation and differentiation of fibroblasts with transition into a protomyofibroblast/myofibroblast phenotype. These mechanical phenotypic and actin isoform genotypic characteristic differences were observed in normal and pathological (scar and Dupuytren's) fibroblasts (Babu et al., 2018). Another factor that could have contributed to the activation of fibroblasts with conversion into their contractile phenotype is the fact that we plated scar fibroblasts on substrates similar to their native environment in this study. For example, cells are stiffer in their native environment than when plated on glass (Xu et al., 2016) or plastic Petri dishes. Despite their phenotypic differences, all three fibroblast types modified the physical structure of the respective decellularized matrix they were seeded onto. Previously, AFM helped to visualise the changes in molecular weight, volume and average height of the ECM protein when coated on a glass coverslip. These measured changes give valuable information on the ECM degradation by cells (Kusick et al., 2005). Here, AFM PeakForce images of decellularized matrices after removing the cells clearly showed misaligned and aggregated ECM fibres and confirmed the ECM remodeling by cells. In addition, the mechanical stiffness of fibroblasts populated decellularized matrices was analyzed by quantitative force maps. Changes in quantitative force mapping were associated with changes in the matrix mechanical environment when the

bare and cell-removed matrices were compared.

Cells sense the mechanical properties of their extracellular matrix by exerting traction forces that are generated by intracellular contractile actin stress fibres. It has been shown that these traction forces linearly contribute to ECM degradation (Jerrell and Parekh, 2014). In accordance, pathological (scar and Dupuytren's) fibroblasts that express large actin stress fibres contribute to soften their microenvironment to a much lower degree than normal fibroblasts. Pro-fibrotic fibroblasts maintain their contractile behaviour via stiffening their environment which is explicitly seen with MatriDerm. Despite of the fact that the liquid environment influenced the Young's modulus to the order of 10^3 Pa in MatriDerm (Figure. 4.2B), the matrix elasticity increased to the order of 10^4 Pa after removing both scar or Dupuytren's fibroblast cell types (Supplementary Figure. 4.12D). Additionally, we confirmed that 1% trypsin, 0.5% Triton X-100 and 1% SDS that were used for cell removal had no effect on matrix topography and Young's modulus (Supplementary Figure. 4.19A & B). This further confirms that changes in topography and mechanics observed in cell-removed matrices are effected by the cells that had been plated onto the matrices. Our results show clearly that contractile myofibroblasts of a dermal scar or palmar fascial Dupuytren's disease origin continuously remodel the extracellular matrix which results ultimately in matrix stiffening (Hinz, 2009). On the other hand, normal fibroblasts soften their microenvironment largely in order to maintain their quiescent state. Previously, AFM nanoindentation tests on idiopathic pulmonary fibrosis and normal lung tissues showed the stiffer tissue properties in lung fibrosis than in normal lung tissues (Booth et al., 2012). Accordingly, our AFM mechanical mapping of pathological (scar and Dupuytren's) and normal fibroblasts on all decellularized matrices shows exactly the same stiffer and softer tissue properties, respectively. This clearly means that the AFM nanoindentation tests on tissue or cells on decellularized matrices are great for distinguishing between fibrotic or scar and normal tissues. Further exploration on the pathological fibroblasts shows that the cancer associated fibroblasts (CAF) isolated from breast cancer environment promotes matrix stiffening and cancer cell invasion by activating intracellular transcriptional regulators-YAP (Calvo et al., 2013). Altogether, our results confirm that the fibroblast mechanics reciprocally influence their surrounding microenvironment mechanics.

Our results further indicate that fibroblast stiffness depends on the composition of the decellularized matrices onto which they are seeded. The Young's modulus values of the three fibroblast types were different on all decellularized matrices, irrespective of matrix stiffness. In this study, the elasticity of most of the decellularized matrices was in the order of 10^5 Pa,

except of the very stiff Amnion. In order to observe the fibroblasts Young's modulus within the decellularized matrices, we filtered the matrix Young's modulus values from the cell populated mechanical maps. With varying ECM composition among the decellularized matrices, there was a distinct influence on the fibroblast stiffness. Therefore, we could evaluate the values of cell stiffness in relation to respective decellularized matrix. Previous studies showed that the reorganisation of ECM components altered the tissue elasticity of damaged livers (Klaas et al., 2016). Obviously, the ECM composition and its stiffness seem to have a direct effect on the regulation and activation of the corresponding cell phenotype (Chaudhuri et al., 2014). In accordance, despite of the variability of the decellularized matrices' stiffness and composition, pathological fibroblasts were stiffer than normal fibroblasts in our study. Furthermore, the pathological fibroblasts greatly maintained their proto-myofibroblast/myofibroblast like phenotype and dermal fibroblasts their regular fibroblast like phenotype while invading into these matrices.

Cellular migration on and invasion into tissues are important for physiological wound repair and for diseases like cancer metastasis and fibrosis (Friedl et al., 2012). With the help of confocal microscopy z stack images, we were able to monitor the degree of fibroblast invasion into the decellularized matrices. Surprisingly, scar and Dupuytren's fibroblasts colonized the top of the Epiflex matrix and were less invasive than normal fibroblasts. On the other hand, normal, scar and Dupuytren's fibroblasts were highly invasive into the collagen rich XenoDerm matrix. Cellular lamellipodia extend into the collagen matrix (Friedrichs et al., 2007a). This conflicting state of fibroblast invasion might be due to the influence of extracellular matrix collagen fibre orientation in cell invasion (Han et al., 2016). Finally, this finding might be important for the clinical application of various matrices. Acellular matrices are currently used for implant coverage in esthetic plastic surgery. Hence, a matrix that prevents fibroblast penetration could also contribute to a reduction of fibrotic capsule formation.

Even if we were unable to assess the influence of ECM protein fibre alignment or cellular integrin expression (Hood and Cheresh, 2002) on cell invasion by biophysical means, we found that contractile pathological fibroblasts are highly invasive in comparison to normal fibroblasts. The mechanically activated myofibroblasts confirmed their phenotypically expected behaviour by vastly invading the ECM. Under pathological conditions, myofibroblasts show an aggressive and invasive phenotype in tissue fibrosis (Li et al., 2011). Extracellular matrix invasion is enhanced by cell stiffness (Mierke et al., 2017). In

accordance, we found large stress fibres in pathological fibroblasts that were stiffer and invaded the decellularized matrices much more profoundly than normal fibroblasts.

4.5 Conclusion

In conclusion, we have shown that the decellularized matrices are suitable substrates to investigate the interdependent reciprocal interplay between cell and ECM mechanics using AFM force spectroscopy. Pathological fibroblasts were stiffer than their normal counterparts and showed higher invasive behaviour into different matrices with subsequent higher stiffening of the decellularized matrices (specifically MatriDerm) used in our study. Furthermore, we showed that cell stiffness depends not only on cell microenvironment mechanical properties but also on the matrix biochemical composition. These findings have a dual important impact in translational research: (1) they will foster further biophysical studies in the field of tissue engineering, and (2) they provide valuable information to improve commercially available acellular matrices that are currently used in various clinical settings, like tissue regeneration and wound healing.

4.6 Methods and Experimental Design

Decellularized matrices and DED Preparation

Human acellular amnion and Epiflex acellular dermal matrix were kindly donated by the German Institute for Cell and Tissue Replacement (Deutsches Institut für Zell- und Gewebeersatz, DIZG, Berlin, Germany). Collagen-elastin rich synthetically produced MatriDerm was purchased from Dr. Otto Suwelack Skin &Health Care AG, Billerbeck, Germany. Porcine XenoDerm acellular dermal matrix was purchased from Medical Biomaterial Products (MBP) GmbH, Neustadt-Glewe, Germany.

De-epidermized dermal (DED) matrix was prepared from excised human tissue as described elsewhere (Mirastschijski et al., 2013). First, tissues were cut and punctured into small circular pieces (diameter ~ 4 mm and thickness ~ 2 mm) by using a trephine and the fat layer beneath the tissue was removed with a scalpel. The tissue was then transferred to the 50 mL falcon tubes containing PBS and incubated in a water bath at $56^{\circ}C$ for 30 min. After that, the epidermis was easily stripped off as the upper dark skin layer was identified as epidermal layer and removed with tweezers. The cells in the dermal layer were destroyed by 10 cycles of freezing and thawing. Then the DEDs were stored at -20 ^{0}C for future experiments.

Primary human fibroblast cultures

Tissues for cell harvest were obtained from patient undergoing plastic reconstructive and hand

surgery. Scar fibroblasts were derived from scar excision and normal from adjacent skin tissue. Dupuytren's fibroblasts were isolated from excised nodules and palmar strands of the same patient who presented with Dupuytren's disease. Patient was informed pre-operatively and had given their informed consent to anonymous tissue donation. The study was approved by the local Ethics Committee (Ärztekammer Bremen, #336/2012). The guidelines of the declaration of Helsinki were followed.

Fibroblast extraction

For cell culture, the tissue was minced and enzymatically disintegrated using a 0.5% collagenase solution (250 U/ml Serva, Heidelberg, Germany) at 37°C in 5% CO_2 for 6 h. After centrifugation, the pellet was resuspended in culture medium (TC 199 with Earle's salts supplemented with 20% fetal bovine serum, 200 IU/ml penicillin, 200 µg/ml streptomycin) and incubated at 37°C in 5% CO_2 air. The culture medium was changed after attachment of the cells. Primary fibroblasts of the three different skin tissues were passaged using trypsin / EDTA solution (0.05% / 0.02% w/v in PBS w//o Ca^{2+}, Biochrom, Berlin, Germany) a split ratio of 1:2 one time a week to preserve monolayer formation.

Cell culture on decellularized matrices

Cells were seeded on the decellularized matrices two weeks before AFM or confocal measurements. In brief, decellularized samples were glued to the Petri dish using the super glue (Tesa Sekundenkleber), taking special care to make sure that glue was in contact only to the bottom layer of the matrices without penetrating through the top layers. We used tiny droplets of super glue, to immobilize our matrix samples, which solidifies faster and thus prevents the contact of glue to the top layer of the samples. PBS was added quickly onto the matrix to prevent drying. Prior to cell seeding, the matrices were extensively washed in PBS for 30 min, and incubated for a few hours with DMEM medium, supplemented with 10% fetal bovine serum (FBS) and 2% penicillin–streptomycin. Then cells were seeded in DMEM medium and incubated at 37°C in a humidified atmosphere of 95% air and 5% CO_2. Cell culture was established for two weeks before proceeding with further measurements. Medium was replenished every three days and supplemented with 10% fetal bovine serum (FBS) and 2% penicillin-streptomycin. Passages between three and eleven were used for all the experiments.

To remove cells from the matrices, the medium was first removed and samples were washed twice with PBS. Then the matrices were treated with 1% trypsin for 3 min and incubated with a solution containing 0.5% Triton X-100 and 1% SDS (sodium dodecyl sulphate) for 5 min at 37 °C. Matrices were washed twice and stored with PBS for AFM imaging and mechanical

measurements.

PeakForce Tapping mode Imaging

A Bruker BioScope Resolve AFM (Bruker Nanotechnologies, Santa Barbara, CA) was used to image the matrices, with and without cells. Commercially available cantilevers (PFQNM-LC probes, Bruker, spring constant 0.1 N/m) were used for imaging. Peak Force Quantitative Nano Mechanical imaging for live cells mode was done at oscillation frequency of 1 kHz using a Peak Force Tapping amplitude of 300 nm (for bare and cells removed matrices) and 600 nm (for cells populated matrices) and a peak force of 400 pN. Scanning was performed at a rate of 0.270 Hz. An optical microscope was combined with the AFM to be able to control tip and sample positioning. The AFM head including the sample was enclosed in a homebuilt polymethacrylate (PMMA) box in order to maintain 5% CO_2 in the atmosphere. Images were recorded with the Nanoscope working software, version 8.15 and image processing was performed with the Nanoscope Analysis software, version 1.8.

AFM force mapping.

A MFP3D AFM (Asylum Research, Santa Barbara, CA, USA) was used to measure mechanical properties of bare, cell-occupied and cell-removed matrices for three types of fibroblasts. An optical microscope (Zeiss Axiovert 135, Zeiss, Oberkochen) was combined with the AFM to be able to control tip and sample positioning. All measurements were performed with the same soft cantilever (MLCT Bio, Bruker, nominal spring constant 0.01 N/m). The Petri dishes with matrix samples were fixed to an aluminum holder with vacuum grease and mounted on the AFM stage with two magnets. The AFM head including the sample was enclosed in a homebuilt polymethacrylate (PMMA) box in order to inject and maintain 5% CO_2. Force maps were recorded on matrices and living cells on matrices to study their mechanical properties. First, the spring constant of the cantilever was calibrated by using the thermal tune method on a cleaned and stiff surface (Sader et al., 1995) and then force curves were recorded. For force curves, we used typically a ramp rate of 1 Hz, corresponding to a maximum loading rate of 1 nN/s and a maximum force of 1nN. Indentation depths were always greater than 500 nm in order to average the stiffness over a large contact area, which gives values that do not depend on local variations of the cytoskeletal or matrix structure. All AFM measurements, imaging and mechanical mapping on matrices after adding cells were performed on living cells.

AFM data analysis.

The data analysis package IGOR (wave metrics, Lake Oswego, OR, USA) was used to evaluate mechanical properties of the cells and decellularized matrices. Details have been

described elsewhere (Carmela Rianna and Radmacher, 2017). Only approach force curves were analysed within the framework of the Hertz model for pyramidal tips in order to obtain the apparent Young's modulus of the samples (Rico et al., 2005; Sneddon, 1965; "Ueber die Berührung fester elastischer Körper.," 1882). At least a total of 10 force maps were recorded at 10 different positions on matrices for each category. Each force map contained 2500 force curves (50 x 50 lines per frame) over an area of typically 30 μm. The median values of 10 force maps (10 x 2500 = 25000 force curves) was considered as a representative modulus of each category (force maps were recorded over 10-12 different positions for each category).

Cell Young's modulus analysis from cell populated matrix force maps.

To study matrix composition dependent cell stiffness, the Young's moduli of cells were calculated from the cell populated matrices. Most of the force maps were taken directly on the cell and in exception some maps contains both cell and matrix regions. The slope (Supplementary Figure. 4.13A) and contact point approach map (Supplementary Figure. 4.13B) helps to distinguish the matrix and cell regions. The AFM tip contact the sample with definite contact point which can be calculated for each force curve in the approach curve. This contact point reflects the height of the sample from which cell and matrix regions are recognized. The slope color-scale shows the slope values above 0.375 (corresponding force curve shown in Supplementary Figure. 4.13C3 and in the respective force maps) falls in the matrix and below 0.375 falls in the cell regions. By substituting 0.375 as threshold value, the Young's modulus values from matrix regions were excluded after careful examination of each force maps. In addition, the force curves obtained in the matrix (Supplementary Figure. 4.13C1) and cell (Supplementary Figure. 4.13C2) clearly shows the distinction. The separation of approach and retract curves in the slope area are smaller in forces curves obtained from matrix than in cell region. The force *versus* indentation graph (Supplementary Figure. 4.13D) shows the larger indentation for cells than the matrix. The separation between approach and retract curves is a measure of the viscosity of the cell, however there is a cross talk with softness of the cell, as we have shown in previous work analyzing the response of step forces of cell (Carmela Rianna and Radmacher, 2017). Thus we used here only the slope to distinguish between cell and matrix rather than more sophisticated but derived quantities like elastic modulus or separation of force curves.

Confocal microscopy and Immunofluorescence staining.

To study cell invasion into matrices, we used a Zeiss LSM 780 Confocal with 40x oil objective lens. Two weeks after seeding of cells on matrices, cells were fixed with 3.7% formaldehyde for 15 min and permeabilized with 0.1% Triton X100 for 3 min. Samples were

washed with PBS after each step and then incubated with a rhodamine phalloidin solution (5:200 dilution in PBS) for F-actin staining for 30 min at 20°C and samples were washed after every step with PBS. Finally, samples were washed and stored in PBS at 4°C prior to image acquisition. The confocal laser lines 561 nm (excitation) and 570-650 nm (emission) were used for obtaining z stack images of cells stained for actin within the matrices. Z stacks were collected and analysed from 3D stacks using ZEN software version 2.0.

Statistical Analysis.

Statistical differences for the median values of Young's moduli of bare, cell occupied and cell removed matrices of the AFM measurements were determined by Wilcoxon test, calculated in IGOR software. * and ** indicate statistically significant differences for p-values <0.05 and p<0.005, respectively.

4.7 Acknowledgements

4.8 Author contributions

PK was performing AFM experiments, confocal experiments, data analysis and manuscript preparation. CR was performing confocal experiments and was involved in data analysis and manuscript preparation. UM designed the experimental setup, provided tissues and different matrices, contributed to data analysis and interpretation, and was involved in the preparation of the manuscript. MR designed the experimental scheme and was involved in data acquisition, data analysis and preparation of the manuscript.

4.9 Additional information

Competing financial interests: The authors declare no competing financial interests.

4.10 Supporting Information
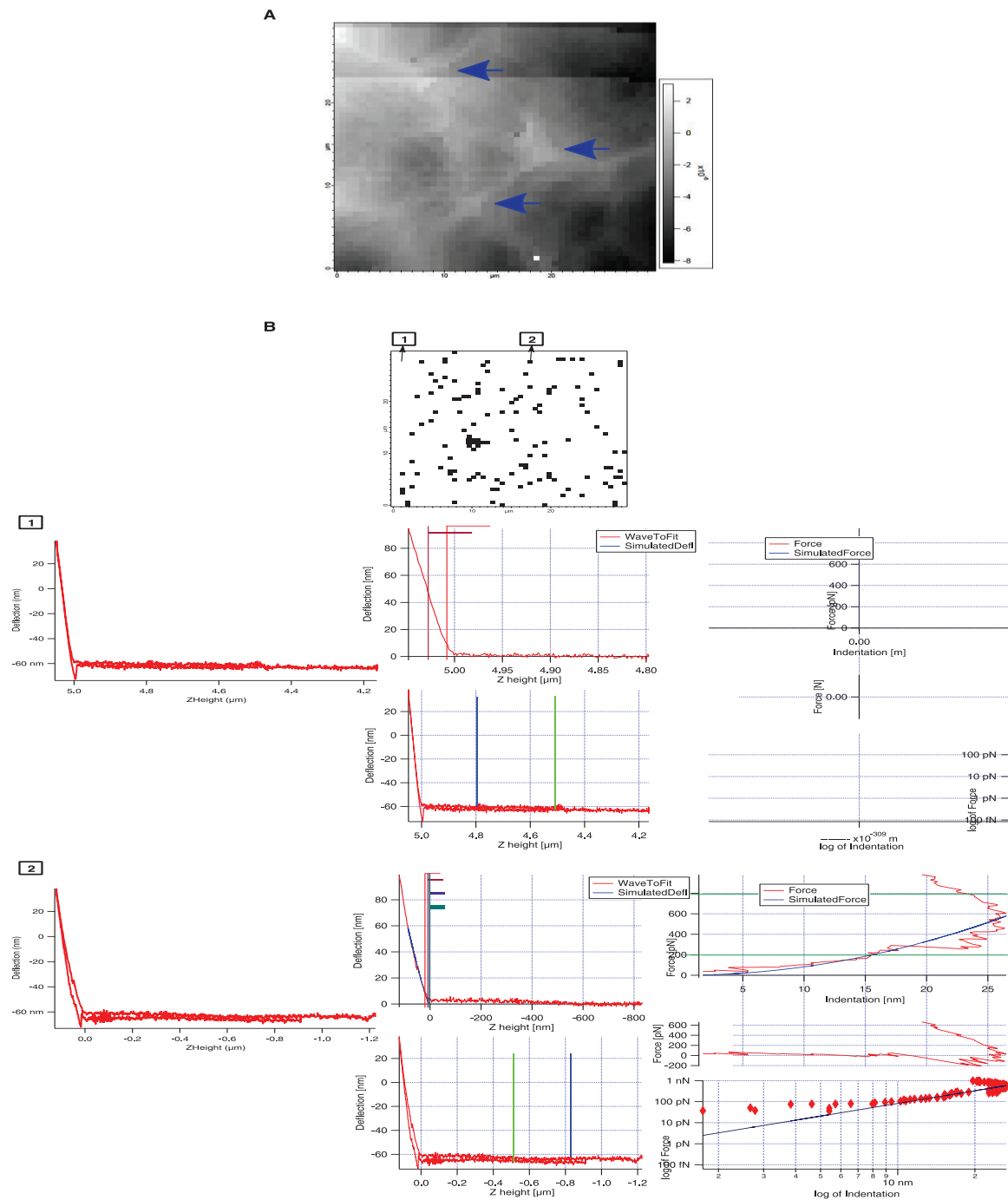
Supplementary figure 4.11 (A) The high resolution map showing the ECM fibers (blue arrows) running along the Amnion decellularized matrix. (B) The force map recorded on the Amnion matrix shows 50 x 50 force curves and the white areas indicates the stiff areas and the black spots indicates the soft areas. Force curve from stiff (1) and soft (2) areas within the Amnion matrix were analyzed and the Hertz Fit window for Young's modulus calculation are shown, respectively.
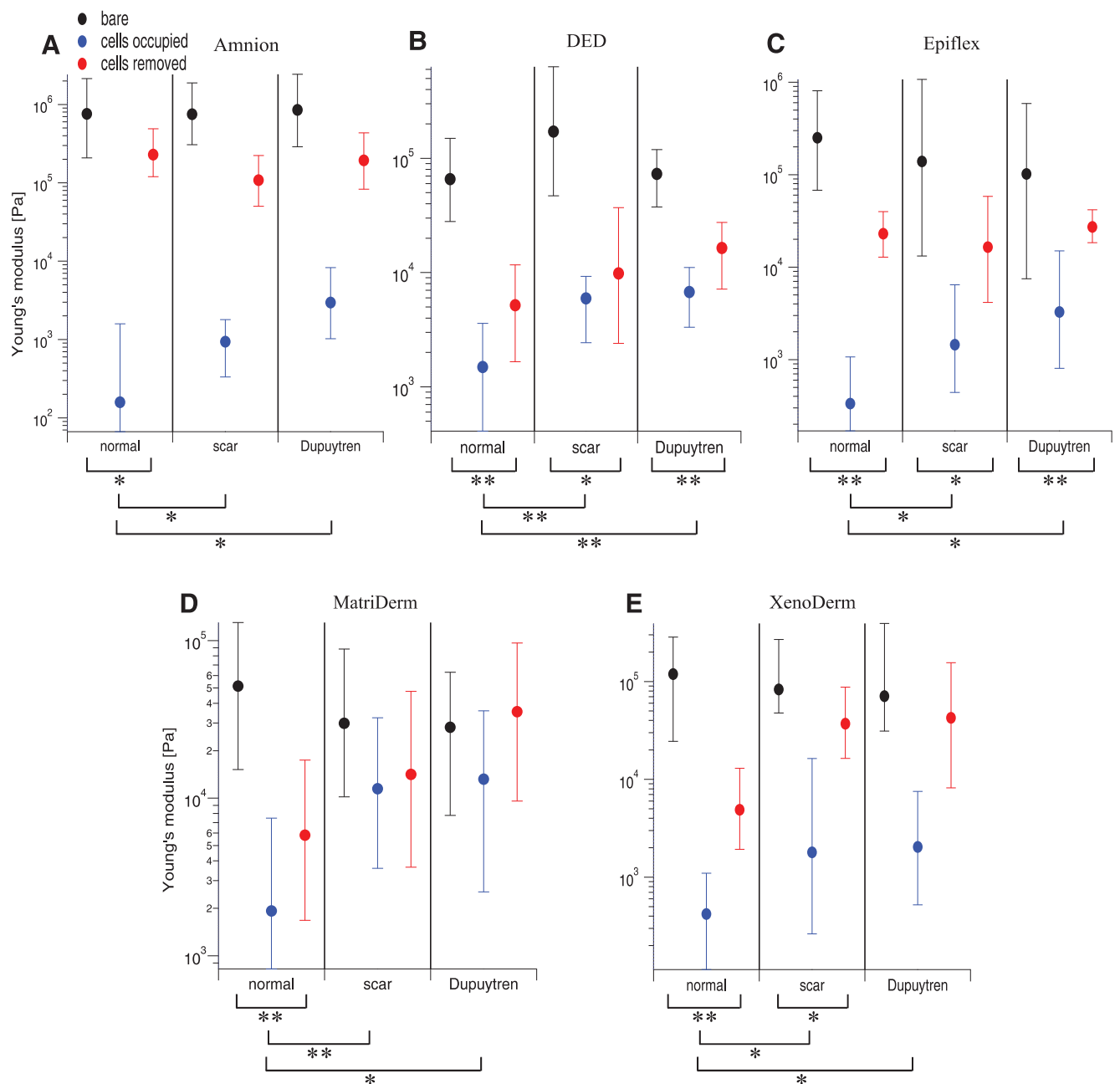
Supplementary figure 4.12 The median of Young's modulus values of the bare (native, black), cell-populated (blue) or cell-removed (red) decellularized matrices for normal, scar and Dupuytren's fibroblasts were plotted for each matrix, i.e. Amnion (A), DED (B), Epiflex (C), MatriDerm (D) and XenoDerm (E). The respective median of Young's moduli values are presented in Table 4.1, 4.2 and 4.3. Statistical results are reported in Methods and Experimental Design section.
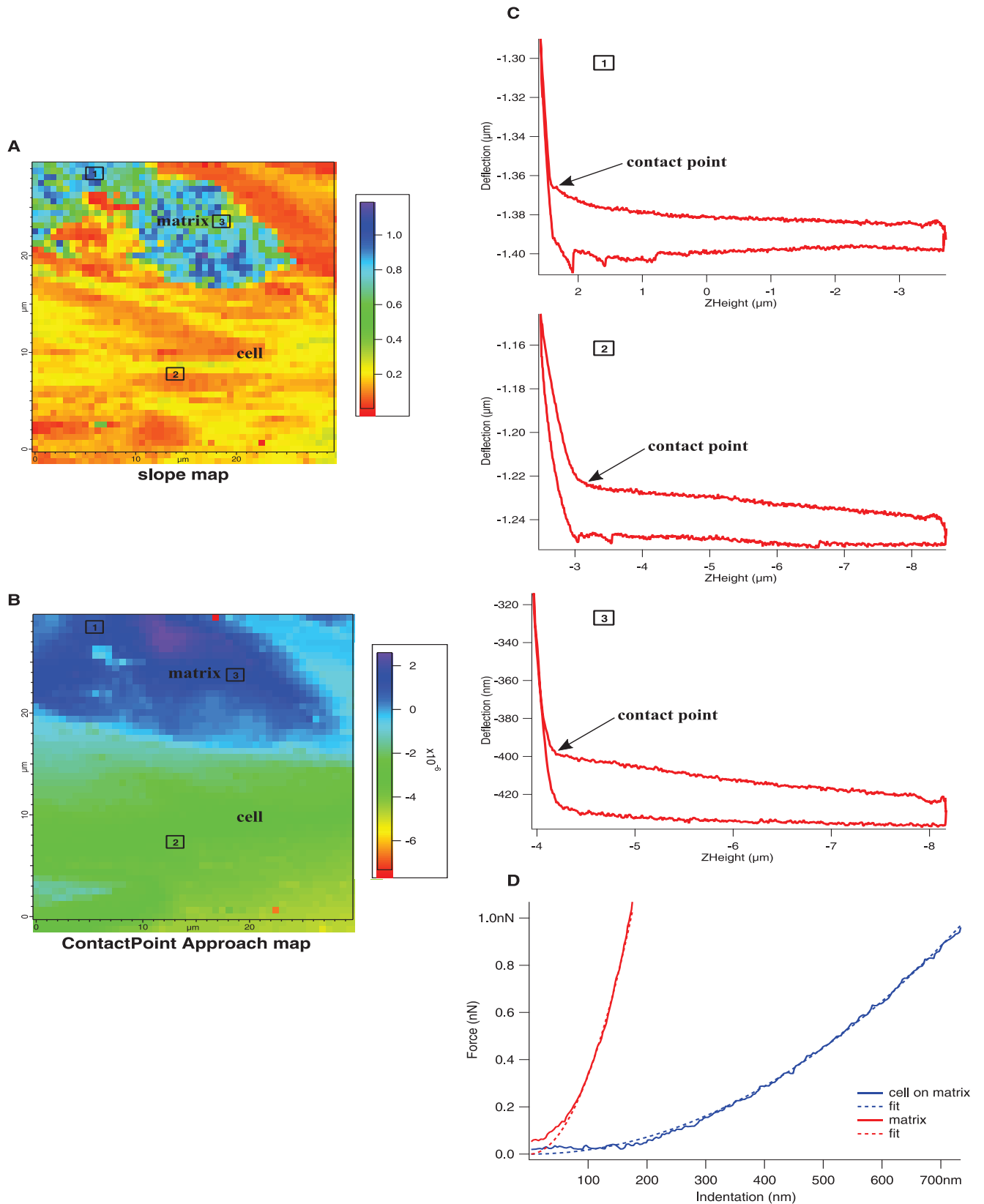
Supplementary figure 4.13 Extrapolation of cell Young's modulus from cell populated matrix. The slope (A) and contactpoint approach (B) map shows the distinctive cell and matrix region. The force curves (C) of the matrix [1] and cell [2] region showing separation of approach and retract curves which is smaller in matrix and comparatively larger in cell. The force curve from the matrix region [3] of the force map corresponds to slope value 0.3748. (D) Force *vs* indentation graph (full line) with Hertz fit (discontinuous line) shows the two slope values of matrix (0.4186) and cells (0.1546). The threshold slope value (0.375) was used as a critical value to neglect the matrix contribution to cell stiffness, after careful analysis of cell-populated mechanical maps.
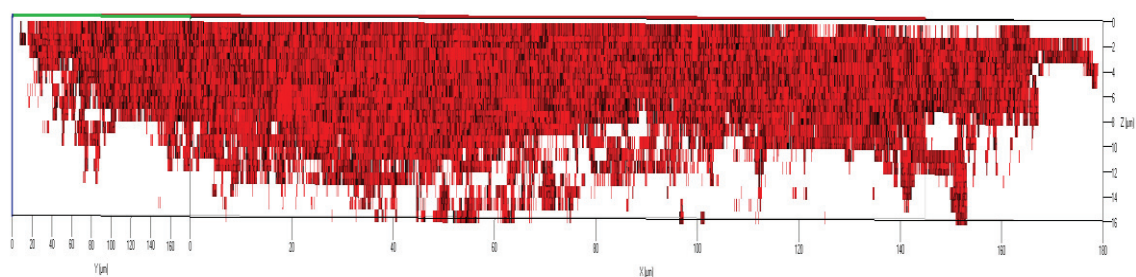
normal
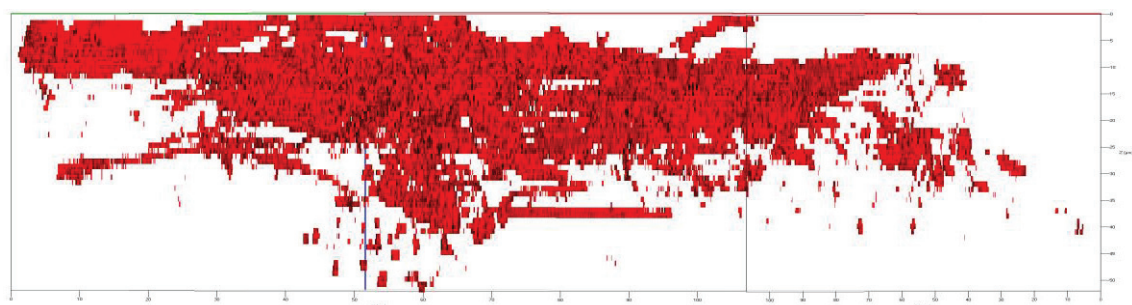
scar
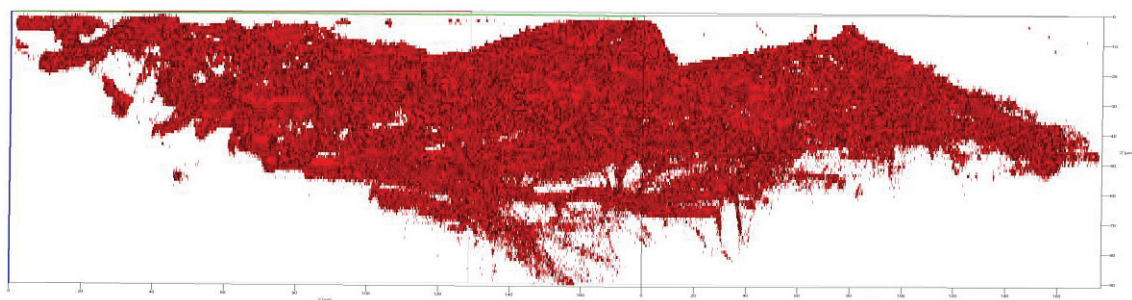
Dupuytren

Supplementary figure 4.14 Cell invasion 3D plot on DED matrix. The 3D plot was created from the z stack images recorded by confocal microscopy. Scar and Dupuytren's fibroblasts were more invasive than normal fibroblasts into the DED matrix.

normal

scar
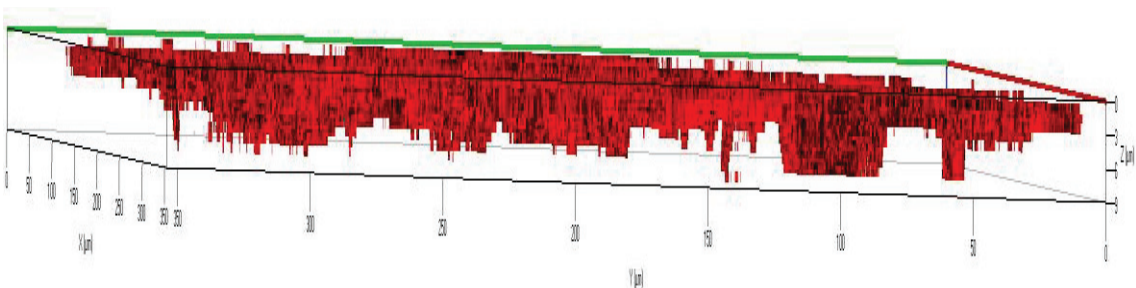
Dupuytren

Supplementary figure 4.15 Cell invasion 3D plot on Epiflex matrix. The 3D plot created from the z stack images shows that normal fibroblasts penetrate more than pathological (scar and Dupuytren's) fibroblasts into the Epiflex matrix.
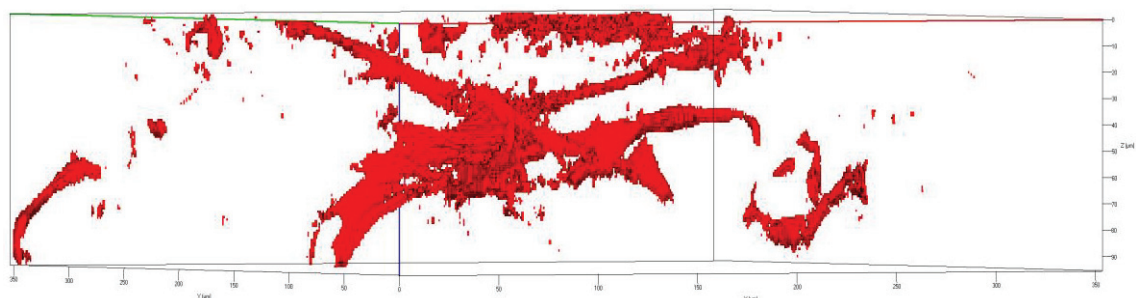
normal
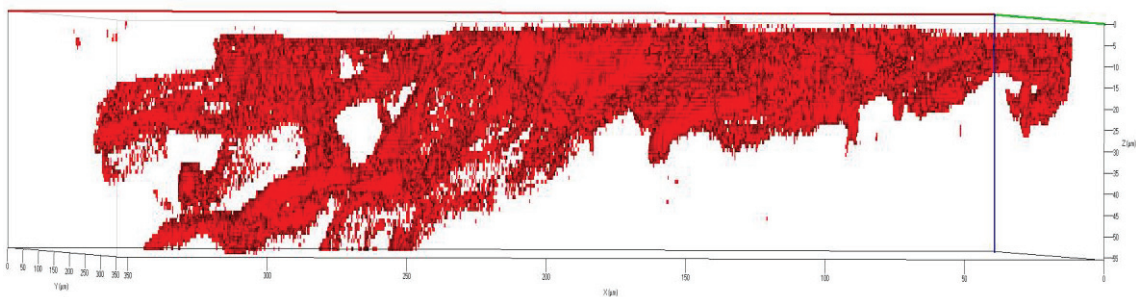
scar
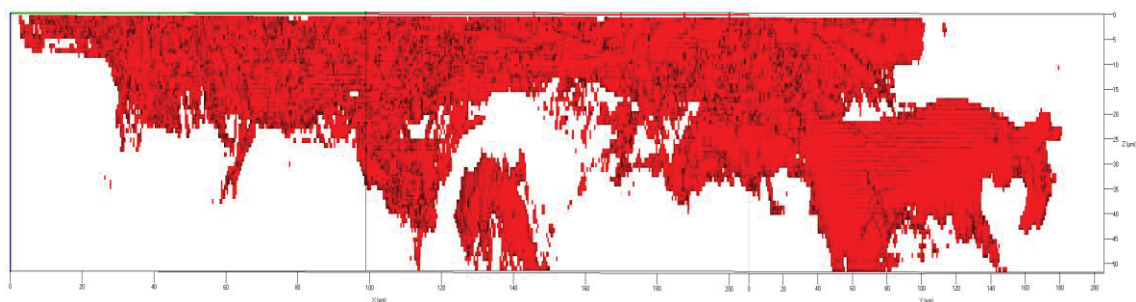
Dupuytren

Supplementary figure 4.16 Cell invasion 3D plot on MatriDerm matrix. The 3D plot was created from the z stack images and shows the invasion of normal, scar and Dupuytren's fibroblasts into the MatriDerm matrix.
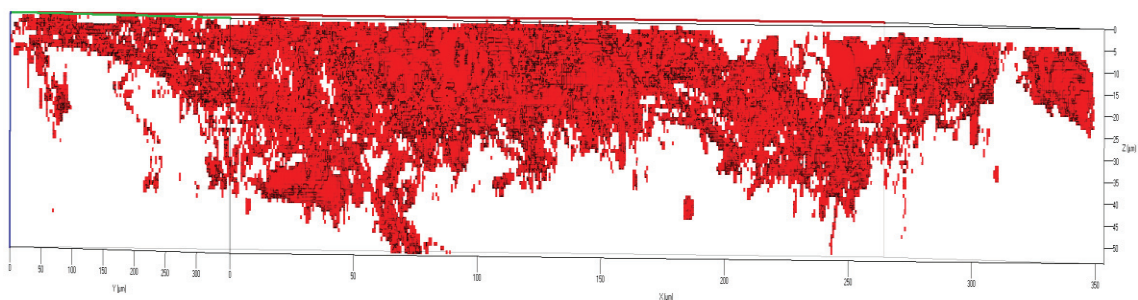
normal
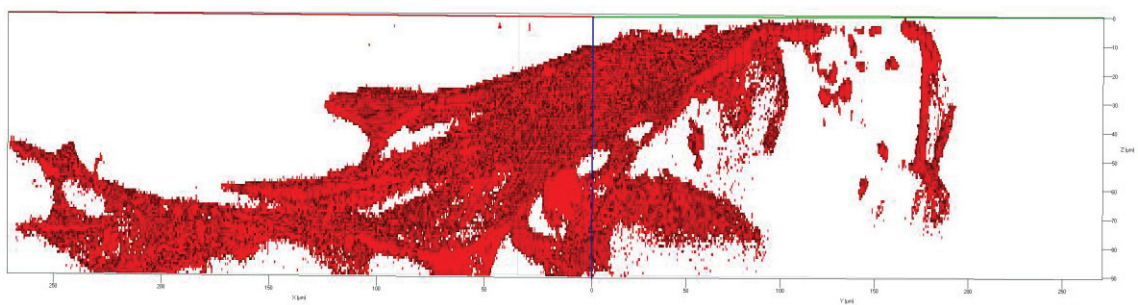
scar
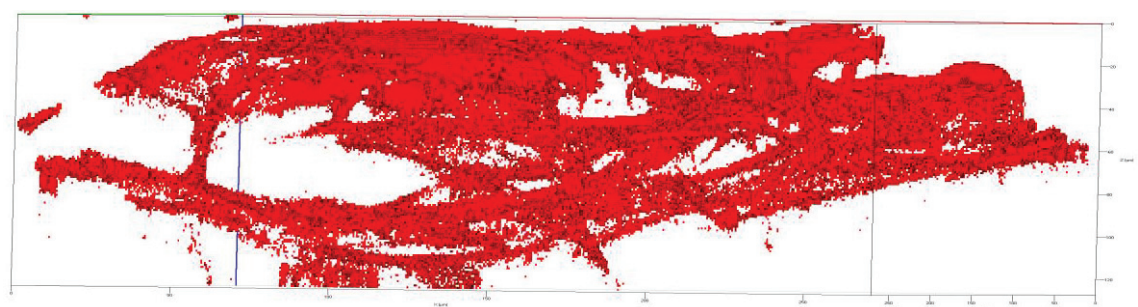
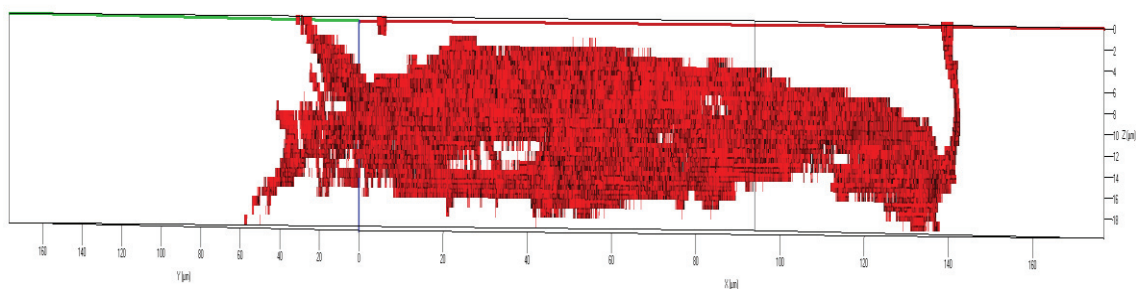

Dupuytren
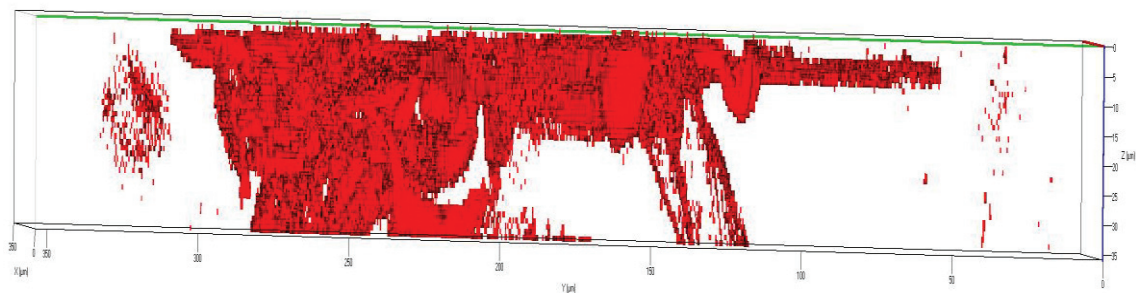
Supplementary figure 4.17 Cell invasion 3D plot on XenoDerm matrix. The 3D plot was created from the z stack images and shows the higher invasive tendency of normal, scar and Dupuytren's fibroblasts into the XenoDerm matrix. With regard to cell types, scar and Dupuytren's fibroblasts were more invasive than normal fibroblasts.
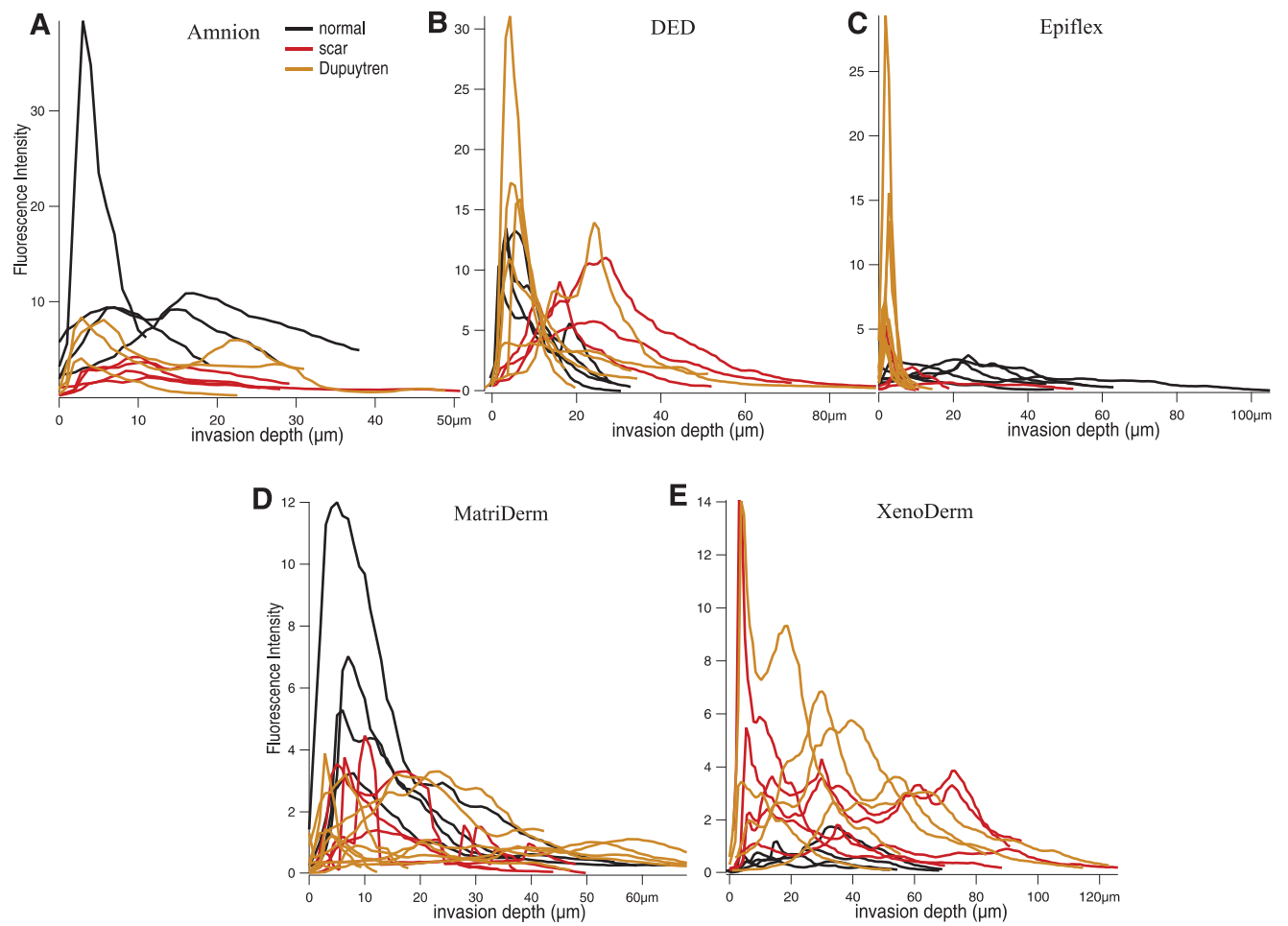
Supplementary figure 4.18 Fluorescence intensity was plotted versus invasion depth from z stack fluorescence images and shows the degree of normal, scar and Dupuytren's fibroblast invasion into Amnion (A), DED (B), Epiflex (C), MatriDerm (D) or XenoDerm (E).
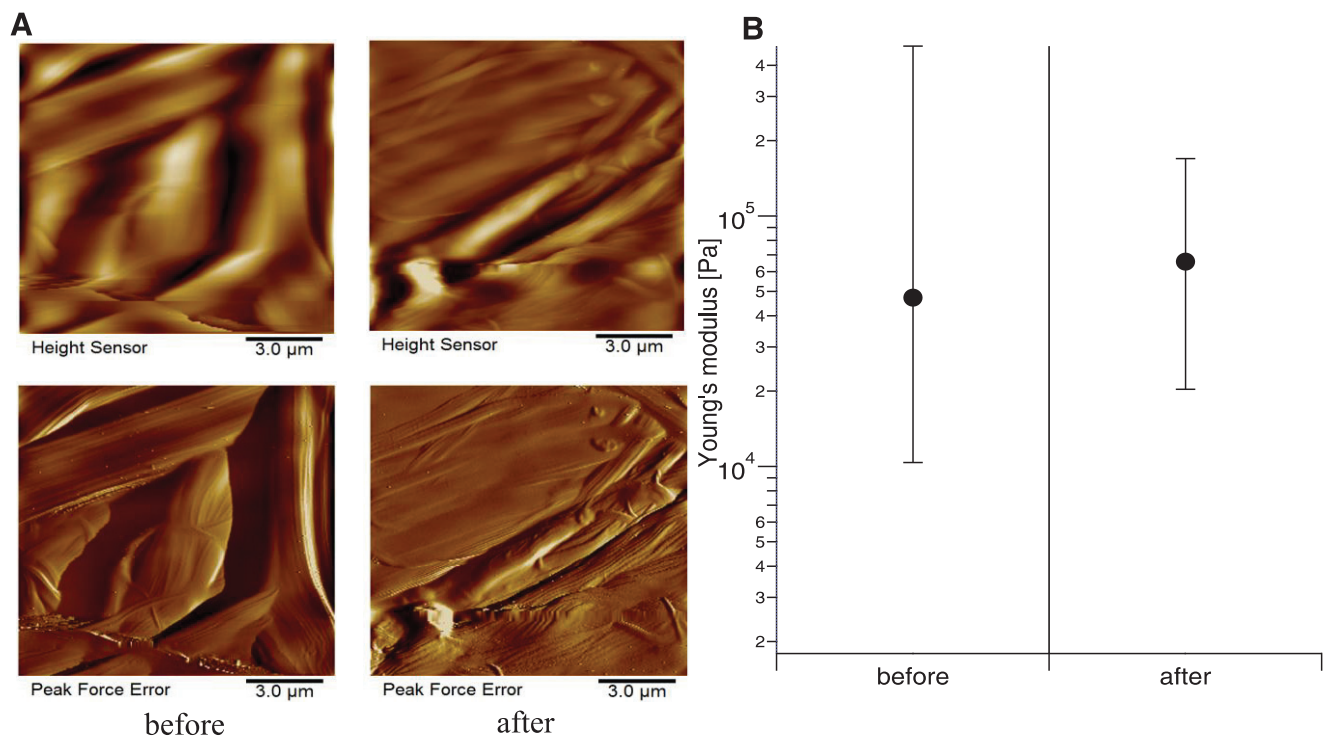
Supplementary figure 4.19 Effect of trypsin, Triton X-100 and SDS on XenoDerm decellularized matrix. (A) Height and PeakForce Error images from AFM PeakForce Tapping and (B) median of Young's modulus values obtained from mechanical force maps before and after treating the matrix with 1% trypsin, 0.5% triton X-100 and 1% SDS. AFM images and Young's modulus plot show that there is no significant effect on XenoDerm's topography and elasticity, respectively.

Chapter 5

This is a verbatim copy of an article that has been submitted in a peer reviewed journal: Viji Babu, P.K., Mirastschijski, U. and Radmacher, M., 2020. Homophilic and heterophilic cadherin bond rupture forces in homo- or hetero-cellular systems measured by AFM based SCFS. *PlosOne*.

Cadherin homophilic and heterophilic binding and influence of actomyosin contraction

Prem Kumar Viji Babu[1,4], Ursula Mirastschijski[2], Ganzanfer Belge[3], Manfred Radmacher[1,4]

[1]Institute of Biophysics, University of Bremen, Bremen, Germany

[2]Wound Repair Unit, Centre for Biomolecular Interactions Bremen, University of

Bremen, Bremen, Germany

[3]Faculty of Biology and Chemistry, University of Bremen, Bremen, Germany

[4]Authors to whom any correspondence should be addressed.

5.1 Abstract

Cadherins enable intercellular adherens junctions to withstand tensile forces in tissues, e.g. generated by intracellular actomyosin contraction. Single molecule force spectroscopy experiments in *in-vitro* experiments can reveal the cadherin-cadherin extracellular region binding dynamics such as bond formation and strength. However, characterization of cadherin homophilic and heterophilic binding in their native conformational and functional state in living cells has rarely been done. Here, we used Atomic Force Microscopy (AFM) based Single cell force Spectroscopy (SCFS) to measure rupture forces of homophilic and heterophilic bond formation of N-, OB- and E- cadherins in living fibroblast and epithelial cells in homo- and hetero-cellular arrangements, i.e. between same type of cells and between cells of different type. In addition, we used indirect immunofluorescence labelling to study and correlate the expression of these cadherins in intercellular adherens junctions. We showed

that N/N and E/E cadherin homophilic bindings are stronger than N/OB, E/N and E/OB heterophilic bindings. Disassembly of intracellular actin filaments reduces the cadherin bond rupture forces suggesting a contribution of actin filaments in cadherin extracellular binding. Inactivation of myosin did not affect the cadherin rupture force in both homo- and hetero-cellular arrangements. Whereas, myosin inactivation particularly strengthened the N/OB heterophilic bond and reinforced the other cadherins homophilic bonds.

5.2 Introduction

Cell adhesion to neighboring cells or the extracellular matrix (ECM) envirnment is a very important process in regulating crucial biological activities such as embryonic development, tissue assembly and dynamics, wound healing and cancer metastasis. Generally, cells communicate with other cells through adherens, gap or mechanosensitive junctions (Verhoekx et al., 2013b). Cadherins from adherens junctions are a class of calcium dependent cell adhesion molecules (CAMs) which comprise three different domains: (i) an intracellular or cytoplasmic domain which binds to the actin cytoskeleton through adaptor proteins such as α-catenin, β-catenin and p120 catenin, (ii) a transmembrane domain and (iii) an extracellular domain. The extracellular domain consists of five extracellular cadherin (EC) repeats. A dimer of EC1-EC5 of one cell interacts with the corresponding cadherin dimer of a neighboring cell through homophilic and heterophilic interaction (Brasch et al., 2018; Hinz and Gabbiani, 2003).

Several assays have been developed to investigate cell-cell interactions in the last two decades, such as dual micropipette assay (Chu et al., 2004), flipping assay (Carmona-Fontaine et al., 2011), FRET (Borghi et al., 2012) and AFM based SCFS (Benoit et al., 2000; Puech et al., 2006). Comparing all assays, AFM based SCFS assay provides a wide range of forces (10 pN to 10^6 pN) (Helenius et al., 2008) and a controlled force application (loading rate) on the cell-cell adhesion cadherin bond by retracting the AFM cantilever at a well-defined velocity (Müller et al., 2009).). In SCFS, cell adhesion force measurements are performed in near physiological conditions. Being a multifunctional toolbox in nanobiotechnology (Müller and Dufrêne, 2008), AFM provides a functionalized cantilever to pick up a live cell guided by optical microscopy. It allows probing the rupture force between cadherin molecules present in two cells, by separating the two cells. The rupture force can be quantified and reveals differences in the specific type of cadherins present in different cell types.

According to the presence or absence of the HAV (His-Ala-Val) cell recognition sequence in the EC1 domain, classical cadherins are classified into type I (E-, N- and others) and type II

cadherins (OB- and others) (Brasch et al., 2018; Hinz and Gabbiani, 2003). The most commonly expressed cadherin found in fibroblast is N-cadherin (cad-2) (Hatta and Takeichi, 1986). Primary rat fibroblasts differentiate into myofibroblasts *in vitro* using transforming growth factor- β1 (TGF-β1). TGF- β1 induces the expression of alpha-smooth muscle actin (α-sma), an increased expression of OB-cadherins (cad-11) and a decreased expression of N-cadherin (Hinz et al., 2004). This TGF-β1 induced cadherin switch from N-cadherin to OB-cadherin increases the intercellular adhesion strength between myofibroblasts by strengthening individual OB-cadherin bonds. Single molecule force spectroscopy (SMFS) measurements on OB- and N-cadherins showed that the rupture force between OB-cadherins homophilic interaction is larger than between N-cadherins (Pittet et al., 2008). A biochemical analysis of N- and OB-cadherins expression in human dermal fibroblast and Dupuytren's myofibroblast shows increased OB-cadherin and decreased N-cadherin expression in myofibroblasts compared to dermal fibroblasts (Verhoekx et al., 2013b). The E (epithelial)-cadherin (cad-1) is the dominant cadherin expressed in most epithelial cell lines like MDCK cells (Wu et al., 1993). The more motile trypsin sensitive subpopulation of MDCK shows low levels of N-cadherin expression (Youn et al., 2005).

Hetero-cellular interactions between different cell types occur in tissue and organ morphogenesis. Involvement of specific cadherins in these interactions plays a huge role in cancer cell metastasis (Apostolopoulou and Ligon, 2012) whereas heterophilic interactions between cell specific cadherins mediates cancer cell invasion (Labernadie et al., 2017). Direct interactions between fibroblast and epithelial cells may play an important role in the epithelial to mesenchymal transition (EMT) process (Nishioka et al., 2015). In certain tissue functional phenomenon, hetero-cellular interactions between normal fibroblasts and gastric cancer cells induce E-cadherin loss and increase metastasis in gastric cancer, which was induced by EMT (Xu et al., 2014). The investigation of hetero-cellular interactions between fibroblast and epithelial cells using biophysical techniques such as SCFS will help to understand better the role of classical cadherins interactions both in EMT and Mesenchymal to Epithelial cell transition (MET) process.

Actin filaments associated with myosin are the major contractile component responsible for intracellular force generation. Generally, these forces are generated by the myosin assembly and motility on the actin filaments. Myosin light chain is phosphorylated by the myosin light chain kinase (MLCK) and this activates the myosin cross linking to the actin filaments with actomyosin contractile force generation. Intracellular forces are then transmitted to the neighbouring cells and to the extracellular environment through cadherins and focal adhesion

complexes, respectively that are connected to actin filaments. Disassembling actin filament rich stress fibres by treating fibroblasts with Cytochalasin D results in decreased cell stiffness (Rotsch and Radmacher, 2000). Addition of Cytochalasin D reduces the cadherin mediated binding forces between myofibroblasts, as measured by SCFS, and shows that cadherins are linked structurally and possibly functionally to the intracellular actin network (Pittet et al., 2008). Inactivating myosin-II activity by treating fibroblasts with ML-7 inhibits the MLCK, which further prevents myosin mediated actomyosin contractility which results in actin cytoskeleton softening and thus decreased cell stiffness (Schäfer and Radmacher, 2005).

In the present study, we have studied the expression of N- and OB-cadherins in three types of fibroblasts extracted from the same patient with Dupuytren's disease using fluorescence microscopy: (1) normal fibroblasts-NFs from normal healthy skin, (2) scar fibroblasts-SFs from cutaneous scar tissue and (3) Dupuytren's myofibroblast-DFs from the nodules of the palmar fascial strands. Using AFM-SCFS, we measured the rupture forces between fibroblasts grown in a confluent monolayer and fibroblasts attached to the AFM cantilever (NF-NF, SF-SF and DF-DF). Loading rate dependent rupture force measurements showed that NF and SF exhibit larger rupture forces than DFs. These results correlated with the cadherin types present in the adherens junctions of respective fibroblast types. Hetero-cellular interaction forces were also measured between fibroblasts grown in monolayers and epithelial cells attached to the cantilever. Regarding the epithelial cell, we used epithelial cell line called MDCK cells to study the hetero-cellular interactions between MDCK and fibroblasts mediated by cadherins expression and binding dynamics. Immunofluorescence studies of MDCK and fibroblast co-cultures showed the presence of N-cadherins at the fibroblast-MDCK junction and E-cadherin loss in MDCK. Cytochalasin D treatment decreases the interaction forces in both homo-cellular and hetero-cellular interactions. In ML-7 treatment, no change in interaction forces observed in homo-cellular and hetero-cellular interactions except for DF-DF interaction. Contrarily, there is an increase in DF-DF rupture forces after ML-7 treatment and reveals that OB- and N-cadherin heterophilic bond strengthens the cell-cell interaction when there is no intracellular contractile force.

5.3 Results

N/OB heterophilic binding is weaker than N- and OB- homophilic binding

Investigation of cell-cell interactions using AFM becomes more possible using a simple cell force spectroscopic setup. AFM based SCFS setup is explained with the simple schematics shown in Fig 5.1A. A tipless cantilever, functionalized with concanavalin A (conA), was

placed on a cell, which makes initial adhesion to the substrate and is appropriately round in shape. The cantilever was approached towards that cell until a certain loading force has been reached. After a dwell time of 2 s the cell has adhered sufficiently and stays attached to the cantilever when the cantilever is retracted from the support as shown in Fig. 5.1B. The force curve obtained during cell capture is shown in Fig. 5.1C. After a recovery time of 10 minutes, the cantilever with the attached cell was approached towards and retracted from another cell attached to the Petri dish. Cell-cell interactions and rupture forces between cells were probed. Fig. 5.1D shows a cell-cell (NF-NF) interaction force curve. The force curve contains approach (red arrows) and retract curve (blue arrows). The cell capturing and cell-cell interaction events are visible in the retract curve. In case of cell-cell interactions, two distinct features can be seen in the retract curve: rupture (continuous line arrows) and tether events (discontinuous line arrows). The adhesion molecules that are well anchored to the intracellular actin filaments interact with their counterparts on the other cell, and the breakage of these bonds can be seen as a rupture event. This rupture event can be due to a single bond breakage or to multiple bond breakages. The rupture force was calculated from the height of the rupture event. When adhesion molecules are not anchored to actin filaments membrane, tethers can be pulled over large distances, which eventually will also break (tether events). The rupture and tether events observed during cell capture were due to the interaction and bond breakage of either specific adhesion molecules or other non-specific interactions, which were not characterized here.
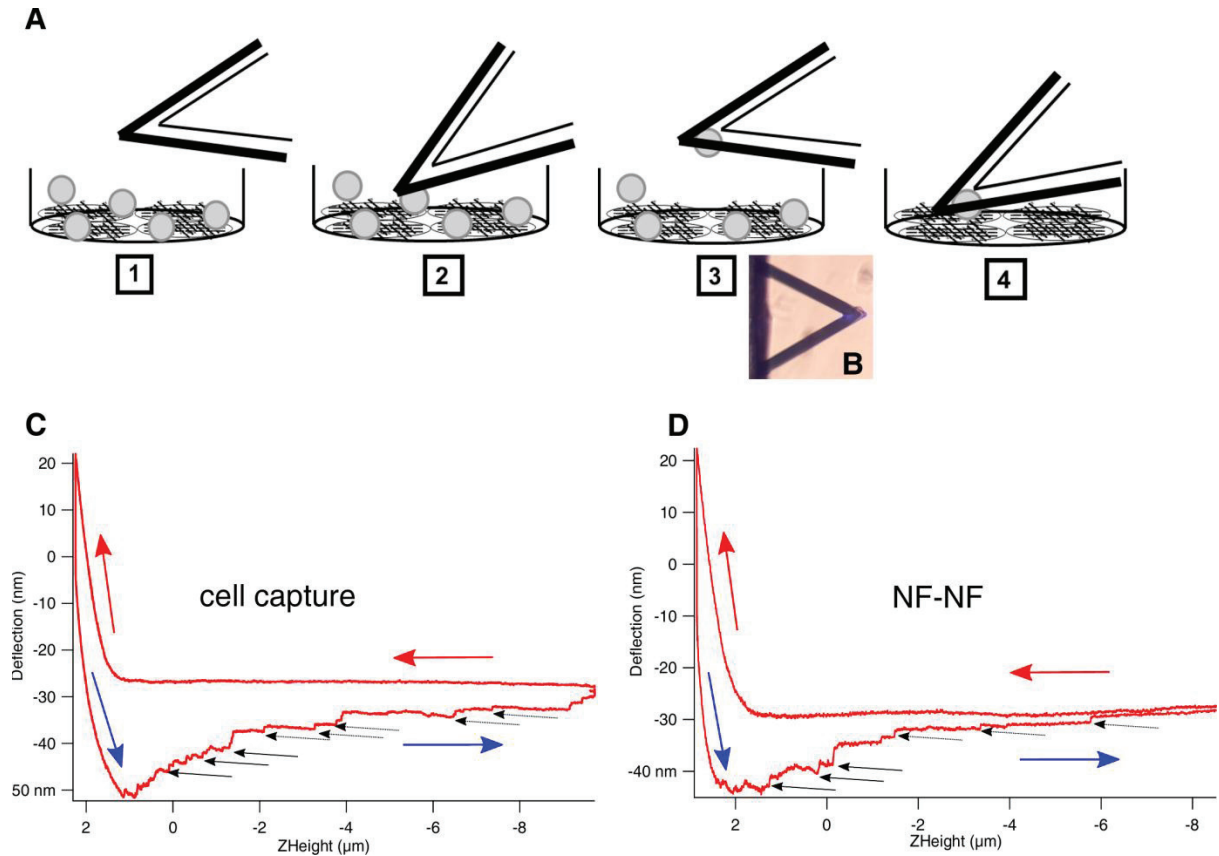
Figure 5.1. Schematic representation AFM based SCFS experimental setup. (A) A simple cartoon represents the capturing of cell by a tipless cantilever in a stepwise manner. 1- The conA functionalized tipless cantilever and a cell with round morphology is chosen with the aid of optical microscopy. 2- The cantilever is approached towards the cell at certain velocity (3 µm/s) and contact force (3 nN). 3- Given the contact time of 2 s, the cell attached cantilever is retracted with the same velcotiy (3 µm/s). (B) Optical image shows the cell attached cantilever. (C) Force curve recorded during cell pick up was shown and retract curve (blue arrow) contains rupture (continuous line black arrow) and tether (discontinuous line black arrow) events. 4- After a recovery time of 10 min, the interaction between cell attached to the cantilever and cell grown as monolayer was conducted. (D) Cell-cell interaction force curve shows rupture events that corresponded to the extracellular cadherin-cadherin bond breakage. Here, multiple rupture events were recorded.

Here we determined rupture forces between three types of fibroblasts isolated from primary human cells using SCFS and assessed the specific cadherins at the interaction site using fluorescence microscopy. The cell-cell rupture force was measured using a approach and retraction velocity of 3 µm/s, a maximum loading force of 3 nN and the contact time of 2 s. The histogram plot of measured rupture forces versus the number of rupture events shows the force distribution for each fibroblast type (NF-NF Fig. 5.2A, SF-SF Fig. 5.2B and DF-DF Fig. 5.2C- red bar). NF-NF interaction showed a larger rupture force (51.91 pN) compared with SF-SF (45.21 pN) or DF-DF (35.71 pN). (See Table 5.1 which lists the corresponding 25, 50 and 75 percentile values). To verify that these rupture forces were due to the cadherin-cadherin bond breakages, the rupture events were recorded in the presence of EGTA (ethylene glycol tetraacetic acid, a calcium chelating agent) in the SCFS setup, effectively removing all

free calcium from the extracellular space. Addition of EGTA completely inhibited the cadherin mediated cell-cell interaction with reduced numbers of rupture events (Fig. 5.2A, B and C, blue bar). Under normal conditions, force curves showed multiple rupture events due to interactions of multiple cadherins (Supplementary Fig. 5.7A), whereas in the absence of Ca^{2+}, i.e. in the presence of EGTA, such rupture events were not seen in force curves (Supplementary Fig. 5.7B). To understand the cadherin-cadherin binding strength, we exerted varying force (loading) rates on the bonds by approaching and retracting the AFM cantilever at different velocities (3, 5, 7.5 and 10 μm/s), which named "pulling rate" in force spectroscopy. For all three fibroblast types, the corresponding rupture forces showed a linear increase depending on the pulling rate applied (Fig. 5.2D). The median rupture force values for respective pulling rates for all three fibroblast types were listed in Table 5.1. NF-NF (Fig. 5.2D black square) and SF-SF (Fig. 5.2D red upper triangle) rupture forces were similar at all velocities except 3 μm/s. In contrast, DF-DF (Fig. 5.2D blue lower triangle) attachments showed smaller rupture forces compared to NF-NF and SF-SF at all velocities.
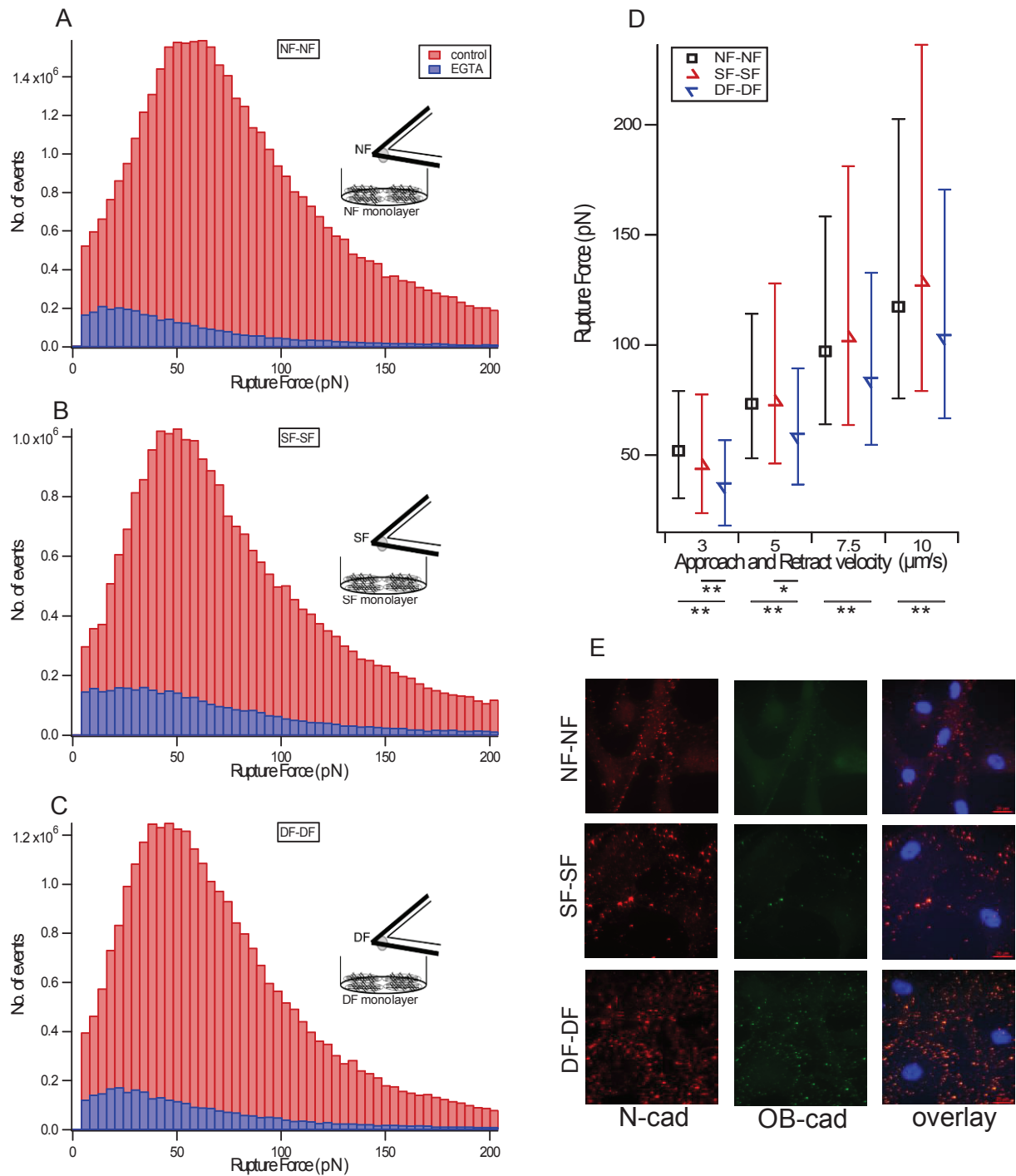
Figure 5.2. Fibroblast intercellular cadherin expression and rupture force measurement. Histogram shows the rupture force (red bar) recorded for (A) NF-NF, (B) SF-SF and (C) DF-DF interactions. Cadherin involvement in the rupture events (Supplementary Fig. 5.7A) was controlled by EGTA (blue bar) addition to the cell-cell interaction setup. This leads to the respective loss of rupture events (Supplementary Fig. 5.7B). (D) Increasing the approach and retract velocity of the cantilever linearly increases the cadherin rupture force for NF-NF (black square), SF-SF (red upper triangle) and DF-DF (blue lower triangle). NF and SF displays large rupture forces than DF at all velocities. Statistical results are reported in Materials and Methods section. (E) Dual immunofluorescence data shows N-cadherin expression (red fluorescence) in all fibroblasts adherens junctions. OB-cadherin expression (green fluorescence) was seen only in DF. The overlay (orange fluorescence) represents the heterophilic binding of N-cadherin and OB-cadherin which is encountered only in DF. Blue fluorescence indicates the nuclei. Scale bar 20 μm.

In order to assess the presence of specific cadherin types in cell-cell interaction sites, all three fibroblast types were immunostained for N- and OB- cadherin. Dual immunostaining for N- (red) and OB- (green) cadherins showed that NF and SF express exclusively N-cadherin whereas DF express both N- and OB- cadherin at the interaction site between cells (Fig. 5.2E). In the overlay (orange-yellow), heterophilic interactions between the N- and OB-cadherins are visible. Single immunostaining for N-cadherin (red) showed that all three fibroblast types express N-cadherin at the interaction site (Supplementary Fig. 5.8A). Similarly, single staining for OB-cadherin (red) in all fibroblasts showed that only DF-DF express OB-cadherin with absent OB-cadherin expression found at the NF-NF and SF-SF interaction site (Supplementary Fig. 5.8B). Controls with no primary antibody for N- (Supplementary Fig. 5.8C) and OB-cadherins (Supplementary Fig. 5.8D) shows no fluorescence that proves no unwanted or unspecific binding of fluorescently tagged secondary antibodies, thus showing the specificity of the secondary antibodies for the primary antibodies used here. This further confirms that the red and green fluorescence seen in Fig. 5.2E and Supplementary Fig. 5.8A&B are due to specific expression of N-cadherin in all three fibroblast types and OB-cadherin only in DF. This reveals homophilic N-cadherin binding in NF and SF and heterophilic N-cadherin/OB-cadherin binding in DF. Homophilic N-cadherin intercellular binding exhibited stronger interaction forces than N/OB-cadherin heterophilic binding when immunostaining results were compared to cadherin-cadherin bond rupture mechanical measurements.

Table 5.1: The median (bold values) rupture force (pN) values of cadherin mediated homocellular and heterocellular adherens junctions at each approach and retract velocities.

Approach and Retract velocity (µm/s) Cell-cell interaction	3			5			7.5			10		
	25th	**Median**	75th	25th	**Median**	75th	25th	**Median**	75th	25th	**Median**	75th
NF-NF	21.53	**51.91**	27.20	24.77	**73.40**	40.72	33.18	**97.18**	61.16	41.63	**117.39**	85.12
SF-SF	21.56	**45.21**	32.33	28.00	**74.22**	53.77	39.56	**103.28**	77.95	49.35	**128.51**	107.84
DF-DF	17.59	**35.71**	21.08	21.57	**58.23**	31.23	28.92	**83.54**	49.22	36.28	**103.05**	67.51
MDCK-MDCK	35.83	**75.51**	50.04	39.74	**98.48**	58.59	47.88	**124.08**	82.34	60.41	**149.68**	111.48
NF- MDCK	20.34	**55.85**	30.04	22.23	**70.48**	35.55	29.08	**91.44**	48.63	35.93	**111.28**	66.59
SF- MDCK	30.53	**39.68**	40.66	29.14	**68.19**	48.56	31.12	**92.36**	61.87	34.45	**106.62**	74.06
DF- MDCK	20.30	**46.70**	26.19	21.84	**63.62**	32.67	27.17	**83.20**	42.12	32.78	**99.42**	53.18

E-, N- and OB- cadherin at the fibroblast-epithelial hetero-cellular adherens junctions

The significance of studying hetero-cellular interactions may lead to sorting out different cell types by their expression and assembly of cell specific cadherins at the interaction site. The investigation of cadherin homophilic and heterophilic interactions may pave the way for a better understanding of cadherin mediated intracellular signalling. Heterophilic cadherin rupture forces were measured between epithelial cells and fibroblasts. A monolayer of fibroblasts was grown in a Petri dish and MDCK epithelial cells were attached to a tipless cantilever functionalized with conA. Fibroblast MDCK interactions were studied by approaching a cantilever with attached MDCK cells towards the fibroblast cell monolayer at 3 µm/s velocity with 3 nN maximum contact force and 2s contact time. In a similar fashion, MDCK-MDCK interactions were studied and the resulting median rupture force value was 75.51 pN. Regarding fibroblast-MDCK interaction, the median rupture force values were

55.85 pN for NF-MDCK, 39.68 pN for SF-MDCK and 46.70 pN for DF-MDCK. (See Table 5.1 which lists the corresponding 25, 50 and 75 percentile values) In order to confirm the cadherin mediated rupture force, the force curves were recorded in the presence of EGTA. The histogram plot (Fig. 5.3A, B, C and D) showed a decrease in rupture events (blue bar) comparative to the rupture events (red bar) obtained without EGTA. The binding strength of the cadherins present in the membrane of these cell types was measured by approaching and retracting the cantilever with the attached MDCK cell at different velocities. All fibroblast-MDCK hetero-cellular interactions and also MDCK-MDCK binding (Fig. 5.3E) showed a linear increase in rupture force as a function of loading rate. The median rupture force values calculated for each pulling velocity for all three types of fibroblasts and MDCK or MDCK-MDCK interactions are listed in Table 5.1. Comparing the rupture forces, NF-MDCK (55.85 pN) (Fig. 3E black filled square), SF-MDCK (39.68 pN) (red filled upper triangle) and DF-MDCK (46.70 pN) (blue filled lower triangle) showed no significant differences between each other; however MDCK-MDCK interactions (sandal filled circle) showed substantially larger rupture forces (75.51 pN).
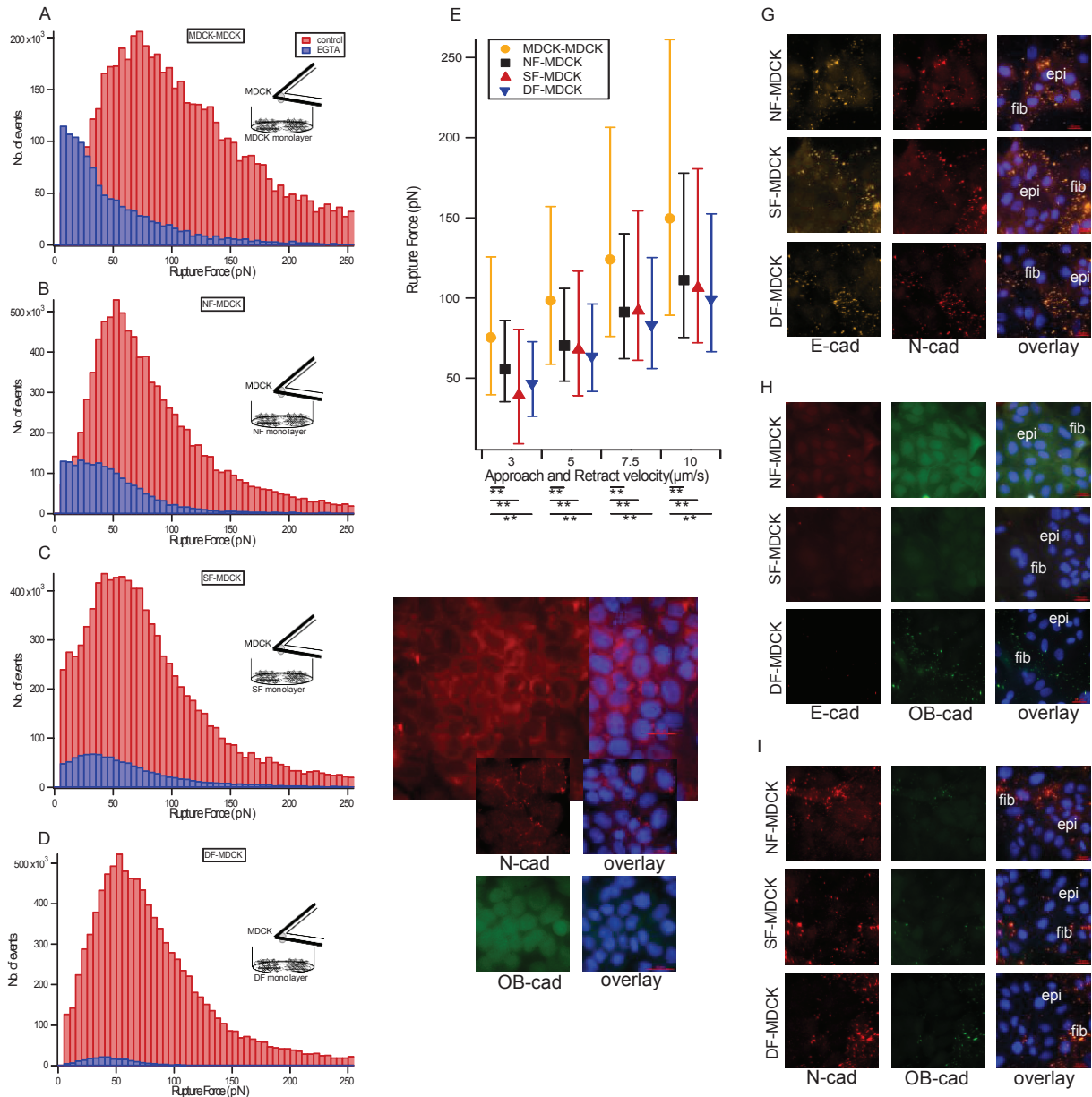
Figure 5.3. Heterocellular fibroblasts-MDCK interactions rupture force measurement and cadherin expression. Ruptures forces displayed as histograms recorded with (blue bar) and without EGTA (red bar) for (A) MDCK-MDCK, (B) NF-MDCK, (C) SF-MDCK and (D) DF-MDCK. (E) The cadherin rupture force shows linear relationship with cantilever approach and retract velocity for MDCK-MDCK (sandal circle), NF-MDCK (black filled square), SF-MDCK (red filled upper triangle), DF-MDCK (blue filled lower triangle). Statistical results are reported in Materials and Methods section. (F) Immunofluorescence data shows predominant E-cadherin expression in MDCK-MDCK adherens junction. Subpopulations of MDCK express N-cadherin but not OB-cadherin. Dual immunofluorescence data shows N-cadherin (red fluorescence in G, I) homophilic binding and loss of E-cadherin (H) in NF-MDCK, SF-MDCK and DF-MDCK. Due to the similar excitation and emission wavelength of fluorescence tags (secondary antibody), dual immunostaining (G) for N-cadherin (red fluorescence) and E-cadherin (sandal fluorescence) is difficult to interpret. The E-cadherin loss seen in (H) confirms the N-cadherin homophilic binding in (G). Only faint OB-cadherin expression (green fluorescence) observed in DF-MDCK (I). Blue fluorescence indicates DAPI-stained nuclei. Scale bar 20 μm.

We examined the distribution of different cadherin subtypes in MDCK-MDCK homo-cellular and fibroblast-MDCK hetero-cellular adherens junctions. MDCK monolayers were immuno-

stained for E-, N- and OB-cadherin (Fig. 5.3F). We observed E-cadherin in the MDCK cell-cell junctions with a subpopulation of MDCK cells expressing very little N-cadherin. In addition, there was no OB-cadherin expression in MDCK cells. To verify the cadherin expression in fibroblast-epithelial cell interaction sites, NF-MDCK, SF-MDCK and DF-MDCK were dual immuno-stained against the different cadherin subtypes (E/N, E/OB and N/OB). The secondary antibody with fluorescent tags that was used for detection of the primary anti-N-cadherin and anti-E-cadherin share almost the same excitation and emission wavelength. This made it difficult to differentiate between the E- and N-cadherin heterophilic interaction in NF-, SF- and DF- MDCK adherens junctions (Fig. 5.3G). Dual immunostaining for E- and OB-cadherins showed a reduction of E-cadherin and absence of OB-cadherin expression in co-cultures with NF-MDCK or SF-MDCK. The loss of E-cadherin was accompanied with faint expression of OB-cadherin in DF-MDCK cultures as well (Fig. 5.3H). In dual immunostaining for N- and OB-cadherins (Fig. 3I), only N-cadherin expression and no OB-cadherin expression were seen at the NF-MDCK and SF-MDCK and very little OB-cadherin at the DF-MDCK adherens junctions. The observation from these cadherin (E/OB and N/OB) subtypes helped to solve the E/N subtype issue and confirms the presence of N-cadherin in Fig. 5.3G. Control experiments showed no E-cadherin expression in NF-NF, SF-SF and DF-DF (Supplementary Fig. 5.9). In summary, the immunofluorescence data (Fig. 5.3I) showed that N-cadherin is the predominant cadherin in the fibroblasts-MDCK adherens junctions. N-cadherin was exclusively seen in the fibroblasts-MDCK and not between MDCK-MDCK junctions in co-cultures. Initially, MDCK-MDCK interaction in MDCK cell cultures showed more E-cadherin and very little N-cadherin expression.

Role of actin assembly in homo- and hetero-cellular adherens junctions

Cytochalasin D disrupts the actin assembly and results in cell softening (Rotsch and Radmacher, 2000). Here, we used 5 μM cytochalasin D to disassemble actin filaments to investigate the role of actin in both homo-cellular and hetero-cellular adherens junctions. As the drug was dissolved in DMSO, any effect of DMSO in cell-cell interaction had to be ruled out in control experiments before. The cityscape plot showed the rupture forces recorded from homo-cellular (Fig. 5.4A-D) and hetero-cellular (Fig. 5.4E-G) cadherins bond rupture before and after the addition of cytochalasin D. The retract curves from control experiments (defined as no drug and no DMSO) (Supplementary Fig. 5.10A) or with DMSO (Supplementary Fig. 5.10B) showed no differences in the rupture patterns whereas with cytochalasin D (Supplementary Fig. 5.10C) dissimilar rupture events were observed. Treatment with cytochalasin D resulted in a reduction of the peak rupture force (Fig. 5.4 blue line) compared

to DMSO addition (Fig. 5.4 red line) or control (Fig. 5.4 black line). The respective median rupture force values calculated for each condition for both homo-cellular and hetero-cellular junctions are listed in Table 5.2. The plot of median rupture forces (Supplementary Fig. 5.11) showed that the cadherin bond rupture force values were decreased in the presence of cytochalasin D for both homo- and hetero-cellular interactions; whereas, no significant differences were observed between control and DMSO rupture force values. This illustrates that the regulation of cadherin extracellular binding dynamics by intracellular actin filaments through their interaction with cadherin cytoplasmic domain.

Table 5.2: The median (bold values) rupture force (pN) values of cadherin mediated homocellular and heterocellular adherens junctions without drug (control), DMSO and cytochalasin D (5 µM).

	control			DMSO			cytochalasinD		
Cell-cell interaction	25th	**Median**	75th	25th	**Median**	75th	25th	**Median**	75th
NF-NF	25.39	**61.86**	41.51	25.23	**60.24**	39.15	14.92	**31.06**	18.48
SF-SF	24.29	**58.41**	36.81	23.44	**48.34**	38.03	10.82	**30.47**	15.79
DF-DF	28.13	**48.41**	33.46	25.93	**45.64**	48.17	10.07	**25.65**	12.43
MDCK-MDCK	28.80	**75.61**	38.40	30.04	**75.24**	53.00	19.70	**43.21**	24.16
NF- MDCK	21.49	**57.04**	30.16	23.24	**64.70**	39.18	23.14	**25.54**	27.56
SF- MDCK	25.04	**56.77**	35.07	21.82	**57.19**	27.98	15.78	**14.98**	18.77
DF- MDCK	23.69	**60.13**	35.41	25.29	**68.42**	40.01	20.50	**23.36**	24.50
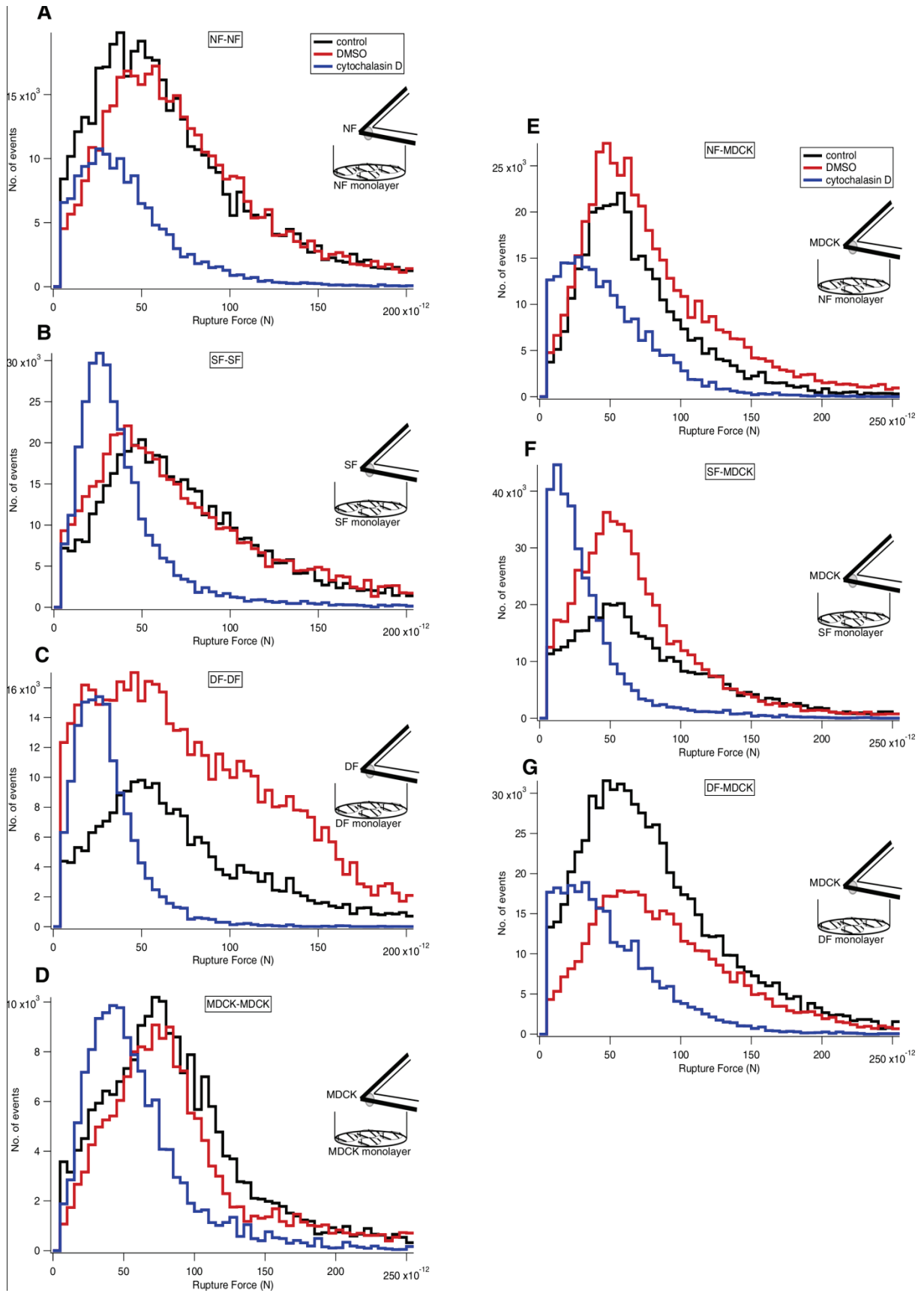
Figure 5.4. Effects of Cytochalasin D Treatment on the rupture force of homocellular and heterocellular adherens junctions. The cityscape plot summarize the effect of cytochalasin D (5 µM) on homocellular- (A) NF-NF, (B) SF-SF, (C) DF-DF, (D) MDCK-MDCK and heterocellular- (E) NF-MDCK, (F) SF-MDCK, (G) DF-MDCK adherens junctions. Rupture events were recorded without the drug as control (black line), with DMSO

(red line) and with cytochalasin D (blue line). The corresponding median values were listed in Table 5.2 and plotted in Supplementary Figure. 5.11.

Myosin inactivation strengthens the N/OB cadherin heterophilic binding

ML-7 inhibits the MLCK activity by inhibition of myosin cross-linking to the actin filaments. As a consequence, there is reduction in contractile stresses, which leads to a softening of the intracellular actin cytoskeleton (Lyapunova et al., 2016). Here we used 5 µM ML-7 to inhibit the myosin activity and determined the role of myosin in both homo-cellular and hetero-cellular adherens junctions. The cityscape plot showed the rupture forces recorded from homo-cellular (Fig. 5.5A-D) and hetero-cellular (Fig. 5.5E-G) cadherin bond ruptures before and after the addition of ML-7. The retract curves from control (no drug and no DMSO) (Supplementary Fig. 5.12A), DMSO (Supplementary Fig. 5.12B) and with ML-7 (Supplementary Fig. 5.12C) showed no difference in the rupture patterns except for DF-DF. No significant shift in rupture force peaks was observed in control (Fig. 5.5 black line), DMSO (Fig. 5.5 red line) and ML-7 (Fig. 5.5 blue line). Only DF-DF showed an increase in the rupture force after treatment with ML-7 (Fig. 5.5C blue line). Comparing the retract curves of controls (Supplementary Fig. 5.13A), DMSO (Supplementary Fig. 5.13B) or ML-7 (Supplementary Fig. 5.13C) treatment of different fibroblast cultures, DF-DF showed distinctive large rupture events in ML-7 treated force curves. The respective median rupture force values calculated for each condition for both homo-cellular and hetero-cellular junctions

Table 5.3: The median (bold values) rupture force (pN) values of cadherin mediated homocellular and heterocellular adherens junctions without drug (control), DMSO and ML-7 (5 µM).

Cell-cell interaction	control			DMSO			ML-7		
	25th	**Median**	75th	25th	**Median**	75th	25th	**Median**	75th
NF-NF	24.48	**58.81**	45.80	19.67	**52.04**	38.84	16.49	**48.87**	33.25
SF-SF	27.37	**66.20**	38.17	34.66	**53.12**	41.96	28.72	**48.98**	36.52
DF-DF	24.29	**53.19**	34.65	23.19	**45.49**	31.87	48.01	**99.69**	75.06
MDCK-MDCK	24.53	**69.71**	43.41	27.11	**67.22**	56.11	26.03	**69.69**	42.50
NF- MDCK	18.58	**52.06**	25.22	17.71	**54.74**	23.17	17.82	**54.41**	22.91
SF- MDCK	17.42	**48.95**	16.58	15.51	**53.87**	17.37	15.05	**41.44**	16.73
DF- MDCK	11.99	**48.35**	18.55	12.98	**47.05**	18.15	15.24	**52.32**	23.10

were listed in Table 5.3. The median plot (Supplementary Fig. 5.14A, B, D, E, F, and G) showed no significant change in the rupture force values for cell-cell interactions in NF-NF or SF-SF cultures in the presence of ML-7 comparing to that of control and DMSO. In case of DF-DF, the median rupture force value (Supplementary Fig. 5.14C) increased significantly after the addition of ML-7. Interestingly, no significant differences were observed in control and DMSO rupture force values in DF-DF. Possibly, the intracellular myosin inactivation by MLCK inhibition does not affect the cadherin homophilic binding. In case of DF-DF which express N-cadherin/OB-cadherin heterophilic binding, myosin inactivity seems to strengthen heterophilic cadherin interactions.
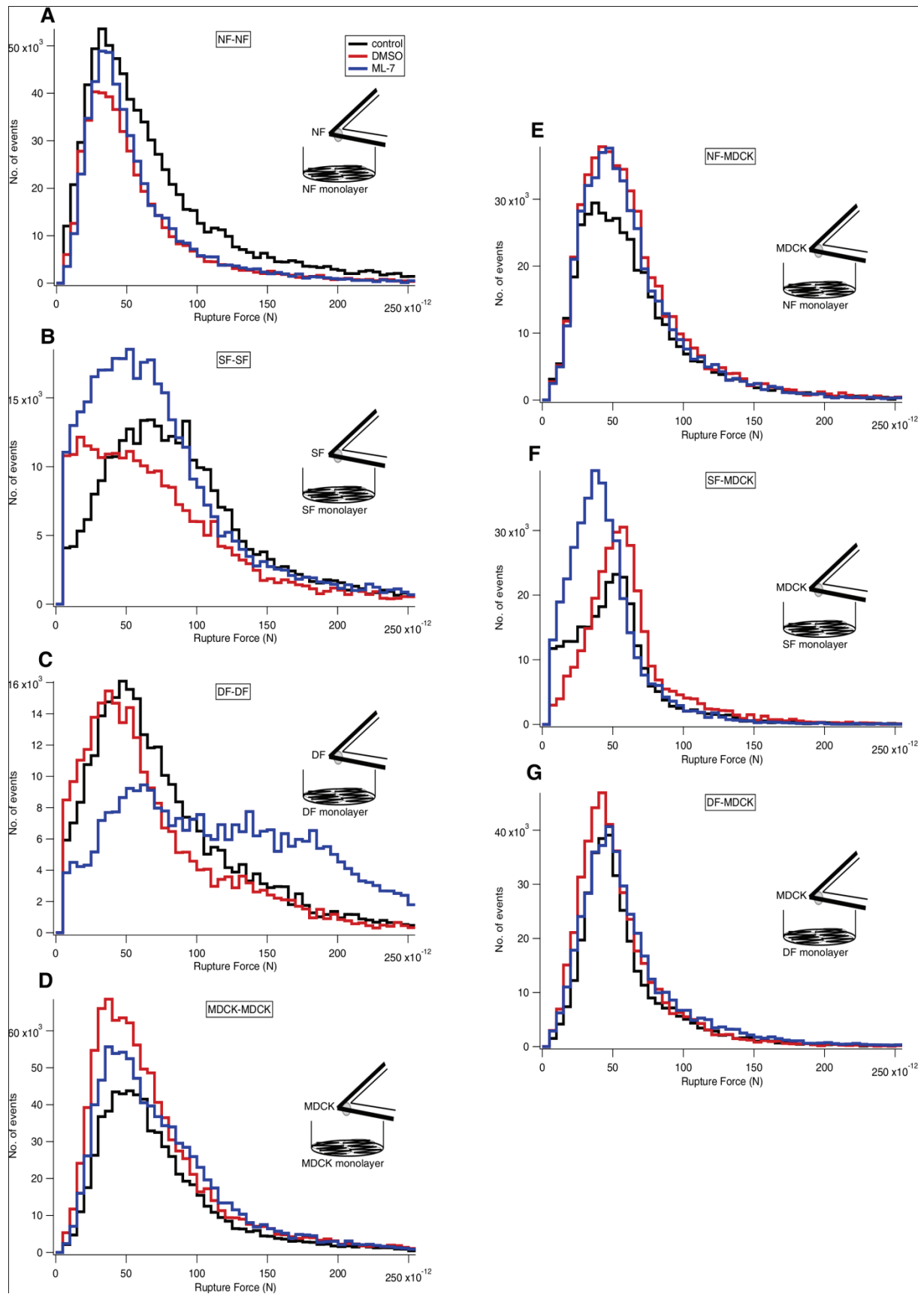
Figure 5.5. Effects of ML-7 Treatment on the rupture force of homocellular and heterocellular adherens junctions. The cityscape plot summarize the effect of ML-7 (5 µM) on homocellular- (A) NF-NF, (B) SF-SF, (C) DF-DF, (D) MDCK-MDCK and heterocellular- (E) NF-MDCK, (F) SF-MDCK, (G) DF-MDCK adherens

junctions. Rupture events were recorded without the drug as control (black line), with DMSO (red line) and with ML-7 (blue line). The corresponding median values were listed in Table 5.3 and plotted in Supplementary Figure. 5.14.

5.4 Discussion

In this work, we performed AFM-based SCFS on homo- and hetero-cellular arrangements between different fibroblasts (NF, SF and DF) and MDCK cells. We measured the homophilic and heterophilic cadherin adhesion rupture forces. Immunofluorescence staining allowed us to visualize the presence of such homophilic and heterophilic pairs of E, N and OB cadherins. Our results showed that homophilic adhesions were stronger than heterophilic adhesions. In addition, our results suggest a role of the intracellular actin cytoskeleton in homophilic and heterophilic cadherin bonds modulating extracellular binding strength. With differing binding capacity and specificity, cadherins of cellular adherens junction play an important role in intra- and inter-cellular mechano-signalling for force transmission. So far, AFM and optical tweezers based SMFS explored the binding strength and kinetics of various cadherin types - both homophilic and heterophilic binding (Baumgartner et al., 2003, 2000; Pittet et al., 2008; Rakshit et al., 2012). Most of these studies were carried out with cadherins which were overexpressed or purified and lacking certain domains (for example, recombinant constructs lacking the cytoplasmic domain). Here, we used AFM based SCFS to measure the rupture forces of cadherin-cadherin bonds in or between cells, i.e. the cadherins measured were in their native state. This setup allowed us to study the cadherin pair formation and their bond rupture forces in physiologically relevant homo- and hetero-cellular arrangements. Previously, using this setup VE-, E- and N- cadherin homophilic pair formation, their binding strength and kinetics were studied using the homo-cellular arrangements made with HUVEC, L-M (TK-) and CHO cells, respectively (Panorchan et al., 2006a, 2006b). In a similar way, we attached different types of fibroblasts (NF, SF and DF) to the AFM cantilevers and put them into contact with monolayers of the same type of fibroblasts. The measured rupture forces showed that NF-NF and SF-SF exhibit stronger interactions than DF-DF. Immunofluorescence studies revealed that N/N-cadherin homophilic pairs enforced the intercellular junctions in NF and SF. Whereas in the case of DF, N-/OB-cadherin heterophilic pairs were seen in the cellular junctions and this contributes to their weaker interaction. NF and SF were shown to express α-sma, but no large stress fibres running in the cell body. Thus both cell types were considered as fibroblast phenotype (Babu et al., 2018). When SF was seeded in a physiological environment such as a decellularized dermal matrix, cells expressed large stress fibres and thus showed a proto-myofibroblast or myofibroblast phenotype (Babu

et al., 2019). In contrast, DF showed α-sma positive large stress fibres and thus were considered as myofibroblast phenotype (Babu et al., 2018). In comparison to earlier reports (Pittet et al., 2008; Verhoekx et al., 2013b), N-cadherin N-cadherin expression was seen in the normal fibroblast phenotype (in this study: NF and SF) and OB-cadherin expression in the myofibroblast phenotype (DF). In contrast to rat fibroblasts, which show a transition in expression from N- to OB-cadherin triggered by TGF-β1 (Pittet et al., 2008), we found in our study that DF expressed both N- and OB-cadherins and exhibited N/OB heterophilic binding. Fibroblasts from patients with Dupuytren's disease express stress fibres and a myofibroblastic phenotype without mechanical or biochemical stimulation such as TGF-β1 (Pittet et al., 2008). Biochemical expression of N-cadherin was observed in Dupuytren's myofibroblast and results from a collagen gel contraction study showed that myofibroblasts displayed reduced contraction in the presence of N-cadherin blocking peptide (Verhoekx et al., 2013b). Obviously, N-cadherin has an important function in myofibroblast intercellular junctions and adherens kinetics. By immunofluorescence, N-cadherin and OB-cadherin expression and their homophilic (in NF and SF) and heterophilic (in DF) pair formation were observed in all three fibroblast phenotypes. In this study, we found that the presence of different cadherins was strongly correlated with the rupture forces measured by SCFS.

In our study, the E/E-cadherin homophilic interactions in MDCK showed rupture force values closely related to previous studies (Panorchan et al., 2006b). This confirms the initial adhesion in MDCK homo-cellular arrangements could be largely dominated by E-cadherin homophilic binding that displays the larger rupture force. MDCK sub-populations such as trypsin sensitive MDCK are characterized by N-cadherin expression (Youn et al., 2005) which we could confirm the N-cadherin expression seen in MDCK cultures with our immunofluorescence analyses.

In tissue and sub-tissue level biology, multicellular interactions are orchestrated through various cell-cell junction mechanisms which, in turn, coordinate individual cell type actions such as directed cellular migration and wound contraction. As central component of the adherens junction, the cadherin transmembrane proteins plays a key role in force transmission between the intracellular environment of different cell types and the intercellular space through cadherin type binding specificity. This phenomenon could have implications for biological analytical methods, e.g. for cell sorting. In response to tissue injury and during wound healing, direct contact between epithelial cells and underlying fibroblasts modulate the necessary protein expression levels which are important for the wound healing process (Krieg et al., 2007). Through activation by the cytokine TGF-β1 in the ECM or by mechanical injury

of epithelial cells, the biochemical expression of α-sma and type I and III collagen was induced in epithelial cell co-cultured fibroblasts (Morishima et al., 2001). These observations brought the knowledge of investigating the adhesion proteins involved in hetero-cellular interactions such as epithelial cell-fibroblasts interaction. For SCFS hetero-cellular studies, MDCK epithelial cells were attached on the cantilever and brought in contact with fibroblasts grown in monolayers in a Petri dish. This experimental set-up was chosen to measure the rupture forces of the N/N homophilic and E/N, E/OB and N/OB heterophilic bonds. Distinct peaks were not observed in the rupture force histograms (Fig. 5.3B, 5.3C and 5.3D), but the observed heterophilic bond results are able to be discussed with previous results. For example, an earlier SCFS study did not show any occurrence of heterophilic interactions between E-cadherin and N-cadherin (Panorchan et al., 2006b). Contrarily, a single molecule study shows the existence of such E/N cadherin heterophilic interactions (Prakasam et al., 2006) and in this study, we observed such E/N cadherin heterophilic interactions from the cell-cell adherens site. Presumably, shorter contact/dwell times (millisecond) used in the former studies could be the reason for not recognizing heterophilic interactions as found in our study (Prakasam et al., 2006). In standard experimental settings, shorter contact times between the cells in the petri dish and on the cantilever were used to prevent nonspecific binding. Deliberately, we chose a different experimental design with longer contact time of 2 sec. in the SCFS setup which enabled us to follow both homophilic and heterophilic cadherin interactions. Despite of the changed protocol, distinct peaks could not be resolved in the histograms. This might be due to the possibility that N/N and E/N rupture forces share similar values. In case of DF-MDCK, no distinct peaks of E/OB and N/OB were seen which could be due to similar rupture forces. This leads to the question if single molecule kinetic studies using AFM or optical tweezers are suitable to measure homophilic and heterophilic cadherin pairs.

E-/N-cadherin heterotypic adhesion sites reinforced by local cytoskeletal reorganization were observed between IAR-2 epithelial cells and RAT-1 fibroblasts using immunofluorescence staining (Omelchenko et al., 2001). This mechanically active heterotypic contact between N-cadherin expressing cancer associated fibroblasts and an E-cadherin expressing epithelial cancer cell line (A431) enables fibroblasts to steer cancer cell invasion (Labernadie et al., 2017). Loss of E-cadherin was observed in co-cultures of fibroblast with epithelial cells, whereas normal fibroblasts can induce E-cadherin loss to promote EMT in gastric cancer (Xu et al., 2014). Epithelial cell-fibroblast interactions stimulate EMT in human bronchial epithelial cells from chronic obstructive pulmonary patients (Nishioka et al., 2015). Accordingly, we found reduced E-cadherin and increased N-cadherin in our multi-cell

cultures with immunofluorescence which might implies the initiation of an EMT process. Furthermore, N/N homophilic adhesion (NF-MDCK and SF-MDCK) and N/OB heterophilic adhesion (DF-MDCK) were present at the interaction sites between epithelial cells and fibroblasts.

In AFM based SCFS, a varying cantilever pulling rate allowed for characterizing the cadherin binding strength. Rupture forces generally increase with increasing pulling rate, which leads to increased loading rates (Taubenberger et al., 2013). In this study, E-cadherin and N-cadherin homophilic and OB-cadherin heterophilic binding rupture forces showed a linear relationship related to the pulling rate. In the fibroblast homo-cellular arrangement, N-cadherin homophilic binding was stronger in NF and SF compared to N/OB-cadherin heterophilic binding in DF. Similarly, in fibroblast-epithelial cell hetero-cellular arrangement, all three fibroblast types interacting with MDCK show similar rupture forces. In general, E-cadherin homophilic binding in MDCK homo-cellular arrangement displayed the strongest binding strength which reflects previous findings (Panorchan et al., 2006a, 2006b; Pittet et al., 2008).

Differences in force peak values can be found when results are compared to other studies. Due to the stochastic process of cadherin protein binding forces can be distributed differentially. Rupturing of molecular bonds is always effected by thermal fluctuations, leading to varying rupture forces and thus cadherin binding events are stochastic (Rico et al., 2013). Even the VE-, N- and OB-cadherin SMFS and SCFS measurements showed three different interaction forces, as the three force peaks were present in rupture force histograms (Baumgartner et al., 2000; Pittet et al., 2008). However, cadherin pairs (VE-, E- and N-) exhibited single force states as well which correlates well to results found in earlier SCFS studies (Panorchan et al., 2006a). Similarly, we observed one single force peak in the histograms which correspond to a single rupture force of cadherin bond unbinding.

Cell-cell adhesion is mediated by cadherins in adherens junctions. Cadherins are linked with their cytoplasmic domain to the intracellular actin cytoskeleton through adaptor proteins such as α- and β-catenin (Weis and Nelson, 2006). Disruption of actin filaments by cytochalasin D affected the cadherin extracellular domain homophilic and heterophilic binding dynamics in our study. It seems that the inactivation of actin filaments with cytochalasin D has a direct effect on the cadherin extracellular binding activity by altering the cadherin cytoplasmic link to the actin filaments (Pittet et al., 2008). However, this phenomenon was found exclusively for OB-cadherin homophilic binding (Pittet et al., 2008). In our study we could show a similar effect for both homophilic (N/N and E/E) and heterophilic (E/N, N/OB and E/OB) adhesion in

homo- and hetero-cellular arrangements.

ML-7 inhibits the activity of MLCK by interacting with the phosphorylation of myosin light chain (MLC). The binding of myosin to actin filaments and ATPase driven contractile force generation are inhibited (Hamacher et al., 2018; Rigor et al., 2013; Simões and Fierro, 2005). In the current study, disabling actin-myosin contraction using ML-7 showed no effect on the cadherin extracellular binding dynamics except for N-/OB-cadherin heterophilic binding. Myosin inactivation particularly strengthened the N-/OB- cadherin extracellular binding activity demonstrated by the change of rupture forces. A hypothetical signalling pathway that could explain the observed N/OB- cadherin reinforcement effect is stated in Fig. 6. Myosin II acts as an actin crosslinker (Laevsky and Knecht, 2003) whereas myosin VI acts as a mediator protein, which binds cadherin to actin filaments (Budnar and Yap, 2013). From our current findings and previous results from others, we speculate that: (1) There is no influence of actomyosin contraction or inactivated myosin on homophilic or heterophilic cadherin extracellular binding dynamics (excluding N/OB); (2) myosin is creating tension in actin filament network, which weakens the N/OB-cadherin heterophilic bond, while inactivation of myosin strengthens this bond; (3) myosin inactivation enhances the N/OB-cadherin reinforcement by the detachment from the cadherin-actin complex. (4) As a consequence, actin filaments per se reinforce and stabilize the cadherin extracellular binding. Loss of myosin II selectively inhibits myofibroblast differentiation in fibroblasts of fibrotic lung when compared to healthy phenotype (Southern et al., 2016).
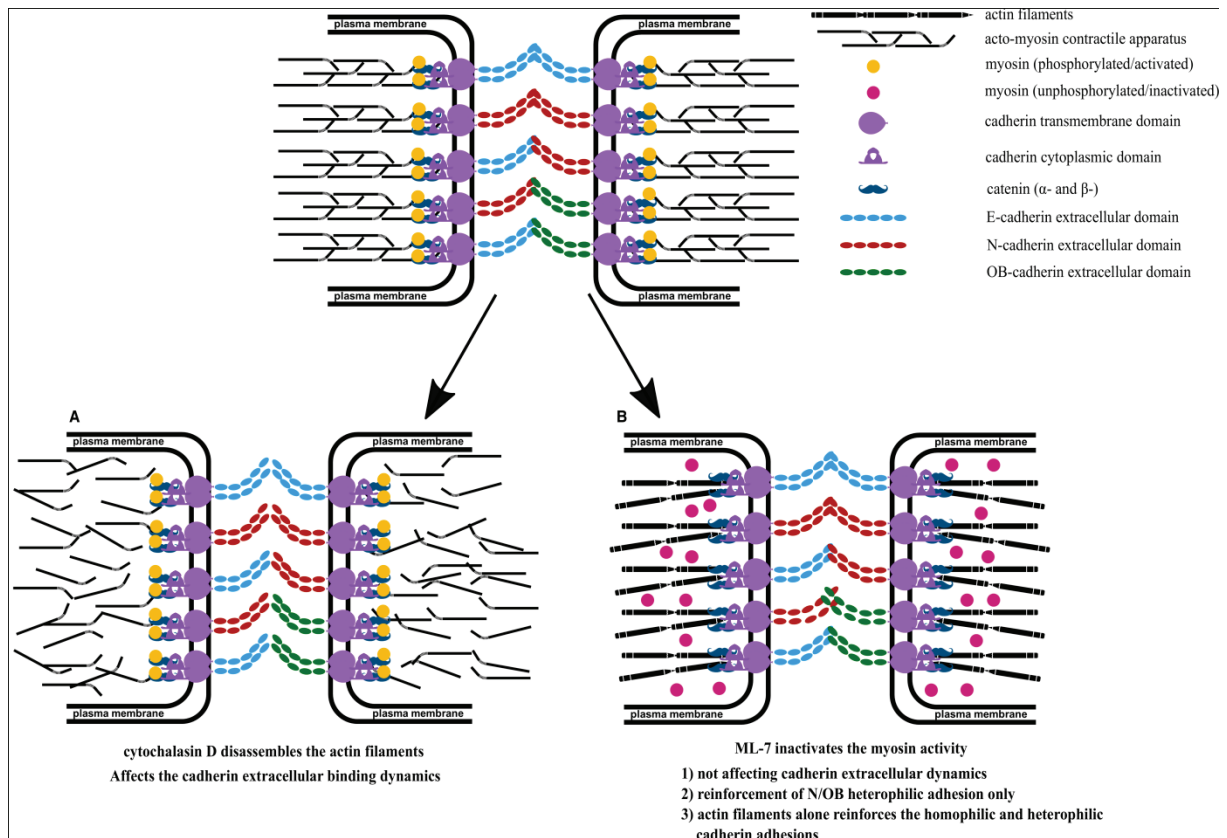
Figure 5.6. Acto-myosin contractility influence cadherin extracellular domain binding dynamics. Cartoon representations depict the effect of actin filaments disruption (A) and myosin inactivation (B) on cadherin homophilic and heterophilic adhesion pairs. (A) Actin filaments disassembly achieved by cytochalasin D treatment leads to weakening of homophilic and heterophilic cadherin adhesions. (B) Myosin inactivation by inhibiting myosin light chain kinase (MLCK) using ML-7 treatment leads to N/OB heterophilic adhesion reinforcement whereas no effects were seen in other cadherin homophilic and heterophilic adhesions. This pictures the stabilization and reinforcement of cadherin homophilic and heterophilic adhesion by actin filaments with no cross linkers-myosin generating contractile forces and with myosin inactivation at the cadherin-catenin-actin complex.

Draw-backs of the current study include the analysis of biochemical expression levels of all myosin types (1-6) and respective localization associated with other functional abilities such as anchoring cadherin-catenin complex to the actin filaments in the cell-cell adhesion sites. Investigations into downstream intracellular signalling pathways are necessary to study further details on the involvement of other signalling molecules (adaptor proteins) in cadherin homophilic and heterophilic adhesion.

5.5 Conclusion

So, in understanding the biophysical dynamics of cell-cell adhesion the underlying actin/adherens junctions and its associated proteins have also to be considered. Our findings showed that myosin inactivation provides mechanical strengthening of N/OB heterophilic adhesion and dissimilar effects on other homophilic and heterophilic adhesion. Based on our

results, further studies are required to investigate the multifunctional role of myosin types, actin filaments and other associated proteins in cell-cell adhesion. SCFS can be a suitable experimental setting to examine the role of intracellular proteins involved in various cellular processes specifically cell-ECM adhesion and here cell-cell adhesion, if one can design the experiments accordingly.

5.6 Methods and Experimental Design

Cell culture

Cell culture was done as previously described (Babu et al., 2018). Fibroblasts were harvested from tissues of patients undergoing hand surgery (approved by the local Ethics Committee-Ärztekammer Bremen, #336/2012) and isolated as described previously. Cells were grown until the passage-9 for fibroblasts and 13 for MDCK in DMEM medium and incubated at 37°C in a humidified atmosphere of 95% air and 5% CO_2. Cell culture was established for two days before proceeding with further SCFS measurements. Medium was supplemented with 10% fetal bovine serum (FBS) and 2% penicillin-streptomycin.

Cantilever functionalization

The silicon-nitride tipless cantilevers (Nanoprobe SPM Tips, NP-OW 9861) were washed with 1 % SDS (sodium dodecyl sulphate), Helizyme (B. Braun Vet Care GmbH) and distilled water solution each for overnight. The cantilevers were then treated with plasma (Ar) at high power for 4 min. In order to functionalize the plasma treated cantilevers with concanavalin A (conA) (C2010, Sigma-Aldrich), the cantilevers were placed in a phosphate buffered saline (PBS) solution containing conA (2 mg/ml) for 2 h at room temperature. The conA coated cantilevers were stored in PBS at 4°C (Friedrichs et al., 2010).

Cell attachment to the cantilever

Prior to cell-cell adhesion measurements, cells that were used for attachment to the cantilever were released from the culture flask by treatment with trypsin for 2 min and trypsin was neutralized by centrifugation and replenishment with new medium. The trypsinized cells were transferred into the Petri dish containing a firmly attached cell monolayer. After 5 min incubation at 37°C, the Petri dishes were used for the single-cell force spectroscopy-AFM setup. The conA functionalized cantilever was then placed over a suitable cell with round morphology which initiated its attachment to the cell monolayer. Then, the conA coated cantilever was approached towards the cell with a 3.5 nN maximum loading force for 2s at a velocity 5 µm/sec until the cell was captured. The cantilever with attached cell was taken few µm away from the cell monolayer and the whole setup was left undisturbed for 10 min in

order to establish firm cell adhesion to the cantilever.

AFM cell adhesion force measurements and data analysis

Single-cell experiments were conducted using a MFP3D AFM (Asylum Research, Santa Barbara, CA, USA). An optical microscope (Zeiss Axiovert 135, Zeiss, Oberkochen) was combined with the AFM to be able to control cantilever and sample positioning. All measurements were performed with 15 tipless cantilevers with a nominal spring constant 60 pN/nm. The Petri dishes with the cell monolayer were fixed to an aluminium holder with vacuum grease and mounted on the AFM stage with two magnets. The AFM head including the sample was enclosed in a homebuilt polymethacrylate (PMMA) box in order to inject and maintain 5% CO_2. Force maps were recorded on cell monolayer to obtain cell-cell rupture force. First, the spring constant of the conA coated cantilever was calibrated by using the thermal tune method on a cleaned and stiff surface (Sader et al., 1995) and then cell capturing followed by cell-cell adhesion force curves were recorded. For force curves, we used typically a maximum loading force of 3nN with 2 s dwell time at a velocity (approach and retract) of 3 µm/sec.

The data analysis package IGOR (wave metrics, Lake Oswego, OR, USA) was used to evaluate the rupture force from the retract force curve. The retract curve contains two different patterns - jumps and tethers. Jumps in the retract curve correspond to the rupture of cadherin bonds, whereas plateaus correspond to pulling of membrane tethers. The height of all jumps was multiplied to the cantilever spring constant in order to obtain the rupture force. By changing the approach and retract velocity (5, 7.5 and 10 µm/sec), we measured the loading rate dependent rupture forces within the cadherin bonds. Rupture forces calculated from all rupture events were presented in histograms. Each category of experiments was repeated two to four times (n=2 to 4). For each category, 30 to 40 force maps (one force map contains 24 force curves) were analyzed.

EGTA, Cytochalasin D and ML-7 addition

For demonstrating Ca^{2+} specific cell-cell interactions, control experiments were performed with 7.5 mM EGTA (Sigma-Aldrich). For drug induced changes on cell-cell adhesion measurements, cytochalasin D (C8273, Sigma-Aldrich) and ML-7 (I2764, Sigma-Aldrich) were used at 5 µM working concentration. Substances were solubilized in DMSO to a stock solution of 200 µM. From this stock solution, 100 µL were added to cultures to a final concentration of 5 µM. To exclude the nonspecific effects of DMSO, control experiments with DMSO were performed in parallel and plotted with drug induced changes in cell-cell adhesion.

Immunofluorescence staining

Regarding immunofluorescence experiment for fibroblast-epithelial cell interaction, co-culturing of fibroblast and epithelial cells was performed in 1:2 ratio. Two days after seeding, cells were fixed with 3.7% formaldehyde for 15 min and permeabilized with 0.1% Triton X100 for 3 min. Samples were washed with PBS after each step and blocked with 3 % goat serum and then incubated with primary antibodies, anti-N-cadherin 1:200 dilution (rabbit polyclonal; sc-7939, Santa Cruz Biotechnology), anti-OB-cadherin 1:50 dilution (mouse monoclonal; sc-365867, Santa Cruz Biotechnology) and anti-E-cadherin 1:50 dilution (goat polyclonal; AF748, R&D systems) at 4°C overnight. After incubation, samples were washed with PBS containing goat serum. Then samples were blocked with 3 % goat serum and then incubated with respective secondary antibodies, e.g. cy3 anti-rabbit IgG (711-165-152, Jackson ImmunoResearch Laboratories, Inc.) at 1:200 dilution, FITC anti-mouse IgM (315-095-020, Jackson ImmunoResearch Laboratories, Inc.) at 1:100 dilution and Rhodamine/TRITC anti-goat IgG (305-025-045, Jackson ImmunoResearch Laboratories, Inc.) at 1:100 in a dark environment. For multicolor staining (dual staining), a sequential (staining one protein after another) incubation of primary and secondary antibodies was performed. Then samples were washed with PBS and stored with ProLong Diamond Antifade Mountant with DAPI (P36966, ThermoFisher Scientific) at 4°C prior to image acquisition. The cells were visualized with a 100x oil-immersion objective mounted on Nikon Eclipse Ti Inverted epifluorescence Microscope (Nikon Instruments Inc., Melville, New York).

Statistical analysis

Statistical differences for the median values of rupture force of cadherins present in homo-cellular and hetero-cellular arrangement of the AFM measurements were determined by Wilcoxon test, calculated in IGOR software. * and ** indicate statistically significant differences for p-values < 0.05 and p < 0.005, respectively.

5.7 Acknowledgements

5.8 Author contributions

PK designed and performed the research and was also performing AFM experiments, fluorescence experiments, data analysis and manuscript preparation. UM provided the different fibroblast types, analytical material and substances and, was involved in the manuscript preparation. GB isolated and provided the cells and also provided antibodies. MR designed the experimental setting and was involved in data acquisition, data analysis and preparation of the manuscript.

## 5.9 Additional information

Competing financial interests: The authors declare no competing financial interests.

5.10 Supporting Information
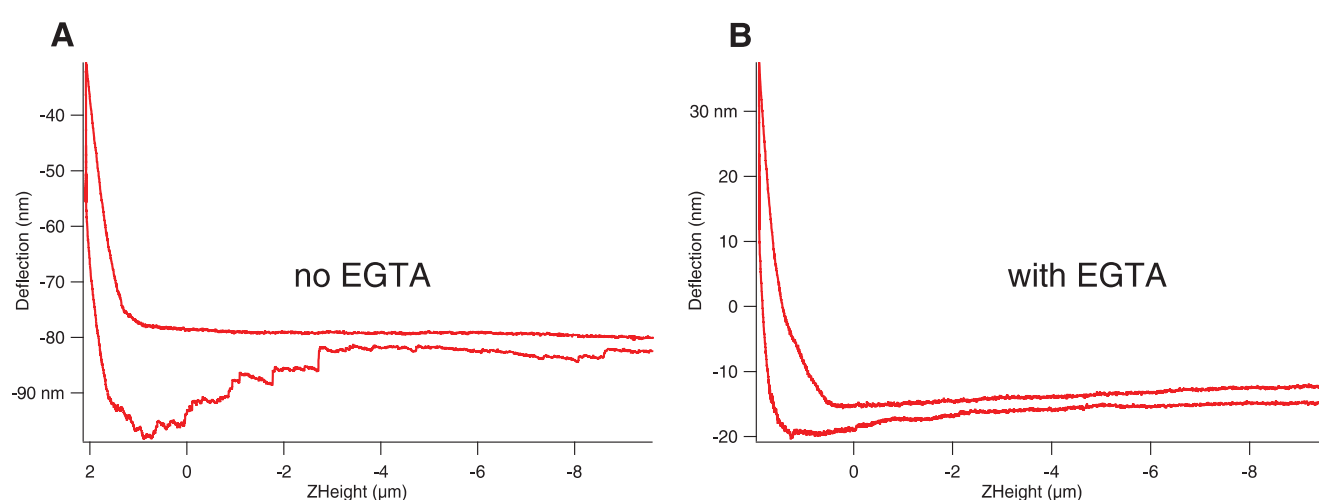
Supplementary figure 5.7 Force curves obtained during cell-cell interaction (here MDCK-MDCK) show distinct rupture events under normal conditions (no EGTA) (A), which in the presence of EGTA, corresponding to low or no Ca^{2+} present, disappear (B).
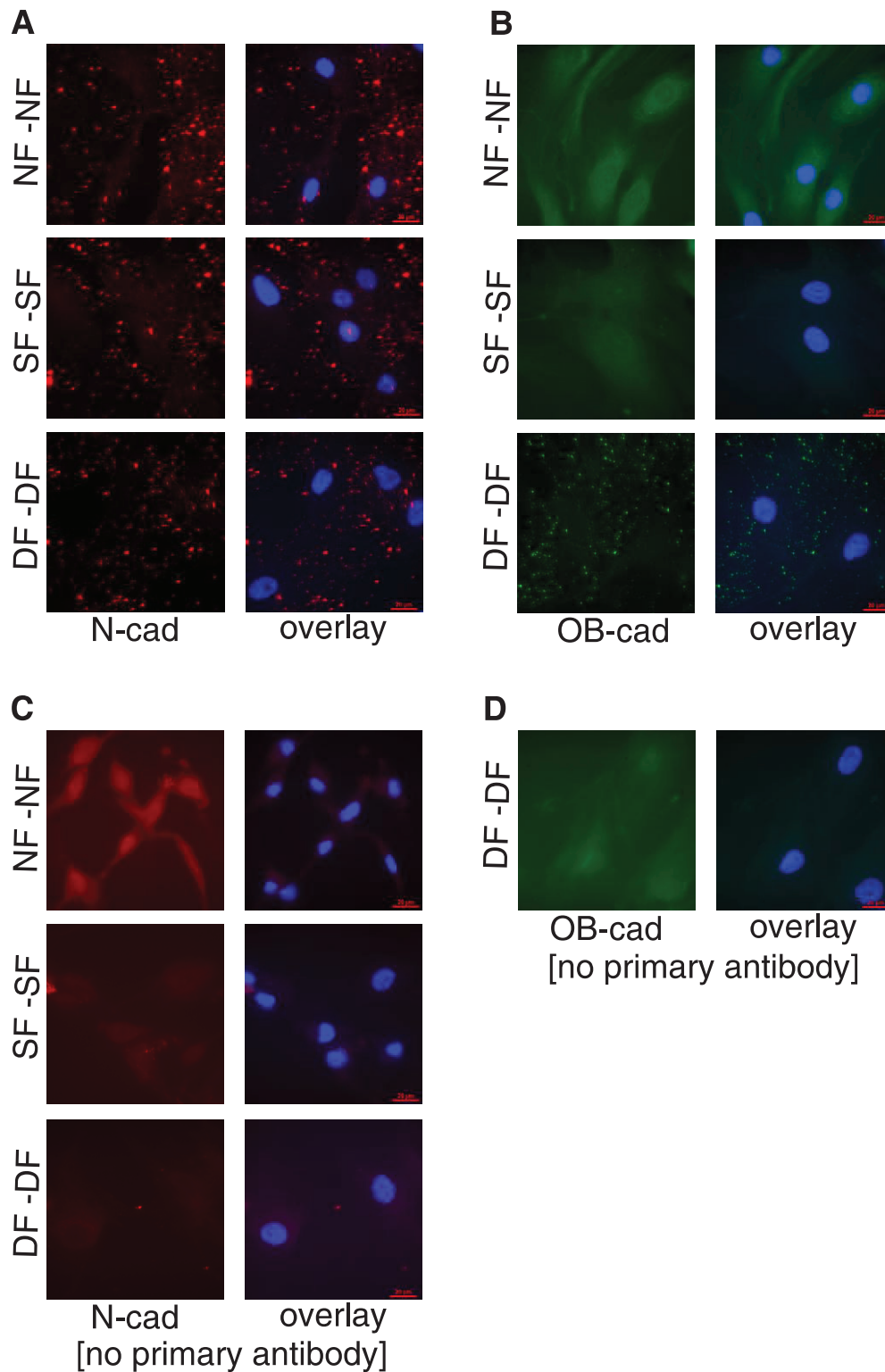
Supplementary figure 5.8 Immunostaining of fibroblasts adherens junctions for N- and OB- cadherin shows N-cad expression (red fluorescence) in all fibroblasts (A) and OB-cad expression (green fluorescence) only in DF interaction sites (B). In the right column (overlay) DAPI staining of the nucleus is overlayed with the corresponding antibody staining. In the control measuremnts (C&D) unspecific binding of the secondary antibody was checked by staining without the corresponding primary antibody for N-cad (C) and OB-cad (D). Only a weak homogenous background fluorescence signal was detected showing that the secondary antibody specifically binds the primary antibody. Scale bar 20 µm.
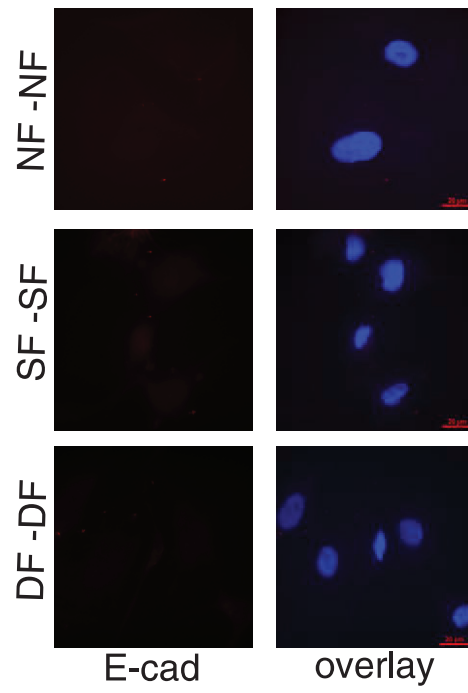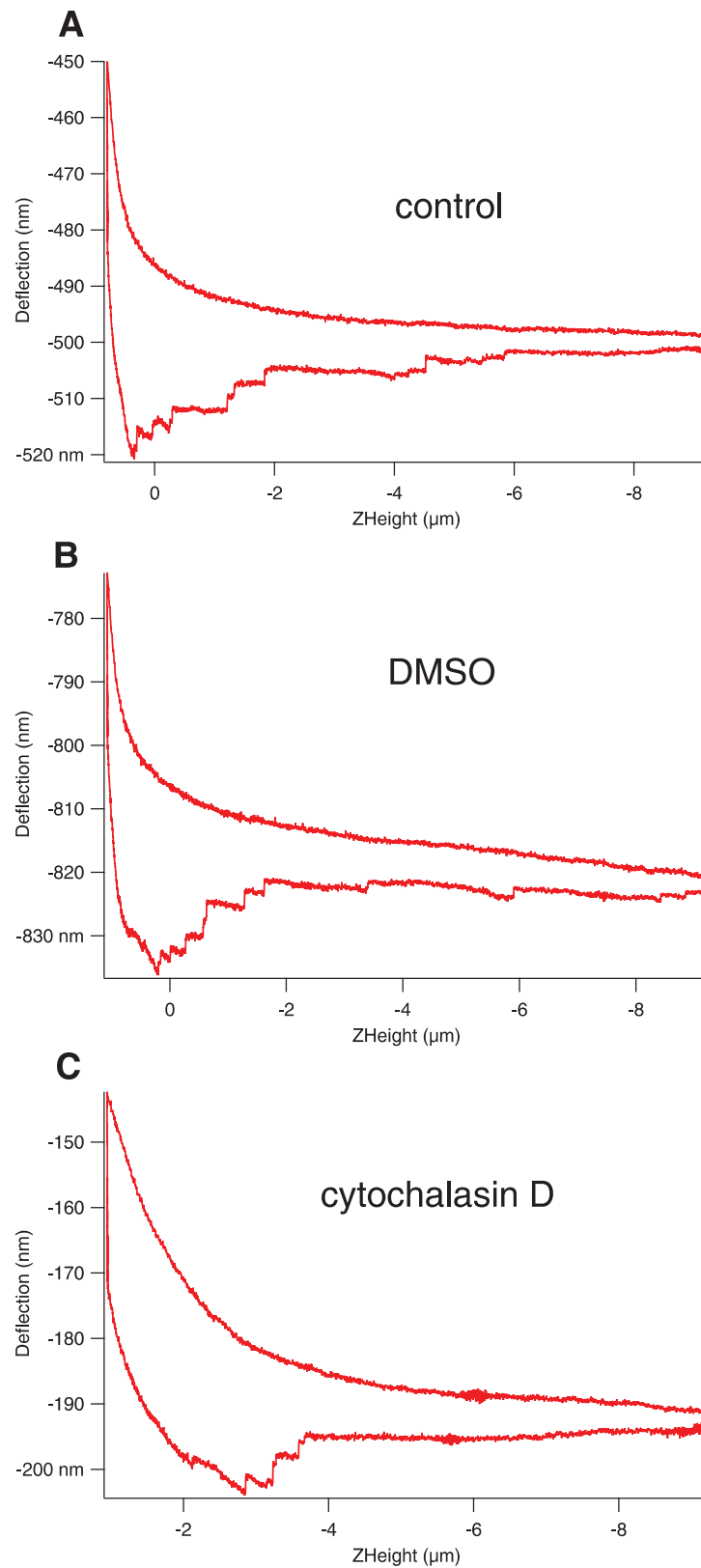
Supplementary figure 5.9 Immunostaining of fibroblasts adherens junctions for E-cadherin shows no expression of E-cad in the NF-NF, SF-SF and DF-DF interaction sites. Scale bar 20 μm.

Supplementary figure 5.10 Force curves measured during cell-cell interaction (here for NF-NF) shows rupture events in all three experimental conditions: control in normal DMEM medium (A), medium plus DMSO (B), and medium with cytochalasin D (C).
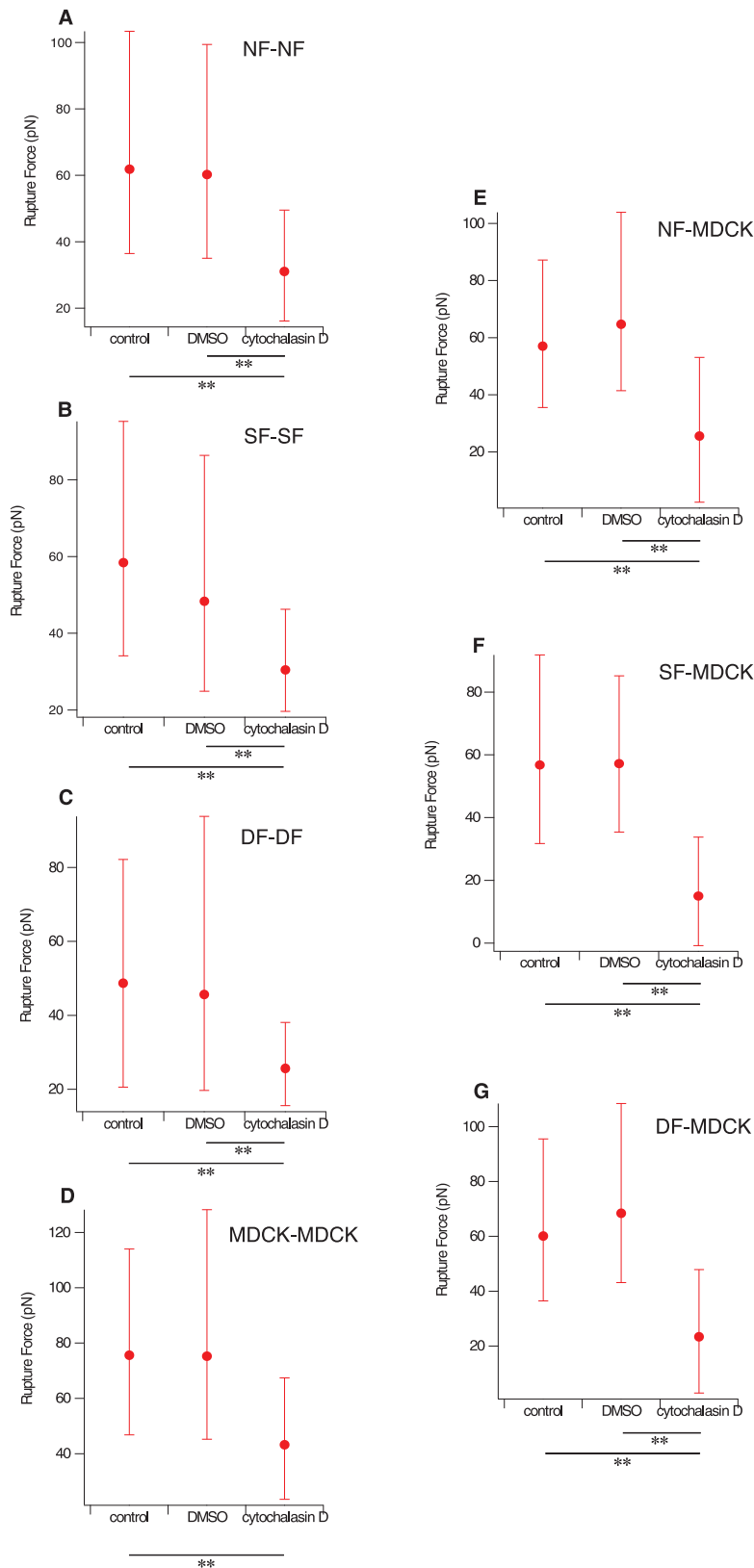
Supplementary figure 5.11 Plot of the median values with the 25th and 75th percentile added as error bars of rupture forces in cell-cell interactions between several cells under control, DMSO and cytochalasin D (5 µM) conditions. (A) NF-NF, (B) SF-SF, (C) DF-DF, (D) MDCK-MDCK, (E) NF-MDCK, (F) SF-MDCK and (G) DF-MDCK. The respective median values are also listed in Table 5.2. Statistical results are reported in Materials and Methods section.
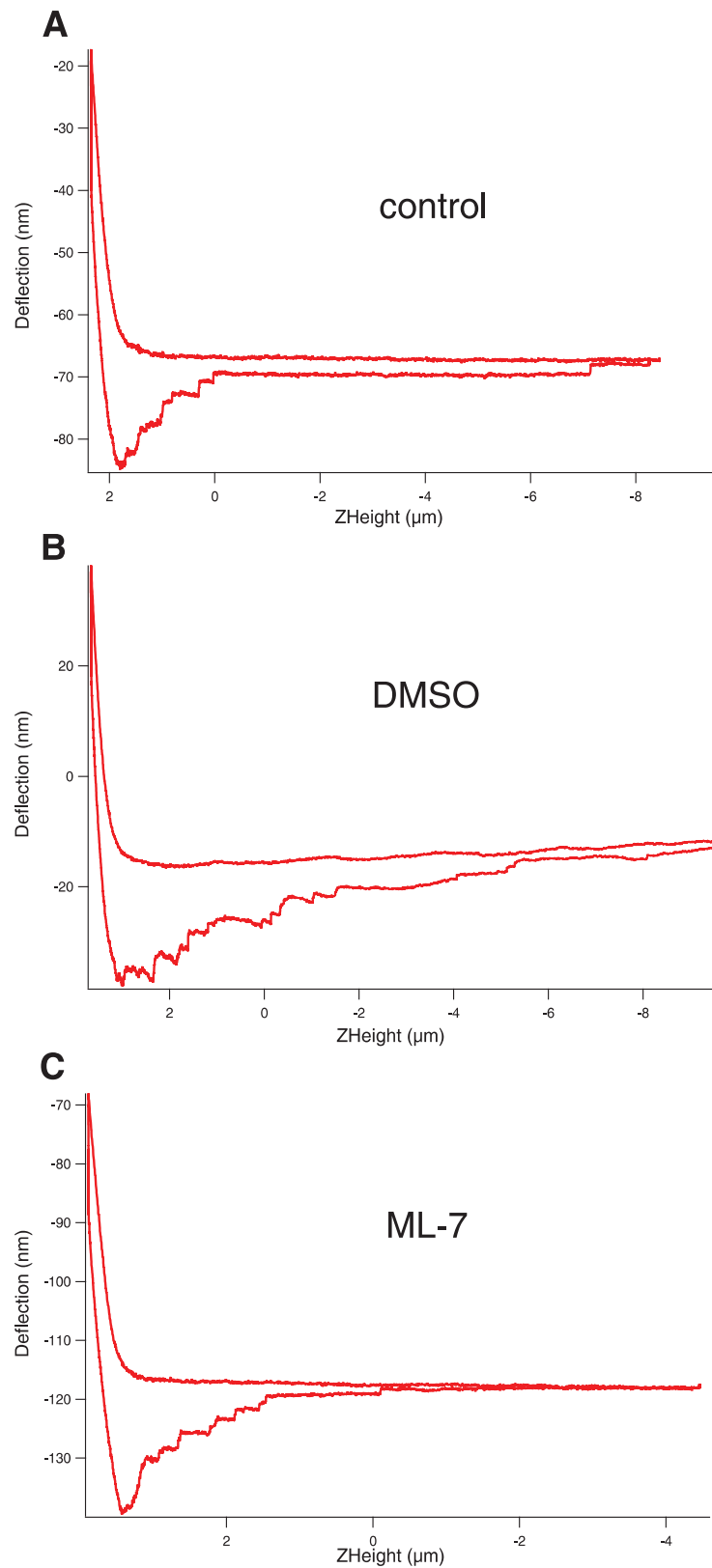
Supplementary figure 5.12 Force curves measured during cell-cell interaction of normal fibroblasts (NF-NF) shows rupture events in all three experimental conditions: control in normal medium (A), medium plus DMSO (B), and medium with ML-7 (C).
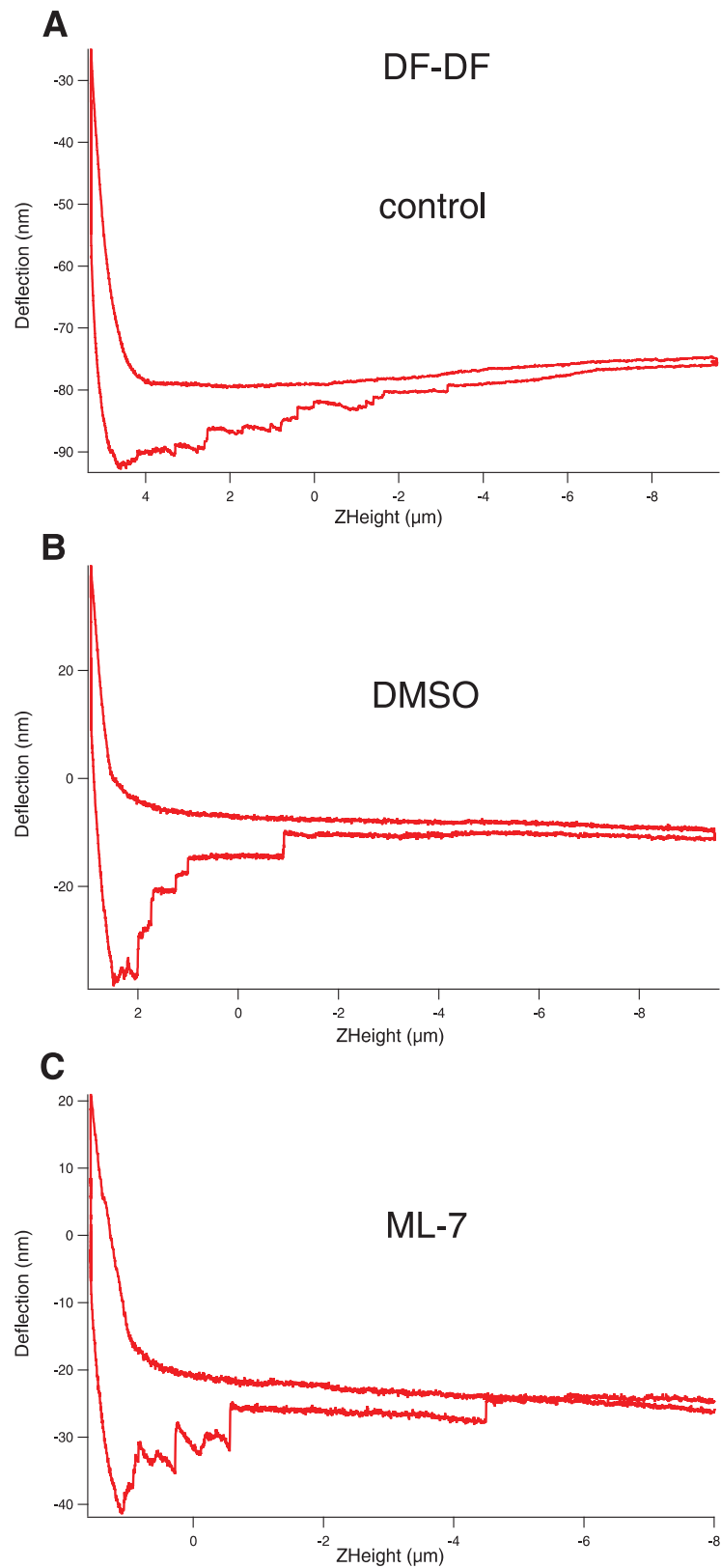
Supplementary figure 5.13 Force curves measured during cell-cell interaction of Dupuytren fibroblasts (DF-DF) shows rupture events in all three experimental conditions: control in normal medium (A), medium plus DMSO (B), and medium with ML-7 (C).
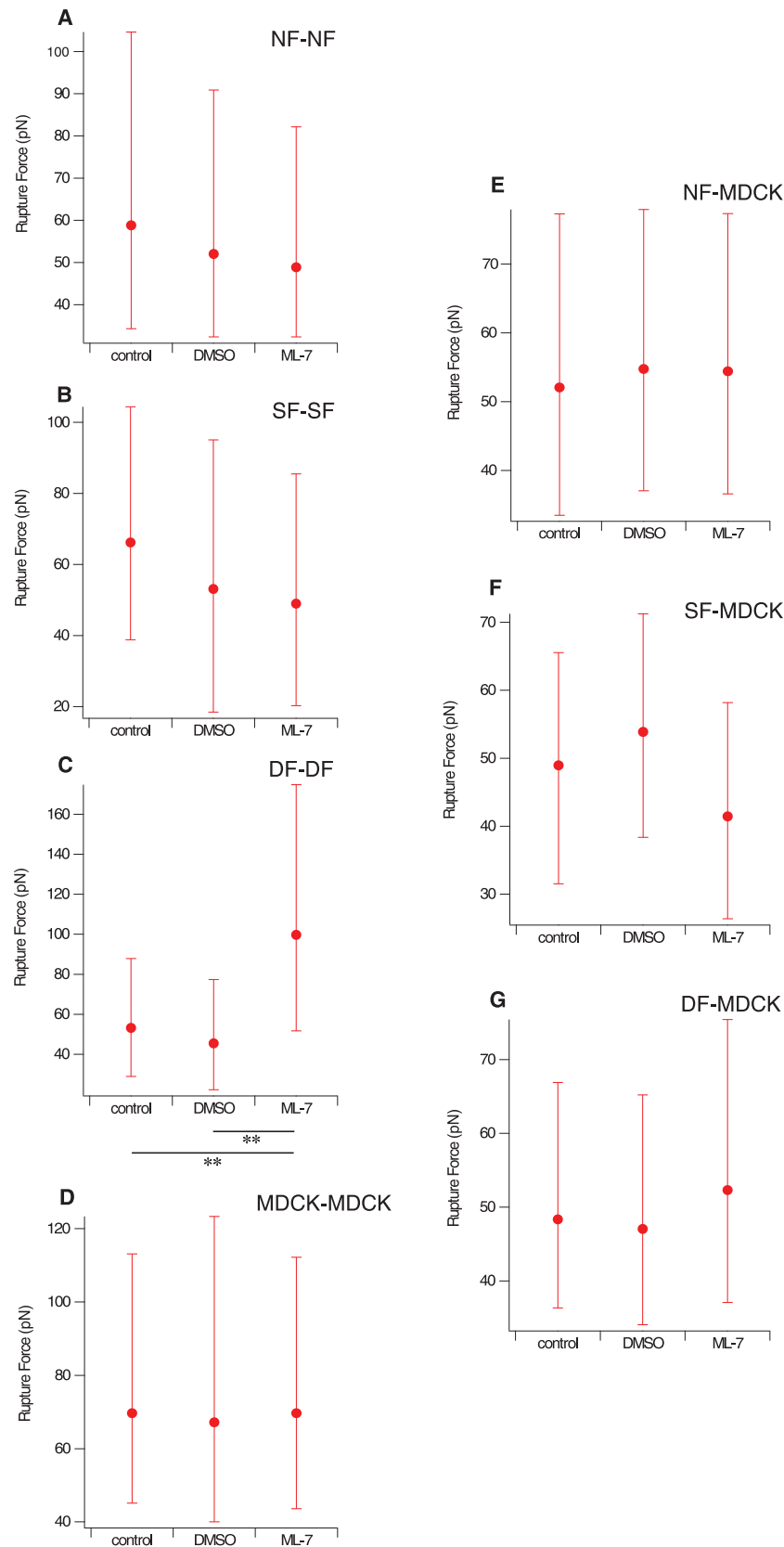
Supplementary figure 5.14 Plot of the median values with the 25th and 75th percentile added as error bars of rupture forces in cell-cell intaractions between several cells under control, DMSO and ML-7 (5 µM) conditions. (A) NF-NF, (B) SF-SF, (C) DF-DF, (D) MDCK-MDCK, (E) NF-MDCK, (F) SF-MDCK and (G) DF-MDCK. The respective median values are also listed in Table 5.3. Statistical results are reported in Materials and Methods section.

IV   Conclusions and Future Prospects

Chapter 6

6.1 Performed and Achieved Results

The primary focus of this thesis was the investigation of mechanical properties of different fibroblast phenotypes obtained from Dupuytren's patient using Atomic Force Microscopy based force spectroscopic techniques such as force mapping and single cell force spectroscopy.

Understanding the cell viscoelastic properties and cell-cell adhesion molecules dynamics dictates the central aspect of the cell mechanobiology. Mechanical loads in the sub-tissue level area induce changes in composition, structure and function of the living cell and its surrounding matrices. Mostly cells are responsible for these changes that they create intracellular force generation through mechanotransduction signalling pathways and results in the physiological or pathological alteration in the ECM and also in the neighbouring and distant cells. Particular cell types such as fibroblasts and their differentiated phenotypes are even more responsible for such sub-tissue dynamics in most of the tissues. The ECM created by fibroblasts performs very important genotypic and phenotypic regulation of cells. This raises the necessity of studying the fibroblast's mechanics in accordance with the substrate that is well designed with topography and biochemical molecules. The mechanical properties of ECM contribute to the fibroblast's viscoelastic properties through outside-in mechanotransduction pathway. Reversibly, through inside-out signalling mechanism, cell response to those signals with the cascade of complex proteins. These cascades of proteins include the major actin cytoskeleton networks and integrins constituted focal adhesions force-points. Force measurements on mechanical load-sensitive fibroblasts and its ECM will probe their mechanical properties and help to describe the relation between cell deformations and ECM substrate stiffness gradients. Force assays can quantify the ECM stiffness that are transmitting forces to the cell's nucleus through mechanotransduction pathways and thus contribute to the nuclear genetic regulations.

The current cellular and ECM mechanobiology requires the need for understanding the interdependent cell-ECM mechanical properties *in vitro* using and creating advanced microscopic and spectroscopic techniques. With the current progress in AFM imaging and spectroscopy, and sample preparation (mostly ECM substrate), topographical evaluation and mechanical properties of cell and ECM can be quantified. AFM mechanical mapping enables to follow the mechanobiology of cell and ECM in the physiological conditions. The imaging ability of AFM enables to visualize cell and ECM topography with far better resolution. AFM based cell force spectroscopy enables to measure the cell adhesion molecules strength and helps to understand the following complex cascade proteins dynamics that lies beneath the cell membranes.

In chapter 1, an introductory review has been given on the topic entitled to AFM, the determination of cell's Young's modulus, fibroblast and myofibroblast, myofibroblast role in organ fibrosis and finally, AFM based SCFS.

In chapter 3, measurement of viscoelastic properties of three different fibroblasts and corresponding phenotypes were discussed on AFM mechanical mapping results. The correlation between cell mechanics and fibroblasts α-sma positive stress fibres were studied using AFM and immunofluorescence techniques. The effects of TGF-β1 and microenvironment stiffness on cell viscoelastic properties were studied. From the wound healing assay, the motility of fibroblasts and their migration patterns were studied.

In chapter 4, the interdependent interplay between cell and ECM mechanics of three fibroblasts were investigated using AFM mechanical mapping. The elastic modulus determination showed that the pathological fibroblasts (scar and Dupuytren's) were stiffer than the normal fibroblasts and they stiffen the decellularized matrices (specifically MatriDerm) thus clarifying the role of myofibroblasts in tissue stiffening in tissue fibrosis. Confocal z-stack imaging on the decellularized matrices populated with fibroblasts showed the highly invasive behaviour of pathological fibroblasts.

In chapter 5, AFM based SCFS setup was established to study the interaction of cadherins (N-, OB- and E-) in homo- and hetero-cellular arrangements. Immunofluorescence studies showed the localization of homophilic and heterophilic cadherin pairs at the cell-cell adheren junctions and demonstrated the EMT transition of epithelia cells by E-cadherin loss and N-cadherin gain. SCFS rupture force measurement showed that the homophilic interactions are stronger than heterophilic interactions. Cadherin mechanical bond rupture force

measurements on cytochalasin D and ML-7 treatment showed that actin filaments and myosin play a crucial role in cadherin extracellular binding dynamics.

6.2 Future Directions

Investigation of cell mechanics in response to certain biochemical and biophysical cues will be helpful to understand the role of various mechano-signalling pathways in cell mechanobiology. Cells seeded and observed on decellularized matrices or commercially available matrigels provides closer or native microenvironment for conducting mechanical studies. Generally, other than normal culture systems, decellularized matrices introduce cells with rich native biochemical environment. As ECM serve as a structural scaffold, cell mechanics investigation conducted on ECM matrices or gels could be more appropriate for understanding the role of cell mechanics in 3D microenvironment. The goal of using matrices is to maintain the cell functionality with supplement of protein factors and overall, mimicking tissue. Retaining ECM architecture and also restoring tissue specific function can make AFM mechanical measurements on cells more relevant in respect to tissue mechanics. Durotaxis and chemotaxis effect can be studied on these matrices populated with cells in order to find the real missing pieces of cell adhesion, dynamics and migration. Even measurement of cellular traction forces on cell populated matrices can be assured with proper experimental design of introducing fluorescent beads tagged with antibody specific to any ECM components of the matrices and able to follow the displacement of beads through fluorescence microscopy.

Force-sensitive fibroblasts loading force on ECM affects not only tissue composition and structure but also modulate the tissue mechanics. Evaluation and comparison of physiological and pathological tissues mechanical properties will be able to broaden the knowledge on various organ specific tissue dynamics. It will provide more opportunity for creating biocompatible tissue engineering products such as bio-scaffolds of varying compositions and stiffness. Careful preparation of tissue samples for AFM studies will enable to study sub-tissue mechanics that does not alter the cell and ECM structure and mechanics (Xu et al., 2016). Such carefully prepared tissue samples could be relevant mechanical cues for carrying AFM mechanical studies. Fibroblast enriched connective tissue under physiological and pathological states could be more interesting for AFM mechanical studies. Biological tissues are an ensemble of cells and ECM, which two components are tightly regulated to facilitate

tissue functions and mechanics. Tissues extracted from connective tissue disorders will be of more interesting platform to visualize ECM networks arrangement and cellular stiffness.

AFM based SCFS can unravel intracellular signalling mechanism by measuring extracellular biomolecular mechanical bond unbinding force. These biomolecules, mostly cadherins or integrins from cell membranes promotes cell-cell and cell-ECM interactions, are of large interest to study their binding dynamics. In this thesis, the role of actomyosin networks in extracellular domains of cadherins dynamics were studied by measuring the cadherin homophilic and heterophilic mechanical bond rupture force. In the similar fashion, other intracellular signalling pathways and their cascade protein complexes role in cadherin dynamics can be studied. For example, the role of adaptor proteins such as α-, β- and p120 catenins in cadherin binding dynamics can be investigated with the appropriate assignment of anti-peptides that could bind to one of the adaptor proteins and thus inactivate the protein of interest. Calcium depletion affects the cadherin binding. The link between Ca^{2+} channels, intracellular calcium signalling and cell adhesion mechanotransduction pathways could be an initiative to find the interlinked proteins and their dynamics that are shared among the pathways.

Integrins from the adhesome complex withstand extra- and intracellularly generated forces. SCFS adhesion force measurement between integrins expressed in fibroblasts and fibronectin (FN) demonstrated the biphasic cellular adhesion behavior of fibroblasts mediated by $\alpha5\beta1$ integrins (Strohmeyer et al., 2017). The mechanical catch bond formed in FN reinforces the cell adhesion before adhesion clusters are formed. SCFS also enables the influence of Arp2/3 signaling pathway in FN-engaged $\alpha5\beta1$ integrins activation of focal adhesion kinase and strengthening of αV-class integrins. The cell-ECM mechanotransduction pathways can be elicited in SCFS measurements only by measuring the unbinding force of extracellular domains of cell adhesion molecules.

The overall conclusion from the AFM based force spectroscopic techniques draws the attention of investigating the biophysical aspects of cell and ECM. This involves the interdependent reciprocal interplay between cell and ECM and also exploration of the interaction mechanism in cell-cell adhesion. Fibroblast and their phenotypes mechanics will open a huge convention, which in many key biomolecular players are still to be explored using biophysical techniques such as force spectroscopy.

Chapter 7

Appendix

Analysis of creep response data

To analyze creep response data we assume that the sample can be described with the general linear solid model as presented in supplementary figure 3.6. When applying a step in z of size Δz, the deflection will follow a single exponential creep, which is characterized by an increase Δd after creep has settled, and an amplitude a of the exponential decay. So, the deflection will obey the following function:

1. $\qquad d = \Delta d + a * e^{-t/\tau}$

As described elsewhere, this can be derived from the dynamic force balance in the Zener element. The parameters of the Zener element can be calculated from the fit parameters in the following way:
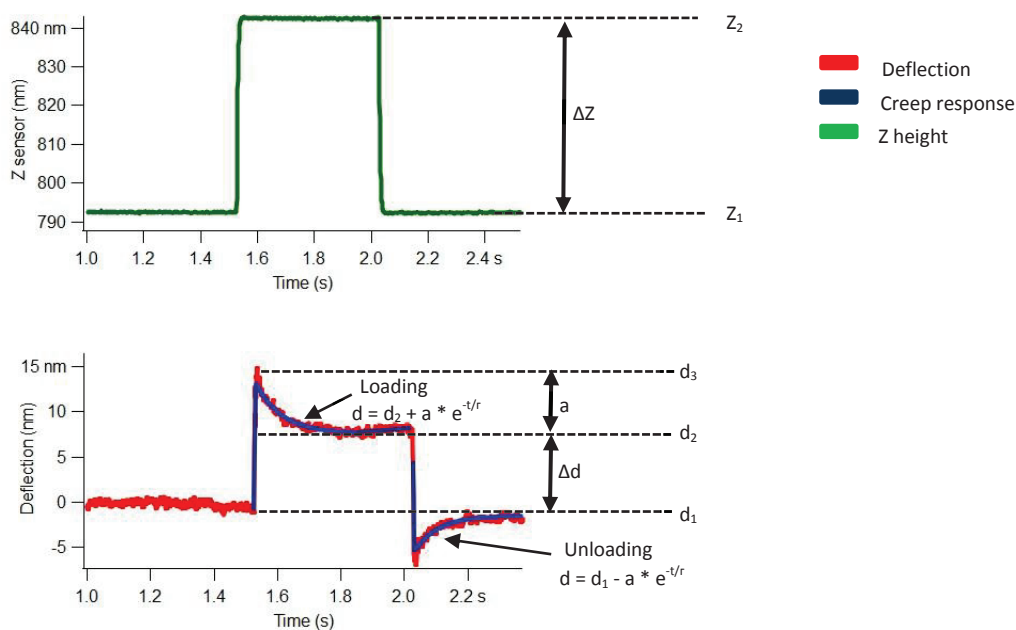
(2a) $\quad k_1 = k_c \frac{\Delta d}{\Delta z - \Delta d}$

(2b) $\quad k_2 = k_c \frac{\Delta d + a}{\Delta z - \Delta d - a} - k_1$

(2c) $\quad f = k_2 * \tau * \frac{k_c + k_1}{k_2 + k_c + k_1}$

The experimentally derived time constant τ is the relaxataion time of the complete mechanical circuit, which comprises the sample (the Zener element above) and the cantilever, as can be seen from the fact, that all quantities above are dependent on k_c. The intrinsic relaxation time constant τ* of the sample, should be defined as f/k_2, and can be calculated from these quantties as shown in eq. 3.

(3) $\quad \tau^* = \frac{f}{k_2} = \tau * \frac{k_c + k_1}{k_2 + k_c + k_1}$

Calculating elastic moduli and dynamic viscosity

The Hertz model describes how the indentation of a sample changes with loading force, for certain tip geometries. In the case of pyramidal indenters we will have a quadratic function. , In the case of a pyramidal tip with opening angle α, elastic modulus E and Poisson ratio ν⬚ of the sample, we find the following relation between indentation δ and loading force F:

(4) $\quad F = \frac{1}{\sqrt{2}} * \frac{E}{1 - \nu^2} * \tan \alpha * \delta^2$

The slope of this force indentation relation, which is the spring constant of the sample, will obviously depend on the loading force F_0 or the loading indentation δ_0 at which it is calculated (or measured):

(5) $\quad k_{Hertz} = \frac{\partial F}{\partial \delta}\Big|_{\delta = \delta_0} = 2 * \frac{1}{\sqrt{2}} * \frac{E}{1 - \nu^2} * \tan \alpha * \delta_0$

138

In the step response measurement, we basically measure the spring constant at given loading force, and we have to use the Hertz model in reverse to calculate these stiffness values in elastic moduli, taking in account the loading force. This results in the following relations:

(6) $\quad E_{1/2} = k_{1/2}^2 * \frac{1}{2*\sqrt{2}} * \frac{1}{\tan \alpha} * (1 - v^2) * \frac{1}{F_0}$

The dynamic viscosity η in the linear standard solid model can be written as:

(7) $\quad \eta = E_2 * \tau^*$

where τ^* is the intrinsic relaxation time as defined in eq. 3.

List of Publications

1. The role of the microenvironment in the biophysics of cancer. [Review Article] Rianna, Carmela, **Prem Kumar**, and Manfred Radmacher. In *Seminars in cell & developmental biology*, vol. 73, pp. 107-114. (**2018**).

2. Mechanical and migratory properties of normal, scar, and Dupuytren's fibroblasts. [Research Article] **Viji Babu, Prem Kumar**, Carmela Rianna, Gazanfer Belge, Ursula Mirastschijski, and Manfred Radmacher. *Journal of Molecular Recognition* 31, no. 9 (**2018**): e2719.

3. Mechanics of Brain Tissues Studied by Atomic Force Microscopy: A Perspective. [Review Article] **Viji Babu, Prem Kumar**, and Manfred Radmacher. *Frontiers in neuroscience* 13 (**2019**).

4. Nano-mechanical mapping of interdependent cell and ECM mechanics by AFM force spectroscopy. [Research Article] **Viji Babu, Prem Kumar**, Carmela Rianna, Ursula Mirastschijski, and Manfred Radmacher. *Scientific reports* 9, no. 1 (**2019**): 1-19.

Manuscripts in Preparation

1. Homo- and Hetero-cellular adherens junction-cadherins homophilic and heterophilic bond rupture force measured by AFM based SCFS. [Research Article] **Prem Kumar Viji Babu**, Manfred Radmacher, **2020**

2. Investigation of Viscoelastic properties of cells by AFM Sweep frequency. [Research Article] Jeanlex Soares de Sousa, **Prem Kumar Viji Babu**, Carmela Rianna, Sandra Perez, Shruti Kulkarni, Manfred Radmacher, **2020**

3. Dupuytren's Disease. [Chapter from Book] Mechanics of Diseases: Biomedical Aspects of the Mechanical Properties of Cells and Tissues. Editor: M. Radmacher **Prem Kumar Viji Babu**, Manfred Radmacher, **2020**

Chapter 8

Bibliography

Abreu-Blanco, M.T., Verboon, J.M., Liu, R., Watts, J.J., Parkhurst, S.M., 2012. Drosophila embryos close epithelial wounds using a combination of cellular protrusions and an actomyosin purse string. J. Cell Sci. 125, 5984–5997. https://doi.org/10.1242/jcs.109066

Achterberg, V.F., Buscemi, L., Diekmann, H., Smith-Clerc, J., Schwengler, H., Meister, J.-J., Wenck, H., Gallinat, S., Hinz, B., 2014a. The Nano-Scale Mechanical Properties of the Extracellular Matrix Regulate Dermal Fibroblast Function. J. Invest. Dermatol. 134, 1862–1872. https://doi.org/10.1038/jid.2014.90

Achterberg, V.F., Buscemi, L., Diekmann, H., Smith-Clerc, J., Schwengler, H., Meister, J.-J., Wenck, H., Gallinat, S., Hinz, B., 2014b. The Nano-Scale Mechanical Properties of the Extracellular Matrix Regulate Dermal Fibroblast Function. J. Invest. Dermatol. 134, 1862–1872. https://doi.org/10.1038/jid.2014.90

Alcaraz, J., Otero, J., Jorba, I., Navajas, D., 2018. Bidirectional mechanobiology between cells and their local extracellular matrix probed by atomic force microscopy. Semin. Cell Dev. Biol., Application of Atomic Force Microscopy in cell biology 73, 71–81. https://doi.org/10.1016/j.semcdb.2017.07.020

Apostolopoulou, M., Ligon, L., 2012. Cadherin-23 Mediates Heterotypic Cell-Cell Adhesion between Breast Cancer Epithelial Cells and Fibroblasts. PLOS ONE 7, e33289. https://doi.org/10.1371/journal.pone.0033289

Ascione, F., Vasaturo, A., Caserta, S., D'Esposito, V., Formisano, P., Guido, S., 2016. Comparison between fibroblast wound healing and cell random migration assays in vitro. Exp. Cell Res. 347, 123–132. https://doi.org/10.1016/j.yexcr.2016.07.015

Babu, P.K.V., Rianna, C., Belge, G., Mirastschijski, U., Radmacher, M., 2018. Mechanical and migratory properties of normal, scar, and Dupuytren's fibroblasts. J. Mol. Recognit. 31, e2719. https://doi.org/10.1002/jmr.2719

Babu, P.K.V., Rianna, C., Mirastschijski, U., Radmacher, M., 2019. Nano-mechanical mapping of interdependent cell and ECM mechanics by AFM force spectroscopy. Sci. Rep. 9, 1–19. https://doi.org/10.1038/s41598-019-48566-7

Baranyi, U., Winter, B., Gugerell, A., Hegedus, B., Brostjan, C., Laufer, G., Messner, B., 2019. Primary Human Fibroblasts in Culture Switch to a Myofibroblast-Like Phenotype Independently of TGF Beta. Cells 8, 721. https://doi.org/10.3390/cells8070721

Baumgartner, W., Golenhofen, N., Grundhöfer, N., Wiegand, J., Drenckhahn, D., 2003. Ca2+ Dependency of N-Cadherin Function Probed by Laser Tweezer and Atomic Force Microscopy. J. Neurosci. 23, 11008–11014. https://doi.org/10.1523/JNEUROSCI.23-35-11008.2003

Baumgartner, W., Hinterdorfer, P., Ness, W., Raab, A., Vestweber, D., Schindler, H., Drenckhahn, D., 2000. Cadherin interaction probed by atomic force microscopy. Proc. Natl. Acad. Sci. 97, 4005–4010. https://doi.org/10.1073/pnas.070052697

Beckmann, J., Schubert, R., Chiquet-Ehrismann, R., Müller, D.J., 2013. Deciphering Teneurin Domains That Facilitate Cellular Recognition, Cell–Cell Adhesion, and Neurite Outgrowth Using Atomic Force Microscopy-Based Single-Cell Force Spectroscopy. Nano Lett. 13, 2937–2946. https://doi.org/10.1021/nl4013248

Bell, E., Ivarsson, B., Merrill, C., 1979. Production of a tissue-like structure by contraction of collagen lattices by human fibroblasts of different proliferative potential in vitro. Proc. Natl. Acad. Sci. 76, 1274–1278. https://doi.org/10.1073/pnas.76.3.1274

Benoit, M., Gabriel, D., Gerisch, G., Gaub, H.E., 2000. Discrete interactions in cell adhesion measured by single-molecule force spectroscopy. Nat. Cell Biol. 2, 313–317. https://doi.org/10.1038/35014000

Binnig, G., Quate, C.F., Gerber, Ch., 1986. Atomic Force Microscope. Phys. Rev. Lett. 56, 930–933. https://doi.org/10.1103/PhysRevLett.56.930

Bisson, M.A., Mcgrouther, D.A., Mudera, V., Grobbelaar, A.O., 2003. The Different Characteristics of Dupuytren's Disease Fibroblasts Derived from either Nodule or Cord: Expression of α-Smooth Muscle Actin and the Response to Stimulation by TGF-β1. J. Hand Surg. Br. Eur. Vol. 28, 351–356. https://doi.org/10.1016/S0266-7681(03)00135-9

Bochaton-Piallat, M.-L., Gabbiani, G., Hinz, B., 2016. The myofibroblast in wound healing and fibrosis: answered and unanswered questions. F1000Research 5. https://doi.org/10.12688/f1000research.8190.1

Bongartz, T., Nannini, C., Medina-Velasquez, Y.F., Achenbach, S.J., Crowson, C.S., Ryu, J.H., Vassallo, R., Gabriel, S.E., Matteson, E.L., 2010. Incidence and mortality of interstitial lung disease in rheumatoid arthritis: A population-based study. Arthritis Rheum. 62, 1583–1591. https://doi.org/10.1002/art.27405

Bonnans, C., Chou, J., Werb, Z., 2014. Remodelling the extracellular matrix in development and disease. Nat. Rev. Mol. Cell Biol. 15, 786–801. https://doi.org/10.1038/nrm3904

Booth, A.J., Hadley, R., Cornett, A.M., Dreffs, A.A., Matthes, S.A., Tsui, J.L., Weiss, K., Horowitz, J.C., Fiore, V.F., Barker, T.H., Moore, B.B., Martinez, F.J., Niklason, L.E., White, E.S., 2012. Acellular Normal and Fibrotic Human Lung Matrices as a Culture System for In Vitro Investigation. Am. J. Respir. Crit. Care Med. 186, 866–876. https://doi.org/10.1164/rccm.201204-0754OC

Borghi, N., Sorokina, M., Shcherbakova, O.G., Weis, W.I., Pruitt, B.L., Nelson, W.J., Dunn, A.R., 2012. E-cadherin is under constitutive actomyosin-generated tension that is increased at cell–cell contacts upon externally applied stretch. Proc. Natl. Acad. Sci. 109, 12568–12573. https://doi.org/10.1073/pnas.1204390109

Bott, K., Upton, Z., Schrobback, K., Ehrbar, M., Hubbell, J.A., Lutolf, M.P., Rizzi, S.C., 2010. The effect of matrix characteristics on fibroblast proliferation in 3D gels. Biomaterials 31, 8454–8464. https://doi.org/10.1016/j.biomaterials.2010.07.046

Boudreau, N.J., Jones, P.L., 1999. Extracellular matrix and integrin signalling: the shape of things to come. Biochem. J. 339, 481–488. https://doi.org/10.1042/bj3390481

Brasch, J., Katsamba, P.S., Harrison, O.J., Ahlsén, G., Troyanovsky, R.B., Indra, I., Kaczynska, A., Kaeser, B., Troyanovsky, S., Honig, B., Shapiro, L., 2018. Homophilic and Heterophilic Interactions of Type II Cadherins Identify Specificity Groups Underlying Cell-Adhesive Behavior. Cell Rep. 23, 1840–1852. https://doi.org/10.1016/j.celrep.2018.04.012

Brickley-Parsons, D., Glimcher, M., Smith, R., Albin, R., Adams, J., 1981. Biochemical changes in the collagen of the palmar fascia in patients with Dupuytren's disease. J. Bone Jt. Surg. 63, 787–797.

Budnar, S., Yap, A.S., 2013. A mechanobiological perspective on cadherins and the actin-myosin cytoskeleton. F1000Prime Rep. 5. https://doi.org/10.12703/P5-35

Calvo, F., Ege, N., Grande-Garcia, A., Hooper, S., Jenkins, R.P., Chaudhry, S.I., Harrington, K., Williamson, P., Moeendarbary, E., Charras, G., Sahai, E., 2013. Mechanotransduction and YAP-dependent matrix remodelling is required for the generation and maintenance of cancer-associated fibroblasts. Nat. Cell Biol. 15, 637–646. https://doi.org/10.1038/ncb2756

Cappella, B., 2016. Force–Distance Curves in Practice, in: Cappella, B. (Ed.), Mechanical Properties of Polymers Measured through AFM Force-Distance Curves, Springer Laboratory. Springer International Publishing, Cham, pp. 67–91. https://doi.org/10.1007/978-3-319-29459-9_2

Carmona-Fontaine, C., Theveneau, E., Tzekou, A., Tada, M., Woods, M., Page, K.M., Parsons, M., Lambris, J.D., Mayor, R., 2011. Complement Fragment C3a Controls Mutual Cell Attraction during Collective Cell Migration. Dev. Cell 21, 1026–1037. https://doi.org/10.1016/j.devcel.2011.10.012

Chaudhuri, O., Koshy, S.T., Cunha, C.B. da, Shin, J.-W., Verbeke, C.S., Allison, K.H., Mooney, D.J., 2014. Extracellular matrix stiffness and composition jointly regulate the induction of malignant phenotypes in mammary epithelium. Nat. Mater. 13, 970–978. https://doi.org/10.1038/nmat4009

Chu, Y.-S., Thomas, W.A., Eder, O., Pincet, F., Perez, E., Thiery, J.P., Dufour, S., 2004. Force measurements in E-cadherin–mediated cell doublets reveal rapid adhesion strengthened by actin cytoskeleton remodeling through Rac and Cdc42. J. Cell Biol. 167, 1183–1194. https://doi.org/10.1083/jcb.200403043

Colorado, P.C., Torre, A., Kamphaus, G., Maeshima, Y., Hopfer, H., Takahashi, K., Volk, R., Zamborsky, E.D., Herman, S., Sarkar, P.K., Ericksen, M.B., Dhanabal, M., Simons, M., Post, M., Kufe, D.W., Weichselbaum, R.R., Sukhatme, V.P., Kalluri, R., 2000. Anti-angiogenic cues from vascular basement membrane collagen. Cancer Res. 60, 2520–2526.

Coughlin, M.F., Fredberg, J.J., 2013. Changes in cytoskeletal dynamics and nonlinear rheology with metastatic ability in cancer cell lines. Phys. Biol. 10, 065001. https://doi.org/10.1088/1478-3975/10/6/065001

Cox, T.R., Erler, J.T., 2011. Remodeling and homeostasis of the extracellular matrix: implications for fibrotic diseases and cancer. Dis. Model. Mech. 4, 165–178. https://doi.org/10.1242/dmm.004077

Culav, E.M., Clark, C.H., Merrilees, M.J., 1999. Connective Tissues: Matrix Composition and Its Relevance to Physical Therapy. Phys. Ther. 79, 308–319. https://doi.org/10.1093/ptj/79.3.308

Dabiri, G., Campaner, A., Morgan, J.R., Van De Water, L., 2006. A TGF-β1-Dependent Autocrine Loop Regulates the Structure of Focal Adhesions in Hypertrophic Scar Fibroblasts. J. Invest. Dermatol. 126, 963–970. https://doi.org/10.1038/sj.jid.5700187

Denisin, A.K., Pruitt, B.L., 2016. Tuning the Range of Polyacrylamide Gel Stiffness for Mechanobiology Applications. ACS Appl. Mater. Interfaces 8, 21893–21902. https://doi.org/10.1021/acsami.5b09344

Desmoulière, A., Geinoz, A., Gabbiani, F., Gabbiani, G., 1993. Transforming growth factor-beta 1 induces alpha-smooth muscle actin expression in granulation tissue myofibroblasts and in quiescent and growing cultured fibroblasts. J. Cell Biol. 122, 103–111. https://doi.org/10.1083/jcb.122.1.103

Dufrêne, Y.F., Ando, T., Garcia, R., Alsteens, D., Martinez-Martin, D., Engel, A., Gerber, C., Müller, D.J., 2017. Imaging modes of atomic force microscopy for application in molecular and cell biology. Nat. Nanotechnol. 12, 295–307. https://doi.org/10.1038/nnano.2017.45

Dulińska, I., Targosz, M., Strojny, W., Lekka, M., Czuba, P., Balwierz, W., Szymoński, M., 2006. Stiffness of normal and pathological erythrocytes studied by means of atomic force microscopy. J. Biochem. Biophys. Methods 66, 1–11. https://doi.org/10.1016/j.jbbm.2005.11.003

Elder, B.D., Kim, D.H., Athanasiou, K.A., 2010. Developing an Articular Cartilage Decellularization Process Toward Facet Joint Cartilage Replacement. Neurosurgery 66, 722–727. https://doi.org/10.1227/01.NEU.0000367616.49291.9F

Enemchukwu, N.O., Cruz-Acuña, R., Bongiorno, T., Johnson, C.T., García, J.R., Sulchek, T., García, A.J., 2016. Synthetic matrices reveal contributions of ECM biophysical and biochemical properties to epithelial morphogenesisSynthetic ECMs for epithelial morphogenesis. J. Cell Biol. 212, 113–124. https://doi.org/10.1083/jcb.201506055

Fan, D., Takawale, A., Lee, J., Kassiri, Z., 2012. Cardiac fibroblasts, fibrosis and extracellular matrix remodeling in heart disease. Fibrogenesis Tissue Repair 5, 15. https://doi.org/10.1186/1755-1536-5-15

Fausther, M., Dranoff, J.A., 2014. Integrins, Myofibroblasts, and Organ Fibrosis. Hepatol. Baltim. Md 60, 756–758. https://doi.org/10.1002/hep.27155

Follonier, L., Schaub, S., Meister, J.-J., Hinz, B., 2008. Myofibroblast communication is controlled by intercellular mechanical coupling. J. Cell Sci. 121, 3305–3316. https://doi.org/10.1242/jcs.024521

Frantz, C., Stewart, K.M., Weaver, V.M., 2010. The extracellular matrix at a glance. J. Cell Sci. 123, 4195–4200. https://doi.org/10.1242/jcs.023820

Friedl, P., Locker, J., Sahai, E., Segall, J.E., 2012. Classifying collective cancer cell invasion. Nat. Cell Biol. 14, 777–783. https://doi.org/10.1038/ncb2548

Friedrichs, J., Helenius, J., Muller, D.J., 2010. Quantifying cellular adhesion to extracellular matrix components by single-cell force spectroscopy. Nat. Protoc. 5, 1353–1361. https://doi.org/10.1038/nprot.2010.89

Friedrichs, J., Taubenberger, A., Franz, C.M., Muller, D.J., 2007a. Cellular Remodelling of Individual Collagen Fibrils Visualized by Time-lapse AFM. J. Mol. Biol. 372, 594–607. https://doi.org/10.1016/j.jmb.2007.06.078

Friedrichs, J., Torkko, J.M., Helenius, J., Teräväinen, T.P., Füllekrug, J., Muller, D.J., Simons, K., Manninen, A., 2007b. Contributions of Galectin-3 and -9 to Epithelial Cell Adhesion Analyzed by Single Cell Force Spectroscopy. J. Biol. Chem. 282, 29375–29383. https://doi.org/10.1074/jbc.M701867200

Friedrichs, J., Werner, C., Müller, D.J., 2013. Quantifying Cellular Adhesion to Covalently Immobilized Extracellular Matrix Proteins by Single-Cell Force Spectroscopy, in: Coutts, A.S. (Ed.), Adhesion Protein Protocols, Methods in Molecular Biology. Humana Press, Totowa, NJ, pp. 19–37. https://doi.org/10.1007/978-1-62703-538-5_2

Fung, Y.C., 1985. Biomechanics. Appl. Mech. Rev. 38, 1251–1255. https://doi.org/10.1115/1.3143684

Gal, N., Weihs, D., 2012. Intracellular Mechanics and Activity of Breast Cancer Cells Correlate with Metastatic Potential. Cell Biochem. Biophys. 63, 199–209. https://doi.org/10.1007/s12013-012-9356-z

García, J.R., García, A.J., 2014. Sensing rigidity. Nat. Mater. 13, 539–540. https://doi.org/10.1038/nmat3996

Geiger, B., Bershadsky, A., 2002. Exploring the Neighborhood: Adhesion-Coupled Cell Mechanosensors. Cell 110, 139–142. https://doi.org/10.1016/S0092-8674(02)00831-0

Geiger, B., Bershadsky, A., Pankov, R., Yamada, K.M., 2001. Transmembrane crosstalk between the extracellular matrix and the cytoskeleton. Nat. Rev. Mol. Cell Biol. 2, 793–805. https://doi.org/10.1038/35099066

Gershlak, J.R., Hernandez, S., Fontana, G., Perreault, L.R., Hansen, K.J., Larson, S.A., Binder, B.Y.K., Dolivo, D.M., Yang, T., Dominko, T., Rolle, M.W., Weathers, P.J., Medina-Bolivar, F., Cramer, C.L., Murphy, W.L., Gaudette, G.R., 2017. Crossing kingdoms: Using decellularized plants as perfusable tissue engineering scaffolds. Biomaterials 125, 13–22. https://doi.org/10.1016/j.biomaterials.2017.02.011

Gilkes, D.M., Semenza, G.L., Wirtz, D., 2014. Hypoxia and the extracellular matrix: drivers of tumour metastasis. Nat. Rev. Cancer 14, 430–439. https://doi.org/10.1038/nrc3726

Gilpin, A., Yang, Y., 2017. Decellularization Strategies for Regenerative Medicine: From Processing Techniques to Applications [WWW Document]. BioMed Res. Int. https://doi.org/10.1155/2017/9831534

Goffin, J.M., Pittet, P., Csucs, G., Lussi, J.W., Meister, J.-J., Hinz, B., 2006. Focal adhesion size controls tension-dependent recruitment of α-smooth muscle actin to stress fibers. J. Cell Biol. 172, 259–268. https://doi.org/10.1083/jcb.200506179

Grande, M.T., Sánchez-Laorden, B., López-Blau, C., Frutos, C.A.D., Boutet, A., Arévalo, M., Rowe, R.G., Weiss, S.J., López-Novoa, J.M., Nieto, M.A., 2015. Snail1-induced partial epithelial-to-mesenchymal transition drives renal fibrosis in mice and can be targeted to reverse established disease. Nat. Med. 21, 989–997. https://doi.org/10.1038/nm.3901

Guedes, A.F., Carvalho, F.A., Malho, I., Lousada, N., Sargento, L., Santos, N.C., 2016. Atomic force microscopy as a tool to evaluate the risk of cardiovascular diseases in patients. Nat. Nanotechnol. 11, 687–692. https://doi.org/10.1038/nnano.2016.52

Guilak, F., Cohen, D.M., Estes, B.T., Gimble, J.M., Liedtke, W., Chen, C.S., 2009. Control of Stem Cell Fate by Physical Interactions with the Extracellular Matrix. Cell Stem Cell 5, 17–26. https://doi.org/10.1016/j.stem.2009.06.016

Haase, K., Pelling, A.E., 2015. Investigating cell mechanics with atomic force microscopy. J. R. Soc. Interface 12, 20140970. https://doi.org/10.1098/rsif.2014.0970

Hamacher, J., Hadizamani, Y., Borgmann, M., Mohaupt, M., Männel, D.N., Moehrlen, U., Lucas, R., Stammberger, U., 2018. Cytokine–Ion Channel Interactions in Pulmonary Inflammation. Front. Immunol. 8. https://doi.org/10.3389/fimmu.2017.01644

Han, W., Chen, S., Yuan, W., Fan, Q., Tian, J., Wang, X., Chen, L., Zhang, X., Wei, W., Liu, R., Qu, J., Jiao, Y., Austin, R.H., Liu, L., 2016. Oriented collagen fibers direct tumor cell intravasation. Proc. Natl. Acad. Sci. 113, 11208–11213. https://doi.org/10.1073/pnas.1610347113

Haslik, W., Kamolz, L.-P., Nathschläger, G., Andel, H., Meissl, G., Frey, M., 2007. First experiences with the collagen-elastin matrix Matriderm® as a dermal substitute in severe burn injuries of the hand. Burns 33, 364–368. https://doi.org/10.1016/j.burns.2006.07.021

Hatta, K., Takeichi, M., 1986. Expression of N-cadherin adhesion molecules associated with early morphogenetic events in chick development. Nature 320, 447–449. https://doi.org/10.1038/320447a0

Hecht, F.M., Rheinlaender, J., Schierbaum, N., Goldmann, W.H., Fabry, B., Schäffer, T.E., 2015. Imaging viscoelastic properties of live cells by AFM: power-law rheology on the nanoscale. Soft Matter 11, 4584–4591. https://doi.org/10.1039/C4SM02718C

Helenius, J., Heisenberg, C.-P., Gaub, H.E., Muller, D.J., 2008. Single-cell force spectroscopy. J. Cell Sci. 121, 1785–1791. https://doi.org/10.1242/jcs.030999

Helvert, S. van, Storm, C., Friedl, P., 2018. Mechanoreciprocity in cell migration. Nat. Cell Biol. 20, 8–20. https://doi.org/10.1038/s41556-017-0012-0

Hinz, B., 2010. The myofibroblast: Paradigm for a mechanically active cell. J. Biomech., Special Issue on Cell Mechanobiology 43, 146–155. https://doi.org/10.1016/j.jbiomech.2009.09.020

Hinz, B., 2009. Tissue stiffness, latent TGF-β1 Activation, and mechanical signal transduction: Implications for the pathogenesis and treatment of fibrosis. Curr. Rheumatol. Rep. 11, 120. https://doi.org/10.1007/s11926-009-0017-1

Hinz, B., Gabbiani, G., 2003. Cell-matrix and cell-cell contacts of myofibroblasts: role in connective tissue remodeling. Thromb. Haemost. 90, 993–1002. https://doi.org/10.1160/TH03-05-0328

Hinz, B., Pittet, P., Smith-Clerc, J., Chaponnier, C., Meister, J.-J., 2004. Myofibroblast Development Is Characterized by Specific Cell-Cell Adherens Junctions. Mol. Biol. Cell 15, 4310–4320. https://doi.org/10.1091/mbc.E04-05-0386

Hoffman, B.D., Grashoff, C., Schwartz, M.A., 2011. Dynamic molecular processes mediate cellular mechanotransduction. Nature 475, 316–323. https://doi.org/10.1038/nature10316

Hood, J.D., Cheresh, D.A., 2002. Role of integrins in cell invasion and migration. Nat. Rev. Cancer 2, 91–100. https://doi.org/10.1038/nrc727

Hoshiba, T., Tanaka, M., 2016. Decellularized matrices as in vitro models of extracellular matrix in tumor tissues at different malignant levels: Mechanism of 5-fluorouracil resistance in colorectal tumor cells. Biochim. Biophys. Acta BBA - Mol. Cell Res. 1863, 2749–2757. https://doi.org/10.1016/j.bbamcr.2016.08.009

Houghton, A.M., Grisolano, J.L., Baumann, M.L., Kobayashi, D.K., Hautamaki, R.D., Nehring, L.C., Cornelius, L.A., Shapiro, S.D., 2006. Macrophage elastase (matrix metalloproteinase-12) suppresses growth of lung metastases. Cancer Res. 66, 6149–6155. https://doi.org/10.1158/0008-5472.CAN-04-0297

Huang, X., Yang, N., Fiore, V.F., Barker, T.H., Sun, Y., Morris, S.W., Ding, Q., Thannickal, V.J., Zhou, Y., 2012. Matrix Stiffness–Induced Myofibroblast Differentiation Is Mediated by Intrinsic Mechanotransduction. Am. J. Respir. Cell Mol. Biol. 47, 340–348. https://doi.org/10.1165/rcmb.2012-0050OC

Ingber, D.E., 2006. Cellular mechanotransduction: putting all the pieces together again. FASEB J. 20, 811–827. https://doi.org/10.1096/fj.05-5424rev

Ingber, D.E., 1997. Tensegrity: The Architectural Basis of Cellular Mechanotransduction. Annu. Rev. Physiol. 59, 575–599. https://doi.org/10.1146/annurev.physiol.59.1.575

Jemec, B., Linge, C., Grobbelaar, A.O., Smith, P.J., Sanders, R., McGrouther, D.A., 2000. The effect of 5-fluorouracil on Dupuytren fibroblast proliferation and differentiation. Chir. Main 19, 15–22. https://doi.org/10.1016/s1297-3203(00)73455-x

Jerrell, R.J., Parekh, A., 2014. Cellular traction stresses mediate extracellular matrix degradation by invadopodia. Acta Biomater. 10, 1886–1896. https://doi.org/10.1016/j.actbio.2013.12.058

Jorba, I., Uriarte, J.J., Campillo, N., Farré, R., Navajas, D., 2017. Probing Micromechanical Properties of the Extracellular Matrix of Soft Tissues by Atomic Force Microscopy. J. Cell. Physiol. 232, 19–26. https://doi.org/10.1002/jcp.25420

Jungbauer, S., Gao, H., Spatz, J.P., Kemkemer, R., 2008. Two Characteristic Regimes in Frequency-Dependent Dynamic Reorientation of Fibroblasts on Cyclically Stretched Substrates. Biophys. J. 95, 3470–3478. https://doi.org/10.1529/biophysj.107.128611

Kalluri, R., Zeisberg, M., 2006. Fibroblasts in cancer. Nat. Rev. Cancer 6, 392–401. https://doi.org/10.1038/nrc1877

Kalwarczyk, T., Ziębacz, N., Bielejewska, A., Zaboklicka, E., Koynov, K., Szymański, J., Wilk, A., Patkowski, A., Gapiński, J., Butt, H.-J., Hołyst, R., 2011. Comparative Analysis of Viscosity of Complex Liquids and Cytoplasm of Mammalian Cells at the Nanoscale. Nano Lett. 11, 2157–2163. https://doi.org/10.1021/nl2008218

Kim, J., Feng, J., Jones, C.A.R., Mao, X., Sander, L.M., Levine, H., Sun, B., 2017. Stress-induced plasticity of dynamic collagen networks. Nat. Commun. 8, 1–7. https://doi.org/10.1038/s41467-017-01011-7

Kim, J., Lee, S.M., Her, S.-H., Lee, K.E., Kim, J.Y., Ahn, J.H., Oh, S.-B., Kwon, J.B., 2013. Newly developed porcine acellular dermal matrix (XenoDerm) for adhesion prevention and rreconstruction of aabdominal wall defect in rat. Tissue Eng. Regen. Med. 10, 102–109. https://doi.org/10.1007/s13770-013-0381-9

Klaas, M., Kangur, T., Viil, J., Mäemets-Allas, K., Minajeva, A., Vadi, K., Antsov, M., Lapidus, N., Järvekülg, M., Jaks, V., 2016. The alterations in the extracellular matrix composition guide the repair of damaged liver tissue. Sci. Rep. 6, 1–12. https://doi.org/10.1038/srep27398

Kloen, P., Jennings, C.L., Gebhardt, M.C., Springfield, D.S., Mankin, H.J., 1995. Transforming growth factor-beta: possible roles in Dupuytren's contracture. J. Hand Surg. 20, 101–108. https://doi.org/10.1016/S0363-5023(05)80067-X

Kole, T.P., Tseng, Y., Jiang, I., Katz, J.L., Wirtz, D., 2004. Intracellular Mechanics of Migrating Fibroblasts. Mol. Biol. Cell 16, 328–338. https://doi.org/10.1091/mbc.e04-06-0485

Kollmannsberger, P., Fabry, B., 2007. BaHigh-force magnetic tweezers with force feedback for biological applications. Rev. Sci. Instrum. 78, 114301. https://doi.org/10.1063/1.2804771

Kreis, T.E., Birchmeier, W., 1980. Stress fiber sarcomeres of fibroblasts are contractile. Cell 22, 555–561. https://doi.org/10.1016/0092-8674(80)90365-7

Krieg, T., Abraham, D., Lafyatis, R., 2007. Fibrosis in connective tissue disease: the role of the myofibroblast and fibroblast-epithelial cell interactions. Arthritis Res. Ther. 9, S4. https://doi.org/10.1186/ar2188

Kusick, S., Bertram, H., Oberleithner, H., Ludwig, T., 2005. Nanoscale imaging and quantification of local proteolytic activity. J. Cell. Physiol. 204, 767–774. https://doi.org/10.1002/jcp.20328

Labernadie, A., Kato, T., Brugués, A., Serra-Picamal, X., Derzsi, S., Arwert, E., Weston, A., González-Tarragó, V., Elosegui-Artola, A., Albertazzi, L., Alcaraz, J., Roca-Cusachs, P., Sahai, E., Trepat, X., 2017. A mechanically active heterotypic E-cadherin/N-cadherin adhesion enables fibroblasts to drive cancer cell invasion. Nat. Cell Biol. 19, 224–237. https://doi.org/10.1038/ncb3478

Łabuś, W., Glik, J., Klama-Baryła, A., Kitala, D., Kraut, M., Maj, M., Nowak, M., Misiuga, M., Marcinkowski, A., Trzebicka, B., Poloczek, R., Kawecki, M., 2018. Atomic force microscopy in the production of a biovital skin graft based on human acellular dermal matrix produced in-

house and in vitro cultured human fibroblasts. J. Biomed. Mater. Res. B Appl. Biomater. 106, 726–733. https://doi.org/10.1002/jbm.b.33883

Laevsky, G., Knecht, D.A., 2003. Cross-linking of actin filaments by myosin II is a major contributor to cortical integrity and cell motility in restrictive environments. J. Cell Sci. 116, 3761–3770. https://doi.org/10.1242/jcs.00684

Lehenkari, P.P., Horton, M.A., 1999. Single Integrin Molecule Adhesion Forces in Intact Cells Measured by Atomic Force Microscopy. Biochem. Biophys. Res. Commun. 259, 645–650. https://doi.org/10.1006/bbrc.1999.0827

Li, Y., Jiang, D., Liang, J., Meltzer, E.B., Gray, A., Miura, R., Wogensen, L., Yamaguchi, Y., Noble, P.W., 2011. Severe lung fibrosis requires an invasive fibroblast phenotype regulated by hyaluronan and CD44Matrix regulates fibroblast invasion. J. Exp. Med. 208, 1459–1471. https://doi.org/10.1084/jem.20102510

Li, Y., Wang, J., Asahina, K., 2013. Mesothelial cells give rise to hepatic stellate cells and myofibroblasts via mesothelial–mesenchymal transition in liver injury. Proc. Natl. Acad. Sci. 110, 2324–2329. https://doi.org/10.1073/pnas.1214136110

Li, Z., Dranoff, J.A., Chan, E.P., Uemura, M., Sévigny, J., Wells, R.G., 2007. Transforming growth factor-β and substrate stiffness regulate portal fibroblast activation in culture. Hepatology 46, 1246–1256. https://doi.org/10.1002/hep.21792

Lillie, M.A., Gosline, J.M., 2002. The viscoelastic basis for the tensile strength of elastin. Int. J. Biol. Macromol. 30, 119–127. https://doi.org/10.1016/S0141-8130(02)00008-9

Lü, W.-D., Zhang, L., Wu, C.-L., Liu, Z.-G., Lei, G.-Y., Liu, J., Gao, W., Hu, Y.-R., 2014. Development of an Acellular Tumor Extracellular Matrix as a Three-Dimensional Scaffold for Tumor Engineering. PLOS ONE 9, e103672. https://doi.org/10.1371/journal.pone.0103672

Lyapunova, E., Nikituk, A., Bayandin, Y., Naimark, O., Rianna, C., Radmacher, M., 2016. Passive microrheology of normal and cancer cells after ML7 treatment by atomic force microscopy. AIP Conf. Proc. 1760, 020046. https://doi.org/10.1063/1.4960265

Ma, X., Schickel, M.E., Stevenson, M.D., Sarang-Sieminski, A.L., Gooch, K.J., Ghadiali, S.N., Hart, R.T., 2013. Fibers in the Extracellular Matrix Enable Long-Range Stress Transmission between Cells. Biophys. J. 104, 1410–1418. https://doi.org/10.1016/j.bpj.2013.02.017

Martens, J.C., Radmacher, M., 2008. Softening of the actin cytoskeleton by inhibition of myosin II. Pflüg. Arch. - Eur. J. Physiol. 456, 95–100. https://doi.org/10.1007/s00424-007-0419-8

McAnulty, R.J., 2007. Fibroblasts and myofibroblasts: Their source, function and role in disease. Int. J. Biochem. Cell Biol. 39, 666–671. https://doi.org/10.1016/j.biocel.2006.11.005

Mierke, C.T., Fischer, T., Puder, S., Kunschmann, T., Soetje, B., Ziegler, W.H., 2017. Focal adhesion kinase activity is required for actomyosin contractility-based invasion of cells into dense 3D matrices. Sci. Rep. 7, 1–18. https://doi.org/10.1038/srep42780

Mirastschijski, U., Kerzel, C., Schnabel, R., Strauss, S., Breuing, K.-H., 2013. Complete Horizontal Skin Cell Resurfacing and Delayed Vertical Cell Infiltration into Porcine Reconstructive Tissue Matrix Compared to Bovine Collagen Matrix and Human Dermis. Plast. Reconstr. Surg. 132, 861–869. https://doi.org/10.1097/PRS.0b013e31829fe461

Moeendarbary, E., Valon, L., Fritzsche, M., Harris, A.R., Moulding, D.A., Thrasher, A.J., Stride, E., Mahadevan, L., Charras, G.T., 2013. The cytoplasm of living cells behaves as a poroelastic material. Nat. Mater. 12, 253–261. https://doi.org/10.1038/nmat3517

Morishima, Y., Nomura, A., Uchida, Y., Noguchi, Y., Sakamoto, T., Ishii, Y., Goto, Y., Masuyama, K., Zhang, M.J., Hirano, K., Mochizuki, M., Ohtsuka, M., Sekizawa, K., 2001. Triggering the Induction of Myofibroblast and Fibrogenesis by Airway Epithelial Shedding. Am. J. Respir. Cell Mol. Biol. 24, 1–11. https://doi.org/10.1165/ajrcmb.24.1.4040

Mouw, J.K., Ou, G., Weaver, V.M., 2014. Extracellular matrix assembly: a multiscale deconstruction. Nat. Rev. Mol. Cell Biol. 15, 771–785. https://doi.org/10.1038/nrm3902

Muiznieks, L.D., Keeley, F.W., 2013. Molecular assembly and mechanical properties of the extracellular matrix: A fibrous protein perspective. Biochim. Biophys. Acta BBA - Mol. Basis

Dis., Fibrosis: Translation of basic research to human disease 1832, 866–875. https://doi.org/10.1016/j.bbadis.2012.11.022

Müller, D.J., Dufrêne, Y.F., 2008. Atomic force microscopy as a multifunctional molecular toolbox in nanobiotechnology. Nat. Nanotechnol. 3, 261–269. https://doi.org/10.1038/nnano.2008.100

Müller, D.J., Helenius, J., Alsteens, D., Dufrêne, Y.F., 2009. Force probing surfaces of living cells to molecular resolution. Nat. Chem. Biol. 5, 383–390. https://doi.org/10.1038/nchembio.181

Nishioka, M., Venkatesan, N., Dessalle, K., Mogas, A., Kyoh, S., Lin, T.-Y., Nair, P., Baglole, C.J., Eidelman, D.H., Ludwig, M.S., Hamid, Q., 2015. Fibroblast-epithelial cell interactions drive epithelial-mesenchymal transition differently in cells from normal and COPD patients. Respir. Res. 16, 72. https://doi.org/10.1186/s12931-015-0232-4

Ohashi, T., Kiehart, D.P., Erickson, H.P., 1999. Dynamics and elasticity of the fibronectin matrix in living cell culture visualized by fibronectin–green fluorescent protein. Proc. Natl. Acad. Sci. 96, 2153–2158. https://doi.org/10.1073/pnas.96.5.2153

Omelchenko, T., Fetisova, E., Ivanova, O., Bonder, E.M., Feder, H., Vasiliev, J.M., Gelfand, I.M., 2001. Contact interactions between epitheliocytes and fibroblasts: Formation of heterotypic cadherin-containing adhesion sites is accompanied by local cytoskeletal reorganization. Proc. Natl. Acad. Sci. 98, 8632–8637. https://doi.org/10.1073/pnas.151247698

Orlandi, A., Ropraz, P., Gabbiani, G., 1994. Proliferative Activity and α-Smooth Muscle Actin Expression in Cultured Rat Aortic Smooth Muscle Cells Are Differently Modulated by Transforming Growth Factor-β1 and Heparin. Exp. Cell Res. 214, 528–536. https://doi.org/10.1006/excr.1994.1290

Pakshir, P., Alizadehgiashi, M., Wong, B., Coelho, N.M., Chen, X., Gong, Z., Shenoy, V.B., McCulloch, C.A., Hinz, B., 2019. Dynamic fibroblast contractions attract remote macrophages in fibrillar collagen matrix. Nat. Commun. 10, 1–17. https://doi.org/10.1038/s41467-019-09709-6

Panorchan, P., George, J.P., Wirtz, D., 2006a. Probing Intercellular Interactions between Vascular Endothelial Cadherin Pairs at Single-molecule Resolution and in Living Cells. J. Mol. Biol. 358, 665–674. https://doi.org/10.1016/j.jmb.2006.02.021

Panorchan, P., Thompson, M.S., Davis, K.J., Tseng, Y., Konstantopoulos, K., Wirtz, D., 2006b. Single-molecule analysis of cadherin-mediated cell-cell adhesion. J. Cell Sci. 119, 66–74. https://doi.org/10.1242/jcs.02719

Pillet, F., Gibot, L., Madi, M., Rols, M.-P., Dague, E., 2017. Importance of endogenous extracellular matrix in biomechanical properties of human skin model. Biofabrication 9, 025017. https://doi.org/10.1088/1758-5090/aa6ed5

Pittet, P., Lee, K., Kulik, A.J., Meister, J.-J., Hinz, B., 2008. Fibrogenic fibroblasts increase intercellular adhesion strength by reinforcing individual OB-cadherin bonds. J. Cell Sci. 121, 877–886. https://doi.org/10.1242/jcs.024877

Porter, K.E., Turner, N.A., 2009. Cardiac fibroblasts: At the heart of myocardial remodeling. Pharmacol. Ther. 123, 255–278. https://doi.org/10.1016/j.pharmthera.2009.05.002

Prakasam, A.K., Maruthamuthu, V., Leckband, D.E., 2006. Similarities between heterophilic and homophilic cadherin adhesion. Proc. Natl. Acad. Sci. 103, 15434–15439. https://doi.org/10.1073/pnas.0606701103

Puech, P.-H., Poole, K., Knebel, D., Muller, D.J., 2006. A new technical approach to quantify cell–cell adhesion forces by AFM. Ultramicroscopy, Proceedings of the Seventh International Conference on Scanning Probe Microscopy, Sensors and Nanostructures 106, 637–644. https://doi.org/10.1016/j.ultramic.2005.08.003

Radmacher, M., 2002. Measuring the elastic properties of living cells by the atomic force microscope. Methods Cell Biol. 68, 67–90. https://doi.org/10.1016/s0091-679x(02)68005-7

Radmacher, M., 1997. Measuring the elastic properties of biological samples with the AFM. IEEE Eng. Med. Biol. Mag. 16, 47–57. https://doi.org/10.1109/51.582176

Radmacher, M., Fritz, M., Kacher, C.M., Cleveland, J.P., Hansma, P.K., 1996. Measuring the viscoelastic properties of human platelets with the atomic force microscope. Biophys. J. 70, 556–567. https://doi.org/10.1016/S0006-3495(96)79602-9

Raines, E.W., 2000. The extracellular matrix can regulate vascular cell migration, proliferation, and survival: relationships to vascular disease. Int. J. Exp. Pathol. 81, 173–182. https://doi.org/10.1046/j.1365-2613.2000.00155.x

Rakshit, S., Zhang, Y., Manibog, K., Shafraz, O., Sivasankar, S., 2012. Ideal, catch, and slip bonds in cadherin adhesion. Proc. Natl. Acad. Sci. 109, 18815–18820. https://doi.org/10.1073/pnas.1208349109

Rana, D., Zreiqat, H., Benkirane-Jessel, N., Ramakrishna, S., Ramalingam, M., 2017. Development of decellularized scaffolds for stem cell-driven tissue engineering. J. Tissue Eng. Regen. Med. 11, 942–965. https://doi.org/10.1002/term.2061

Rianna, C., Kumar, P., Radmacher, M., 2018. The role of the microenvironment in the biophysics of cancer. Semin. Cell Dev. Biol., Application of Atomic Force Microscopy in cell biology 73, 107–114. https://doi.org/10.1016/j.semcdb.2017.07.022

Rianna, C., Radmacher, M., 2017. Influence of microenvironment topography and stiffness on the mechanics and motility of normal and cancer renal cells. Nanoscale 9, 11222–11230. https://doi.org/10.1039/C7NR02940C

Rianna, Carmela, Radmacher, M., 2017. Comparison of viscoelastic properties of cancer and normal thyroid cells on different stiffness substrates. Eur. Biophys. J. EBJ 46, 309–324. https://doi.org/10.1007/s00249-016-1168-4

Rianna, C., Radmacher, M., 2016. Cell mechanics as a marker for diseases: Biomedical applications of AFM. AIP Conf. Proc. 1760, 020057. https://doi.org/10.1063/1.4960276

Rico, F., Rigato, A., Picas, L., Scheuring, S., 2013. Mechanics of proteins with a focus on atomic force microscopy. J. Nanobiotechnology 11, S3. https://doi.org/10.1186/1477-3155-11-S1-S3

Rico, F., Roca-Cusachs, P., Gavara, N., Farré, R., Rotger, M., Navajas, D., 2005. Probing mechanical properties of living cells by atomic force microscopy with blunted pyramidal cantilever tips. Phys. Rev. E Stat. Nonlin. Soft Matter Phys. 72, 021914. https://doi.org/10.1103/PhysRevE.72.021914

Rigor, R.R., Shen, Q., Pivetti, C.D., Wu, M.H., Yuan, S.Y., 2013. Myosin Light Chain Kinase Signaling in Endothelial Barrier Dysfunction. Med. Res. Rev. 33, 911–933. https://doi.org/10.1002/med.21270

Rock, J.R., Barkauskas, C.E., Cronce, M.J., Xue, Y., Harris, J.R., Liang, J., Noble, P.W., Hogan, B.L.M., 2011. Multiple stromal populations contribute to pulmonary fibrosis without evidence for epithelial to mesenchymal transition. Proc. Natl. Acad. Sci. 108, E1475–E1483. https://doi.org/10.1073/pnas.1117988108

Roessner, E.D., Vitacolonna, M., Hohenberger, P., 2012. Confocal Laser Scanning Microscopy Evaluation of an Acellular Dermis Tissue Transplant (Epiflex®). PLOS ONE 7, e45991. https://doi.org/10.1371/journal.pone.0045991

Rønnov-Jessen, L., Petersen, O.W., 1996. A function for filamentous alpha-smooth muscle actin: retardation of motility in fibroblasts. J. Cell Biol. 134, 67–80. https://doi.org/10.1083/jcb.134.1.67

Rotsch, C., Radmacher, M., 2000. Drug-induced changes of cytoskeletal structure and mechanics in fibroblasts: an atomic force microscopy study. Biophys. J. 78, 520–535. https://doi.org/10.1016/S0006-3495(00)76614-8

Rudolph, R., Vande Berg, J., 1991. The myofibroblast in Dupuytren's contracture. Hand Clin. 7, 683–692; discussion 693-694.

Sader, J.E., Larson, I., Mulvaney, P., White, L.R., 1995. Method for the calibration of atomic force microscope cantilevers. Rev. Sci. Instrum. 66, 3789–3798. https://doi.org/10.1063/1.1145439

Sakar, M.S., Eyckmans, J., Pieters, R., Eberli, D., Nelson, B.J., Chen, C.S., 2016. Cellular forces and matrix assembly coordinate fibrous tissue repair. Nat. Commun. 7, 1–8. https://doi.org/10.1038/ncomms11036

Samuel, M.S., Lopez, J.I., McGhee, E.J., Croft, D.R., Strachan, D., Timpson, P., Munro, J., Schröder, E., Zhou, J., Brunton, V.G., Barker, N., Clevers, H., Sansom, O.J., Anderson, K.I., Weaver, V.M., Olson, M.F., 2011. Actomyosin-Mediated Cellular Tension Drives Increased Tissue Stiffness

and β-Catenin Activation to Induce Epidermal Hyperplasia and Tumor Growth. Cancer Cell 19, 776–791. https://doi.org/10.1016/j.ccr.2011.05.008

Schäfer, A., Radmacher, M., 2005. Influence of myosin II activity on stiffness of fibroblast cells. Acta Biomater. 1, 273–280. https://doi.org/10.1016/j.actbio.2005.02.004

Schillers, H., Medalsy, I., Hu, S., Slade, A.L., Shaw, J.E., 2016. PeakForce Tapping resolves individual microvilli on living cells. J. Mol. Recognit. 29, 95–101. https://doi.org/10.1002/jmr.2510

Schillers, H., Rianna, C., Schäpe, J., Luque, T., Doschke, H., Wälte, M., Uriarte, J.J., Campillo, N., Michanetzis, G.P.A., Bobrowska, J., Dumitru, A., Herruzo, E.T., Bovio, S., Parot, P., Galluzzi, M., Podestà, A., Puricelli, L., Scheuring, S., Missirlis, Y., Garcia, R., Odorico, M., Teulon, J.-M., Lafont, F., Lekka, M., Rico, F., Rigato, A., Pellequer, J.-L., Oberleithner, H., Navajas, D., Radmacher, M., 2017. Standardized Nanomechanical Atomic Force Microscopy Procedure (SNAP) for Measuring Soft and Biological Samples. Sci. Rep. 7, 1–9. https://doi.org/10.1038/s41598-017-05383-0

Schindelin, J., Arganda-Carreras, I., Frise, E., Kaynig, V., Longair, M., Pietzsch, T., Preibisch, S., Rueden, C., Saalfeld, S., Schmid, B., Tinevez, J.-Y., White, D.J., Hartenstein, V., Eliceiri, K., Tomancak, P., Cardona, A., 2012. Fiji: an open-source platform for biological-image analysis. Nat. Methods 9, 676–682. https://doi.org/10.1038/nmeth.2019

Schleip, R., Klingler, W., Lehmann-Horn, F., 2005. Active fascial contractility: Fascia may be able to contract in a smooth muscle-like manner and thereby influence musculoskeletal dynamics. Med. Hypotheses 65, 273–277. https://doi.org/10.1016/j.mehy.2005.03.005

Schultz, G.S., Davidson, J.M., Kirsner, R.S., Bornstein, P., Herman, I.M., 2011. Dynamic reciprocity in the wound microenvironment. Wound Repair Regen. 19, 134–148. https://doi.org/10.1111/j.1524-475X.2011.00673.x

Serini, G., Bochaton-Piallat, M.-L., Ropraz, P., Geinoz, A., Borsi, L., Zardi, L., Gabbiani, G., 1998. The Fibronectin Domain ED-A Is Crucial for Myofibroblastic Phenotype Induction by Transforming Growth Factor-β1. J. Cell Biol. 142, 873–881. https://doi.org/10.1083/jcb.142.3.873

Shi, X., Qin, L., Zhang, X., He, K., Xiong, C., Fang, J., Fang, X., Zhang, Y., 2011. Elasticity of cardiac cells on the polymer substrates with different stiffness: an atomic force microscopy study. Phys. Chem. Chem. Phys. 13, 7540–7545. https://doi.org/10.1039/C1CP20154A

Simões, R.L., Fierro, I.M., 2005. Involvement of the Rho-Kinase/Myosin Light Chain Kinase Pathway on Human Monocyte Chemotaxis Induced by ATL-1, an Aspirin-Triggered Lipoxin A4 Synthetic Analog. J. Immunol. 175, 1843–1850. https://doi.org/10.4049/jimmunol.175.3.1843

Sisson, T.H., Ajayi, I.O., Subbotina, N., Dodi, A.E., Rodansky, E.S., Chibucos, L.N., Kim, K.K., Keshamouni, V.G., White, E.S., Zhou, Y., Higgins, P.D.R., Larsen, S.D., Neubig, R.R., Horowitz, J.C., 2015. Inhibition of Myocardin-Related Transcription Factor/Serum Response Factor Signaling Decreases Lung Fibrosis and Promotes Mesenchymal Cell Apoptosis. Am. J. Pathol. 185, 969–986. https://doi.org/10.1016/j.ajpath.2014.12.005

Smithmyer, M.E., Sawicki, L.A., Kloxin, A.M., 2014. Hydrogel scaffolds as in vitro models to study fibroblast activation in wound healing and disease. Biomater. Sci. 2, 634–650. https://doi.org/10.1039/C3BM60319A

Sneddon, I.N., 1965. The relation between load and penetration in the axisymmetric boussinesq problem for a punch of arbitrary profile. Int. J. Eng. Sci. 3, 47–57. https://doi.org/10.1016/0020-7225(65)90019-4

Sollich, P., 1998. Rheological constitutive equation for a model of soft glassy materials. Phys. Rev. E 58, 738–759. https://doi.org/10.1103/PhysRevE.58.738

Solon, J., Levental, I., Sengupta, K., Georges, P.C., Janmey, P.A., 2007. Fibroblast Adaptation and Stiffness Matching to Soft Elastic Substrates. Biophys. J. 93, 4453–4461. https://doi.org/10.1529/biophysj.106.101386

Southern, B.D., Grove, L.M., Rahaman, S.O., Abraham, S., Scheraga, R.G., Niese, K.A., Sun, H., Herzog, E.L., Liu, F., Tschumperlin, D.J., Egelhoff, T.T., Rosenfeld, S.S., Olman, M.A., 2016. Matrix-driven Myosin II Mediates the Pro-fibrotic Fibroblast Phenotype. J. Biol. Chem. 291, 6083–6095. https://doi.org/10.1074/jbc.M115.712380

Stolz, M., Gottardi, R., Raiteri, R., Miot, S., Martin, I., Imer, R., Staufer, U., Raducanu, A., Düggelin, M., Baschong, W., Daniels, A.U., Friederich, N.F., Aszodi, A., Aebi, U., 2009. Early detection of aging cartilage and osteoarthritis in mice and patient samples using atomic force microscopy. Nat. Nanotechnol. 4, 186–192. https://doi.org/10.1038/nnano.2008.410

Strohmeyer, N., Bharadwaj, M., Costell, M., Fässler, R., Müller, D.J., 2017. Fibronectin-bound α5β1 integrins sense load and signal to reinforce adhesion in less than a second. Nat. Mater. 16, 1262–1270. https://doi.org/10.1038/nmat5023

Taubenberger, A.V., Hutmacher, D.W., Muller, D.J., 2013. Single-Cell Force Spectroscopy, an Emerging Tool to Quantify Cell Adhesion to Biomaterials. Tissue Eng. Part B Rev. 20, 40–55. https://doi.org/10.1089/ten.teb.2013.0125

Tomasek, J., Rayan, G.M., 1995. Correlation of α-smooth muscle actin expression and contraction in Dupuytren's disease fibroblasts. J. Hand Surg. 20, 450–455. https://doi.org/10.1016/S0363-5023(05)80105-4

Tomasek, J.J., Gabbiani, G., Hinz, B., Chaponnier, C., Brown, R.A., 2002. Myofibroblasts and mechano-regulation of connective tissue remodelling. Nat. Rev. Mol. Cell Biol. 3, 349–363. https://doi.org/10.1038/nrm809

Tondon, A., Hsu, H.-J., Kaunas, R., 2012. Dependence of cyclic stretch-induced stress fiber reorientation on stretch waveform. J. Biomech., Special Issue on Cardiovascular Solid Mechanics 45, 728–735. https://doi.org/10.1016/j.jbiomech.2011.11.012

TOWNLEY, W.A., CAMBREY, A.D., KHAW, P.T., GROBBELAAR, A.O., 2009. The role of an MMP inhibitor in the regulation of mechanical tension by Dupuytren's disease fibroblasts. J. Hand Surg. Eur. Vol. 34, 783–787. https://doi.org/10.1177/1753193409345188

Tse, J.R., Engler, A.J., 2010. Preparation of Hydrogel Substrates with Tunable Mechanical Properties. Curr. Protoc. Cell Biol. 47, 10.16.1-10.16.16. https://doi.org/10.1002/0471143030.cb1016s47

Ueber die Berührung fester elastischer Körper., 1882. . J. Für Reine Angew. Math. Crelles J. 1882, 156–171. https://doi.org/10.1515/crll.1882.92.156

van Beuge, M.M., ten Dam, E.-J.P.M., Werker, P.M.N., Bank, R.A., 2016. Matrix and cell phenotype differences in Dupuytren's disease. Fibrogenesis Tissue Repair 9, 9. https://doi.org/10.1186/s13069-016-0046-0

van Helvert, S., Friedl, P., 2016. Strain Stiffening of Fibrillar Collagen during Individual and Collective Cell Migration Identified by AFM Nanoindentation. ACS Appl. Mater. Interfaces 8, 21946–21955. https://doi.org/10.1021/acsami.6b01755

Verhoekx, J.S.N., Beckett, K.S., Bisson, M.A., McGrouther, D.A., Grobbelaar, A.O., Mudera, V., 2013a. The mechanical environment in dupuytren's contracture determines cell contractility and associated MMP-mediated matrix remodeling. J. Orthop. Res. 31, 328–334. https://doi.org/10.1002/jor.22220

Verhoekx, J.S.N., Verjee, L.S., Izadi, D., Chan, J.K.K., Nicolaidou, V., Davidson, D., Midwood, K.S., Nanchahal, J., 2013b. Isometric Contraction of Dupuytren's Myofibroblasts Is Inhibited by Blocking Intercellular Junctions. J. Invest. Dermatol. 133, 2664–2671. https://doi.org/10.1038/jid.2013.219

Vertelov, G., Gutierrez, E., Lee, S.-A., Ronan, E., Groisman, A., Tkachenko, E., 2016. Rigidity of silicone substrates controls cell spreading and stem cell differentiation. Sci. Rep. 6, 1–6. https://doi.org/10.1038/srep33411

Viji Babu, P.K., Radmacher, M., 2019. Mechanics of Brain Tissues Studied by Atomic Force Microscopy: A Perspective. Front. Neurosci. 13. https://doi.org/10.3389/fnins.2019.00600

von Versen-Hoeynck, F., Steinfeld, A.P., Becker, J., Hermel, M., Rath, W., Hesselbarth, U., 2008. Sterilization and preservation influence the biophysical properties of human amnion grafts. Biologicals 36, 248–255. https://doi.org/10.1016/j.biologicals.2008.02.001

Walimbe, T., Panitch, A., Sivasankar, M.P., 2017. An in vitro scaffold-free epithelial–fibroblast coculture model for the larynx. The Laryngoscope 127, E185–E192. https://doi.org/10.1002/lary.26388

Wang, J.H.-C., Lin, J.-S., Yang, Z.-C., 2007. Cell Traction Force Microscopy, in: Qin, L., Genant, H.K., Griffith, J.F., Leung, K.S. (Eds.), Advanced Bioimaging Technologies in Assessment of the Quality of Bone and Scaffold Materials: Techniques and Applications. Springer, Berlin, Heidelberg, pp. 227–235. https://doi.org/10.1007/978-3-540-45456-4_14

Watt, F.M., Huck, W.T.S., 2013. Role of the extracellular matrix in regulating stem cell fate. Nat. Rev. Mol. Cell Biol. 14, 467–473. https://doi.org/10.1038/nrm3620

Weis, W.I., Nelson, W.J., 2006. Re-solving the Cadherin-Catenin-Actin Conundrum. J. Biol. Chem. 281, 35593–35597. https://doi.org/10.1074/jbc.R600027200

Wells, R.G., 2013. Tissue mechanics and fibrosis. Biochim. Biophys. Acta BBA - Mol. Basis Dis., Fibrosis: Translation of basic research to human disease 1832, 884–890. https://doi.org/10.1016/j.bbadis.2013.02.007

Wen, Q., Janmey, P.A., 2013. Effects of non-linearity on cell–ECM interactions. Exp. Cell Res., Special Issue: Cell Motility and Mechanics 319, 2481–2489. https://doi.org/10.1016/j.yexcr.2013.05.017

Wilshaw, S.-P., Kearney, J.N., Fisher, J., Ingham, E., 2006. Production of an Acellular Amniotic Membrane Matrix for Use in Tissue Engineering. Tissue Eng. 12, 2117–2129. https://doi.org/10.1089/ten.2006.12.2117

Wipff, P.-J., Rifkin, D.B., Meister, J.-J., Hinz, B., 2007. Myofibroblast contraction activates latent TGF-β1 from the extracellular matrix. J. Cell Biol. 179, 1311–1323. https://doi.org/10.1083/jcb.200704042

Wu, J.C., Gregory, C.W., Dephilip, R.M., 1993. P-Cadherin and E-Cadherin Are Co-expressed in MDCK Cells. Biochem. Biophys. Res. Commun. 195, 1329–1335. https://doi.org/10.1006/bbrc.1993.2189

Xu, W., Hu, X., Chen, Z., Zheng, X., Zhang, C., Wang, G., Chen, Y., Zhou, X., Tang, X., Luo, L., Xu, X., Pan, W., 2014. Normal Fibroblasts Induce E-Cadherin Loss and Increase Lymph Node Metastasis in Gastric Cancer. PLOS ONE 9, e97306. https://doi.org/10.1371/journal.pone.0097306

Xu, X., Li, Z., Cai, L., Calve, S., Neu, C.P., 2016. Mapping the Nonreciprocal Micromechanics of Individual Cells and the Surrounding Matrix Within Living Tissues. Sci. Rep. 6, 1–9. https://doi.org/10.1038/srep24272

Yamaguchi, H., Yoshida, N., Takanashi, M., Ito, Y., Fukami, K., Yanagihara, K., Yashiro, M., Sakai, R., 2014. Stromal Fibroblasts Mediate Extracellular Matrix Remodeling and Invasion of Scirrhous Gastric Carcinoma Cells. PLOS ONE 9, e85485. https://doi.org/10.1371/journal.pone.0085485

Yango, A., Schäpe, J., Rianna, C., Doschke, H., Radmacher, M., 2016. Measuring the viscoelastic creep of soft samples by step response AFM. Soft Matter 12, 8297–8306. https://doi.org/10.1039/C6SM00801A

Yeh, Y.-C., Ling, J.-Y., Chen, W.-C., Lin, H.-H., Tang, M.-J., 2017. Mechanotransduction of matrix stiffness in regulation of focal adhesion size and number: reciprocal regulation of caveolin-1 and β1 integrin. Sci. Rep. 7, 1–14. https://doi.org/10.1038/s41598-017-14932-6

Youn, Y.-H., Hong, J., Burke, J.M., 2005. Endogenous N-cadherin in a subpopulation of MDCK cells: distribution and catenin complex composition. Exp. Cell Res. 303, 275–286. https://doi.org/10.1016/j.yexcr.2004.09.023

Zhou, Y., Huang, X., Hecker, L., Kurundkar, D., Kurundkar, A., Liu, H., Jin, T.-H., Desai, L., Bernard, K., Thannickal, V.J., 2013. Inhibition of mechanosensitive signaling in myofibroblasts ameliorates experimental pulmonary fibrosis. J. Clin. Invest. 123, 1096–1108. https://doi.org/10.1172/JCI66700